Title
Assays and Tools for Biomolecular Analysis in Remote and Low-Resource Settings

Author
Henrikson, Richard Harry

Publication Date
2015

Peer reviewed|Thesis/dissertation

Assays and Tools for Biomolecular Analysis in Remote and Low-Resource Settings

By

Richard Harry Henrikson

A dissertation submitted in partial satisfaction of the

requirements for the degree of

Joint Doctor of Philosophy

With University of California, San Francisco

in

Bioengineering

in the

Graduate Division

of the

University of California, Berkeley

Committee in Charge:

Professor Luke P. Lee
Professor Tejal Desai
Professor George Sensabaugh

Summer 2015

Assays and Tools for Biomolecular Analysis in Remote and Low-Resource Settings

By Richard Harry Henrikson

Abstract

Assays and Tools for Biomolecular Analysis in Remote and Low-Resource Settings

By

Richard Harry Henrikson

Joint Doctor of Philosophy in Bioengineering with

University of California, San Francisco

University of California, Berkeley

Professor Luke P. Lee, Chair

The global population faces significant challenges in not only improving health care, but even just in maintaining it. Environmental and economic disparities are increasingly creating a massive population that lacks adequate medical attention. Traditional tools employed to detect, monitor, and treat sickness are woefully inadequate in the face of this grand challenge in medicine. However, a new generation of technologies is under development that promises to increase both the access and the quality of care available on a global scale. These tools provide simple but powerful means for both medical workers and patients to take a predictive and preventative approach to medicine – lowering the overall burden on the system and leading a new state of wellness.

There is no shortage of problems to solve in this effort to vastly energize the medical system. However, at the core, molecular diagnostic tools hold particular promise for revolutionary gains. As the core machinery of life, proteins and nucleic acids tell the full story of health and illness through their rise and fall. The ability to capture these changes, and to draw meaning from them, will be a cornerstone of modern proactive medicine. Early detection of illness often leads to a far reduced burden on the medical system, and significantly improved outcomes for the patient. In this work, I focus on the development of several technologies aimed at bringing health care a step closer to the world that needs it most.

In the first chapter, I provide a brief overview of the acute clinical needs in remote and low-resource settings, as well as an historical perspective on the periodic evolution of medicine over the centuries that has led us to the cusp of a molecular diagnostic world. I also review some of the enabling technologies that have been developed to facilitate point of care medicine.

Chapter 2 focuses on new assays and methods for nucleic acid testing in low-resource settings. I particularly focus on the development of robust isothermal amplification to glean information about both the presence of infection *and* the proper course of treatment. Through genotypic analysis of the invading pathogen, drug susceptibility can be determined. Furthermore, these assays are incorporated into several microfluidic and electronic systems that enable inexpensive and rapid diagnosis.

Chapter 3 provides an insight into the world of protein analysis in point of care settings. In this work, I've focused on robust, DNA-based sensors to detect proteins and initiate a downstream signal that can be quantified through fluorescent or nanophotonic mechanisms. In both cases, there is a focus on maintaining a rapid and robust signal that can be delivered at a low cost.

Chapter 4 deviates slightly, as it explores a means to revolutionize the traditional polymerase chain reaction by leveraging nanoplasmonic phenomena. I provide a description and initial empirical insights on a means to perform multiplexed nucleic acid quantification with little more than an LED driving both thermocycling and specific detection. While this technology certainly has applications in the developed world as well, the primary focus is on facilitating the use of gold standard assays with simple and affordable tools.

The final chapter briefly reviews my work in this doctorate degree program, while providing some insights into next steps to move these tools even closer to applications in the developing world.

For my parents, who taught me curiosity, compassion, and courage.
May they treasure this work as though they were alone in reading it.

Contents

Preface

The world is not like it has ever been before. We are entering a new age of unprecedented advances in technological capability, where your keyboard predicts what you want to say, your media tells you what you want to watch, and your phone takes you where you want to be. Real-time information is already old news. And yet, as we march brazenly forward, we can't help but notice that something has been left behind. Or some*one*, rather. As we live in a time of great hope for the future, we also live in a time of great disparity among humankind. The gap between those who have and those who do not has grown at a breakneck pace. And nowhere is this gap more evident, nor more tragic, than in the very core of that fundamental need that drives everything else: our health.

Martin Luther King, Jr. once said "Of all the forms of inequality, injustice in healthcare is the most shocking and inhumane." This sentiment has been a rally cry for me in my years at Berkeley. With a growing population that faces ever more burdens on health, and resources stretched to the breaking point, it is clear that new solutions are needed to address healthcare in the coming years. We are facing a turning point, where medicine may share in the considerable advances made through technological breakthroughs in computation and automation. These breakthroughs promise to empower doctors and individuals alike with unprecedented access to medical information that will aid in the path towards a true *health*care system that is predictive and preventive, rather than the reactionary sickcare system of the past.

This graduate program has been a long and trying time in which I have had the good fortune to work with many great people on challenging problems that make you want to greet each day with renewed fervor. I've had the opportunity to work with passionate interdisciplinary teams, and to see and live in far-off places across five continents. I know that I am extraordinarily fortunate for these experiences. I know they are not offered frequently, nor do I accept them lightly. I've seen and felt great things during my graduate career, but I have also faced and embraced the hardships that plague our planet.

The work presented in this dissertation has been a focal point for me to build an idea of what the world could and should be like. It is with great humility that I realize just how small these contributions are in the grand schemes they aim to sway. But I take comfort in my knowledge that every grand journey requires that one, simple, unassuming, first step. I believe now it is now time to take what I've learned herein and stride forward.

Acknowledgements

A Ph.D. can be an isolating experience, as you withdraw from the rest of the world into an increasingly narrow domain of esoteric study. However, I can thankfully say this was not the case for me. I've had the good fortune to be surrounded by many smart, passionate, and fun people who have made my Ph.D. not just possible, but a true pleasure. While I'm certain I can't possibly thank everyone, I'll do my best to cover a small portion here.

Of course, none of this would be possible without my parents. And not just for existential reasons. Their unconditional love and respect has given me the confidence to pursue my dreams in the face of any obstacle. They've always believed in me, and pushed me to be my best self. Mom, you've always been my number one fan – I'll never forget the late-night quizzes and early-morning pre-test brain food (chocolate). Dad, you've been an inspiration to me – a model engineer with a sharp wit and good heart. And to the rest of my family – Chris, Scott, and Kim –we've shaped each other in countless immeasurable ways through the decades. Thanks for making me the person I am today.

To my advisor, Luke Lee, thank you for everything you've done to nurture my academic growth. From the very beginning you welcomed me with open arms, and continue to be a central advocate for my scientific career. You gave me the space to build my own projects, and to learn the hard lessons that only failure can teach – though thankfully success came as well (you can't lose them all!). Your passion has inspired and encouraged multiple generations of BioPOETS, and I'm proud to be among their alumni ranks. I would also like to thank my first rotation advisor, Amy Herr, for providing an opportunity to grow in a new lab. And of course, a big thank you to my dissertation committee members, Tejal Desai and George Sensabaugh, for their crucial help in the last leg of the race.

To my fellow BioPOETS, I couldn't have asked for a better team to join me in this journey. Frankie Myers, you've been an amazing partner in crime – the oscilloscope to my pipette. I had an amazing time as we wandered the globe, teaching and supporting each other with patience and good humor. John Waldeisen, Debkishore Mitra, Brendan Turner, Ivan Dimov, Charlie Yeh, Chi-Cheng Fu, Sean Liu, and Brian Kim, it was a pleasure building out the point of care diagnostics branch of the BioPOETS with all of you. David Breslauer, your wisdom belies your success – thank you for all of your guidance, inspiration, and snark. Tanner Nevill, thank you for paving the way for global health technology, both with the BioPOETS and with the POCDx Idea Lab. Megan Dueck, you were always a force of order and calm in the chaos of lab and lecture. Yeonho Choi, Young Geun Park, SoonGweon Hong, Liz Wu, Eric Lee, Hansang Cho, Eunice Lee, Jun Ho Son, Seung-Min Park, Ben Ross, and Sang Hun Lee, thank you for all of your guidance – you've been an example of hard work that pays off. Julian Diaz, Adrian Sprenger, Qiong Pan, Fei Liu, thank you for bringing a diversity of ideas and culture to our group. And I'd especially like to thank the students who volunteered their time to tackle these challenges with me – Michael Song, Lily Xu, Monica Lin, Jennifer Bone, Mauro Poggio, Hinesh Patel, Edwin Li, Lucia Cheung, Andrew Tran, and Samantha Smiley – I know you all have bright careers ahead of you.

I've been blessed with amazing collaborators, both at home and abroad, who have given their invaluable experience in my academic progress. At Berkeley, Jennifer Doudna's Group (especially Mark Luskus), provided enabled our radiolabeled AMProbe testing. Lee Riley and his group (especially Amador Goodridge) provided valuable input in our tuberculosis research. Abroad, I had the opportunity to work with groups in South Africa,

Ireland, and Korea. Paul van Helden and the team from the Centre of Excellence for Biomedical Tuberculosis Research welcomed me into their community and provided guidance for two summers while I developed the μBAR system (with a special thanks to Borna Mueller for hosting and providing bioinformatics advice). Paul Leonard and the Translational Diagnostics Group of Dublin City University further aided in the development of our LAMP assays (and my taste for Beamish). Sunghoon Kwon and the entire team at the Biophotonics and Nano Engineering Lab of Seoul National University made me feel like a part of the family while training me in advanced microfabrication techniques (and a special thanks to Taehong Kwon for hosting me during my time there).

And then there are the countless people who influenced me prior to even entering Berkeley. My time working at the National Cancer Institute in high school was truly formative. I was able to get early experience with *in vitro* and *in vivo* assays that actually touched the lives of patients struggling with disease. I had incredible mentors in both the Lab of Cell Biology (Michael Maurizi) and the Experimental Transplantation and Immunology Branch (Dan Fowler). Pardis Sabeti provided a welcome introduction to bioinformatics research at the MIT Whitehead Institute. Angela Belcher and the Biomolecular Materials Group at MIT gave me rich experiences in nanotechnology and high throughput molecular selection (especially through my work with Saeeda Jaffar, Beau Peelle, and Eric Krauland). I took further steps towards the development of molecular analysis tools at Lawrence Livermore National Lab, receiving valuable guidance from Fred Milanovich, Ted Tarasow, Amy Hiddessen, Kevin Ness, Klint Rose, and Pejman Naraghi-Arani.

Of course, all of this research required substantial funding and I'm deeply indebted to the agencies that supported my work over the years. The National Defense Science & Engineering Graduate (NDSEG) Fellowship gave me the freedom to pursue my own original research. The NIH Training Grant supported me early in my Berkeley career as I found a lab and research topic. Awards from the Berkeley Center for Emerging and Neglected Disease (CEND) facilitated my research in Cape Town. The Center for Integration of Medicine & Innovative Technology (CIMIT) Prize for Primary Healthcare seeded my research in rapid and versatile molecular diagnostics. Grants from both the Defense Advanced Research Projects Agency (DARPA) and the Bill & Melinda Gates Foundation further funded my work on molecular diagnostic tool development. Finally, the National Science Foundation (NSF) East Asia and Pacific Summer Institutes (EAPSI) gave me the opportunity to conduct interdisciplinary research in Seoul.

And finally, I would like to thank the many other friends and colleagues who have made my graduate work a joy. I regret that I simply don't have enough pages to list all of you. You brought me laughter when times were tough, you joined me in adventures big and small, you nudged me forward when I needed it most, and you know exactly who you are. I am so grateful for all of the amazing people in my life. Thank you so much, everyone!

Chapter 1: Introduction to Molecular Diagnostics in Remote and Low-Resource Settings

1.1 Clinical Needs in Remote and Low-Resource Settings

1.1.1 Design Criteria for Healthcare Technology in Remote and Low-Resource Settings

Rapid and distributed diagnostics have the potential to vastly improve healthcare by reducing therapeutic costs to treat progressive diseases, limiting the waste of expensive medicines, providing tools to manage chronic illness, and inhibiting the spread of infectious disease and the associated costs to society. Many medical facilities in the United States are fortunate to have access to a variety of diagnostic technologies, including very powerful nucleic acid and protein quantification equipment. However, these tools come at a large cost, often requiring centralized laboratories and skilled technicians to achieve results that are asynchronous with doctor-patient visits. This bulky infrastructure for routine diagnostics is painfully inadequate in serving remote and low-resource (RLR) settings.

Table 1.1 Example design constraints for an adult pulmonary tuberculosis diagnostic device. Adapted from the WHO consensus meeting report on high-priority target product profiles for new tuberculosis diagnostics[1].

Constraint	Minimally Acceptable	Optimal Goal
Sensitivity	> 65%	> 98%
Specificity	> 98%	> 98%
Quantitation	Qualitative	Quantitative
Finger Prick Sample Volume	< 25 μL	< 10 μL
Sample Preparation and Processing	Limited; No precise measuring	Integrated or Not Required
Reagent Integration	1 external reagent	No external reagents
Time to Result	< 60 mins	< 20 mins
Daily Throughput	> 10 tests per 6 hours	> 25 tests per 6 hours
Power Requirements	Battery or Solar Power	None
Consumable cost	< $6	< $4
Device cost	< $500	$0
Maintenance	After 1 year or >1000 tests	None
Data Analysis	Integrated	Integrated
Operating Environment	5 – 40 °C, 70% humidity	5 – 50 °C, 90% humidity
Storage and Stability	1 year, 5 – 35 °C, 70% humidity	2 years, 5 – 40 °C, 90% humidity
Training	< 3 days for HCP	< 1 day for HCP

An ideal diagnostic solution to address the current gaps in care for RLR settings would be characterized by the World Health Organization's (WHO) "Assured" criteria[2]:

A ffordable by those at risk.
S ensitive (few false negatives).
S pecific (few false positives).
U ser-friendly (simple to perform, requiring minimal training).
R apid (enabling treatment at first visit) and **R**obust (resistant to external stresses).
E quipment-free (including ancillary power sources).
D elivered to those who need it.

These criteria can broadly be categorized as *limits on available resources* (cost, ancillary equipment/power, delivery capabilities) or *performance requirements* (sensitivity, specificity, speed, robustness). The specific values (time, concentration, etc.) for each of these criteria depend on the target application. A broad variety of use cases for clinical diagnosis occur in RLR settings, including global health, emergency response, biothreat analysis, and environmental monitoring. Each presents a unique target product profile (TPP), with limits on cost, performance, and ancillary equipment. Careful selection of these design criteria is necessary for initial technology design and development, performance evaluation, and eventual deployment[3]. A range of common design criteria is presented in Table 1.1.

1.1.2 Environments for Diagnostic Testing

A full spectrum of environments may be found in diagnostics applications, leading to a broad range of design criteria. These locations may broadly be classified as centralized labs and hospitals, remote clinics, and field settings. Although there are many defining constraints for product development, use cases may generally be classified as a function of "remoteness" and "cost". In this way, remoteness defines how far removed the testing site is from traditional infrastructure (power, trained personnel, transportation, etc.). Perhaps one of the most important constraints in diagnostic product design, cost varies dramatically according to the potential application. Whereas a rapid diagnostic test (RDT) for HIV might have to cost $0.01 per assay to be viable, a comparable medical test performed by astronauts in space has a dramatically larger budget. It is thus important to identify all of the product requirements and to optimize the diagnostic solution to meet the desired metrics without exceeding cost requirements with diminishing returns on performance.

Molecular and cellular diagnostic tools are found in a range of settings. The global clinical diagnostics market size has been estimated at ~$50 billion USD, with large commercial reference labs taking an overwhelming majority (>80%). Point-of-care tests performed in clinics or physician office labs represent ~10% market share, and at-home tests contribute to the remaining ~10%[4]. There is thus tremendous potential for expansion of the point-of-care market. Furthermore, tests performed in clinical reference labs are generally incompatible with use in many environments of interest. A listing of several example environments of interest can be found in Table 1.2.

Table 1.2 Diagnostic testing environments.

Environment	Remoteness	Resource Availability	Cost Tolerance
Doctor's office	Low	High	Medium
Remote clinic	High	Low - Medium	Low
Pharmacy	Low	High	Medium
Rural community	High	Low	Low
Emergency response	Medium	Low – Medium	Medium
Disaster response	Medium	Low – Medium	Low
Military deployment	Medium – High	Low – High	High
Forensics	Low – Medium	Medium – High	High
Expedition (space, sea, etc.)	High	Low – Medium	High
Environmental monitoring	Medium – High	Low – Medium	Medium
Food & drug analysis	Low – Medium	Medium – High	Medium
Cleanliness assurance	Low - Medium	Medium - High	Medium

In addition to clinical settings, molecular diagnostics play important roles in a wide array of applications with harsh resource constraints. The ability to rapidly diagnose infectious diseases in military personnel deployed to remote regions remains a critical unmet need. Furthermore, remote tools for detecting and specifically identifying biothreat agents will become increasingly important as rapidly advancing genetic engineering tools vastly reduce the barriers to biological weaponization[5]. Forensic analysis remains a significant burden for law enforcement, creating significant backlogs for the judicial process and potentially even leading to false trial outcomes in cases where adequate tools are unavailable. Remote diagnostic tools are also necessary as humans engage in increasingly remote expeditions of sea and space. These same kinds of tools may further prove invaluable for continuous or periodic environmental monitoring, food and drug quality control, and cleanliness assurance.

Given the tremendous diversity of applications for diagnostic tools in RLR settings, a similarly diverse set of tools is likely to emerge, addressing specific TPPs. However, a core set of enabling technologies will likely be incorporated into many of these solutions. These include automated sample preparation, miniaturized molecular quantification, and mobile data acquisition and transmission.

1.1.3 Acute and Chronic Biomarkers of Disease

Appropriate biomarkers are arguably the most critical component of an effective disease screening and management system. The selected biomarker(s) must provide a specific diagnosis of disease status relevant for clinical intervention. These biomarkers include nucleic acid, protein, and small molecule analytes from either pathogen or host systems. They may be analyzed simply for presence beyond a certain cutoff threshold, or for static or dynamic concentrations of the analyte. These threshold and classification levels are typically selected to segment patient populations into recommended therapeutic regimens.

Biomarkers must be selected to provide adequate signals for sensitive and specific diagnosis of a disease in the clinical settings, and timelines under which a patient is likely to be tested. For example, an acute infection might yield an initially high pathogen load in certain cases, followed by a drastic decline. A subsequent immune response may lead to a high antibody level. The optimal biomarker must be selected depending on the exact time of

testing relative to initial exposure, as well as the availability of biospecimens for analysis. An example plot of time-dependent biomarker level is shown in Figure 1.1.

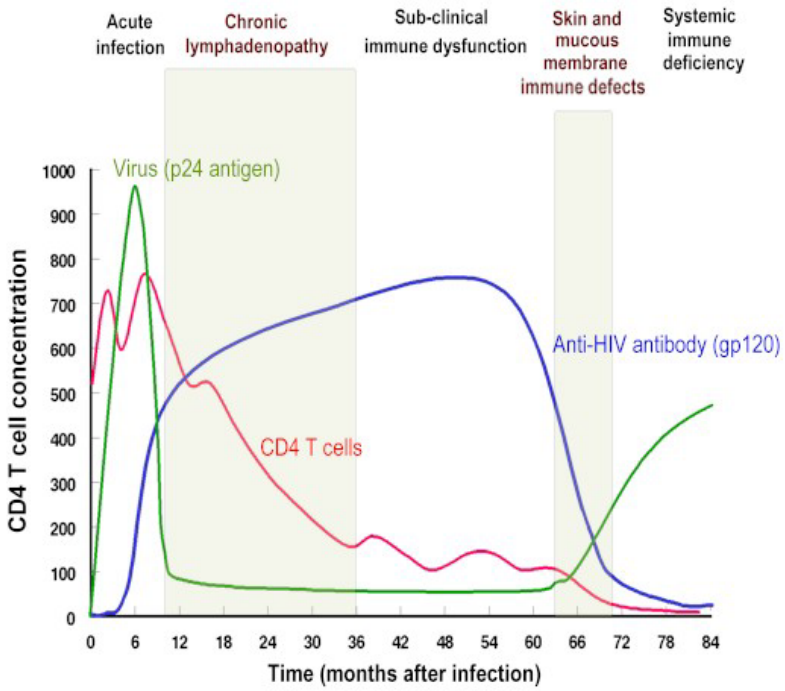

Figure 1.1 Typical biomarker level over the course of a pathogenic infection.
During the course of a viral infection with the human immunodeficiency virus (HIV), the viral load, as measured by quantification of a viral capsid protein, is initially very high (green). The patient's immune system is also intact, and thus has a large number of CD4 T cells (red). Anti-HIV antibodies are generated in acute response to the infection (blue). However, as the virus replicates, it damages host CD4 cells, leading to low white blood counts. Eventually, once the immune response has faded, the HIV viral load recovers. It is thus clear that, for a viral infection, the type of biomarker that is available in high concentrations may vary significantly as a function of time[6].

A number of biomarkers have been leveraged for acute disease screening and monitoring. These vary widely depending on the specific application. Direct detection of nucleic acid or protein from pathogens is commonly used for infectious disease detection, sometimes complemented with host response biomarkers (such as white blood cell count as a proxy for immune response). These markers are selected for their ability to identify acute conditions either through broad population surveillance or through directed analysis based on symptomatic indications.

Once a patient has already been diagnosed with a condition, chronic disease monitoring or therapeutic intervention efficacy assessment may be necessary. These types of tests present different requirements from acute detection of disease. The biomarkers involved are more likely to be direct indicators of disease state (either through pathogen levels or through host response analytes). Immunological tests are generally less relevant in chronic monitoring.

1.2 Traditional Clinical Diagnostic Methods

1.2.1 History of Medical Diagnostics

Healthcare has undergone a drastic (and generally periodic) evolution since ancient times in which medical diagnosis was governed by superstition, anecdotal opinion, and, in some cases, primitive testing[7]. These periods of diagnostic insight may be characterized as anecdotal observation, bulk humoral classification, cellular classification, and molecular analysis. The shift towards more analytical, scientifically-driven diagnosis has generally been accelerated through periodic advances in technology, enabling an unprecedented understanding of deviations from homeostasis that lead to clinical pathology.

As early as ca. 1500 BCE, the ancient Egyptian Edwin Smith Papyrus described methods for diagnosing and rationally treating traumatic injuries[8]. This text is often attributed to Imhotep (2630-2611 BC) and presents the earliest known instance of the application of scientific methods to medicine. However, this scroll was limited to 48 readily-observable indications produced through traumatic injury, and still referenced 8 magic spells. A symptomatic analysis of patients was further delineated in the Babylonian Diagnostic Handbook written by Esagil-kin-apli (1069-1046 BC), applying logical analyses of patient symptoms to obtain diagnoses. Thus, the majority of clinical diagnoses were limited to anecdotal observation, in which subjective analyses were performed, often involving superstition or intangible symptomatic evidence.

A significant shift in medicine occurred as patient samples entered the clinical diagnosis pipeline. By 300 AD, urine was promoted by Hippocrates as the most information-rich fluid available to clinicians[7]. Clinicians were advised to use their own senses to evaluate specimens for color, consistency, and even taste. This course evaluation of urine (known as "uroscopy") became commonplace, and even required practice, during the Middle Ages. However, clinicians still lacked the appropriate tools to evaluate patient specimens in a more robust and objective manner.

While the 17th and 18th centuries brought new tools for course health assessment, including measures for pulse, blood pressure, and lung function, true laboratory medicine did not emerge until the 19th century. Advances in microscopy, including the ability to culture, fix, and stain bacteria, helped give rise to the modern vision of pathogenic medicine described by Koch's postulates in 1890. Infectious diseases could be ascribed to specific microorganisms given that the following criteria were all met:

1. The microorganism is abundantly present in diseased organisms, but not found in healthy organisms.
2. The microorganism can be isolated from the diseased organism and grown in culture.
3. This purely cultured organism should cause disease when introduced into a healthy organism.
4. The microorganism must subsequently be isolated from the inoculated, diseased organism.

By the close of the 19th century, microscopy in the home or office became the primary diagnostic tool leveraged by physicians. The causative agent of disease could be accurately identified through a combination of cell culture and microscopy. Along with symptomatic

analysis, clinical cytology has continued as a primary diagnostic tool through to modern times.

Technological advances in the late 20th century instigated an ongoing shift in clinical diagnostics. While cell culture and microscopy are still considered the gold standard tools for many infectious diseases, molecular analysis has made gradual inroads due to improvements in assay sensitivity, specificity, simplicity, and speed. These technologies are far from standard, even in advanced clinical laboratories, but the many advantages offered through molecular analysis ensure they will soon be a cornerstone for healthcare.

1.2.2 Symptomatic Analysis

Despite its fairly course and subjective nature, the primary method for initial medical intervention remains patient-reported symptomatic assessment. Although this method of detection has come a long way since the early days of magic and superstition, results remain subjective and lack the resolution necessary to sufficiently classify patients for many indications.

A symptomatic analysis involves a complex and subjective integration of many inputs, including patient and family medical history, recent symptoms, vital sign measurements, and course patient observation[9]. The majority of diagnoses are made simply with this first level of patient interaction, though physician accuracy and confidence are generally increased through access to additional test results[10]. Clearly this approach places a substantial burden on hospitals, requiring highly trained personnel to assess each individual, assuming a significant risk associated with human error.

A second level analysis may rely on a clinical exclusion tree[11,12]. This strategy allows physicians to synthesize symptomatic and testing information to identify all possible indications, and subsequently exclude those that are unlikely based on patient-specific inputs. This approach adds an algorithmic nature to clinical diagnosis that may aid in producing higher quality results. However, the lack of rapid tests to provide objective information leaves doctors with few options when a decision must be made. This often leads to misdiagnosis and improper therapeutic approach, especially in RLR settings[13,14].

1.2.3 Microscopy

Developed by the early 17th century[15], microscopy offered an unprecedented view into the microscopic world of healthcare. Anasthasius Kircher first used microscopy in the diagnostic setting, identifying "worms" of *Bacillus pestis* in blood as the causative agent of the plague (though, given the magnification power of his microscope, he likely actually observed blood cells)[7,16]. Robert Hooke later coined the term "cell" in his documentation of the microscopic landscape of living tissues[17]. Antoni van Leeuwenhoek developed over 500 simple lenses for magnification, and was one of the first to document many microscopic structures in biology. Further advances in microscopy included improvements in magnification, illumination, and contrast agents[18].

Microscopy continues to play a vital role in disease diagnosis. Observations of the size, color, morphology, and growth of microorganisms enables a direct method for detecting causative pathogens. Microscopic analysis of host cells can also lead to diagnosis of disorders or secondary effects of pathogenic infection.

However, microscopic analysis requires the use of optical instruments that are costly and require extensive training. Furthermore, direct microscopic analysis of a sample is dependent on the incidence of the imaged target, making it difficult or impossible to detect low-concentration pathogens. Although contrast agents such as chromogenic dyes and fluorophores enhance sensitivity, they also add complexity and reduce overall assay robustness for RLR settings.

1.2.4 Cell Culture

First developed by Robert Koch in 1881, the culture of pure cell lines remains the primary method for clinical laboratory diagnosis of infectious disease[19]. This method involves the collection and isolation of a cellular population from a clinical specimen, followed by growth in a culture medium. Chemical agents such as antibiotics may be added to the culture medium in order to further classify specimens by chemoresistance.

There are many advantages to cell culture over other diagnostic methods, thus leading it to be the gold standard for many conditions. This approach can be very sensitive, enabling the detection of relatively few clones due to signal amplification by proliferation. Cell culture provides additional information beyond basic pathogen classification – including cell morphology, growth and proliferation rates, and chemosensitivity (of which each may advise clinical decisions in some cases). Furthermore, cell culture is relatively cheap, particularly in developing nations where labor costs are low.

However, cell culture is limited in a number of critical ways that likely mark it as a point of care testing modality of the past, to be replaced with more advanced methods. Cell culture requires significant resources, including incubators, growth media, culture vessels, sterile work environments, and trained personnel. Highly trained staff are also required to conduct culture assays and these costs directly scale with throughput requirements. Since cell culture relies on inherent cellular proliferation rates, the process can be slow, taking days to months, depending on the target cell type. Cell culture also presents a challenge for versatility in the face of emerging or rapidly evolving species. Furthermore, many cell types cannot be cultured through any known methods[20]. Cell culture also presents a fairly course level of information, particularly in cases where subtle fluctuations in molecular biomarkers are more indicative of disease state.

1.2.5 Agglutination

Agglutination generally refers to the process by which a set of particles or cells adheres into a large cluster due to a crosslinking by molecules or particles with multiple affinity domains. The specific agglutination of bacteria was first discovered by Herbert Edward Durham and Max von Gruber in 1896[21,22]. The so-called "Gruber-Durham" reaction was subsequently applied to the diagnosis of typhoid fever by Fernand Widal. In the "Widal" reaction, the serum of a typhoid-infected patient caused agglutination of the *Salmonella typhi* bacteria, while non-infected serum let to no agglutination[23,24]. This is due to the immunosensitive antibodies in the infected serum, able to bind to surface markers of the bacteria.

Agglutination has continued to be a powerful diagnostic tool for RLR settings, providing a rapid and simple means of visual target detection, requiring minimal to no external equipment. However, the agglutination assay generally lacks in sensitivity and

quantitative range compared with modern molecular diagnostic tools. Furthermore, the direct use of pathogenic cells poses cost, stability, and safety issues.

1.3 The Rise of Molecular Diagnostics

1.3.1 History of Molecular Diagnostics

The mid- to late- 19th century witnessed the rise of assays and tools for the detection and quantification of molecules in samples to aid in the diagnosis of disease. As opposed to traditional methods of symptomatic or cytologic analysis, molecular diagnostic methods have ushered in a new error of versatile, rapid, robust, and simple medical diagnosis[25]. In particular, these tools enable the detection of protein, nucleic acid, and small molecule biomarkers associated with disease. Rather than observing disease with course visual methods, molecular technologies have facilitated a new digital age in medicine.

1.3.2 Protein Detection

The workhorse of the cell, proteins have become incredibly valuable biomarkers in modern medicine[26]. Both pathogenic and host proteins may be detected in order to assess the presence and severity of a medical disorder. Furthermore, the complex analysis of multiple proteins ("proteomics")[27], as well as the temporal monitoring of protein levels has led to significant improvements in diagnosis. Protein detection has evolved from relatively course agglutination assays to highly sensitive and quantitative immunoassays leveraging a wide variety of biorecognition elements[25].

Although the Widal reaction initially only measured the agglutination of pathogenic cells in response to infected serum, the fundamental agglutination assay has been extended to a broad range of configurations, including the clustering of latex beads[26], nanoparticles[28], and cells[26]. Such assays can be extended for the detection of proteins, small molecules, and nucleic acids[29].

The development of gel electrophoresis enabled the visualization and quantification of proteins in a size-specific manner[30]. This method involves the application of an electric field gradient across a porous material such as an acrylamide gel[31], initiating a size- and charge-specific migration of macromolecules across the gel. Specific probes may be added to enable the identification of target proteins in a gel through the Western blotting process[32,33].

Immunoassays have subsequently been developed to specifically detect a broad range of biomarkers with specific antibodies. Though these assays were first performed using radioactive reporters[34], a range of reporters have been developed that include the use of catalytic[35], fluorescent[36], and nanoplasmonic[37,38] phenomena. Protein diagnostic technologies are further explored in Chapter 3.

1.3.3 Nucleic Acid Detection

The detection and sequencing of nucleic acids has brought clinical diagnosis into the digital age. Although protein levels provide an important view into cellular machinery, nucleic acid analysis enables rich interrogation of a range of sequence-specific biomarkers for chronic illness, acute infection, drug susceptibility and tolerance, and speciation.

Nucleic acid amplification by the polymerase chain reaction (PCR) provided the sensitivity needed to detect extremely low copy numbers of targets in a small volume of

solution[39]. These targets could be amplified and then quantified through a standard gel electrophoresis or through sequence-specific probe tagging in a southern blot[40]. This sequence-specific amplification of a target molecule has been further modified to obviate the need for thermocycling via isothermal techniques[41,42]. In both cases, a range of reporter mechanisms have been developed, including intercalating dyes[43,44], TaqMan probes[45], and chromatogenic or fluorescent byproducts of amplification[46]. Next-generation sequencing techniques have been developed for use in laboratory settings, and have yet to reach a configuration compatible with RLR setting deployment[47,48]. Integrated methods for rapid and simple nucleic acid testing hold great promise for many diagnostic applications in RLR settings[49]. Nucleic acid diagnostic technologies are further explored in Chapter 2.

1.4 Adapting Molecular Diagnostics for the Point of Need

1.4.1 Overview of Diagnostic Design for RLR Settings

Based on the specific design constraints presented by a clinical need, a targeted assay can be developed. Biomarkers should be carefully selected for specificity to the target, as well as compatibility with reasonable bioassays. The biomarker selection process is closely coupled with the target sample matrix. Blood, saliva, urine, tears, nasal swabs, and sweat all provide varying biomarker profiles and sample preparation requirements. Based on the sample matrix, target biomarker type, and other assay constraints, a device substrate must be selected. Some common substrates include porous media such as paper, standard assay tubes, and microfluidic systems. Given a device configuration, an appropriate assay may be implemented, consisting of sample processing, signal transduction, and readout modules. As a whole, the integration of these components leads to advanced systems capable of meeting the needs of RLR settings.

1.4.2 Sample Matrices

A variety of matrices have been analyzed for use as samples in diagnostic assays for RLR settings, including urine, tears, saliva, sputum, nasopharyngeal swabs, and blood. These sample matrices have a range of advantages and disadvantages relating to assay invasiveness, sample availability, biomarker diversity, and mechanical homogeneity.

Urine has long been a fixture in medical diagnosis[7]. A range of conditions may be diagnosed through urinalysis, including metabolic disorders, urinary tract infections, liver and kidney disorders, and sexually-transmitted infections[50]. Urine samples are also generally available in large volumes, except in the case of some medical conditions. However, urine has a lower number and concentration of clinically-relevant protein and nucleic acid biomarkers than blood[51,52], and frequently requires large volumes in order to achieve reasonable sensitivity.

Tears have also become a target for non-invasive diagnosis. Tear fluid exhibits a complex chemical composition that lends itself to a range of assays[53,54]. However, tear fluid has yet to be extensively analyzed for broad use in diagnostic settings beyond certain ocular disorders. Furthermore, tear fluid is generally only available in small volumes, or completely unavailable in patients with certain disorders, such as dry eye syndrome.

Saliva holds promise as a non-invasive matrix with a proteomic makeup comparable to that of blood[55–58]. Saliva samples are generally available in sufficient volumes with minimal patient discomfort. However, saliva exhibits a wide variability in fluidic properties across patients[59,60] and, perhaps more problematically, in response to disease state.

Furthermore, salivary protein levels are generally lower than those found in blood, thus requiring higher sensitivity assays for comparable performance.

Sputum samples are composed of mucus produced by coughing and oral emission from the lower respiratory tract. These samples provide valuable insights into infectious agents present in the respiratory system, especially in the case of tuberculosis. However, sputum samples can be hard to produce in some patients, and have a wide spectrum of fluidic properties that make sample preparation complex. Furthermore, their use is generally limited to diagnosis of respiratory infections.

Nasopharyngeal swabs are commonly used for the detection of a range of microbial pathogens, most commonly in respiratory infections. These samples generally provide very sensitive signals in cell culture or other biomarker amplification assays[61,62]. However, nasopharyngeal swabs require a level of training and patient discomfort that likely precludes their broad use in RLR settings.

Blood has been the workhorse sample matrix for general diagnostic testing. Blood contains a diverse mixture of cells, proteins, nucleic acids, and small molecules. These biomarkers have been adapted into a broad range of blood tests in laboratory settings. However, blood tests generally require an invasive phlebotomy procedure, as well as trained personnel. Alternative assays have been developed to utilize the small volumes of blood available from fingerprick samples[25]. Blood glucose tests are by far the leading example of finger stick assays[63], though a range of new tests are being developed for use in RLR settings[25].

1.4.3 Assay Containers and Substrates

The substrate upon which an assay is incorporated has a significant impact on the overall versatility and performance in RLR settings. Many substrates have been developed for use in RLR settings, including reaction tubes, porous substrates (such as paper), and microfluidic systems. Though the two former methods offer a level of simplicity, microfluidic systems enable a broader range of assay modalities while sample and reagent volumes used.

A number of assays have been developed in a "single-tube" format that enables the addition of a sample and possibly other reagents to a tube for analysis. In particular, these systems have been developed for laboratory use in many nucleic acid amplification assays. Some groups have extended these assays for use in RLR settings, though they generally require larger sample and reagent volumes than paper or microfluidic systems. Tube assays also generally require one or more manual sample processing steps, and lack integrated automation without external equipment that is often incompatible with use in RLR settings.

Paper systems have been implemented extensively for lateral flow assays[64]. These substrates enable passive loading of samples and high surface area exposure to dried reagents. Paper substrates offer simple operation that is compatible with both manual and automated signal readout. However, paper diagnostic tests often lack sensitivity compared with tube-based or microfluidic assays. Furthermore, the simple mechanism of sample wicking has proven incompatible with a number of modalities. Though some groups are developing novel means to replicate microfluidic functions in paper substrates[65–67], a number of hurdles still remain before complex assays become generally available.

The Lab on a Chip (LOC) approach seeks to miniaturize biological assays that would normally require large amounts of reagents and excessive reaction time scales when

performed in traditional bench top apparatuses. Initial LOC approaches have leveraged the remarkable success of microfabrication techniques developed for the silicon chip industry to make high-precision microfluidic devices in a way that has proven to be both reproducible and scalable[68–70]. Recent efforts have focused on developing more affordable LOC platforms that are based on inexpensive substrates, such as plastics[71].

Modular LOC devices are specifically well suited to meet the diagnostic needs of underserved populations living in remote and resource-poor settings[72,73]. Cheap, rapid, and versatile diagnostics can be produced by leveraging the unique properties of microfluidic systems[69,73]. The dramatically reduced length scales lead to highly efficient diffusion-drive heat and mass transfer that can vastly accelerate standard assays as compared with bench top counterparts. Microfluidic systems operate with very low Reynolds flow regimes, leading to highly controlled laminar streams that can readily be manipulated using simple viscous forces. Furthermore, microfluidic devices lend themselves to simple scaling into vast arrays of multiplexed reactions.

1.4.4 Fluidic Actuation

The mechanism of fluidic actuation is often the most important consideration in the design of novel microfluidic systems. A range of active and passive fluid pumping and control techniques have been described in the context of microfluidics over the past several decades. A number of these methods have been incorporated into devices specifically designed for disease diagnostics in remote and resource-limited settings. Although the most common fluidic actuation mechanism found in point of care platforms has traditionally been surface tension (i.e. lateral flow assays), a number of other mechanisms have been investigated. Active fluidic actuation mechanisms require an external source of energy to drive fluid flow at the point of care, whereas passive mechanisms frequently leverage ubiquitous physical phenomena such as surface tension and gravity.

Pressure-driven (or pneumatic) pumps are commonly used in microfluidic systems in a laboratory setting. These pumps may either rely on a syringe to drive flow at an inlet, or vacuum pressure to drive flow at the outlet, leading to Poiseuille flow[74]. Peristaltic pumps have also been developed to provide periodic translational pressure in either a valved[75] or rotary system[76,77]. Pressure-drive flow using syringe pumps offers a consistent means of loading samples in a very controlled manner. As the workhorse tool for microfluidics labs, it is the most commonly used and most well-characterized method for loading samples. However, traditional syringe pumps are prohibitively large, expensive, and power-dependent for use in most point of care settings. Most standard syringe pump setups further require relatively large sample volumes due to “dead space” inherent in the system. Furthermore, these systems frequently present issues with bubble generation, either on-chip or in the off-chip interconnects, which often compromise the assay[78].

Several groups have attempted to integrate pressure-driven flow on chips by manually[79] and electronically[80] triggered application of pressure. The manual controls include simple, hand-activated mechanisms such as screws[81–83] and buttons[84]. Although these methods require active actuation by the user, they may eventually be designed in such a simple way as to reduce or waive the need for advanced training prior to use, making these approaches particular attractive for point of care diagnostic. Further efforts have aimed to automate this mechanical pumping with magnetic[83] and piezoelectric[85] actuators in order to

reduce user error and simplify use. Additionally, several groups have proposed methods for on-chip peristaltic sample loading[76,86]. However, a practical on-chip pressure-driven loading mechanism has yet to be seen in commercial miniaturized point-of-care systems.

Centrifugal force has been implemented for use in compact disc (CD) assay formats, often referred to as a "lab on a CD"[87]. Fluid flow has been well-characterized in CD platforms as a function of channel geometry, fluid properties, and rotation rate[88,89]. Lab on a CD platforms generate flow with properties similar to pneumatic systems, but with some unique applications for sample automated sample processing such as centrifugal separation. CD platforms have been incorporated into some commercial products[87]. However, they require external power and equipment, and a more complex system design than standard microfluidic devices. They thus have yet to reach significant reach in RLR settings.

Electrokinetic actuation leverages electric fields to induce sample migration[90]. Examples of electrokinetic actuation include electrophoretic flow[91–93], electroosmotic flow[94], and dielectrophoretic flow[95,96]. Electrophoretic and electroosmotic flow generally rely on the application of an electric field axially along a fluidic channel, forcing ions to move in a charge-specific direction and yielding bulk flow through frictional forces. While electrophoretic flow relies on ions distributed throughout the bulk of the solution to generate flow, electroosmotic flow only impacts ions in the electric double layer generated at the channel wall. Electrophoretic flow is also used to selectively move charged species in a sample, such as nucleic acids or proteins[97]. Dielectrophoretic flow generates a charge distribution on the surface of a particle with dielectric properties that vary from the bulk solution, leading to a flow towards increasing field density in an electromagnetic field gradient. This method is frequently used for particle separation and preconcentration, though it has also been applied to bulk fluid actuation through frictional forces of moving particles or ions[98].

Electrokinetic actuation mechanisms are attractive due to their lack of moving parts, as well as their well-characterized and sensitive control of flow rates. They can also generally be incorporated into integrated circuit (IC) platforms, enabling companies to leverage the well-established chip manufacturing industry. However, electrokinetic systems require a power supply for actuation, frequently on the order of tens to hundreds of volts[99]. Furthermore, these mechanisms may unintentionally heat[90], lyse, or hydrolyze samples. The kinetics are also highly dependent on the ionic makeup of the medium being introduced, which can vary drastically across different sample types or even across different patients. As opposed to mechanical and acoustic flow regimes, electrokinetic flows generally experience far less sample mixing – which may be desired for diagnostic applications. Finally, these mechanisms generally operate in a continuous-flow manner, which may not be compatible with desired on-chip reaction conditions.

Surface acoustic wave (SAW) technology has also been implemented for fluidic actuation in microfluidic systems[100–102]. SAW devices leverage interdigitated piezoelectric transducers that generate mechanical waves based on the electrode geometry and matrix properties. Like electrokinetic actuation, these transducers lack moving parts and have well-characterized flow rates. They are also compatible with IC platforms. However, SAW actuators also require power for actuation and have a dependency on the sample matrix properties. Unlike electrokinetic actuation, SAW is not as dependent on solution and particle charges for actuation.

Capillary action is the most commonly used form of passive fluid actuation in molecular diagnostic applications[103,104]. Often implemented in lateral flow assays, capillary action depends on the surface tension at the wall-fluid-air interface. Capillary action is particularly attractive as it provides simple and robust actuation without the need for any external power supply. Furthermore, substrates for capillary action are generally inexpensive to fabricate (including paper substrates found in lateral flow systems). However, capillary action has significant dependence on the properties of the sample matrix and substrate material. Capillary action also has thus far only been used in a limited number of assay configurations as compared with microfluidic systems.

Gravity-driven flow functions in a way similar to pressure-driven flow, but with gravitational force on the mass of the sample at an inlet driving a passive loading of the microfluidic chip[104,105]. Gravity-driven flow offers advantages and disadvantages similar to those of pressure driven flow, with the primary difference being that gravity-driven flow does not require an external power source, but also lacks some of the tunable control found in pressure-driven flow. With uncontrolled-flow rates that are highly dependent on sample volume and loading, along with potential issues with bubbles, gravity-driven flow has yet to find a significant foothold in the diagnostics world.

Degas-driven flow is a recently developed fluid actuation mechanism that relies on the degassing of a porous substrate material prior to use, such that the introduction of a sample to an inlet on a closed channel causes gas flux from the channels into the channel walls[106,107]. This flux creates a net lower pressure inside the channels, leading to a pressure gradient between the atmospheric-facing end of the liquid sample and the channel-facing end. A flow regime similar to pressure- and gravity-driven flow is thus observed. However, as gas directly transfers from the channels into the walls, degas-driven flow does not suffer from any issues with bubbles, and is fully compatible with loading dead-end channels. This mechanism is attractive for applications in RLR settings as it retains the low overhead of passive actuation systems while offering much of the functionality found in traditional pressure-driven microfluidic systems. Degas-driven flow is further explored in Chapter 2.

1.5 Discussion

The development of any tool for use in RLR settings will be directly guided by the specific target product profile, usage environment, and diagnostic objective. Through defining these criteria, an optimized solution can be developed that leverages optimal molecular diagnostic assay mechanisms in appropriate control systems. In particular, nucleic acid and protein detection mechanisms are attractive for many diagnostic applications. Blood and saliva are also generally attractive sample matrices for diagnosis, though the optimal matrix depends on the availability of target biomarkers and compatibility with analytical systems. The system substrate and fluidic actuation are also critical components of any diagnostic system. In particular, degas-driven flow in microfluidic systems offers a number of advantages for use in RLR settings.

With these design rules in mind, we have developed several systems for nucleic acid and protein detection in RLR settings. These systems combine multiple biochemical mechanisms into microfluidic systems that yield the performance prescribed by analysis in RLR settings. In Chapter 2, we present a microfluidic biomolecular amplification (μBAR) reader combined with isothermal amplification and degas-driven flow to yield an integrated

nucleic acid analysis device. In Chapter 3, we present an aptamer-mediated probe (AMProbe) for protein recognition that is coupled with both nanoplasmonic and isothermal amplification readout mechanisms downstream. In Chapter 4, we present an improved method of driving and analyzing the polymerase chain reaction through photothermal nanoplasmonic PCR (nanoPCR) that drastically reduces infrastructure needs for robust nucleic acid testing in RLR settings. As these assays and tools continue to evolve, we anticipate a vast array of possibilities to open, leading to improved quality and access to healthcare for the global population.

1.6 References

1. Denkinger, C., Kik, S. & Casenghi, M. High-priority target product profiles for new tuberculosis diagnostics. in *Consensus Meeting on high-priority target product profiles for new tuberculosis diagnostics* (World Health Organization, 2014). at <http://www.who.int/tb/publications/tpp_report/en/>
2. Mabey, D., Peeling, R. W., Ustianowski, A. & Perkins, M. D. Tropical infectious diseases: Diagnostics for the developing world. *Nat Rev Micro* **2,** 231–240 (2004).
3. Banoo, S. *et al.* Evaluation of diagnostic tests for infectious diseases: general principles. *Nat Rev Micro* S16–S18 (2008). at <http://www.nature.com/nrmicro/journal/v6/n11_supp/abs/nrmicro1523.html>
4. Budel. *Molecular Dx Report: Market Size, Segmentation, Growth and Opportunities (5th edition)*. (2013). at <http://decibio.com/MDx>
5. Dougherty, G. M., Clague, D. S. & Miles, R. R. Field-capable biodetection devices for homeland security missions. *Proc. SPIE* **6540,** 654016–654016–10 (2007).
6. Microbiology and Immunology Online. *University of Southern Carolina School of Medicine* (2015). at <http://microbiologybook.org/>
7. Berger, D. A brief history of medical diagnosis and the birth of the clinical laboratory. *Med. Lab. Obs.* **3,** 28–30, 34–40 (1999).
8. Feldman, R. P. & Goodrich, J. T. The Edwin Smith Surgical Papyrus. *Child's Nerv. Syst.* **15,** 281–284 (1999).
9. Kienle, G. S. & Kiene, H. Clinical judgement and the medical profession. *J. Eval. Clin. Pract.* **17,** 621–7 (2011).
10. Bossuyt, P. M. M., Reitsma, J. B., Linnet, K. & Moons, K. G. M. Beyond diagnostic accuracy: the clinical utility of diagnostic tests. *Clin. Chem.* **58,** 1636–43 (2012).
11. Van der Velde, G. Clinical decision analysis: an alternate, rigorous approach to making clinical decisions and developing treatment recommendations. *J. Can. Chiropr. Assoc.* **49,** 258–63 (2005).
12. Bae, J.-M. The clinical decision analysis using decision tree. *Epidemiol. Health* **36,** e2014025 (2014).
13. Garrouste-Orgeas, M. *et al.* Overview of medical errors and adverse events. *Ann. Intensive Care* **2,** 2 (2012).
14. Singh, H. & Sittig, D. F. Advancing the science of measurement of diagnostic errors in healthcare: the Safer Dx framework. *BMJ Qual. Saf.* **24,** 103–10 (2015).
15. Van Helden, A., Dupré, S. & van Gent, R. *The Origins of the Telescope*. (Amsterdam University Press, 2010). at <https://books.google.com/books?id=XguxYlYd-9EC&pgis=1>

16. Kircher, A. & Lange, C. *Scrutinium physico-medicum contagiosae Luis seu pestis*. (1659). at <https://books.google.com/books/about/Scrutinium_physico_medicum_contagiosae_L.html?id=5Ig_AAAAcAAJ&pgis=1>
17. Hooke, R. *Micrographia, or some physiological descriptions of minute bodies made by magnifying glasses with observations and inquiries thereupon*. *Micrographia, or some physiological descriptions of minute bodies made by magnifying glasses with observations and inquiries thereupon* (Dover Publications, Inc., New York, 1665). at <http://apps.webofknowledge.com/full_record.do?product=UA&search_mode=GeneralSearch&qid=5&SID=3DNtuiYjZv1JsnXLbDY&page=1&doc=1>
18. Wollman, A. J. M., Nudd, R., Hedlund, E. G. & Leake, M. C. From Animaculum to single molecules: 300 years of the light microscope. *Open Biol.* **5,** 150019 (2015).
19. Koch, R. *Zur Untersuchung von pathogenen Organismen*. *Messages from the Imperial Health Office* **1,** (Robert Koch-Institut, 1881).
20. Dong, J., Olano, J. P., McBride, J. W. & Walker, D. H. Emerging Pathogens: Challenges and Successes of Molecular Diagnostics. *J Mol Diagn* **10,** 185–197 (2008).
21. Durham, H. E. On a Special Action of the Serum of Highly Immunised Animals, and Its Use for Diagnostic and other Purposes. *Proc. R. Soc. London* **59,** 224–226 (1896).
22. Gruber, M. von & Durham, H. E. Eine neue Methode zur raschen Erkennung des Choleravibrio und des Typhusbacillus. *Münchener Med. Wochenschrift* **43,** 285–286 (1896).
23. Widal, F. Sérodiagnostic de la fièvre typhoide. *Bull. Mem. Soc. Med. Hop. Paris* (1896).
24. Widal, F. & Sicard, A. Étude sur le sérodiagnostic et sur la réaction agglutinante chez les typhiques. *Ann. l'Institut Pasteur* **11,** 353–432 (1897).
25. Song, Y. *et al.* Point-of-care technologies for molecular diagnostics using a drop of blood. *Trends Biotechnol.* **32,** 132–9 (2014).
26. Warsinke, A. Point-of-care testing of proteins. *Anal. Bioanal. Chem.* **393,** 1393–1405 (2009).
27. Adkins, J. N. *et al.* Toward a human blood serum proteome: analysis by multidimensional separation coupled with mass spectrometry. *Mol. Cell. Proteomics* **1,** 947–55 (2002).
28. Costanzo, P. J., Patten, T. E. & Seery, T. A. P. Nanoparticle agglutination: acceleration of aggregation rates and broadening of the analyte concentration range using mixtures of various-sized nanoparticles. *Langmuir* **22,** 2788–94 (2006).
29. Vollenhofer-Schrumpf, S., Buresch, R. & Schinkinger, M. A simple nucleic acid hybridization/latex agglutination assay for the rapid detection of polymerase chain reaction amplicons. *J. Microbiol. Methods* **68,** 568–76 (2007).
30. Tiselius, A. A new apparatus for electrophoretic analysis of colloidal mixtures. *Trans. Faraday Soc.* **33,** 524 (1937).
31. RAYMOND, S. & WEINTRAUB, L. Acrylamide Gel as a Supporting Medium for Zone Electrophoresis. *Science (80-.).* **130,** 711–711 (1959).
32. Towbin, H., Staehelin, T. & Gordon, J. Electrophoretic transfer of proteins from polyacrylamide gels to nitrocellulose sheets: procedure and some applications. *Proc. Natl. Acad. Sci. U. S. A.* **76,** 4350–4354 (1979).
33. Burnette, W. N. 'Western Blotting': Electrophoretic transfer of proteins from sodium dodecyl sulfate-polyacrylamide gels to unmodified nitrocellulose and radiographic

detection with antibody and radioiodinated protein A. *Anal. Biochem.* **112,** 195–203 (1981).
34. Berson, B. S. A. & Yalow, R. S. Quantitative aspects of the reaction between insulin and insulin-binding antibody. 1996–2016 (1959).
35. Engvall, E. & Perlmann, P. Enzyme-linked immunosorbent assay (ELISA) quantitative assay of immunoglobulin G. *Immunochemistry* **8,** 871–874 (1971).
36. Patsenker, L. *et al.* Fluorescent probes and labels for biomedical applications. *Ann. N. Y. Acad. Sci.* **1130,** 179–87 (2008).
37. Baptista, P. *et al.* Gold nanoparticles for the development of clinical diagnosis methods. *Anal. Bioanal. Chem.* **391,** 943–950 (2008).
38. Huser, T. Nano-Biophotonics: new tools for chemical nano-analytics. *Curr. Opin. Chem. Biol.* **12,** 497–504 (2008).
39. Saiki, R. *et al.* Enzymatic amplification of beta-globin genomic sequences and restriction site analysis for diagnosis of sickle cell anemia. *Science (80-.).* **230,** 1350–1354 (1985).
40. Southern, E. M. Detection of specific sequences among DNA fragments separated by gel electrophoresis. *J. Mol. Biol.* **98,** 503–17 (1975).
41. Kim, J. & Easley, C. J. Isothermal DNA amplification in bioanalysis: strategies and applications. *Bioanalysis* **3,** 227–39 (2011).
42. Craw, P. & Balachandran, W. Isothermal Nucleic Acid Amplification Technologies for Point-of-Care Diagnostics: A Critical Review. *Lab Chip* doi:10.1039/c0xx00000x
43. LERMAN, L. S. Structural considerations in the interaction of DNA and acridines. *J. Mol. Biol.* **3,** 18–30 (1961).
44. Bahrami, A. R. *et al.* Use of fluorescent DNA-intercalating dyes in the analysis of DNA via ion-pair reversed-phase denaturing high-performance liquid chromatography. *Anal. Biochem.* **309,** 248–52 (2002).
45. Holland, P. M., Abramson, R. D., Watson, R. & Gelfand, D. H. Detection of specific polymerase chain reaction product by utilizing the 5'----3' exonuclease activity of Thermus aquaticus DNA polymerase. *Proc. Natl. Acad. Sci. U. S. A.* **88,** 7276–80 (1991).
46. Fischbach, J., Xander, N. C., Frohme, M. & Glökler, J. F. Shining a light on LAMP assays - A Comparison of LAMP Visualization Methods Including the Novel Use of Berberine. *Biotechniques* **58,** 189–194 (2015).
47. Biesecker, L. G., Burke, W., Kohane, I., Plon, S. E. & Zimmern, R. Next-generation sequencing in the clinic: are we ready? *Nat. Rev. Genet.* **13,** 818–24 (2012).
48. Van Dijk, E. L., Auger, H., Jaszczyszyn, Y. & Thermes, C. Ten years of next-generation sequencing technology. *Trends Genet.* **30,** 418–26 (2014).
49. Ahmad, F. & Hashsham, S. a. Miniaturized nucleic acid amplification systems for rapid and point-of-care diagnostics: a review. *Anal. Chim. Acta* **733,** 1–15 (2012).
50. Understanding urine tests. (2013). at <http://www.ncbi.nlm.nih.gov/books/PMH0072534/>
51. Adachi, J., Kumar, C., Zhang, Y., Olsen, J. V & Mann, M. The human urinary proteome contains more than 1500 proteins, including a large proportion of membrane proteins. *Genome Biol.* **7,** R80 (2006).
52. Marimuthu, A. *et al.* A comprehensive map of the human urinary proteome. *J. Proteome Res.* **10,** 2734–43 (2011).

53. Shamsi, F. A. *et al.* Analysis and comparison of proteomic profiles of tear fluid from human, cow, sheep, and camel eyes. *Invest. Ophthalmol. Vis. Sci.* **52,** 9156–65 (2011).
54. Zhou, L. *et al.* In-depth analysis of the human tear proteome. *J. Proteomics* **75,** 3877–85 (2012).
55. Loo, J. A., Yan, W., Ramachandran, P. & Wong, D. T. Comparative human salivary and plasma proteomes. *J. Dent. Res.* **89,** 1016–23 (2010).
56. Hu, S., Loo, J. A. & Wong, D. T. Human body fluid proteome analysis. *Proteomics* **6,** 6326–53 (2006).
57. Yan, W. *et al.* Systematic comparison of the human saliva and plasma proteomes. *Proteomics. Clin. Appl.* **3,** 116–134 (2009).
58. Rahim, M. A. A., Rahim, Z. H. A., Ahmad, W. A. W. & Hashim, O. H. Can Saliva Proteins Be Used to Predict the Onset of Acute Myocardial Infarction among High-Risk Patients? *Int. J. Med. Sci.* **12,** 329–335 (2015).
59. Rantonen, P. J. & Meurman, J. H. Viscosity of whole saliva. *Acta Odontol. Scand.* **56,** 210–4 (1998).
60. Stokes, J. R. & Davies, G. A. Viscoelasticity of human whole saliva collected after acid and mechanical stimulation. *Biorheology* **44,** 141–60 (2007).
61. Irving, S. A., Vandermause, M. F., Shay, D. K. & Belongia, E. A. Comparison of nasal and nasopharyngeal swabs for influenza detection in adults. *Clin. Med. Res.* **10,** 215–8 (2012).
62. Cho, M.-C. *et al.* Comparison of sputum and nasopharyngeal swab specimens for molecular diagnosis of Mycoplasma pneumoniae, Chlamydophila pneumoniae, and Legionella pneumophila. *Ann. Lab. Med.* **32,** 133–8 (2012).
63. Newman, J. D. & Turner, A. P. F. Home blood glucose biosensors: a commercial perspective. *Biosens. Bioelectron.* **20,** 2435–53 (2005).
64. Posthuma-Trumpie, G., Korf, J. & van Amerongen, A. Lateral flow (immuno)assay: its strengths, weaknesses, opportunities and threats. A literature survey. *Anal. Bioanal. Chem.* **393,** 569–582 (2009).
65. Connelly, J. T., Rolland, J. P. & Whitesides, G. M. A 'Paper Machine' for Molecular Diagnostics. *Anal. Chem.* **87,** 7595–601 (2015).
66. Carrilho, E., Martinez, A. W. & Whitesides, G. M. Understanding Wax Printing: A Simple Micropatterning Process for Paper-Based Microfluidics. *Anal. Chem.* **81,** 7091–7095 (2009).
67. Yetisen, A. K., Akram, M. S. & Lowe, C. R. Paper-based microfluidic point-of-care diagnostic devices. *Lab Chip* **13,** 2210–51 (2013).
68. Yeo, L. Y., Chang, H.-C., Chan, P. P. Y. & Friend, J. R. Microfluidic devices for bioapplications. *Small* **7,** 12–48 (2011).
69. Hansen, C. & Quake, S. R. Microfluidics in structural biology: smaller, faster... better. *Curr. Opin. Struct. Biol.* **13,** 538–544 (2003).
70. Yager, P. *et al.* Microfluidic diagnostic technologies for global public health. *Nature* **442,** 412–418 (2006).
71. Yager, P., Domingo, G. J. & Gerdes, J. Point-of-Care Diagnostics for Global Health. *Annu. Rev. Biomed. Eng.* (2008). doi:10.1146/annurev.bioeng.10.061807.160524
72. Sia, S. K., Linder, V. & Chin, C. D. Lab-on-a-chip devices for global health: Past studies and future opportunities. *Lab Chip* **7,** 41–57 (2007).

73. Pennathur, S. How to exploit the features of microfluidics technology. *Lab Chip* **8,** 20–22 (2008).
74. Kirby, B. J. *Micro- and Nanoscale Fluid Mechanics: Transport in Microfluidic Devices*. (Cambridge University Press, 2010). at <http://books.google.com/books?id=y7PB9f5zmU4C&pgis=1>
75. Unger, M. a. Monolithic Microfabricated Valves and Pumps by Multilayer Soft Lithography. *Science (80-.).* **288,** 113–116 (2000).
76. Darby, S. G. *et al.* A metering rotary nanopump for microfluidic systems. *Lab Chip* **10,** 3218–26 (2010).
77. Chou, H., Unger, M. A. & Stephen, R. A Microfabricated Rotary Pump. *Biomed. Microdevices* **3,** 323–330 (2001).
78. Zheng, W., Wang, Z., Zhang, W. & Jiang, X. A simple PDMS-based microfluidic channel design that removes bubbles for long-term on-chip culture of mammalian cells. *Lab Chip* **10,** 2906–10 (2010).
79. Weng, K.-Y., Chou, N.-J. & Cheng, J.-W. Triggering vacuum capillaries for pneumatic pumping and metering liquids in point-of-care immunoassays. *Lab Chip* **8,** 1216–9 (2008).
80. Hong, C., Tsai, C., Chen, S. & Chen, C. Disposable microfluidic vacuum modules using inductively-triggered transformative polymers for point-of-care diagnostics. *Transducers* 1472–1475 (2011).
81. Weibel, D. B., Siegel, A. C., Lee, A., George, A. H. & Whitesides, G. M. Pumping fluids in microfluidic systems using the elastic deformation of poly(dimethylsiloxane). *Lab Chip* **7,** 1832–6 (2007).
82. Zheng, Y., Dai, W. & Wu, H. A screw-actuated pneumatic valve for portable, disposable microfluidics. *Lab Chip* **9,** 469–72 (2009).
83. Hulme, S. E., Shevkoplyas, S. S. & Whitesides, G. M. Incorporation of prefabricated screw, pneumatic, and solenoid valves into microfluidic devices. *Lab Chip* **9,** 79–86 (2009).
84. Moorthy, J. *et al.* Microfluidic tectonics platform: A colorimetric, disposable botulinum toxin enzyme-linked immunosorbent assay system. *Electrophoresis* **25,** 1705–13 (2004).
85. Laser, D. J. & Santiago, J. G. A review of micropumps. *J. Micromechanics Microengineering* **14,** R35–R64 (2004).
86. Yokokawa, R., Saika, T., Nakayama, T., Fujita, H. & Konishi, S. On-chip syringe pumps for picoliter-scale liquid manipulation. *Lab Chip* **6,** 1062–6 (2006).
87. Madou, M. *et al.* Lab on a CD. *Annu. Rev. Biomed. Eng.* **8,** 601–628 (2006).
88. Madou, M. J. LabCD: a centrifuge-based microfluidic platform for diagnostics. in *Proc. SPIE* **3259,** 80–93 (SPIE, 1998).
89. Duffy, D. C., Gillis, H. L., Lin, J., Sheppard, N. F. & Kellogg, G. J. Microfabricated Centrifugal Microfluidic Systems : Characterization and Multiple Enzymatic Assays. *Anal. Chem.* **71,** 4669–4678 (1999).
90. Wong, P. K., Wang, T.-H., Deval, J. H. & Ho, C.-M. Electrokinetics in Micro Devices for Biotechnology Applications. *IEEE/ASME Trans. Mechatronics* **9,** 366–376 (2004).
91. Bruin, G. J. Recent developments in electrokinetically driven analysis on microfabricated devices. *Electrophoresis* **21,** 3931–51 (2000).

92. Ermakov, S., Jacobson, S. & Ramsey, J. Computer simulations of electrokinetic injection techniques in microfluidic devices. *Anal. Chem.* **72,** 3512–7 (2000).
93. Bousse, L. *et al.* Electrokinetically controlled microfluidic analysis systems. *Channels* **29,** 155–181 (2000).
94. Schasfoort, R. B. Field-Effect Flow Control for Microfabricated Fluidic Networks. *Science (80-.).* **286,** 942–945 (1999).
95. Cummings, E. B. Streaming dielectrophoresis for continuous-flow microfluidic devices. *IEEE Eng. Med. Biol. Mag.* **22,** 75–84 (2003).
96. Chang, S. & Cho, Y.-H. A continuous size-dependent particle separator using a negative dielectrophoretic virtual pillar array. *Lab Chip* (2008). doi:10.1039/b806614k
97. Salieb-Beugelaar, G. B., Dorfman, K. D., van den Berg, A. & Eijkel, J. C. T. Electrophoretic separation of DNA in gels and nanostructures. *Lab Chip* (2009). doi:10.1039/b905448k
98. Brown, a., Smith, C. & Rennie, a. Pumping of water with ac electric fields applied to asymmetric pairs of microelectrodes. *Phys. Rev. E* **63,** 1–8 (2000).
99. Luo, J. K. *et al.* Moving-part-free microfluidic systems for lab-on-a-chip. *J. Micromechanics Microengineering* **19,** 54001 (2009).
100. Haeberle, S. & Zengerle, R. Microfluidic platforms for lab-on-a-chip applications. *Lab Chip* **7,** 1094–110 (2007).
101. Yeo, L. Y. & Friend, J. R. Ultrafast microfluidics using surface acoustic waves. *Biomicrofluidics* **3,** 12002 (2009).
102. Girardo, S., Cecchini, M., Beltram, F., Cingolani, R. & Pisignano, D. {Polydimethylsiloxane–LiNbO3} surface acoustic wave micropump devices for fluid control into microchannels. *Lab Chip* **8,** 1557 (2008).
103. Kornev, K. G., Callegari, G. & Neimark, A. V. CAPILLARY MICROFLUIDICS FOR VISCOELASTIC FLUIDS Gerardo Callegari , and Alexander V . Neimark. *Interface* 15–16 (2004).
104. Jong, W. R., Kuo, T. H., Ho, S. W., Chiu, H. H. & Peng, S. H. Flows in rectangular microchannels driven by capillary force and gravity. *Int. Commun. Heat Mass Transf.* **34,** 186–196 (2007).
105. Laschi, S. *et al.* A new gravity-driven microfluidic-based electrochemical assay coupled to magnetic beads for nucleic acid detection. *Electrophoresis* **31,** 3727–3736 (2010).
106. Hosokawa, K., Sato, K., Ichikawa, N. & Maeda, M. Power-free poly(dimethylsiloxane) microfluidic devices for gold nanoparticle-based DNA analysis. *Lab Chip* **4,** 181–185 (2004).
107. Liang, D. Y., Tentori, A. M., Dimov, I. K. & Lee, L. P. Systematic characterization of degas-driven flow for poly(dimethylsiloxane) microfluidic devices. *Biomicrofluidics* **5,** 24108 (2011).

Chapter 2: Nucleic Acid Detection with a Microfluidic Biomolecular Amplification Reader

2.1 Introduction

2.1.1 Nucleic Acid Detection and Quantification in Remote and Low-Resource Settings

Clinical diagnostics have undergone a dramatic shift over the last 40 years, with rapid molecular analysis technologies systematically enhancing and replacing traditional phenotypic observation methods[1–5]. Initial efforts in molecular diagnostics focused on detecting nucleic acids and proteins isolated from bulk tissue samples. Cell culture enabled direct observation of phenotypic traits while simultaneously increasing the quantity of genetic and proteomic biomarkers through cellular proliferation. These biomarkers could then be analyzed through standard laboratory techniques including microscopy, gel electrophoresis, and spectroscopy.

However, cell culture suffers from a number of limitations that make it suboptimal or even prohibitive for use in clinical diagnostic settings, particular those in remote or low resource (RLR) settings. Cell proliferation rates are highly heterogeneous, both across species and even across genotypes within a species. *Mycobacterium tuberculosis* famously has a rather long doubling time of ~24 hours, thus requiring up to 6 weeks to achieve an adequate cellular density for phenotypic or molecular analysis[6]. Cell culture requires highly-trained staff with significant hands-on time, as well as multiple large pieces of equipment. Although some initial efforts have been made to miniaturize and automate cell culture[7–9], such strategies still provide less information than can be mined from molecular analysis. Furthermore, a number of pathogens simply cannot be cultured by any known methods, prohibiting standard *in vitro* analysis[10]. New techniques were thus necessary for sensitive and specific, species-agnostic, and rapid detection and quantification of pathogenic disease markers.

The advent of the polymerase chain reaction (PCR) in 1985 ushered in a new era of molecular diagnostic technologies that no longer relied on cell culture for sensitive molecular detection[11,12]. PCR leverages natural biological mechanisms for DNA replication in a cyclic process to yield exponential gains in genetic material. A synthetic set of single-stranded guide oligomers, called primers, are added in excess to the initial target nucleic acid template. An initial heating step (melting) separates the two strands of genomic DNA. A subsequent cooling (annealing) yields primer-genome hybrid pairs. A thermostable polymerase from *Thermus aquaticus* (Taq) extends the primer-genome hybrid in the 3' direction using free deoxynucleotide triphosphates (dNTPs) complementary to the template strand. The entire cycle of melting, annealing, and extension takes 20-90 seconds, depending on the efficiency and speed of the temperature control mechanism and the polymerase. This cycle is generally repeated up to 40 times in order to achieve a quantifiable amount of DNA products, termed amplicons.

Although some groups have attempted to directly adapt PCR for use in RLR settings, either through miniaturization[13] or automation[14], a growing effort has centered on

alternative, isothermal signal amplification techniques[15,16]. These methods present several advantages due to reduced maximal temperature requirements. Less power is required to drive the assay, and simple chemical heating methods have been applied in some instances[17]. Lower temperatures also reduce issues related to evaporation and bubble formation that are frequently problematic in miniaturized diagnostic systems[18]. Furthermore, reducing maximal operational temperature enables the use of a larger diversity of materials and reagents that might otherwise be functionally compromised during traditional PCR.

Through the combination of novel signal amplification mechanisms with inexpensive miniaturization and automation technology (see Section 1.4 for a discussion of miniaturization technology), academic and industrial diagnostic developers have made significant advances towards low-cost, rapid, and portable molecular diagnostic systems.

2.1.2 Current Nucleic Acid Diagnostic Technologies

Nucleic acid detection and quantification techniques have been developed for a broad range of targets and environments, employing a variety of methods for signal amplification and readout in overall platforms that range from simple lateral flow strip tests to complex pump-actuated sample processors.

A growing number of biochemical mechanisms have been developed for nucleic acid amplification. In addition to the traditional PCR method, a number of isothermal amplification techniques have been developed. These include loop-mediated isothermal amplification (LAMP)[19], recombinase polymerase amplification (RPA)[20], rolling cycle amplification (RCA)[21], etc. Each of these methods presents certain advantages and disadvantages with regard to assay performance, as summarized in Table 2.1. Academic and industrial groups are further developing each of these amplification mechanisms towards commercial deployment, with LAMP in the lead with the largest volume of new academic papers to date.

Table 2.1 Nucleic acid amplification technologies for remote and low-resource settings.

Polymerization Reaction	Year	Minimum Time to Answer (min)[22]	Min. Temp (°C)†	Max Temp (°C)	Limitations	Advantages
PCR	1985[12]	15	50	95	Requires thermocycling	Robust Simple design
LAMP	2000[19]	15	55	66	Complex set of 4-6 primers	Robust Isothermal
RPA	2006[20]	< 5	20	42	Complex set of enzymes	Rapid (<5 mins) Isothermal @ RT
RCA	1995[23,24]	65	20	37	Needs circular NA Slower	Localized amplicon Isothermal @ RT
NASBA	1991[25]	60[26]	37	41	RNA amplification Slower	Selective RNA amplification

Researchers have also developed a range of mechanisms to quantify the amount of amplified nucleic acid product. Assays have been designed to yield a fluorescent or

† The minimum and maximum temperatures for each reaction have some dependence on the sequence-specific primer melting temperature.

colorimetric readout of amplification through intercalating dyes[27,28], metal indicators[29], hybridization probes[30], and nanoplasmonic shifts[31,32]. Furthermore, amplification has been directly measured through electrochemical indicators[33–35].

These assays have been optimized and combined into a range of integrated diagnostic systems. However, an adequately simple, robust, rapid, inexpensive, and versatile platform has yet to be developed for use in RLR settings. In this work, we aim to further advance RLR nucleic acid testing through the development of an integrated analysis platform for quantification of nucleic acid targets through isothermal amplification methods.

1.1.1 The Microfluidic Biomolecular Amplification Reader

We have developed an integrated Microfluidic Biomolecular Amplification Reader (μBAR) for multiplexed molecular analysis in RLR settings. This system leverages power-free degas loading into a microfluidic chip, isothermal nucleic acid amplification, and integrated fluorescent readout (Figure 2.1).

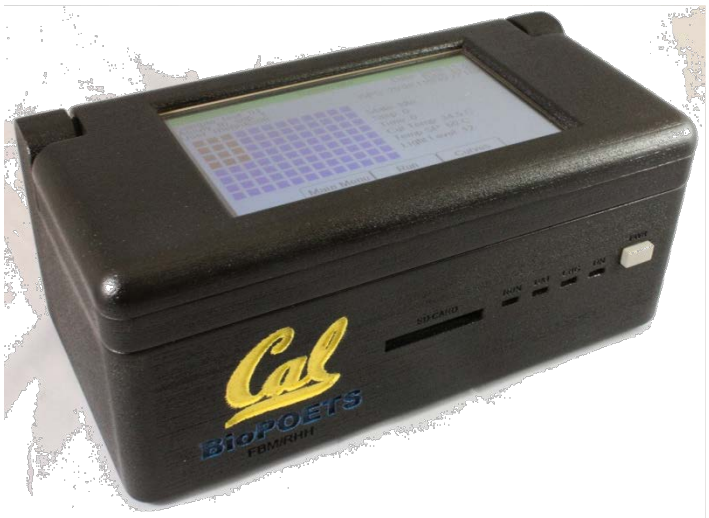

Figure 2.1 The Microfluidic Biomolecular Amplification Reader (μBAR).

2.2 Loop-mediated Isothermal Amplification Assay

2.2.1 LAMP Assay Overview

LAMP was first developed in 2000 by researchers at Eiken Chemical Co., Ltd and has since gained popularity in the field of molecular diagnostics for its specificity, robustness, and speed[19]. LAMP primarily differs from traditional PCR in that it is conducted isothermally at ~60°C using 4-6 primers and a *Bst* polymerase with strand-displacement properties (isolated from *Bacillus stearothermophilus*). Amplification of a single copy of template can be observed in the range of 20-120 minutes, depending on the target sequence and assay conditions. LAMP has been extended for the detection of RNA[36] and single nucleotide polymorphisms (SNPs)[28], with commercial reagent kits available globally.

The LAMP process requires a set of forward and backward inner primers (FIP and BIP, respectively) as well as a set of forward and backward initiator primers (F3 and B3, respectively). The inner primers first generate looping structures that are subsequently displaced from the target template by the initiator primers. A self-amplifying looping structure is finally generated that will undergo continued polymerization without the need

for any thermal melting or annealing steps. Optional forward and backward loop primers may be added to further increase the amplification rate (LPF and LPB)[37]. The mechanism of action is described in Figure 2.2.

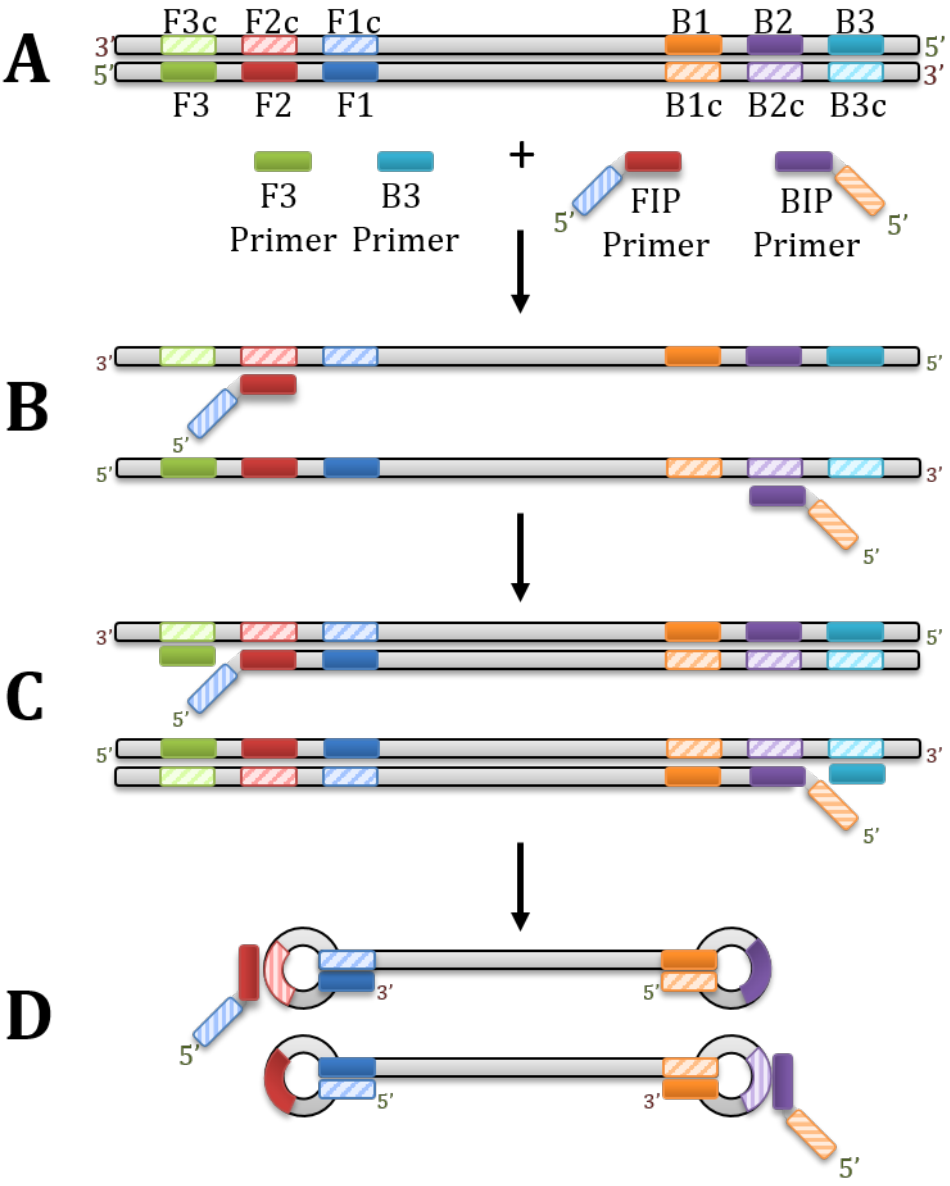

Figure 2.2 Loop mediated isothermal amplification mechanism. (A) An initial template for amplification is mixed with a set of forward and reverse inner primers (FIP and BIP, respectively), as well as a set of forward and backward initiator primers (F3 and B3, respectively). Sense (solid color) and antisense (dashed color) primer binding motifs are labeled on the template sequence. (B) In an excess of primers at amplification temperature (generally ~60°C), FIP and BIP primers will hybridize to their complimentary strands and begin polymerization, displacing any downstream template via the strand-displacement property of the *Bst* polymerase. (C) The newly-extended sequences are now hybridized to the template sense and antisense strands. The F3 and B3 initiator primers displace the new

amplicon via the same strand-displacement property of the *Bst* polymerase. (D) After one more round of polymerization with FIP and BIP primers and release by F3 and B3 primers, the initial looping structures are formed. These structures have complimentary tail ends in the FIP and BIP regions, which will polymerize in a looping manner.

Several readout mechanisms have been adapted for LAMP analysis (Figure 2.3)[29]. Initial work showed amplicon detection through direct measurements of turbidity changes due to precipitation of amplification biproducts[38]. Colorimetric assays have also been developed using naphthalene blue, etc.[39]. However, fluorescence measurements offer more sensitive results. Assays have been developed for fluorescent detection by SYBR Green intercalating dye as well as a calcein metal indicator dye[29].

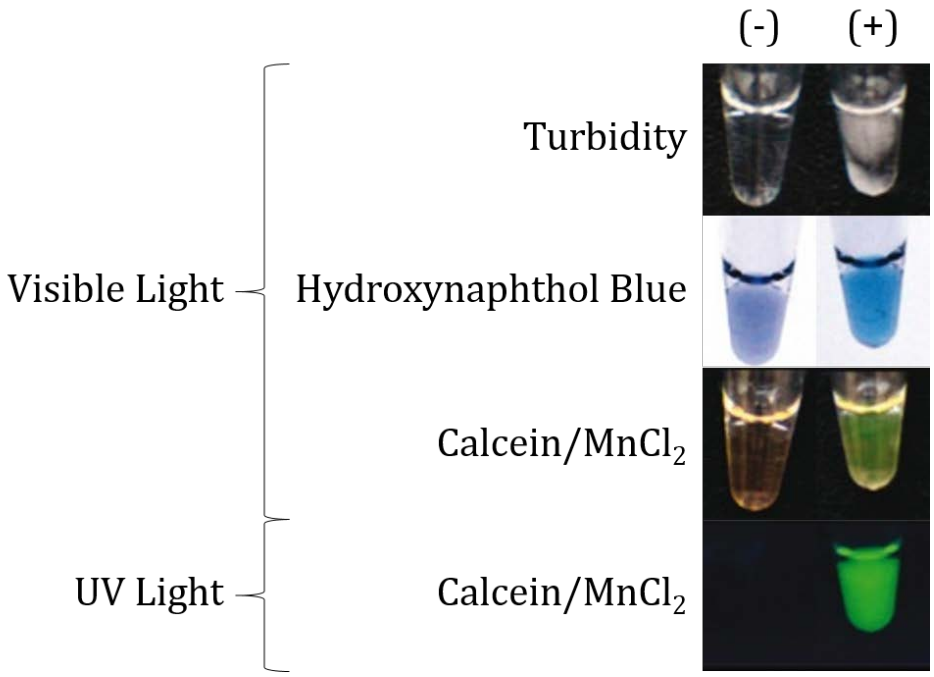

Figure 2.3 Mechanisms of optical readout for loop mediate isothermal amplification. Images of an end point LAMP reaction after a 60 minute incubation at 65°C. A low (-) and a high concentration of initial template (+) are shown. The calcein/$MnCl_2$ detection method generally shows a higher sensitivity detection, with UV excitation enhancing the effect. (Images adapted from Fishbach et al.[29]).

LAMP offers a number of advantages over traditional PCR. Beyond obviating the need for thermocycling and thus reducing device power consumption and thermal limits on materials and reagents, LAMP also generally produces results in a shorter time than traditional PCR. LAMP has also been demonstrated to be more resistant to interferents than PCR[40], facilitating simpler analysis of samples with minimal pre-processing.

LAMP has been applied to a range of applications, including infectious disease diagnosis[41], environmental monitoring[38,42], food administration[34,43,44], and chronic disease screening[28]. Thus far, the vast majority of these efforts have been conducted as benchtop or single-tube assays. Some have incorporated phase-change stabilized exothermic chemical

reactions to maintain the assay operating temperature at ~65°C without the need for electronics[17]. Initial attempts have been made to adapt the LAMP assay for paper-based diagnostics[45]. Several other groups have attempted to miniaturize the LAMP assay[46–48]. Thus far, a fully integrated solution from sample to result has yet to be realized for a broad range of molecular diagnostic applications.

2.2.2 LAMP Primer Design

LAMP primer sets were designed in a deductive constraint process similar to standard PCR primer design, though 6-8 primer binding regions (F1, F2, F3, B1c, B2c, B3c; optional: LPF, LPB) are assessed rather than just 2. In general, LAMP primer binding sites are constrained to be within a specific range of parameters, with some dependence on the target application. Similar to PCR amplification, the general process for primer design consists of exhaustive identification of potential primer binding regions, followed by removal of any sequences violating acceptance criteria. The overall process for LAMP primer design is as follows:

1. Identify a target sequence to be amplified. This may be a conserved region for general species detection, or a region containing SNPs for genotyping.
2. Identify every possible primer binding region, within size primer size, composition, and melting temperature constraints. For standard LAMP, the 3' ends of F1, F2, B1, and B2 should not be AT-rich. Each binding region should have a Tm between ~55°C – 65°C to enable efficient operation in the optimal enzyme temperature range.
3. Exclude primer binding regions with expected secondary structure (such as hairpins) that might lead to decreased target hybridization efficiency.
4. Identify every possible combination of 6 primer binding regions that yield an ordered set of F1, F2, F3, B1c, B2c, and B3c regions. Spacing should also be taken into account to leave sufficient spacing between the F1 and F2 regions for LPF primer design, and between the B1c and B2c regions for LPB primer design. There should be 40 – 60 bp between the 5' ends of F2 and F1, as well as between the 5' ends of B2 and B1. The total length between the 5' ends of F2 and B2 should be less than 200bp[49]. Given the potential number of combinations between 6 regions, this step can be computationally demanding.
5. Exclude any combinations of 6 primers with cross-hybridization that might lead to decreased target hybridization efficiency and/or unwanted products. Combinations may be sorted by their maximal cross-hybridization score.
6. Assess the best scoring primer sets for LPF and LPB primer design. LPF and LPB are designed by following steps 1 – 3 for the sequences between F1/F2 and B1c/B2c regions, respectively. Candidates with excessive secondary structure of cross-hybridization with any other regions are excluded. Either LPF, LPB, or both may be impossible to generate given the input set of 6 binding regions.
7. The final F3 and B3 sequences are directly used as primers. The FIP primer is made as a composite sequence of 5'-F1c-F2-3' and the BIP primer is made as a composite sequence of 5'-B1c-B2-3'. The LPF and LPB primers are just the respective sequences generated in step 6.

Several web-based tools are available to assist in LAMP primer design, including the PrimerExplorer package developed by Eiken[49], and the LAMP Assay Versatile Analysis (LAVA) open source application[50]. We have also developed a MATLAB script for custom automated LAMP primer design. In this work, we have used primer sets for the detection of, HIV-1[51], malaria[52], and tuberculosis, described in Table 2.3.

Table 2.2 Lamp Primers Used in μBAR Assays.

Organism Target	Target Sequence	Primer Type	Primer Sequence
HIV-1[51]	GGUAAGAGAUCAGGCUGAACAUCUUAA GACAGCAGUACAAAUGGCAGUAUUCAU CCACAAUUUUAAAAGAAAAGGGGGGAU UGGGGGGUACAGUGCAGGGGAAAGAAU AGUAGACAUAAUAGCAACAGACAUACA AACUAAAGAAUUACAAAAACAAAUUAC AAAAAUUCAAAAUUUUCGGGUUUAUUA CAGGGACAGCAGAAAUCCACUUUGGAAA GGACCAGC	F3	GGTAAGAGATCAGGCTGAACATC
		B3	GCTGGTCCTTTCCAAAGTGG
		FIP	CCCCAATCCCCCCTTTTCTTAGACA GCAGTACAAATGGCA
		BIP	AGTGCAGGGGAAAGAATAGTAGAC CTGCTGTCCCTGTAATAAACCC
		LPF	TTAAAATTGTGGATGAAT
		LPB	GCAACAGACATACAAACTAAAG
Malaria[52]	TGTAATTGGAATGATAGGAATTTACAAG GTTCCTAGAGAAACAATTGGAGGGCAAG TCTGGTGCCAGCAGCCGCGGTAATTCCA GCTCCAATAGCATATATTAAAATTGTTG CAGTTAAAACGTTCGTAGTTGAATATTA AAGAATCCGATGTTTCATTTAAACTGGT TTGGGAAAACCAAATATATTATATATTT TGCTTTGTTCAAAATAAGGTTTTC	F3	TGTAATTGGAATGATAGGAATTTA
		B3	GAAAACCTTATTTTGAACAAAGC
		FIP	AGCTGGAATTACCGCGGCTGGGTTC CTAGAGAAACAATTGG
		BIP	TGTTGCAGTTAAAACGTTCGTAGCC CAAACCAGTTTAAATGAAAC
		LPF	GCACCAGACTTGCCCT
		LPB	TTGAATATTAAAGAA
Tuberculosis (TB Common)	GTCGCCGCGATCAAGGAGTTCTTCGGCA CCAGCCAGCTGAGCCAATTCATGGACCA GAACAACCCGCTGTCGGGGTTGACCCAC AAGCGCCGACTGTCGGCGCTGGGGCCCG GCGGTCTGTCACGTGAGCGTGCCGGGCT GGAGGTCCGCGACGTGCA	F3	CGGATGACCACCCAGGAC
		B3	ACGTCGCGGACCTCCA
		FIP	ACTCCTTGATCGCGGCGACGGCGAT CACACCGCAGA
		BIP	CCAGAACAACCCGCTGTCGGCACGC TCACGTGACAGAC
		LPF	GGCCGGATGTTGATCAACG
		LPB	GGTTGACCCACAAGCGC

2.2.3 LAMP Reaction Mix Optimization

The LAMP reaction may be performed using a LoopAMP Kit (Eiken,) or by preparing a custom reaction mix from individual components[49]. We tested both methods and found that the custom mix performed at least as well as the LoopAMP Kit, with the advantage of facilitating further customization for implementation in a microfluidic environment (data not shown). The LAMP reaction mix described by Tomita *et al.* consists of the primary components: *Bst* polymerase, dNTPs, salts (Tris, KCl, $MgSO_4$, $(NH_4)_2SO_4$), a DNA hybrid destabilizer (betaine), primers, and colorimetric or fluorescent indicators, as necessary[49].

For a fluorescent readout, we tested the calcein/$MnCl_2$ system relative to the SYBR Green intercalating dye. We found that, in general, the calcein detection system yielded higher fluorescent signals in a shorter period of time. Furthermore, initial background fluorescent signal was lower in our optimized calcein/$MnCl_2$ mix. We have thus used the calcein indicator in all assays moving forward.

For our purposes, the basic LoopAMP DNA Kit exhibited excessive initial fluorescence in the calcein-based detection format. This background signal would make it difficult to detect a signal in a microfluidic platform, and essentially impossible to detect in an equipment-free naked eye readout. In the calcein assay, the fluorescent signal is produced by the precipitation of $MnCl_2$ as a result of pyrophosphate release during DNA polymerization[49]. $MnCl_2$ acts as a quencher for the fluorescent calcein molecule, and thus its removal from solution leads to an increased fluorescent signal. The initial and relative concentrations of these two reagents are critical for the assay performance in a microfluidic platform. We thus conducted an optimization to adjust the relative concentration of calcein and $MnCl_2$ for visual readout, yielding optimal concentrations of 27.28 μM and 1488 μM, respectively (see Appendix D.1.1 for results leading to optimal configuration).

The LAMP assay also shows some dependence on operating temperature, with reactions venturing too high or low yielding significantly reduced amplification rates. This optimal temperature depends to some extent on the specific primer sequence and the salt content, similar to what is observed in optimal annealing temperatures for standard PCR reactions. We found an optimal amplification at ~63°C, with temperatures below 58°C or above 66°C significantly inhibiting amplification (Figure 2.4).

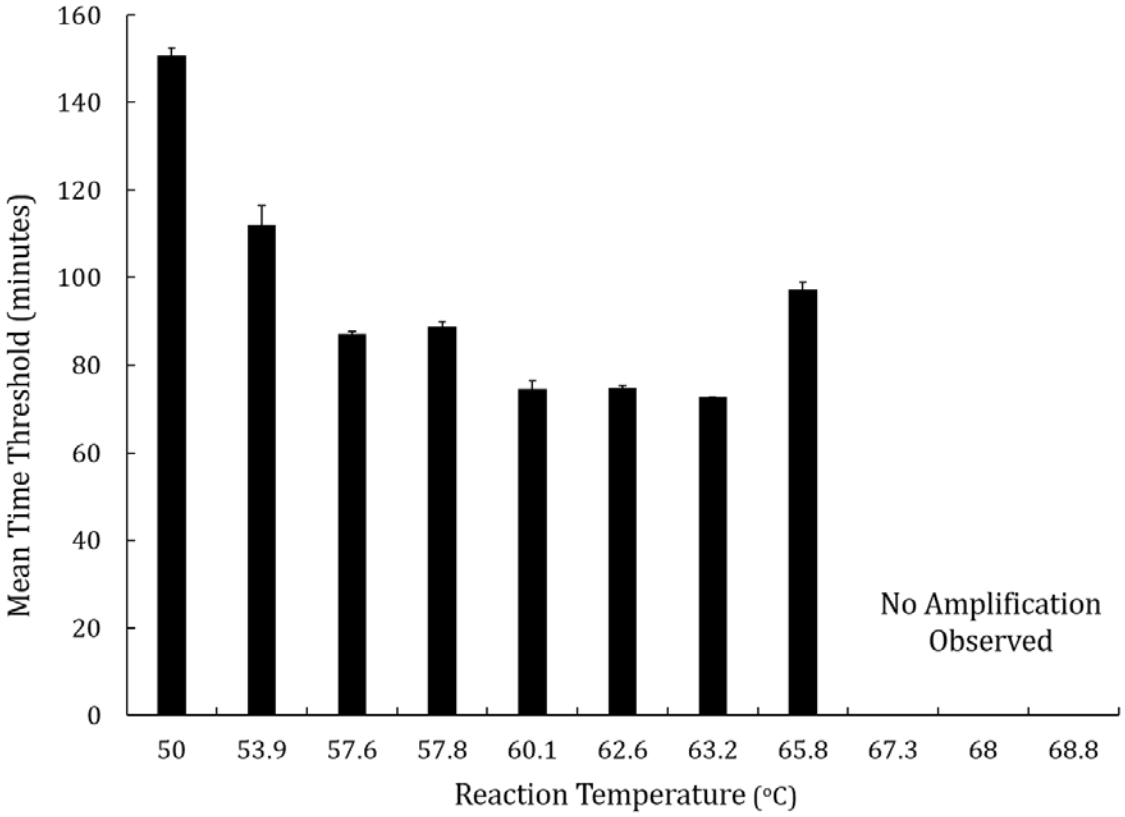

Figure 2.4 Optimization of LAMP amplification temperature. LAMP was performed using our optimized calcein/$MnCl_2$ reaction mix to amplify both positive (10^6 copies/μL malaria target plasmid) and negative template control samples (NTC). Reactions were performed in duplicate on a Biorad CFX96 instrument with a temperature gradient applied across wells.

An optimal temperature for amplification was found to be ~63°C, with no amplification observed above ~66°C. No amplification was observed in any NTC samples (data not shown).

Interferents in whole blood have been shown to inhibit several nucleic acid amplification mechanisms[53]. In particular, hemoglobin has been shown to inhibit amplification[53]. Although LAMP shows a reduced sensitivity to whole blood interferents relative to PCR[40], we characterized the amount of inhibition through spiking a serial dilution of human plasma into LAMP reactions using malaria primers and template (Figure 2.5). We observed significant reaction inhibition at 5% plasma, with reactions proceeding near uncontaminated rates starting with 1 – 2% plasma.

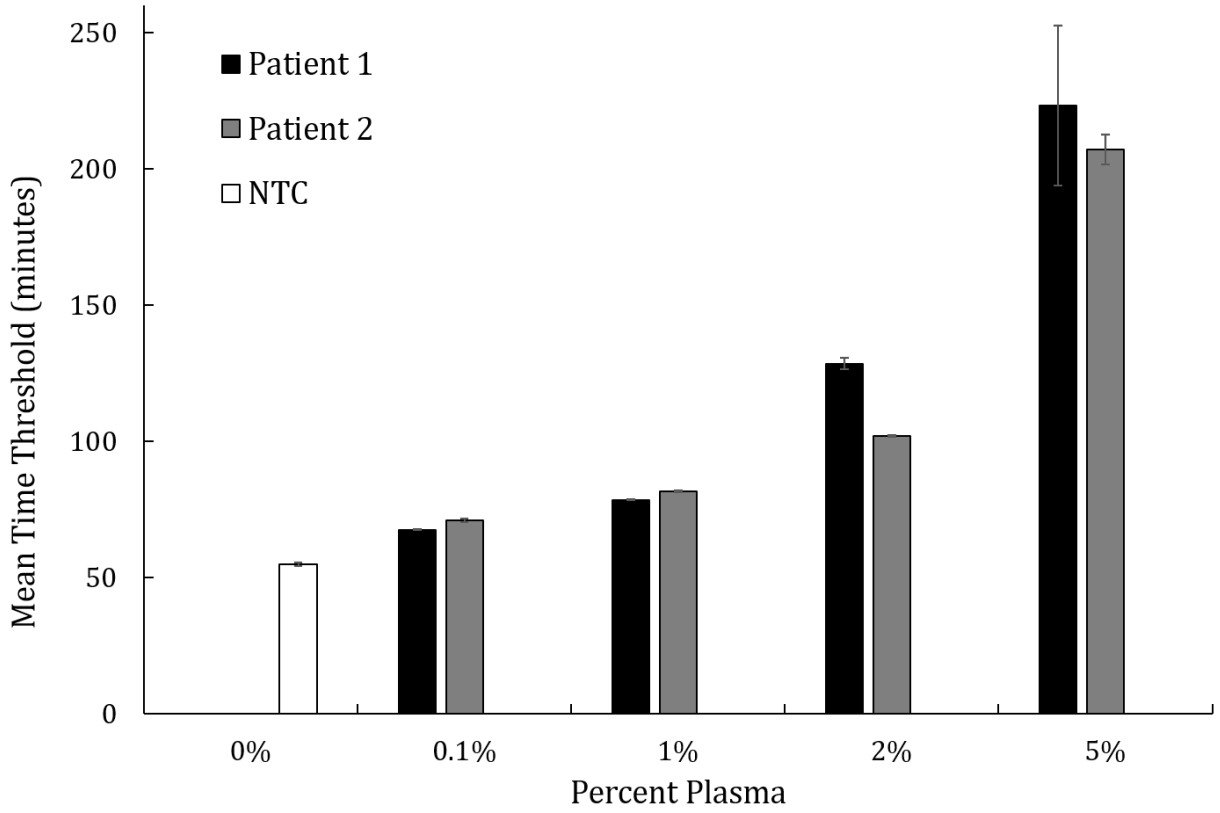

Figure 2.5 LAMP inhibition by plasma. LAMP was performed using our optimized calcein/$MnCl_2$ reaction mix to amplify both positive (10^6 copies/μL malaria target plasmid) and negative samples (NTC). Diluted human plasma from two different patients was spiked into the sample to a final concentration of 0.1%, 1%, 2%, or 5%. A control test was performed with water spiked in rather than diluted plasma (0% plasma). Reactions were performed in triplicate on a Biorad CFX96 instrument. Plasma content of 5% led to significant reduction in amplification rate, with less inhibition observed for the range of 0.1% - 2%. No amplification was observed in any NTC samples (data not shown).

Beyond offering advantages in assay optimization and customization, preparing our own reactions mixes from individual components has offered a significant cost savings over

commercial kit purchase. We have estimated the cost of our custom mix to be $0.02/μL, compared with $0.19/μL with the LoopAMP Kit, with the polymerase making up ~50% of the cost, and the dNTPs making up ~40% in the custom mix (see Appendix A.2 for a detailed analysis of reagent costs for LAMP). A microfluidic system using 50 μL of sample would thus require ~$1.00 or less in reagent costs, prior to any economies of scale or special negotiations.

2.2.4 LAMP Analysis of Single Nucleotide Polymorphisms for Drug Resistance

Single nucleotide polymorphisms (SNPs) are genomic loci of high variability in an organism[54]. A number of SNPs have been associated with microorganism pathogenicity or host susceptibility to disease. These genetic markers offer a powerful method to learn about a target organism with minimal analysis, enabling multiplexed biomolecular analysis without the need for exhaustive sequencing.

LAMP has been applied to SNP analysis for a range of conditions. In SNP analysis, LAMP primers are designed such that the 3' base of the F1 region overlaps with the 3' base of the B1 region. In this way, a single basepair mismatch at the SNP locus can drastically reduce the amplification efficiency of the LAMP reaction, enabling SNP turn-on or turn-off assays (Figure 2.6).

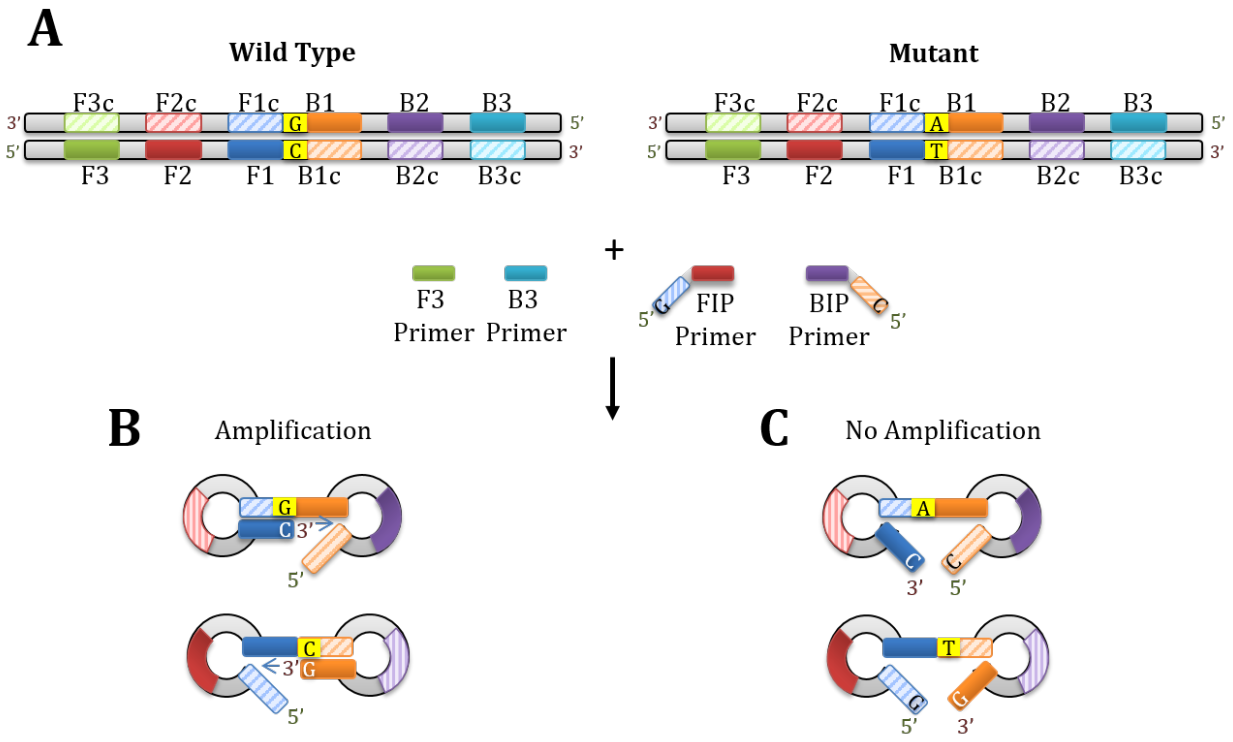

Figure 2.6 LAMP analysis of SNPs. (A) An initial template for amplification is mixed with a set of forward and reverse inner primers (FIP and BIP, respectively), as well as a set of forward and backward initiator primers (F3 and B3, respectively). Sense (solid color) and antisense (dashed color) primer binding motifs are labeled on the template sequence. The template sequence to the left represents a wild type allele (G/C, highlighted in yellow), while the template sequence on the right represents a mutant allele (A/T, highlighted in yellow).

(B) The looping structures generated through amplification of the wild type template will proceed with efficient polymerase binding at the 3' ends. (C) The looping structures generated through amplification off the mutant template will lead to reduce amplification efficiency due the the base mismatch at the 3' ends. FIP and BIP primers may be designed to selectively amplify either the wild type or mutant sequence, enabling turn-on or turn-off assays for SNPs.

SNP typing holds great promise for rapid screening of drug resistance in pathogen-host systems[55]. We have worked with collaborators at the Tuberculosis Centre for Excellence at Stellenbosch University in Cape Town, South Africa to identify SNPs associated with drug resistance in tuberculosis and to subsequently design assays to detect these resistance genotypes.

Mycobacterium tuberculosis (*Mtb*) is the causative pathogen in tuberculosis (TB), an infection of the respiratory system that may eventually spread to peripheral organs, leading to acute disease and death if left untreated. One third of the world's population suffers from latent TB, with 8.8 million new cases of the disease and 2 million deaths annually[56]. These numbers are dramatically skewed towards the developing world, with TB accounting for the majority of HIV-related deaths. It is thus extremely important to avoid wasting precious resources and medicines on misdiagnosis and retreatment. However, sputum smear microscopy (by far the most common TB test performed in low-income countries at 83 million/year) only achieves 40-60% sensitivity in field conditions, with this value dropping to 20% in cases of co-infection with HIV[56]. Furthermore, the confirmatory diagnostic technique of cell culture is prohibitively slow, yielding results in the time frame of months, during which a treatment regimen has already been pursued regardless of drug susceptibility. Genotyping tests adapted to RLR settings present an attractive option for detection of TB and screening for drug resistance due to their speed and low cost.

Tuberculosis is generally treated sequentially with three lines of drugs, summarized in Table 2.4. Multiple lines of drugs have become necessary as drug resistance has become increasingly problematic. This is due to both patient compliance issues, as well as excessive drug prescription in cases where disease or drug resistance status has not been confirmed beyond symptomatic diagnosis. Cases of multi-drug resistant (MDR) TB have become increasingly common, with 2013 global incidences of 3.5% and 20.5% in new cases and previously-treated cases, respectively[57]. The percentage of MDR-TB cases that were also extensively drug resistant (XDR) was 9.0% in the same year. Patients with extensive pulmonary TB typically are infected with $\sim 10^{12}$ bacteria[58]. Drug resistance has been shown to result from spontaneous mutations at rates of 10^{-7} to 10^{-10} mutations per bacterium per generation, depending on the specific drug[58]. Patients are thus frequently treated with multiple drugs at once in order to prevent conversion to MDR or XDR. It is thus critical to develop tools to rapidly identify both TB infection, as well as drug resistance profile for patients presenting with respiratory symptoms in the clinic in order to deliver targeted therapeutics.

Table 2.3 Lines of pharmaceutical treatment for tuberculosis.

Treatment	Pharmaceutical	Abbreviations
First Line	Ethambutol	EMB, E
	Isoniazid	INH, H
	Pyrazinamide	PZA, Z
	Rifampicin	RMP, R
	Streptomycin	STM, S
Second Line **1.** Less effective than first-line drugs (e.g., p-aminosalicylic acid) **2.** Has toxic side-effects (e.g., cycloserine) **3.** Unavailable in many developing countries (e.g., fluoroquinolones)	Amikacin	AMK
	Kanamycin	KM
	Capreomycin	
	Viomycin	
	Enviomycin	
	Ciprofloxacin	CIP
	Levofloxacin	
	Moxifloxacin	MXF
	Ethionamide	
	Prothionamide	
	Cycloserine	
	p-Aminosalicylic acid	PAS, P
Third Line 1. Not very effective (clarithromycin) 2. Efficacy has not been proven (linezolid, R207910). 3. Impractically expensive (rifabutin)	Rifabutin	
	Clarithromycin	CLR
	Linezolid	LZD
	Thioacetazone	T
	Thioridazine	
	Arginine	
	Vitamin D	
	R207910	

The TB Drug Resistance Mutation Database (TBDReaMDB) has become a repository of SNPs that have been associated with drug resistance in cases of tuberculosis[59]. TB SNP genotyping studies are organized with information including their polymorphism, amino acid change, geographical origin, and confidence of associated drug resistance, among other assay parameters. A listing of several important SNPs and the drug for which they have been showed to confer resistance is presented in Table 2.5.

Table 2.4 SNPs conferring drug resistance in *M. tuberculosis.*

Name	Sequence	Location	Drug Resistance	Mutation
fabG1 -15	C	1673425	Isoniazid	C->T
fabG1 -16	A	1673424	Isoniazid	A->G
fabG1 -8	T	1673432	Isoniazid	T->C
fabG1 -8	T	1673432	Isoniazid	T->A
katG s315T	GC	2155167	Isoniazid	AGC->ACA
katG S315T	C	2155168	Isoniazid	AGC->ACC
rrs 1401	A	1473246	Kanamycin	A->G
rrs 1402	C	1473247	Kanamycin	C->T
rrs 1402	C	1473247	Kanamycin	C->A
rrs 1484	G	1473329	Kanamycin	G->T
rrs 1484	G	1473329	Kanamycin	G->A
gyrA A90V	C	7570	Quinolone	GCG->GTG
gyrA D94A	A	7582	Quinolone	GAC->GCC
gyrA D94G	A	7582	Quinolone	GAC->GGC
gyrA D94N	G	7581	Quinolone	GAC->AAC
gyrA D94Y	G	7581	Quinolone	GAC->TAC
gyrA S91P	T	7572	Quinolone	TCG->CCG
rpoB D435V	A	761110	Rifampicin	GAC->GTC
rpoB D435Y	G	761109	Rifampicin	GAC->TAC
rpoB H445D	C	761139	Rifampicin	CAC->GAC
rpoB H445R	A	761140	Rifampicin	CAC->CGC
rpoB H445Y	C	761139	Rifampicin	CAC->TAC
rpoB S450L	C	761155	Rifampicin	TCG->TTG
rpoB S531W	C	761155	Rifampicin	TCG->TGG
rpsL K43R	A	781687	Streptomycin	AAG->AGG
rpsL K43T	A	781687	Streptomycin	AAG->ACG
rpsL K88Q	A	781821	Streptomycin	AAG->CAG
rpsL K88R	A	781822	Streptomycin	AAG->AGG

Within the local population in South Africa, our collaborators identified just three SNPs that accounted for >70% of rifampicin resistant isolates in TB patients: D435V, H445D, and S450L within the *rpoB* gene[‡]. We thus focused our initial proof-of-concept effort on these SNPs, though we designed primer sets for several other SNPs (highlighted in Table 2.5). The SNPs are highlighted within the TB genome in Figure 2.7. The primers were designed using the PrimerExplore V4 Application with relevant SNP locus constraints, as described in Appendix A.2. A close-up of the designed primers for the D435V SNP is shown in Figure 2.9B. A listing of designed primer sequences can be found in Table 2.6.

[‡] SNPs have been annotated to indicate the numerical amino acid locus of mutation within the gene, flanked by the wild type and mutant amino acid abbreviation (located to the left and right of the number, respectively). For example, rpoB D435V represents the mutation occurring at amino acid residue 435 in the rpoB gene, leading to a mutation from aspartic acid (D) to valine (V).

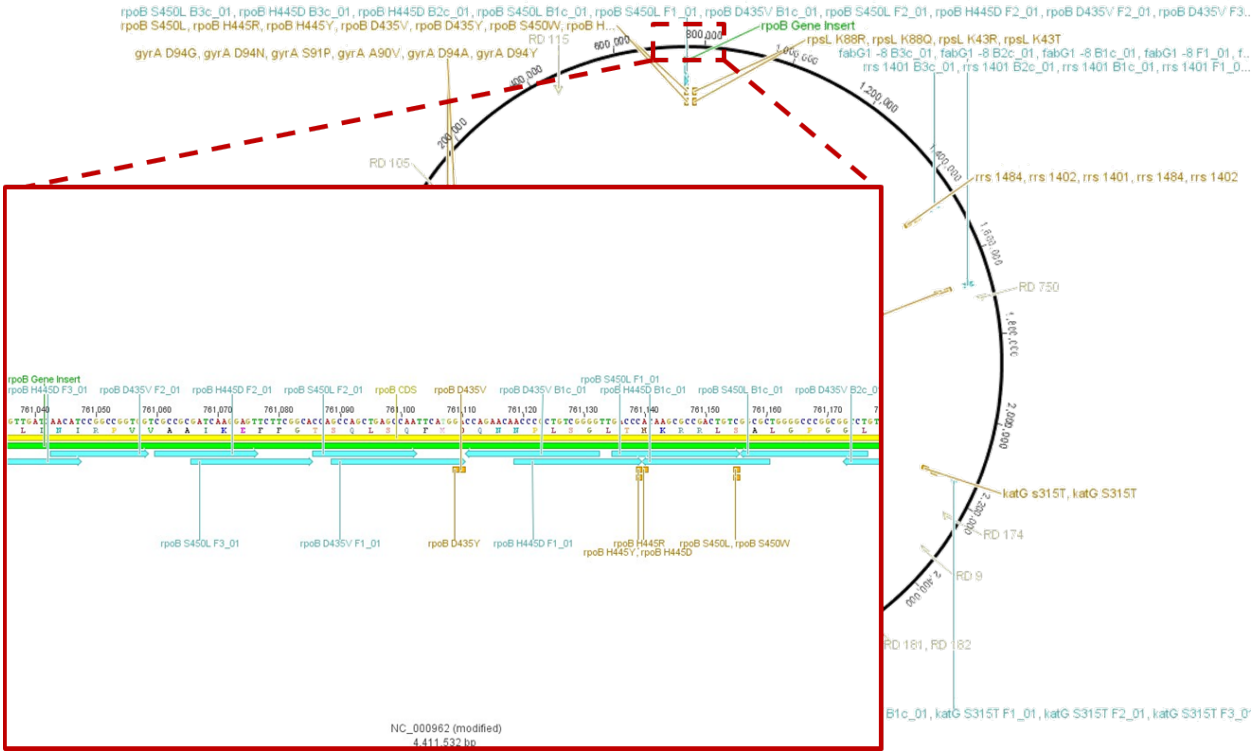

Figure 2.7 *M. tuberculosis* genome annotated with SNPs conferring resistance to commonly-used drugs. The full *Mtb* genome is shown as a circular sequence, with the *rpoB* gene positioned at the top. SNP mutations (yellow) and LAMP primer sequences (blue) are shown in the call-out box.

Table 2.5 LAMP primer sequences for *M. tuberculosis* SNP detection

Organism Target	Target Sequence	Primer Type	Primer Sequence
***M. tuberculosis* rpoB D435V SNP**	CGTGGAGGCGATCACACCGCAGACGTT GATCAACATCCGGCCGGTGGTCGCCGC GATCAAGGAGTTCTTCGGCACCAGCCA GCTGAGCCAATTCATGGACCAGAACAA CCCGCTGTCGGGGTTGACCCACAAGCG CCGACTGTCGGCGCTGGGGCCCGGCGG TCTGTCACGTGAGCGTGCCGGGCTGGA GGTCCGCGACGT	F3	CGTGGAGGCGATCACACC
		B3	TGCACGTCGCGGACCT
		FIP_WT	TCCATGAATTGGCTCAGCTGGCAAC ATCCGGCCGGTGG
		BIP_WT	ACCAGAACAACCCGCTGTCGGGGCA CGCTCACGTGACAGAC
		FIP_MT	ACCATGAATTGGCTCAGCTGGCAAC ATCCGGCCGGTGG
		BIP_MT	TCCAGAACAACCCGCTGTCGGGGCA CGCTCACGTGACAGAC
		LPF	GTGCCGAAGAACTCCTTGATC
		LPB	TTGACCCACAAGCGCCGAC
***M. tuberculosis* rpoB H445D SNP**	CCGCAGACGTTGATCAACATCCGGCCG GTGGTCGCCGCGATCAAGGAGTTCTTC GGCACCAGCCAGCTGAGCCAATTCATG GACCAGAACAACCCGCTGTCGGGGTTG ACCCACAAGCGCCGACTGTCGGCGCTG GGGCCCGGCGGTCTGTCACGTGAGCGT GCCGGGCTGGAGGTCCGCGACGTGCAC CCGTCGCACTACGGCCGGATGTGC	F3	CCGCAGACGTTGATCAACAT
		B3	GCACATCCGGCCGTAGTG
		FIP_WT	GGGTCAACCCCGACAGCGGGTCGCC GCGATCAAGGAGT
		BIP_WT	CACAAGCGCCGACTGTCGGCGCACG TCGCGGACCTCCAG
		FIP_MT	CGGTCAACCCCGACAGCGGGTCGCC GCGATCAAGGAGT

		BIP_MT	GACAAGCGCCGACTGTCGGCGCACG TCGCGGACCTCCAG
		LPF	CTGGCTGGTGCCGAAGA
		LPB	GGTCTGTCACGTGAGCGTGC
***M. tuberculosis* rpoB S450L SNP**	GATCAAGGAGTTCTTCGGCACCAGCCA GCTGAGCCAATTCATGGACCAGAACAA CCCGCTGTCGGGGTTGACCCACAAGCG CCGACTGTCGGCGCTGGGGCCCGGCGG TCTGTCACGTGAGCGTGCCGGGCTGGA GGTCCGCGACGTGCACCCGTCGCACTA CGGCCGGATGTGCCCGATCGAAACCCC TGAGGGG	F3	GATCAAGGAGTTCTTCGGCA
		B3	CCCCTCAGGGGTTTCGA
		FIP_WT	GACAGTCGGCGCTTGTGGGTCCCAG CCAGCTGAGCCAA
		BIP_WT	CGGCGCTGGGGCCCGGCGGTCTAGT GCGACGGGTGCA
		FIP_MT	AACAGTCGGCGCTTGTGGGTCCCAG CCAGCTGAGCCAA
		BIP_MT	TGGCGCTGGGGCCCGGCGGTCTAGT GCGACGGGTGCA
		LPF	CGGGTTGTTCTGGTCCATG
		LPB	N/A

We first conducted LAMP assays using plasmid sequences containing 500bp inserts surrounding the D435V SNP in the *M. tuberculosis* genome (Figure 2.7). Using two different primer sets, designed to detect either the rifampicin sensitive (WT) or resistant (MT) allele, we were able to observe a decreased amplification efficiency (represented as a later time threshold, Tt, in the target mismatch cases) (Figure 2.8). This differential amplification enables real-time determination of *Mtb* susceptibility to rifampicin.

In order to further decrease the relative amplification efficiency for mismatched SNP targets, we introduced destabilizing bases to reduce amplification efficiency. Groups have previously demonstrated enhanced SNP allelic discrimination by the introduction of hybridization destabilization elements in standard PCR[60]. The impact of a 3' mismatch has a strength dependent on the allele pairing of a SNP[61]. We hypothesized similar effects would be observed in LAMP reactions.

We designed variants of the rpoB D435V SNP primer set in which the FIP and BIP primers had the normal complimentary base, as well as all 3 possible destabilizing bases at the -3 position (Table 2.7). As we intended to place a destabilizing base in the -3 position on the 3' end of F1 and B1 sequences (to maximally inhibit amplification), we designed FIP and BIP primers to have this destabilizing base in the -3 position from the 5' end (which is the F1c and B1c sequence, respectively). The -3 position of the 5' end becomes the -3 position of the 3' end in the complimentary sequence.

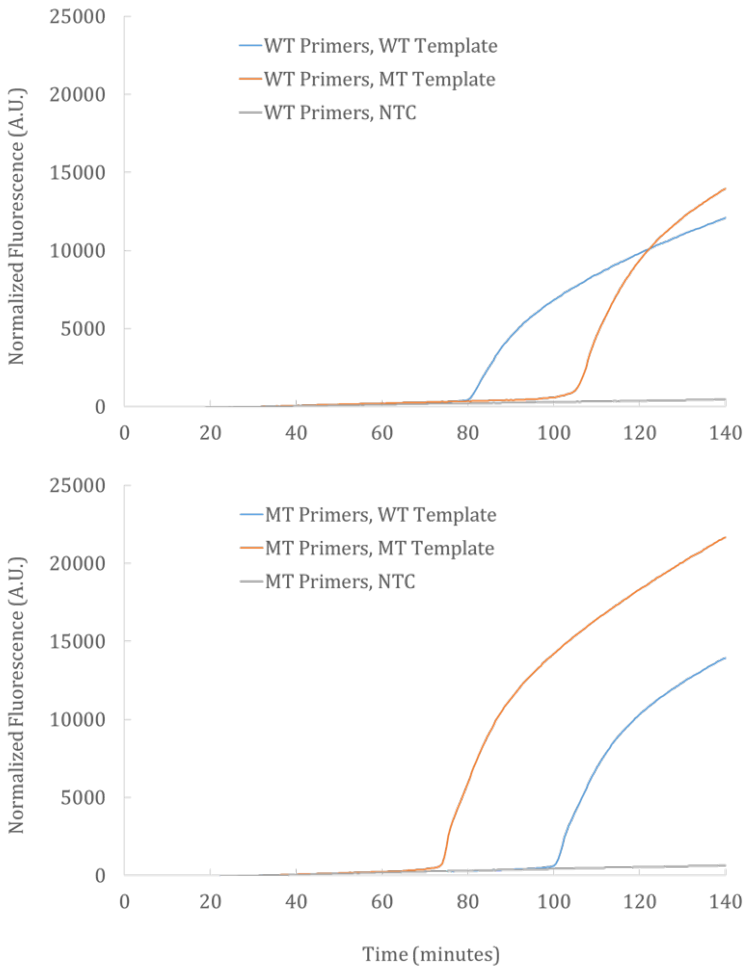

Figure 2.8 LAMP analysis of rifampicin-resistance D435V SNP with both wild type (WT) and Mutant (MT) primer sets. Water samples spiked with ~10^4 copies/μL of plasmids containing a 500bp insert from the *rpoB* gene of the H37Rv strain of *Mtb* were amplified via LAMP at 63°C for 150 minutes. Optimized calcein-based reaction mixes were used (see Appendix D.1.1) and fluorescence was measured on a Biorad CFX96 thermocycler. The insert either contained a wild type (WT) or mutant (MT) allele at the D435V SNP locus. (A) WT primers were used to amplify WT, MT, and NTC samples. Differential amplification of the WT target was observed, with a Tt of ~80 minutes versus ~105 minutes for the MT target. (B) MT primers were used to amplify WT, MT, and NTC samples. Differential amplification of the MT target was observed, with a Tt of ~75 minutes versus ~105 minutes for the WT target. No amplification was observed in any NTC samples.

Table 2.6 LAMP primers with -3 destabilized bases. The destabilized base options are indicated in bold under the primer sequence column.

Organism Target	Target Sequence	SNP	Primer	-3 bp	Primer Sequence
***M. tuberculosis* rpoB D435V SNP**	CGTGGAGGCGATCACACC GCAGACGTTGATCAACAT CCGGCCGGTGGTCGCCGC GATCAAGGAGTTCTTCGG CACCAGCCAGCTGAGCCA ATTCATGGACCAGAACAA CCCGCTGTCGGGGTTGAC CCACAAGCGCCGACTGTC GGCGCTGGGGCCCGGCGG TCTGTCACGTGAGCGTGC CGGGCTGGAGGTCCGCGA CGT	WT	FIP	C	TC**C**ATGAATTGGCTCAGCTGGCA ACATCCGGCCGGTGG
				G	TC**G**ATGAATTGGCTCAGCTGGCA ACATCCGGCCGGTGG
				A	TC**A**ATGAATTGGCTCAGCTGGCA ACATCCGGCCGGTGG
				T	TC**T**ATGAATTGGCTCAGCTGGCA ACATCCGGCCGGTGG
			BIP	C	AC**C**AGAACAACCCGCTGTCGGGG CACGCTCACGTGACAGAC
				G	AC**G**AGAACAACCCGCTGTCGGGG CACGCTCACGTGACAGAC
				A	AC**A**AGAACAACCCGCTGTCGGGG CACGCTCACGTGACAGAC
				T	AC**T**AGAACAACCCGCTGTCGGGG CACGCTCACGTGACAGAC
		MT	FIP	C	AC**C**ATGAATTGGCTCAGCTGGCA ACATCCGGCCGGTGG
				G	AC**G**ATGAATTGGCTCAGCTGGCA ACATCCGGCCGGTGG
				A	AC**A**ATGAATTGGCTCAGCTGGCA ACATCCGGCCGGTGG
				T	AC**T**ATGAATTGGCTCAGCTGGCA ACATCCGGCCGGTGG
			BIP	C	TC**C**AGAACAACCCGCTGTCGGGG CACGCTCACGTGACAGAC
				G	TC**G**AGAACAACCCGCTGTCGGGG CACGCTCACGTGACAGAC
				A	TC**A**AGAACAACCCGCTGTCGGGG CACGCTCACGTGACAGAC
				T	TC**T**AGAACAACCCGCTGTCGGGG CACGCTCACGTGACAGAC

These tests proved successful, yielding an increased ΔTt for destabilized primer sets relative to standard sets (Figure 2.9). This enhanced differential amplification improves the ability to differentiate between tuberculosis cases that are drug susceptible versus drug resistant.

Although these results are promising, the non-specific amplification of mismatched SNP target sequences poses a significant challenge for false positive results, particular in cases of low initial target concentration. In order to decouple the target concentration from the resistance genotype, both sets of primers should be used in parallel to observe a combined differential amplification. Furthermore, a common set of primers that amplifies both WT and MT sequences may be used as a bar for relative amplification efficiency.

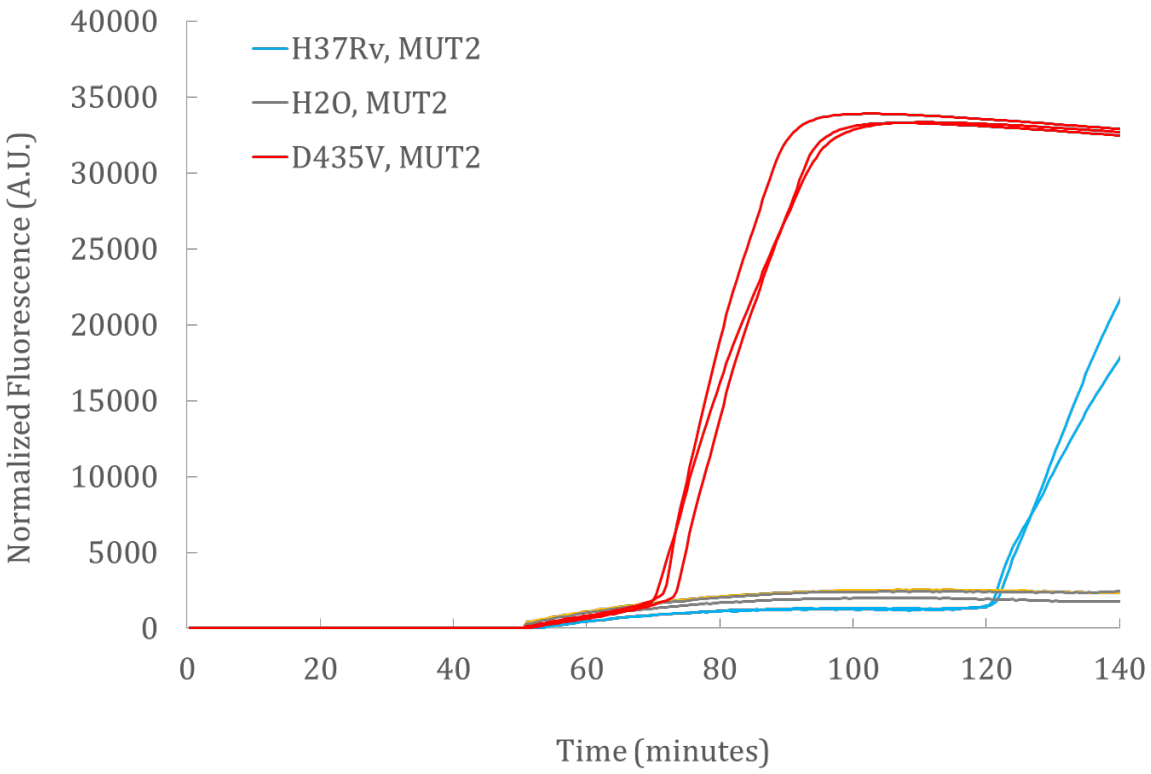

Figure 2.9 Increased amplification differentiation with destabilized bases in LAMP primer sequences. Water samples spiked with 10^4 copies/μL of plasmids containing a 500bp insert from the *rpoB* gene of the H37Rv strain of *Mtb* were amplified via LAMP at 63°C for 150 minutes. Optimized calcein-based reaction mixes were used (see Appendix D.1.1) and fluorescence was measured on a Biorad CFX96 thermocycler. Here we show results for the MT primers with the destabilizing G nucleotide at the -3 position (Table 2.7). The MT primers selectively amplified the MT D435V plasmid (Tt ≈ 70 minutes) versus the WT H37Rv plasmid (Tt ≈ 120 minutes). No amplification was observed in the NTC samples.

2.2.5 LAMP Analysis of Clinical Sputum Samples

Drug susceptibility testing (DST) is generally performed as a secondary diagnostic in order to assess *M. tuberculosis* sensitivity to several drugs through titrated drug culture[62]. This process requires significant infrastructure, personnel, and power requirements, and can take up to 8 weeks in order to yield a result. A recent alternative has been introduced with the Cepheid GeneXpert[14]. The GeneXpert is a benchtop machine for automated sample preparation and nucleic acid amplification. Assays have been designed for a range of targets, including *M. tuberculosis*. However, this system is prohibitively expensive and time-consuming for unsubsidized use in RLR settings[63,64]. Efforts have also been made to develop lateral flow assays for M. tuberculosis genotyping, however these methods still require expensive and time-consuming PCR equipment and require highly-trained staff in order to minimize erroneous results. Table 2.8 compares current methods for TB diagnosis with our proposed system.

Table 2.7 Comparison of TB diagnostic technologies for RLR settings.

Technology	Time to Answer	Sensitivity	Drug Susceptibility?	Automated Components	Cost	Commercial Example
Sputum Smear Microscopy	2 hours	40 - 60%	No	None	$	QBC FAST AFB
Cell Culture	8 weeks		No	Analysis	$	
Drug Susceptibility Culture	8 weeks	80+%	Yes	Analysis	$$	TB MODS Test Kit
Benchtop PCR	4 hours	85+%	Yes	None	$$$	CFX96
Automated PCR	2 hours	85+%	Yes	Sample Prep, Analysis	$$$$	Genexpert
Isothermal Amplification	1 hour	N/A	Yes	Analysis	$$	TwistDx
µBAR	1 hour	N/A	Yes	Analysis	$	N/A

In our first iteration, we tested our LAMP assay with patient samples provided by our collaborators at Stellenbosch. We confirmed that our assay performs adequately on boiled (inactivated) sputum samples (Figure 2.10).

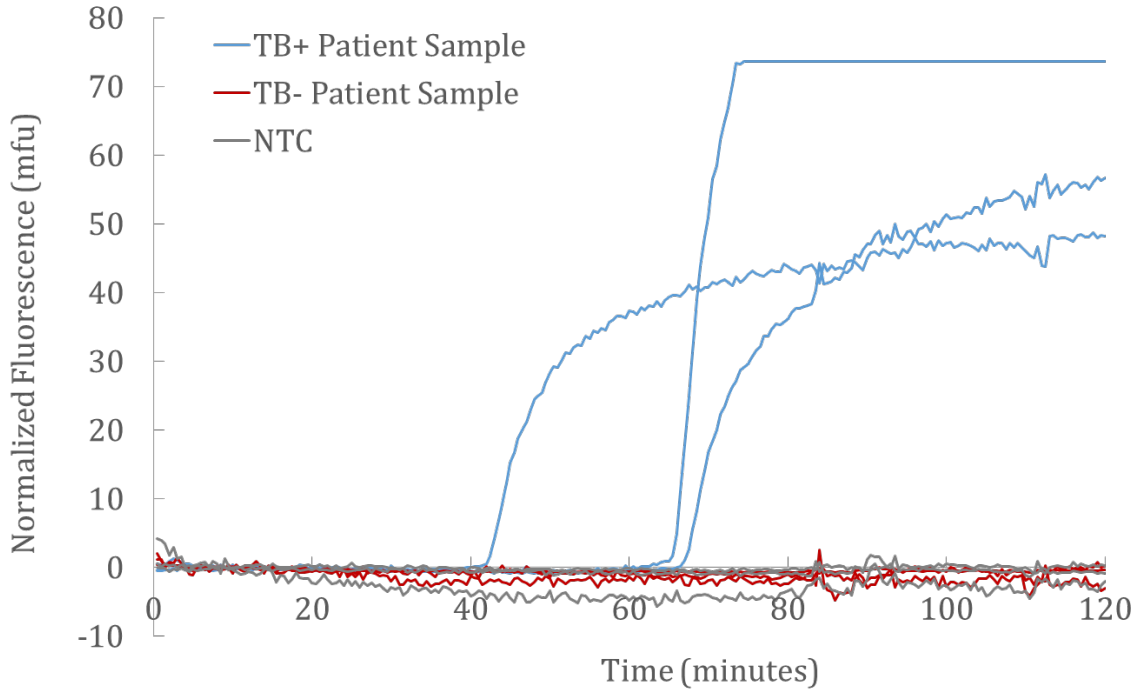

Figure 2.10 LAMP analysis of boiled sputum samples. Patient samples were provided by collaborators at Stellenbosch, pretreated by incubation with NALC-NaOH and boiling (see Appendix A.2.**8**). Optimized calcein-based reaction mixes were used (see Appendix D.1.1) to amplify a TB+, TB-, and NTC sample in triplicate. WT FIP and BIP primers were used in all reactions (Table 2.6). Real-time fluorescence was measured on a Roche LightCycler thermocycler. This reaction configuration showed amplification within 40 -60 minutes for a TB+ patient sample. No amplification was seen for the TB- or NTC samples within 120 minutes.

These results represent a first step in the development of a system for *Mtb* detection, quantification, and drug susceptibility testing. We believe this technology can be further extended for use in an integrated system containing sample preparation components to work with viscous sputum samples.

2.2.6 Lyophilization of LAMP Reagents

Diagnostic tools deployed in RLR settings should offer user-friendly and equipment-free operation (**see section 1.1.1**). In particular, most molecular diagnostic assays require environmentally-sensitive reagents. These reagents add complexity to the assay (requiring a user to manually dispense them into the diagnostic system) while further necessitating temperature and humidity control that is often unreliable or entirely unavailable. A common method to address both of these issues involves the direct immobilization of reagents on diagnostic system substrates through lyophilization (commonly referred to as "freeze-drying"). In this way, diagnostic systems can be pre-assembled with all required reagents dried in place, for passive resuspension with the sample fluid.

The lyophilization procedure involves cooling a liquid material below its critical point, followed by sublimation in a low-pressure environment. This process is leveraged in the pharmaceutical and diagnostics industries to facilitate the functional preservation of sensitive reagents at room temperature. Lyophilization further accelerates resuspension of the dried reagents through the formation of pores during the process.

We tested a number of configurations for lyophilization, including off- and on-chip reaction mixes. However, we were unable to achieve a reproducible lyophilization process that would lead to a significant fluorescence change from start to finish of a LAMP reaction (see Appendix A.2.7 for details on lyophilization reaction conditions tested). We thus used fresh reagents in all on-chip reactions.

2.3 Design of Microfluidic Chips for Multiplexed NA Assay

2.3.1 LAMP Analysis Chip Design

We have designed a microfluidic chip in a 96-well format for the simultaneous analysis of up to 6 different samples for up to 16 different nucleic acid biomarkers. The chip was designed to meet the following criteria: (1) Detect one or more target sequences in parallel, (2) Provide an assay sensitivity as low as 1 copy/μL, (3) Prevent cross-contamination due to amplicon exposure between wells and between chips, (4) Operate under passive sample loading, (5), Minimize bubble formation during operation, (6) Facilitate replicate analysis, (7) Facilitate a simple and scalable fabrication process, and (8) Facilitate optional readout on standard fluorescent plate readers. These design constraints, and their associated design outputs are summarized in Table 2.9.

Table 2.8 Design inputs and outputs for LAMP analysis chip.

Requirement Input	Design Output
Multiplexed detection	Multiple reaction chambers
Assay sensitivity < = 1 copy/μL	Total reaction chamber volume per analyte > = 1 μL (ensures a minimum of 1 copy amplified)
Prevention of cross-contamination	Sealed, dead-end reaction chambers Disposable

Passive sample loading	Degas-driven flow Microfluidic solution-isolated pump
Prevention of bubble formation	Degas-driven flow Microfluidic solution-isolated pump Sealing layer
Replicate analysis	Multiple sample inlets per chip
Simple and scalable fabrication	Soft lithography compatible with injection-molding techniques
Readout on fluorescent plate readers	Reaction chamber pitch equivalent to 384-well plates

The wells were designed to range from 1.5 to 3 mm in diameter and set at a pitch of 4.5 mm (equivalent to a 384 well plate, allowing comparative analysis in a plate reader). The chamber heights were designed to be between 100 - 300 μm, yielding individual chamber volumes ranging from 176 nL to 2,120 nL. Channels were designed to yield identical fluidic resistance between the inlet and each of its connected reaction chambers. The chip design is shown in Figure 2.11.

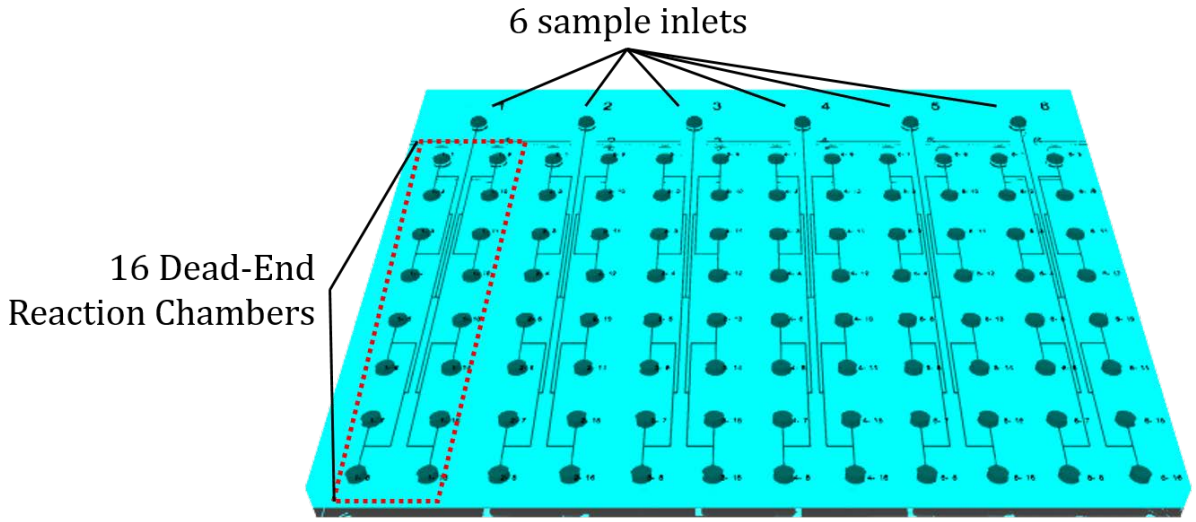

Figure 2.11 Microfluidic chip for multiplexed LAMP analysis. Six separate sample inlets enable testing of multiple analytes or replicates of a single analyte on one chip. The PDMS substrate has 16 dead-end reaction chambers positioned with equal fluidic resistance from each sample inlet (see Appendix B.1 for CAD designs).

The chambers are cast in polydimethylsiloxane (PDMS) using standard soft lithography techniques[65] and bonded to a thin transparent elastomer base using oxygen plasma[66]. The chip is UV sterilized for 24 hours after bonding. After bonding, the device is exposed to a vacuum of ~300 mTorr for >1 hour, and then vacuum sealed using a commercial food sealer. Due to the elastomeric pore structure of the PDMS, the chip will begin drawing in sample introduced into the inlets immediately upon exposure to atmospheric pressure. Samples can be completely loaded in less than 1 hour. This time can be significantly reduced with smaller reaction chambers and from design modifications (described later). Chips can

be stored vacuum sealed for at least one month (likely much longer) without loss of vacuum. This degas-driven loading method enables us to use dead-end reaction chambers which help ensure that amplicons remain on chip and reduce the risk of contamination between amplification runs.

The expected assay sensitivity can be calculated as a function of sample volume analyzed, with the assumption that a minimum of 1 amplicon is required for a signal to be observed[67]. In practice, an additional assay efficiency factor would reduce this sensitivity based on practical limitations (amplification inefficiency, damage to the target strand, and loss of target strand due to non-specific absorption to device walls). Reaction chamber dimensions were selected in order to meet assay sensitivity requirements.

2.3.2 Characterization of Degas Loading

Degas-driven fluidic actuation (DFA) is a nascent technique that facilitates passive loading of microfluidic devices. DFA leverages gas-permeable substrate materials (such as polydimethylsiloxane, PDMS) to enable sample loading by the negative pressure stored in a device that has been pre-treated in a low-pressure environment (Figure 2.12). DFA obviates the need for any external equipment or power sources at the point of use, while providing more controlled and rapid flow rates than other passive loading methods (such as capillary action or gravity-driven flow). Furthermore, DFA offers a passive mechanism to load fluid into complex geometries and dead-end channels. DFA was first implemented by Maeda et al.[68,69] and was further coupled with trench-based blood separation by Lee et al.[70,71].

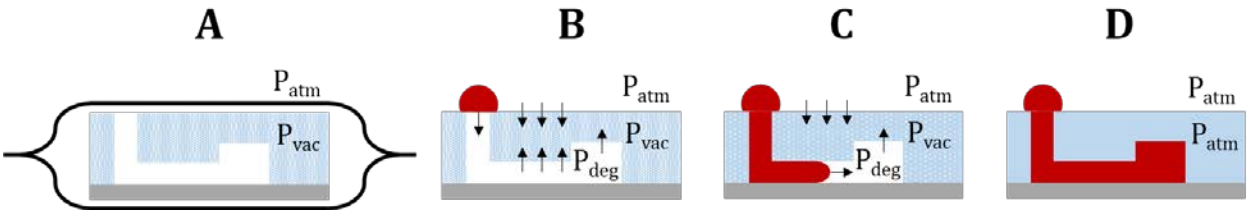

Figure 2.12 Degas-driven fluidic actuation (DFA). (A) A DFA chip is previously incubated in a vacuum chamber and hermetically sealed. The porous material of the chip has a reduced gas pressure ($P_{vac} < P_{atm}$). (B) The DFA chip is removed from the sealed package and a sample is placed on an inlet to a dead-end channel. A flux of gas from the channels and the external environment begins ($P_{vac} < P_{deg} < P_{atm}$). The higher P_{atm} relative to P_{deg} creates a pressure gradient across the liquid sample, generating a pressure-driven flow into the channel. (C) The liquid sample continues to load into the channel, with any potential bubbles removed through the flux of gas from the channel to the porous material. As the porous material is exposed to atmospheric pressure, the pressure inside begins to equilibrate towards P_{atm}.

In an example DFA system, a PDMS microfluidic chip is initially placed in a vacuum chamber to lower the gas content and thus pressure in the PDMS material (it can take up to ~30 minutes for the PDMS to reach an equilibrium pressure with the vacuum, depending on the material properties). This chip may be used immediately or vacuum-sealed for later use. Upon exposure to atmospheric pressure, gas will begin to dissolve into the "degassed" PDMS material at a rate defined by Fick's First Law (Equation 2.1). Gas will pass through all

surfaces of the chip, including the microfluidic channel walls. When liquid is placed on an inlet, gas will be isolated in the microfluidic channels between the liquid plug and the microfluidic channel walls. As this isolated gas passes through the surfaces of the microfluidic channels, a pressure gradient develops in the channels by which the leading edge of the plug is at a lower pressure than the external liquid at atmospheric pressure. The liquid is thus pushed into the channel by the higher atmospheric pressure at the inlet, leading to Poiseuille flow.

$$J = -D\frac{\delta C}{\delta x}$$

Equation 2.1 Fick's first law.

The concentration gradient within the microfluidic channel walls is defined by Fick's Second law (Equation 2.2). By solving for the gas concentration in the chip with a microfluidic geometry of one-dimensional diffusion in a plane sheet[72] (Equation 2.3), the effective flux of gas as a function of time can be calculated.

$$\frac{\delta C}{\delta t} = D\frac{\delta^2 C}{\delta x^2}$$

Equation 2.2 Fick's second law.

$$C = C_1 + (C_2 - C_1)\frac{x}{l} + \frac{2}{\pi}\sum_{l}^{\infty}\frac{C_2\cos n\pi - C_1}{n}\sin\left(\frac{n\pi x}{l}\right)exp\left(-D\frac{n^2\pi^2 t}{l^2}\right) + \frac{2}{l}\sum_{l}^{\infty}\sin\left(\frac{n\pi x}{l}\right)exp\left(-D\frac{n^2\pi^2 t}{l^2}\right)\int_0^l f(x')\sin\left(\frac{n\pi x'}{l}\right)dx'$$

Assume:

C = C1, x = 0, $t \geq 0$,
C = C2, x = l, $t \geq 0$,
C = f(x), $0 < x < l$, $t = 0$,

Equation 2.3 Solution to Fick's second law for a planar surface.

Microfluidic devices have traditionally been fabricated through rapid prototyping techniques involving a limited variety of materials, including polydimethyl siloxane (PDMS), glass, and several polymers. Most microfluidic systems include a molded "device" component that is bonded to a flat substrate component. Although a number of substrates have been used in the literature, glass has been the workhorse base due to its optical transparency, versatile surface chemistry, and biocompatibility. For point of care diagnostics (POC-Dx) applications, however, thin polymeric films promise to reduce device costs while facilitating simpler assembly.

In order to meet the needs of our chip development prototyping for the mBAR, we developed a technique using commercially available PCR seals (Biorad) (see Appendix A.6).

These devices are cheaper, more versatile, and easier to assemble than comparable glass-based devices. With this optimization, LAMP chips could be fully loaded within 20 minutes.

2.3.3 Optimization of Degas Loading with Solution-Isolated Pumps

Although DFA offers a number of advantages over existing active and passive actuation mechanisms, it yields flow rates and loading times that are sensitive to pre-treatment conditions, as well as operation timing at the point of use. Furthermore, as the loading rate is proportional to the surface area of the channels through which the plugged gas is diffusing, the flow rate of solution decreases drastically as the channel loads.

In order to address these issues, we have developed a microfluidic solution-isolated pump (μSIP) for use in RLR settings. The system was initially developed specifically to enhance the loading of dead-end chambers in PDMS chips (see Appendix B.3). The basic system consists of a solution loading channel and proximal degas channels (Figure 2.13). The fluidic loading channel must be plugged at one end with the liquid sample, and have no other fluid outlets. The proximal degas channels may either be actively pumped through a suction mechanism, or passively pumped through degas chambers with a large surface area (thus maintaining a reduced pressure in the degas channels).

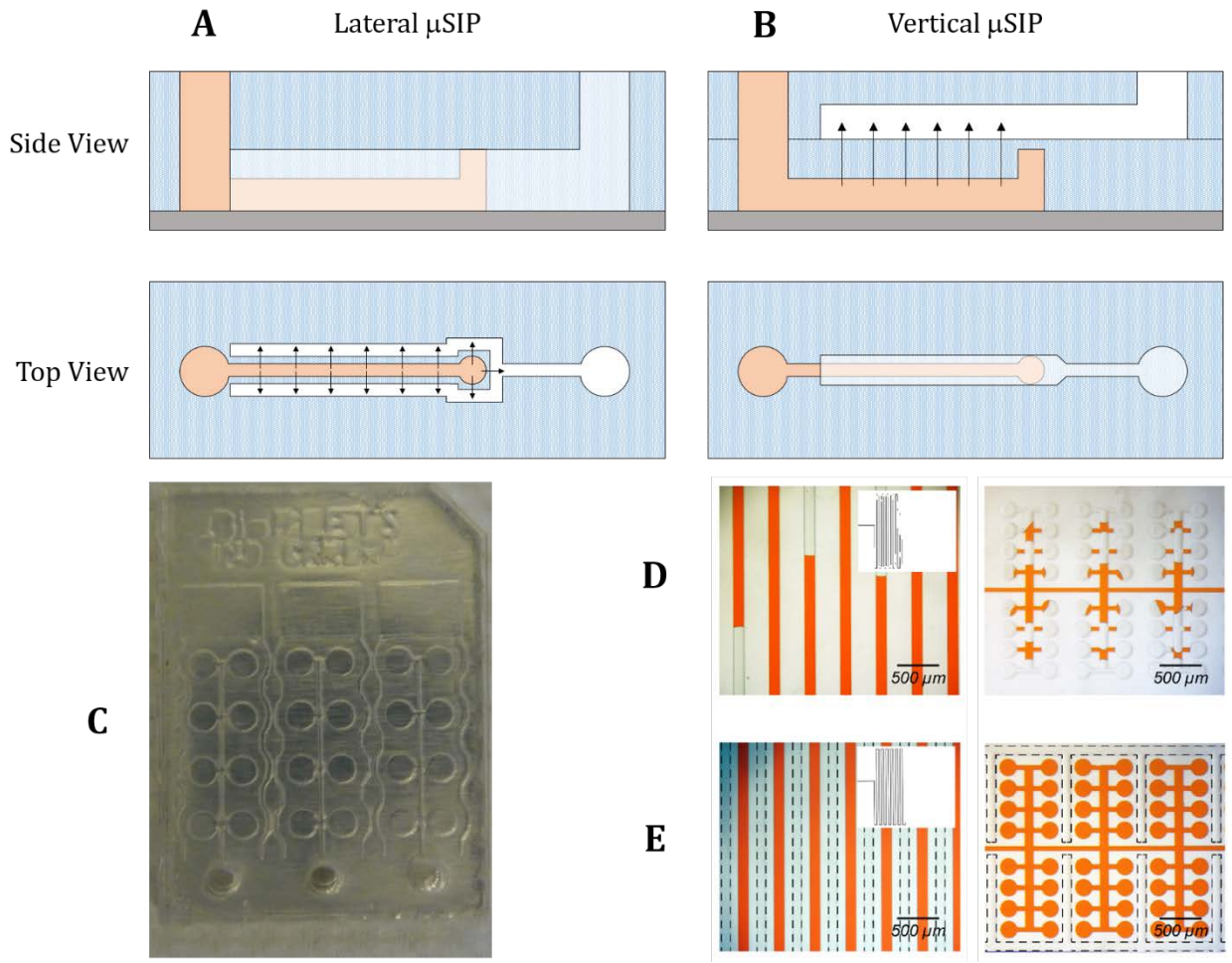

Figure 2.13 Microfluidic solution isolated pump (μSIP). (A) In the lateral μSIP configuration, flanking degas channel (white) provide a lower pressure to generate flow in the solution loading channel (orange). This pressure may be provided in a passive manner (by a large chamber in a degassed porous substrate) or an active manner (by an active pumping of gas from the outlet of the flanking degas channel). This configuration has the advantage of only needing a single device layer for fabrication. (B) In the vertical mSIP configuration, flanking degas channels (white) are made in a second substrate which is bound to the top of the top of the substrate containing the solution loading channel (orange). Similarly to the lateral configuration, a lower pressure in the degas flanking channel generates flow in the solution loading channel. (C) Initial prototype of a passive μSIP device. This device was fabricated with an aluminum substrate and layered pressure-sensitive adhesive to form channels, with a thin PDMS membrane placed on top. Inlets and dead-end reaction chambers were designed similar to the standard LAMP chip design, with the addition of flanking channels joined to a degas pump chamber. While this is a passive chamber (adding additional surface area for degassing), active pumps may also be developed (see Appendix B.1 for CAD designs of chips). (D) Conventional pressure-driven loading of a chip leads to bubbles and is impossible to load dead-end chambers. (E) μSIP enables dead-end channel loading with no bubbles.

We found the addition μSIP components could significantly reduce sample loading time in DFA systems. We further characterized μSIP performance as a function of channel geometry and the driving degas pressure (Figure 2.14). As expected, a decrease in the thickness of the wall between the proximal degas and solution loading channels also reduced the loading time (due to reduced diffusion barrier length). Similarly, increasing the channel width increased the loading time due to a reduced surface area to volume ratio. We further demonstrated that a decrease in the driving pressure of the proximal degas channel would increase sample loading rate due to an increased pressure gradient driving the in the solution loading channel.

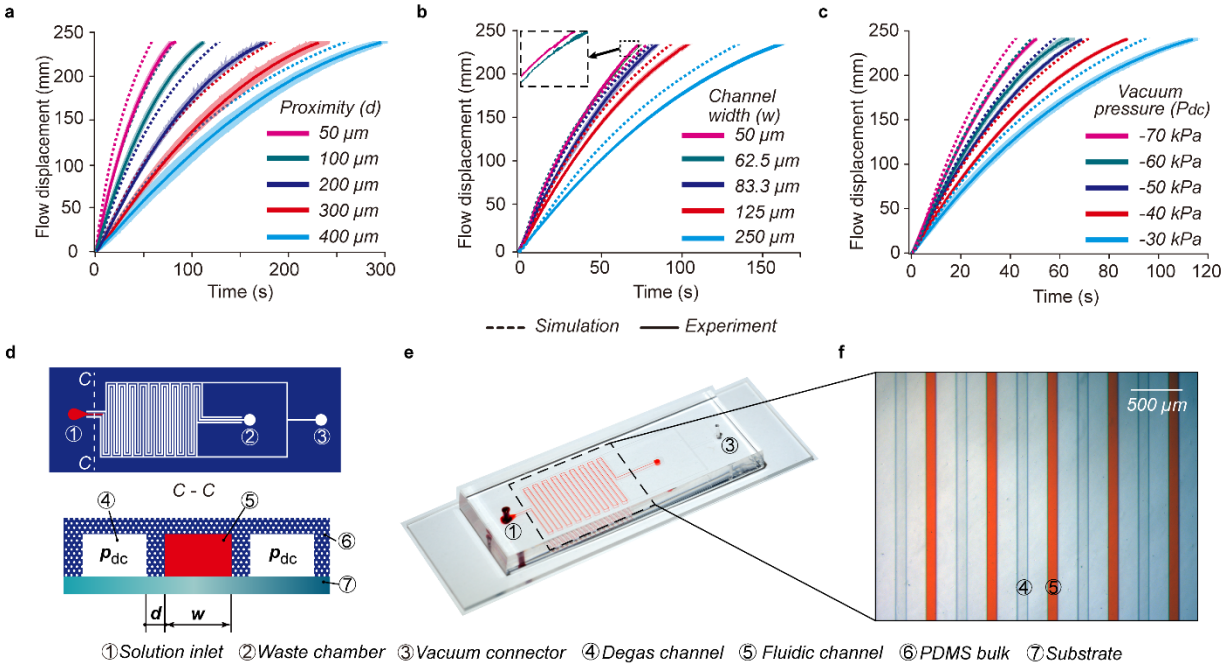

Figure 2.14 Characterization of μSIP Flow. The dotted lines represent simulation results, while the solid line depicts the experimental data. The experimental data is plotted as an average (central solid line) and two standard deviations (shaded region) from three independent measurements. (A) The fluid displacement (in mm) into the fluidic channels is plotted as a function of time for different proximity distances, d. It was observed that an increase in proximity resulted in an increase in the fluid flow velocity. (B) The fluid displacement into the fluidic channels is plotted as a function of time for different fluidic channel widths, which affects the degassing surface area to channel volume ratio (SAVR). An increase in the fluidic channel width, which leads to a reduction in SAVR, was observed to result in a decrease in the fluid flow velocity. (C) The fluid displacement into the fluidic channels is plotted as a function of time for different vacuum pressures (relative to atmospheric pressure) applied to the degas channel network. It was observed that a decrease in the applied pressure resulted in an increase in the fluid flow velocity. (D) Layout of the devices used for characterization. The device layout consisted of serpentine fluidic channels surrounded by flanking degas channels on both sides. A vacuum was applied to the degas channels using an external vacuum source through the port. (E) Image of the single layer PDMS chip bonded onto a glass substrate device used for characterization. (F) Microscope image of the degas channel and fluidic channel networks.

2.4 Integrated Microfluidic Biomolecular Amplification Reader

2.4.1 μBAR System Overview

We further developed an automated system to analyze fluorescent signals produced produced as a result of isothermal amplification assays. Termed a "microfluidic biomolecular amplification reader" (μBAR), this system generates and maintains an isothermal assay temperature, illuminates the microfluidic chip, and detects fluorescence emission from the reaction chambers via a phototransistor array (Figure 2.15)[73,74]. The μBAR provides a user with a simple, inexpensive, and contained system in which a chip may be placed for isothermal amplification and analysis. The system provides users with a touch screen interface to initiate, monitor, and review test. A thorough characterization of μBAR power, heating, and photometric performance can be found in Appendix D.1.2.

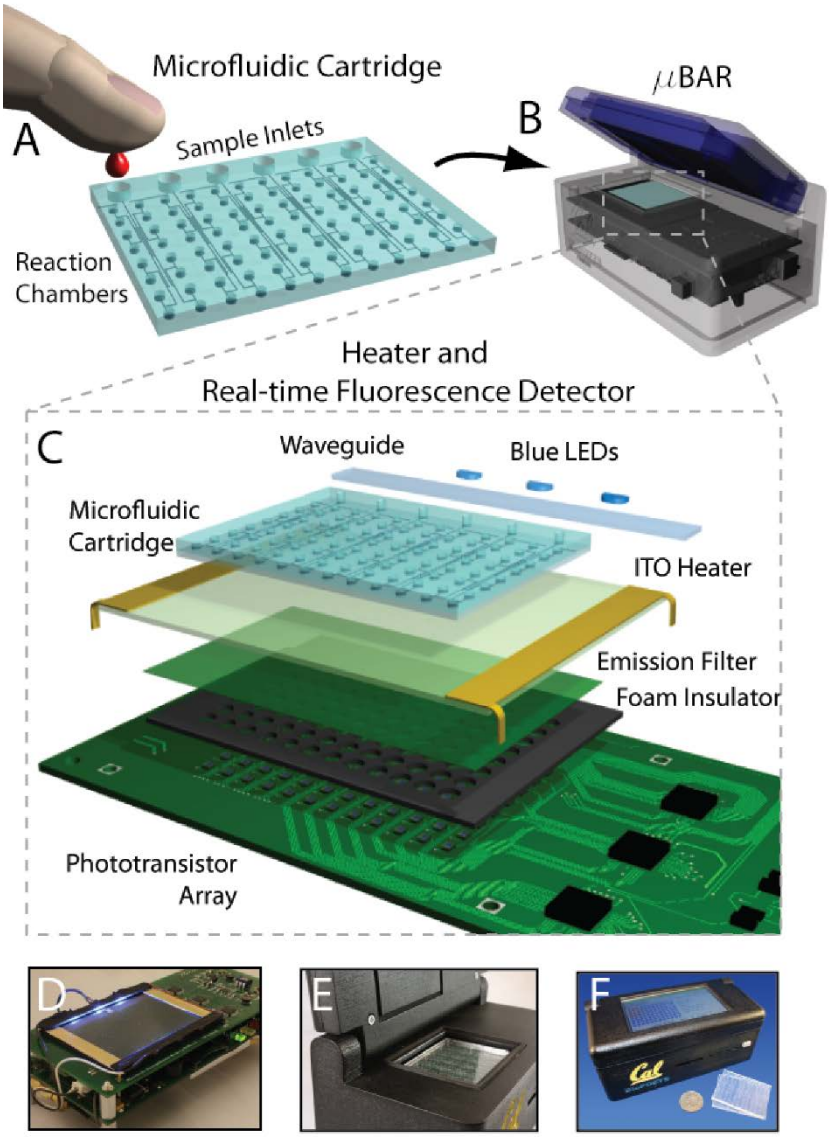

Figure 2.15 The μBAR System Overview. (A) A disposable microfluidic cartridge is loaded with sample fluid (e.g. blood) via SIMBAS degas-driven flow. This technique proceeds

automatically without any pumping or external power. LAMP reaction mix (primers, enzymes, dNTPs, etc.) may be lyophilized on-chip or mixed with the sample before loading. After 30 min, the chip is fully loaded and is placed in the μBAR instrument. (B–C) The instrument features blue excitation LEDs to the side of the chip. Waveguides help to ensure the light is efficiently coupled to the PDMS chip without stray scattering. An ITO substrate provides uniform heating across the reaction chambers of the chip. Below this substrate is a green plastic emission filter following by a neoprene foam barrier with holes which optically isolate each phototransistor on the PCB underneath. The neoprene provides both thermal and optical insulation to the system. The microfluidic chip sticks to the surface of the ITO via van der Waals forces, maximizing thermal transfer and ensuring that the chip does not move during heating. (D) μBAR with case removed, showing side LED illumination through waveguides. (E) μBAR with chip inserted. (D) Assembled handheld μBAR instrument and microfluidic cartridges with a US quarter for size comparison.

2.4.2 Analysis of μBAR Performance for HIV Detection

We performed a proof-of-concept assay to quantify fluorescent signals generated by a LAMP assay to detect HIV spiked into solution (Figure 2.16). Two independent samples are shown, one containing a plasmid with the target gene at a concentration of 10^3 copies/μL, and the other containing no DNA (negative template control, NTC). The chips were vacuum treated at 300 mTorr, samples were dropped onto the chip (20 μL per inlet), and the chip was placed into the μBAR instrument upon completion of sample loading. Amplification is clearly visible in the chambers with the target HIV integrase plasmid as compared with the NTC chambers (Figure 2.16A). Within 70 minutes, the positive samples exhibit readily detectable signals above the NTC background (Figure 2.16B). When run on a conventional quantitative PCR thermocycler (Bio-Rad CFX96), the amplification occurs somewhat earlier (around 40 minutes). This discrepancy in time may be due to the differences in reaction volumes and surface-to-volume ratios of the two assays (each on-chip chamber contains about 1.2 μL sample volume, whereas the full 20 μL is in one reaction tube on the thermocycler). LAMP reagents may be adsorbing to the PDMS channels as they enter the chip, leading to lower concentrations overall within the wells and a heterogeneity from well-to-well (note that the final intensity varies somewhat from well to well). More work needs to be done to find an effective surface treatment method which enables vacuum-driven loading but prevents adsorption. As with qPCR (which can also be quite heterogeneous from well to well), we recommend running assays in duplicate or triplicate with the μBAR to mitigate this heterogeneity. Despite these shortcomings, our results indicate that the μBAR is able to detect amplification.

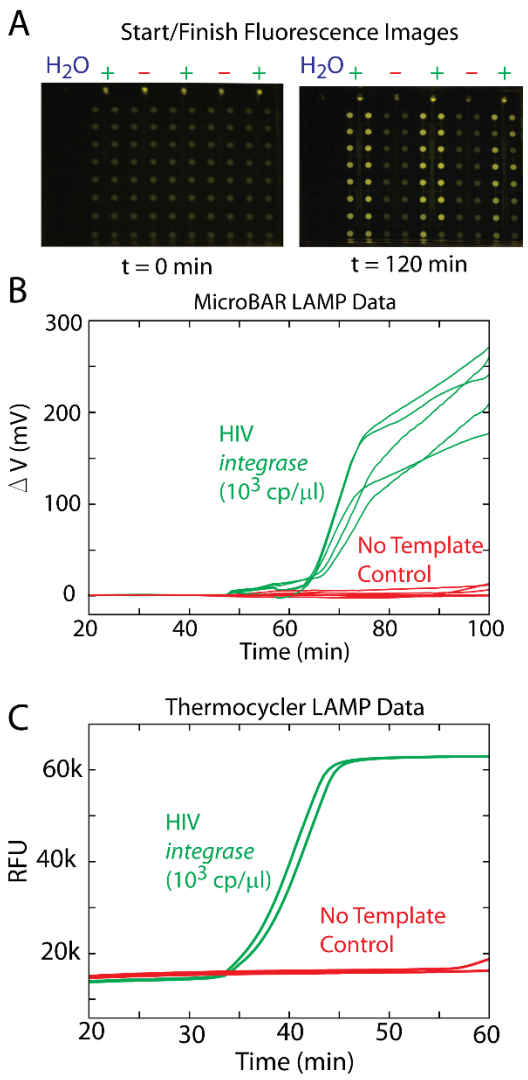

Figure 2.16 μBAR LAMP vs. Thermocycler LAMP. Results of the LAMP reaction for detection of the HIV integrase gene using both the μBAR and a conventional thermocycler. (A) Presence of the HIV integrase gene target results in an increase in fluorescence from the reaction wells, as seen in these before and after chip photos. (B) Photoamplifier voltages from 5 independent reaction wells are displayed here, all showing a positive result after about 70 minutes. (C) The same assay run on a conventional thermocycler shows positive results slightly faster (40 minutes), possibly due to the differences in assay volumes and thermal transfer characteristics.

2.5 Discussion

In this chapter we demonstrated the development of a nucleic acid analysis system for use in RLR settings. We first developed primers for isothermal amplification of target sequences in a LAMP reaction. These primers were designed to selectively detect SNPs encoding drug resistance in *M. tuberculosis*. We demonstrated differential amplification rates with these initial primer designs, and further enhanced the selectivity through the addition of 3' destabilizing bases. We demonstrated the function of our LAMP primer set in the detection of *M. tuberculosis* in samples from infected patients.

We further developed a microfluidic system to enable rapid and multiplexed analysis while avoiding any issues with bubble formation. We developed a DFA mechanism for passive loading of reaction chambers, and further enhanced loading rate through the addition of a μSIP mechanism. Although our initial implementation of μSIP was in a passive DFA system, this technology can be extended to active systems with alternate pumping mechanisms.

We further developed an integrated μBAR system for automated real-time analysis of fluorescence in microfluidic chips during isothermal amplification. We demonstrated critical system performance parameters, including signal linearity, thermal uniformity, and battery discharge. We demonstrated amplification in the μBAR system with a model LAMP system. We believe these tools hold great promise for implementation into a fully-integrated diagnostic system for use in RLR settings.

2.6 References

1. Tang, Y.-W., Procop, G. W. & Persing, D. H. Molecular diagnostics of infectious diseases. *Clin Chem* **43,** 2021–2038 (1997).
2. Debnath, M., Prasad, G. B. K. S. & Bisen, P. S. *Molecular Diagnostics: Promises and Possibilities*. (Springer Netherlands, 2010). at <http://www.springerlink.com/content/978-90-481-3260-7#section=656588&page=1>
3. Gilbert, G. L. Molecular diagnostics in infectious diseases and public health microbiology: cottage industry to postgenomics. *Trends Mol. Med.* **8,** 280–287 (2002).
4. Rao, J. R. *Molecular Diagnostics: Current Technology and Applications*. (Taylor & Francis, 2006). at <http://www.amazon.com/dp/190493319X>
5. Pang, T. & Peeling, R. W. Diagnostic tests for infectious diseases in the developing world: two sides of the coin. *Trans. R. Soc. Trop. Med. Hyg.* **101,** 856–857 (2007).
6. Ginsberg, A. M. & Spigelman, M. Challenges in tuberculosis drug research and development. *Nat. Med.* **13,** 290–4 (2007).
7. Halldorsson, S., Lucumi, E., Gómez-Sjöberg, R. & Fleming, R. M. T. Advantages and challenges of microfluidic cell culture in polydimethylsiloxane devices. *Biosens. Bioelectron.* **63,** 218–31 (2015).
8. Rameez, S., Mostafa, S. S., Miller, C. & Shukla, A. A. High-throughput miniaturized bioreactors for cell culture process development: reproducibility, scalability, and control. *Biotechnol. Prog.* **30,** 718–27
9. Sasaki, N. *et al.* A palmtop-sized microfluidic cell culture system driven by a miniaturized infusion pump. *Electrophoresis* **33,** 1729–35 (2012).
10. Wilson, M. J., Weightman, A. J. & Wade, W. G. Applications of molecular ecology in the characterization of uncultured microorganisms associated with human disease. *Rev. Med. Microbiol.* **8,** (1997).
11. Mullis, K. Process for amplifying nucleic acid sequences. (1987). at <http://www.google.com/patents/US4683202>
12. Saiki, R. *et al.* Enzymatic amplification of beta-globin genomic sequences and restriction site analysis for diagnosis of sickle cell anemia. *Science (80-.).* **230,** 1350–1354 (1985).

13. Zhang, C. & Xing, D. Miniaturized PCR chips for nucleic acid amplification and analysis: latest advances and future trends. *Nucl. Acids Res.* **35,** 4223–4237 (2007).
14. Zeka, A. N., Tasbakan, S. & Cavusoglu, C. Evaluation of the GeneXpert MTB/RIF assay for rapid diagnosis of tuberculosis and detection of rifampin resistance in pulmonary and extrapulmonary specimens. *J. Clin. Microbiol.* **49,** 4138–41 (2011).
15. Craw, P. & Balachandran, W. Isothermal Nucleic Acid Amplification Technologies for Point-of-Care Diagnostics: A Critical Review. *Lab Chip* (2012). doi:10.1039/c2lc40100b
16. Gill, P. & Ghaemi, A. Nucleic acid isothermal amplification technologies: a review. *Nucleosides. Nucleotides Nucleic Acids* **27,** 224–43 (2008).
17. Liu, C., Mauk, M. G., Hart, R., Qiu, X. & Bau, H. H. A self-heating cartridge for molecular diagnostics. *Lab Chip* **11,** 2686–92 (2011).
18. Kirby, B. J. *Micro- and Nanoscale Fluid Mechanics: Transport in Microfluidic Devices*. (Cambridge University Press, 2010). at <http://books.google.com/books?id=y7PB9f5zmU4C&pgis=1>
19. Notomi, T. *et al.* Loop-mediated isothermal amplification of DNA. *Nucleic Acids Res* **28,** E63 (2000).
20. Piepenburg, O., Williams, C. H., Stemple, D. L. & Armes, N. A. DNA Detection Using Recombination Proteins. *PLoS Biol* **4,** e204 (2006).
21. Ali, M. M. *et al.* Rolling circle amplification: a versatile tool for chemical biology, materials science and medicine. *Chem. Soc. Rev.* **43,** 3324–41 (2014).
22. Zanoli, L. M. & Spoto, G. Isothermal amplification methods for the detection of nucleic acids in microfluidic devices. *Biosensors* **3,** 18–43 (2013).
23. Fire, a & Xu, S. Q. Rolling replication of short DNA circles. *Proc. Natl. Acad. Sci. U. S. A.* **92,** 4641–4645 (1995).
24. Liu, D., Daubendiek, S. L., Zillman, M. a, Ryan, K. & Kool, E. T. Rolling Circle DNA Synthesis: Small Circular Oligonucleotides as Efficient Templates for DNA Polymerases. *J. Am. Chem. Soc.* **118,** 1587–1594 (1996).
25. Compton, J. Nucleic acid sequence-based amplification. *Nature* **350,** 91–2 (1991).
26. Deiman, B., van Aarle, P. & Sillekens, P. Characteristics and applications of nucleic acid sequence-based amplification (NASBA). *Mol. Biotechnol.* **20,** 163–179 (2002).
27. Bahrami, A. R. *et al.* Use of fluorescent DNA-intercalating dyes in the analysis of DNA via ion-pair reversed-phase denaturing high-performance liquid chromatography. *Anal. Biochem.* **309,** 248–52 (2002).
28. Iwasaki, M. *et al.* Validation of the Loop-Mediated Isothermal Amplification Method for Single Nucleotide Polymorphism Genotyping with Whole Blood. *Genome Lett.* **2,** 119–126(8) (2003).
29. Fischbach, J., Xander, N. C., Frohme, M. & Glökler, J. F. Shining a light on LAMP assays - A Comparison of LAMP Visualization Methods Including the Novel Use of Berberine. *Biotechniques* **58,** 189–194 (2015).
30. Whitcombe, D., Theaker, J., Guy, S. P., Brown, T. & Little, S. Detection of PCR products using self-probing amplicons and fluorescence. *Nat. Biotechnol.* **17,** 804–7 (1999).
31. Larsson, E. M., Langhammer, C., Zoric, I. & Kasemo, B. Nanoplasmonic Probes of Catalytic Reactions. *Science (80-.).* **326,** 1091–1094 (2009).

32. Chen, W. *et al.* Nanoparticle Superstructures Made by Polymerase Chain Reaction: Collective Interactions of Nanoparticles and a New Principle for Chiral Materials. *Nano Lett.* doi:10.1021/nl900726s
33. Lin, Y. *et al.* Electrochemical Branched-DNA Assay for Polymerase Chain Reaction-Free Detection and Quantification of Oncogenes in Messenger RNA. *Anal. Chem.* (2008). at <http://pubs3.acs.org/acs/journals/doilookup?in_doi=10.1021/ac801263r>
34. Ahmed, M. U. *et al.* Electrochemical genosensor for the rapid detection of GMO using loop-mediated isothermal amplification. *Analyst* **134,** 966–972 (2009).
35. Carpini, G., Lucarelli, F., Marrazza, G. & Mascini, M. Oligonucleotide-modified screen-printed gold electrodes for enzyme-amplified sensing of nucleic acids. *Biosens. Bioelectron.* **20,** 167–75 (2004).
36. Kurosaki, Y. *et al.* Rapid and simple detection of Ebola virus by reverse transcription-loop-mediated isothermal amplification. *J Virol Methods* **141,** 78–83 (2007).
37. Nagamine, K., Hase, T. & Notomi, T. Accelerated reaction by loop-mediated isothermal amplification using loop primers. *Mol. Cell. Probes* **16,** 223–229 (2002).
38. Aoi, Y., Hosogai, M. & Tsuneda, S. Real-time quantitative LAMP (loop-mediated isothermal amplification of DNA) as a simple method for monitoring ammonia-oxidizing bacteria. *J. Biotechnol.* **125,** 484–491 (2006).
39. Goto, M., Honda, E., Ogura, A., Nomoto, A. & Hanaki, K.-I. Colorimetric detection of loop-mediated isothermal amplification reaction by using hydroxy naphthol blue. *Biotechniques* **46,** 167–172 (2009).
40. Francois, P. *et al.* Robustness of a loop-mediated isothermal amplification reaction for diagnostic applications. *FEMS Immunol. Med. Microbiol.* **62,** 41–8 (2011).
41. Mori, Y. & Notomi, T. Loop-mediated isothermal amplification (LAMP): a rapid, accurate, and cost-effective diagnostic method for infectious diseases. *J. Infect. Chemother.* **15,** 62–69 (2009).
42. Lu, X., Mo, Z.-Y., Zhao, H.-B., Yan, H. & Shi, L. LAMP-based method for a rapid identification of Legionella spp. and Legionella pneumophila. *Appl. Microbiol. Biotechnol.* **92,** 179–87 (2011).
43. Han, F., Wang, F. & Ge, B. Detecting Potentially Virulent Vibrio vulnificus Strains in Raw Oysters by Quantitative Loop-Mediated Isothermal Amplification. *Appl. Environ. Microbiol.* **77,** 2589–95 (2011).
44. Ahmed, M. U., Hasan, Q., Mosharraf Hossain, M., Saito, M. & Tamiya, E. Meat species identification based on the loop mediated isothermal amplification and electrochemical DNA sensor. *Food Control* **21,** 599–605 (2010).
45. Connelly, J. T., Rolland, J. P. & Whitesides, G. M. A 'Paper Machine' for Molecular Diagnostics. *Anal. Chem.* **87,** 7595–601 (2015).
46. Fang, X., Liu, Y., Kong, J. & Jiang, X. Loop-Mediated Isothermal Amplification Integrated on Microfluidic Chips for Point-of-Care Quantitative Detection of Pathogens. *Anal. Chem.* **82,** 3002–3006 (2010).
47. Asiello, P. J. & Baeumner, A. J. Miniaturized isothermal nucleic acid amplification, a review. *Lab Chip* (2011). doi:10.1039/c0lc00666a
48. Ahmad, F. & Hashsham, S. a. Miniaturized nucleic acid amplification systems for rapid and point-of-care diagnostics: a review. *Anal. Chim. Acta* **733,** 1–15 (2012).

49. Tomita, N., Mori, Y., Kanda, H. & Notomi, T. Loop-mediated isothermal amplification (LAMP) of gene sequences and simple visual detection of products. *Nat. Protoc.* **3,** 877–882 (2008).
50. Torres, C. *et al.* LAVA: an open-source approach to designing LAMP (loop-mediated isothermal amplification) DNA signatures. *BMC Bioinformatics* **12,** 240 (2011).
51. Hosaka, N. *et al.* Rapid detection of human immunodeficiency virus type 1 group M by a reverse transcription-loop-mediated isothermal amplification assay. *J. Virol. Methods* **157,** 195–199 (2009).
52. Poon, L. L. M. *et al.* Sensitive and Inexpensive Molecular Test for Falciparum Malaria: Detecting Plasmodium falciparum DNA Directly from Heat-Treated Blood by Loop-Mediated Isothermal Amplification. *Clin Chem* **52,** 303–306 (2006).
53. Wilson, I. G. Inhibition and facilitation of nucleic acid amplification. *Appl. Environ. Microbiol.* **63,** 3741–3751 (1997).
54. Sachidanandam, R. *et al.* A map of human genome sequence variation containing 1.42 million single nucleotide polymorphisms. *Nature* **409,** 928–33 (2001).
55. Arnold, C. *et al.* Single-nucleotide polymorphism-based differentiation and drug resistance detection in Mycobacterium tuberculosis from isolates or directly from sputum. *Clin. Microbiol. Infect.* **11,** 122–30 (2005).
56. *Diagnostics for tuberculosis: Global demand and market potential*. (2006). at <http://www.who.int/tdr/publications/publications/tbdi.htm>
57. *Global tuberculosis report*. (World Health Organization, 2014). at <http://www.who.int/tb/publications/global_report/en/>
58. David, H. L. Probability Distribution of Drug-Resistant Mutants in Unselected Populations of Mycobacterium tuberculosis. *Appl. Microbiol.* **20,** 810–814 (1970).
59. Sandgren, A. *et al.* Tuberculosis drug resistance mutation database. *PLoS Med.* **6,** e2 (2009).
60. Ye, S., Dhillon, S., Ke, X., Collins, A. R. & Day, I. N. M. An efficient procedure for genotyping single nucleotide polymorphisms. *Nucleic Acids Res.* **29,** e88 (2001).
61. You, F. *et al.* BatchPrimer3: A high throughput web application for PCR and sequencing primer design. *BMC Bioinformatics* **9,** 253 (2008).
62. Dowdy, D. W., Chaisson, R. E., Maartens, G., Corbett, E. L. & Dorman, S. E. Impact of enhanced tuberculosis diagnosis in South Africa: A mathematical model of expanded culture and drug susceptibility testing. *Proc. Natl. Acad. Sci.* **105,** 11293–11298 (2008).
63. Evans, C. A. GeneXpert--a game-changer for tuberculosis control? *PLoS Med.* **8,** e1001064 (2011).
64. Meyer-Rath, G. *et al.* The impact and cost of scaling up GeneXpert MTB/RIF in South Africa. *PLoS One* **7,** e36966 (2012).
65. Duffy, D. C., McDonald, J. C., Schueller, O. J. A. & Whitesides, G. M. Rapid Prototyping of Microfluidic Systems in Poly(dimethylsiloxane). *Anal. Chem.* **70,** 4974–4984 (1998).
66. Eddings, M. A., Johnson, M. A. & Gale, B. K. Determining the optimal PDMS–PDMS bonding technique for microfluidic devices. *J. Micromechanics Microengineering* **18,** 067001 (2008).
67. Kreutz, J. E. *et al.* Theoretical Design and Analysis of Multivolume Digital Assays with Wide Dynamic Range Validated Experimentally with Microfluidic Digital PCR. *Anal. Chem.* **83,** 8158–8168 (2011).

68. Hosokawa, K., Sato, K., Ichikawa, N. & Maeda, M. Power-free poly(dimethylsiloxane) microfluidic devices for gold nanoparticle-based DNA analysis. *Lab Chip* **4,** 181–185 (2004).
69. Hosokawa, K., Omata, M., Sato, K. & Maeda, M. Power-free sequential injection for microchip immunoassay toward point-of-care testing. *Lab Chip* **6,** 236–241 (2006).
70. Dimov, I. K. *et al.* Stand-alone self-powered integrated microfluidic blood analysis system (SIMBAS). *Lab Chip* **11,** 845–850 (2011).
71. Liang, D. Y., Tentori, A. M., Dimov, I. K. & Lee, L. P. Systematic characterization of degas-driven flow for poly(dimethylsiloxane) microfluidic devices. *Biomicrofluidics* **5,** 24108 (2011).
72. Crank, J. The mathematics of diffusion. (1975).
73. Myers, F. B., Henrikson, R. H., Xu, L. & Lee, L. P. A point-of-care instrument for rapid multiplexed pathogen genotyping. *Proc. Annu. Int. Conf. IEEE Eng. Med. Biol. Soc. EMBS* 3668–3671 (2011). doi:10.1109/IEMBS.2011.6090619
74. Myers, F. B., Henrikson, R. H., Bone, J. & Lee, L. P. A Handheld Point-of-Care Genomic Diagnostic System. *PLoS One* **8,** (2013).

Chapter 3: Protein Detection by Aptamer-Mediated Amplification Probe Release

3.1 Introduction

3.1.1 Protein Detection and Quantification in Remote and Low-Resource Settings

Although many significant advances have been made in the design and implementation of protein-targeted molecular diagnostics since the first radio immunoassay performed in 1959[1], a commercial deployment meeting all of the needs for testing in remote and low-resource (RLR) settings has yet to be realized. The first experiments performed by Berson and Yalow demonstrated the potential sensitivity and specificity of antibody-mediated detection of target antigens[1]. The sensitivity of this biorecognition technique was further enhanced with the development of the enzyme immunoassay, enabling catalytic signal amplification and colorimetric readout in remote settings[2]. The enzyme-linked immunosorbent assay (ELISA) was developed in 1971 as a "sandwich" assay to further improve sensitivity and specificity of immunodiagnostics[3,4]. Subsequent efforts have aimed to improve assay speed, sensitivity, portability, and robustness.

Proteins have becoming increasingly popular diagnostic biomarkers for point-of-care testing (POCT). While nucleic acids provide the DNA or RNA blueprints for cellular machinery, they do not adequately represent the final protein expression and post-translational modification levels that are often closely tied to disease state. Through direct analysis of protein targets, a more accurate picture of actual disease state may be provided. Furthermore, an internal amplification of signal may be observed as multiple copies of the protein may be generated per pathogen or host cell. Protein targets include those derived directly from a target pathogen (e.g. HIV p24 capsid protein[5]), directly from a host organism (e.g. prostate-specific antigen (PSA)[6], human epidermal growth factor receptor 2 (HER2)[7]), or immunogenically synthesized by a host in response to a target antigen (e.g. immunoglobulins, or antibodies[8]).

Immunologic tests are most commonly used for protein detection in RLR settings. These techniques leverage the high affinity binding between antigens and their matching antibodies, frequently coupled with some form of catalytic signal amplification. These assays, though sensitive, frequently suffer from issues with cost, ease of use, robustness, and versatility. However, a number of next generation affinity agents and detection mechanisms promise to enhance and extend POCT for more protein targets in more RLR settings.

3.1.2 Affinity Biomolecules in Protein Diagnostics

The vast majority of existing molecular diagnostic tools rely on affinity-based target recognition events coupled with some form of downstream signal transduction[9]. These assays primarily leverage biomolecules (antibodies, peptides, or DNA/RNA oligos) to selectively bind target proteins. Each biomolecular recognition element offers a number of advantages and disadvantages, as summarized in Table 3.1.

Table 3.1 Comparison of biomolecular recognition elements.

Recognition Element	Size	Stability	Design Simplicity	Cost	Combinatorial Diversity
Antibody	~1500 amino acids (~150 kDa)	Low	Complex	$$$	Very High
Peptide	< 50 amino acids (<5 kDa)	Medium	Easy	$$	High
DNA aptamer	< 40 base pair (<13 kDa)	High	Easy	$	Low
RNA aptamer	< 40 base pair (<13 kDa)	Low	Easy	$$	Low
Non-native base aptamer	< 40 base pair (<13 kDa)	Variant	Easy	$$	Medium - High

The workhorse in this field has traditionally been the antibody, a protein complex that is active in the vertebrate immune response[10,11]. Vertebrates generally carry a large diversity of antibodies with variable domains that each specifically bind to a target molecule, such as a viral particle fragment, based on the specific charge, hydrophobicity, and geometric conformation of the antibody polypeptide chains[12]. Antibodies are used for specific target recognition in a wide array of biological assays, including ELISA[3], FACS[13], and western blotting[14].

Antibodies are primarily discovered through an immunogenic process by which a target molecule engenders an immune response in a mammalian host (rabbit, goat, rat, etc.). This is a lengthy procedure, requiring significant resources for host immunoactivation and subsequent antibody collection, purification, and analysis[15]. This *in vivo* batch production scheme is difficult to scale. Antibodies are thus generally manufactured via recombinant techniques[16]. Antibody coding sequences must be determined and incorporated into transfection vectors for cellular expression or transgenic production, a process that can take several months to several years.

Short peptides (< 50 amino acids) are attractive alternatives to comparatively large antibodies (~ 1500 amino acids) for molecular recognition applications. Peptides can be selected through phage display techniques[17], using a large random sequence library to obtain the highest affinity molecules. The resulting peptides are readily sequenced and can be synthesized *in vivo* or *in vitro*. Some initial efforts have been made to incorporate peptide biorecognition elements into diagnostic systems[18], though they have yet to be incorporated into commercial diagnostic platforms. Like antibodies, short peptides may suffer from sensitivity to environmental perturbations including temperature, pH, and salt concentration.

Recently, a growing interest in leveraging nucleic acids as molecular recognition elements has led to a surge of innovation that may transform the diagnostics industry (Figure 3.1). Like protein-based antibodies, nucleic acids are composed of discrete chemical residues that can be recombined to produce a massive diversity of sequential permutations and associated chemical properties (for example, a nucleic acid molecule just 20 base pairs (bp) long can yield over 10^{12} different sequences). Although this rich chemical diversity has traditionally been applied to information coding that ultimately leads to some downstream effector production (such as the translation of a protein via triplet codons), it has recently

been shown that nucleic acid molecules themselves can be powerful biochemical tools with affinity and enzymatic properties that rival their proteinaceous counterparts[19].

Aptamers are short nucleic acid sequences (generally less than 40 bp) that bind to a corresponding target molecule with extraordinarily high sensitivity and specificity. These binding properties come from an aptamer's specific three dimensional shape and functional group positioning (Figure 3.2). Aptamers may be composed of DNA, RNA, or non-native nucleoside bases (with additional functional groups to increase the diversity of molecules and affinity properties that can be generated)[20]. Although computational techniques are being developed for *in silico* aptamer design[21], the primary method for designing new aptamers is systematic evolution of ligands by exponential enrichment (SELEX)[22]. In this process, an initial pool of up to 10^{15} random nucleic acid sequences (the DNA library) are iteratively screened, amplified, and mutated to yield a final pool of oligomers that meet the specific selection criteria of the SELEX (Figure 3.2). Although the bench top SELEX procedure initially took weeks to identify a single target, the protocol has been optimized to yield acceptable results within just a couple of days[23]. With SELEX, functional nucleic acid sequences can be generated extremely rapidly, making them attractive alternatives to protein-based biosensors.

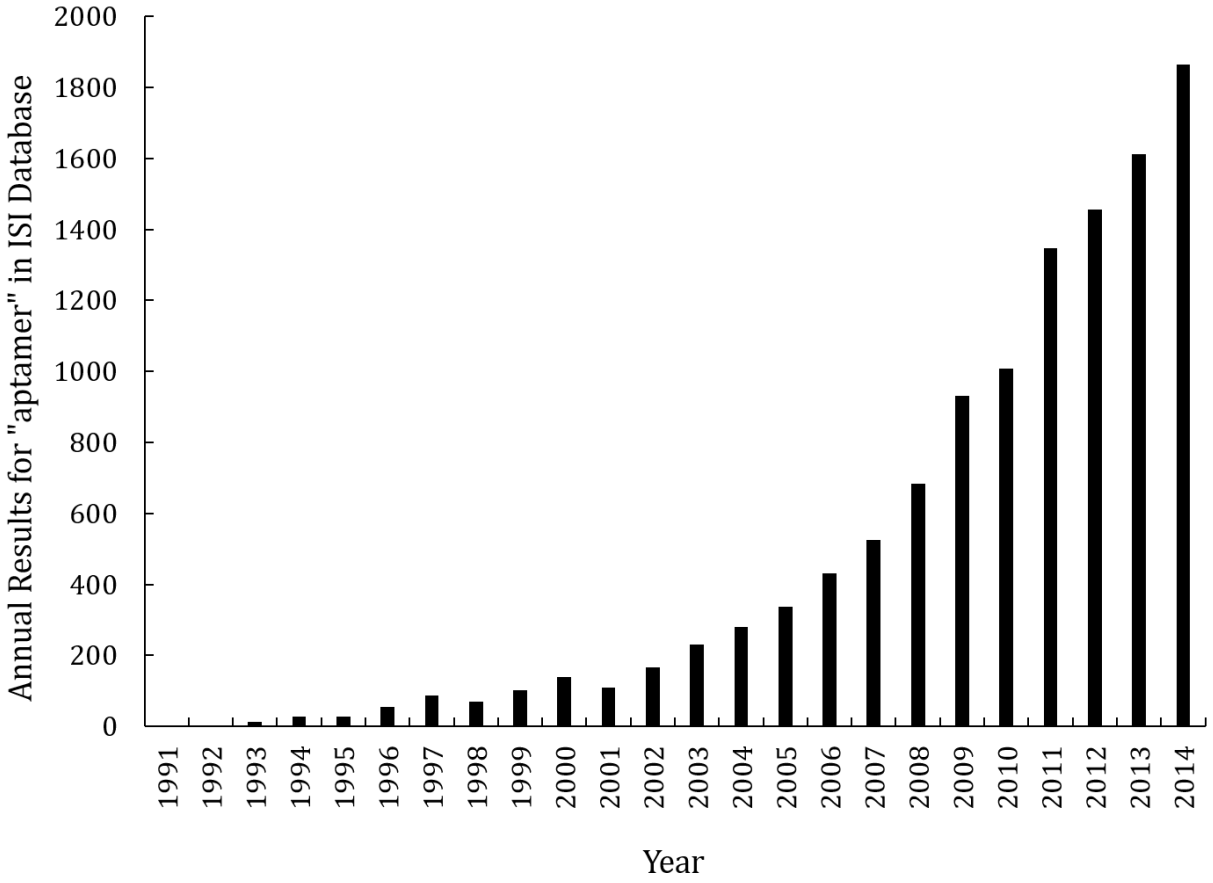

Figure 3.1 The rise of aptamers. The total number of results for a search of "aptamer" as a topic in the ISI Web of Knowledge Database. Although nucleic acids have only recently been

designed for non-hybridization affinity purposes, aptamers have already proven extremely valuable as molecular recognition elements. The keyword "aptamer" has experienced a 25-fold increase in annual citations since 1998.

Beyond their affinity properties, nucleic acids have been developed to perform catalytic functions such as nucleolytic cleavage[24–28]. Aptazymes are nucleic acid molecules containing aptamer regions that have been coupled with enzymatic sequences (ribozymes or deoxyribozymes) by "communication" elements that translate a binding event into catalytic activity (Figure 3.2B). In this way, the entire signal transduction is accomplished by a single molecule. These modular aptazyme-mediated signal transduction probes can be readily modified and designed with openly available thermodynamic modeling software[29–31]. It is even possible to incorporate several aptazyme elements in concert to produce logical AND, OR, NOT, and NOR gates[32,33]. With their rich functional diversity, simple design, and robust performance, aptamer probes promise to play a disruptive role in the diagnostics industry.

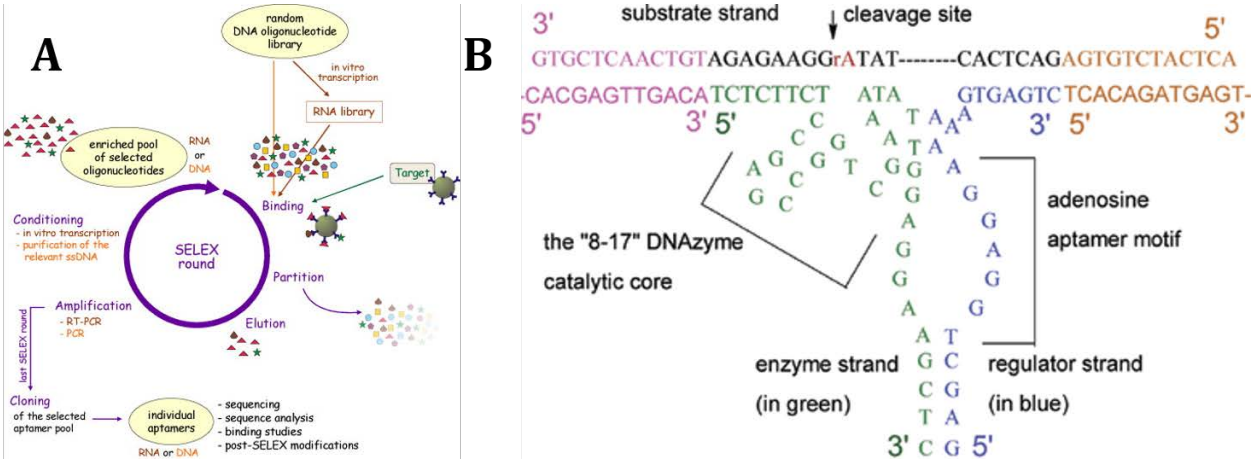

Figure 3.2 Aptamer selection and aptazyme structure. (A) Sequential evolution of ligands by exponential enrichment is a cyclic process that is generally iterated several times before yielding a pool of aptamers meeting specific affinity and activity requirements[23]. (B) Two dimensional hybridization structure of the adenosine aptazyme we will use in preliminary testing. The individual aptamer and catalytic components were discovered through the SELEX process[34].

3.1.3 Signal Transduction in Protein Diagnostics

Signal transduction elements are required for efficient conversion of a protein biorecognition event into a readable signal. Often referred to as "labels", a number of molecular tags have been developed to couple biorecognition with optical, electrical, radioactive, and magnetic labels[35]. Other systems have been developed for "label-free" analysis, obviating the need for secondary tags or even biorecognition elements altogether[36]. Although each method offers a range of analytical options with accompanying advantages and disadvantages, most protein detection assays for RLR settings incorporate some form of tag that provides catalytic signal amplification or high-intensity optical visibility.

Table 3.2 Signal transduction methods.

	Type	Technology
Labeled	Linear	Beads
		Gold nanoparticles
		Fluorophores
		Chromatic dyes
		Nanowires
	Amplified	Electrochemical
		Enzymatic color change
		Enzymatic light production
		Particle aggregation
		Radioisotopes
Direct	Optical	UV-Vis spectrometry
		IR spectrometry
		Raman spectrometry
		Mass spectrometry

The majority of tags used in molecular diagnostics rely on optical detection[37,38], either by naked eye readout or automated image processing. Fluorescent tags have been widely applied for molecular detection due to their large signal intensity relative to a dark background under proper illumination and filtering conditions[39]. Fluorophores, such as fluorescein, emit light in response to stimulation by an excitation light source. The emitted light generally has a lower energy (longer wavelength) than the excitation light, facilitating sensitive detection through longpass filters. Quantum dots have also been developed to provide bright signals that are not subject to the photobleaching that plagues most fluorophores[40]. However, the cost and complexity of including excitation light sources and optical components have generally prevented the commercial use of fluorescence in RLR settings, with a few recent exceptions.

Nanoplasmonic particles exhibit a number of properties that have made them popular for a number of diagnostic applications in RLR settings. Briefly, nanoparticles display a large light scattering cross section, without the photobleaching that's observed with dyes or fluorophores (see Chapter 4 for a more detailed discussion of nanoplasmonic materials). These particles are generally fairly stable for dry and ambient storage, and are compatible with a wide range of surface functionalizations for conjugation to biorecognition elements[41]. Gold nanoparticles (GNPs) have been adapted for use in a range of lateral flow ("dip stick") assays, including many pregnancy tests[42]. However, traditional use of these nanoparticles does not yield any signal amplification, limiting the potential diagnostic sensitivity.

A number of enzymatic chemical reactions have been adapted for biomolecular assays, enhancing the signal observed for a signal labeling event through a catalytic

amplification. Both organic and inorganic catalysts have been conjugated to biorecognition elements, such as antibodies, to yield products that can be detected through optical or electrical means. Enzymes have been developed to generate color change, chemiluminescence, fluorescence, or electrochemical redox[43]. These methods provide a diversity of sensitive signal detection mechanisms, though the enzymes used can be expensive and frequently suffer from stability issues under assay conditions found in RLR settings.

Radioactive isotopes have also been conjugated to biorecognition molecules to serve as robust and highly-sensitive labels[1,44–46]. This radio immunoassay method leverages the natural emission of ionizing radiation from radioactive isotopes such as 125-Iodine (^{125}I)[47]. A standard radio immunoassay generally consists of a competitive binding assay in which a radiolabeled target antigen is bound to a specific antibody, with a subsequent concentration-specific binding exchange with non-radioactive target antigens. The concentration of target antigen can be determined based on the remaining percentage of radiolabeled antibody-antigen complexes through use of standard dosimetry methods. Radio immunoassay methods are extremely sensitive and relatively inexpensive. However, the use of ionizing radiation requires special training and reagent handling, precluding many applications in RLR settings.

Magnetically active tags have also been employed as labels for signal transduction in biomolecular assays[48]. Magnetic tags are appealing for diagnostic applications as they are generally stable, inexpensive to manufacture, and biocompatible. As most specimens of interest do not exhibit any magnetic properties at standard assay temperatures, magnetic markers can provide highly sensitive and specific signals. A number of tools have been developed for direct detection of magnetic tags, including magnetoresistive sensors[49,50], superconducting quantum interference devices (SQUIDs)[51], and Hall effect sensors[52,53]. However, magnetic sensor technology has yet to be adapted for commercial use in RLR settings.

Some efforts have been made to reduce the reliance on secondary labels by direct detection of ligand-receptor binding through associated physical phenomena, or by analysis of intrinsic molecular properties of the target protein. Target binding can be directly detected through surface plasmon resonance[54], acoustic attenuation of micro- and nanostructures[55], and impedence on nanowire substrates[56]. These systems all still require biorecognition elements or other surface modifications to yield specific detection results. The intrinsic molecular properties of a target molecule can be analyzed through optical spectroscopy (UV-Vis, IR, Raman), mass spectroscopy, or calorimetry. However, these systems have yet to be widely applied in RLR diagnostic devices due to the high non-specific background found in untreated patient samples.

3.1.4 Assay Platforms for Protein Diagnostics

The diagnostic elements described above (biorecognition, signal transduction, signal amplification) have been incorporated into a broad range of formats for use in RLR settings. Antibody-based agglutination assays are frequently performed on paper substrates[57]. Lateral flow assays are also performed on porous substrates that exhibit capillary-driven sample wicking. A number of assays have been simply applied in traditional microcentrifuge tubes to yield visible or quantifiable results. These methods are often cheap and simple to

use, though they frequently suffer from issues with sensitivity and reproducibility. Furthermore, their simplicity limits the ability to perform additional sample preparation and analytical workflows in an automated manner.

Microfluidic platforms have been leveraged to bring significant improvements to assay sensitivity, cost, and versatility (see **Section 1.4** for more details on microfluidic technologies). Simple flow-through platforms have been developed to bring affinity assays similar to lateral flow predecessors into the microfluidic environment[58,59]. Furthermore, catalytic assays have been implemented in microfluidic systems to improve sensitivity. A range of miniaturized sensors have been developed for optical, electrical, radioactive, and magnetic analysis of microfluidic assays. The miniaturization of sample handling and analysis will be critical in the development of protein diagnostic systems for RLR settings.

3.2 Aptamer-Mediated Release of Amplification Probes

3.2.1 AMProbe Assay Overview

We have leveraged aptamer-mediated signal transduction to reduce the cost, complexity, and instability often found in antibody counterpart assays. In these systems, a biorecognition event between a target molecule and the designed aptamer sequence yields the selective release of a reporter strand for downstream analysis (Figure 3.3). We have designed configurations that leverage either nucleolytic or competitive binding mechanisms to release the reporter strand. In the nucleolytic release design, the 10-23 deoxyribozyme (DNAzyme)[60,61] has been adapted into a system for reporter release in response to target binding to an aptamer sequence (Figure 3.3A). Alternatively, the competitive binding mechanism enables release directly upon destabilization of the reporter hybridization following target binding (Figure 3.3B). We have focused our efforts on the latter affinity competition mechanism in order to mitigate any potential risk associated with the nucleolytic cleavage mechanism (matrix-specific interference, instability, or background leakage signal). Furthermore, as the thermodynamic properties of these functional nucleic acid structures are well-understood, optimal *in silico* design is possible with a range of tools[62]. These aptamer-mediated amplification probes (AMProbe) may be adapted to a diversity of target molecules and downstream signal amplification mechanisms.

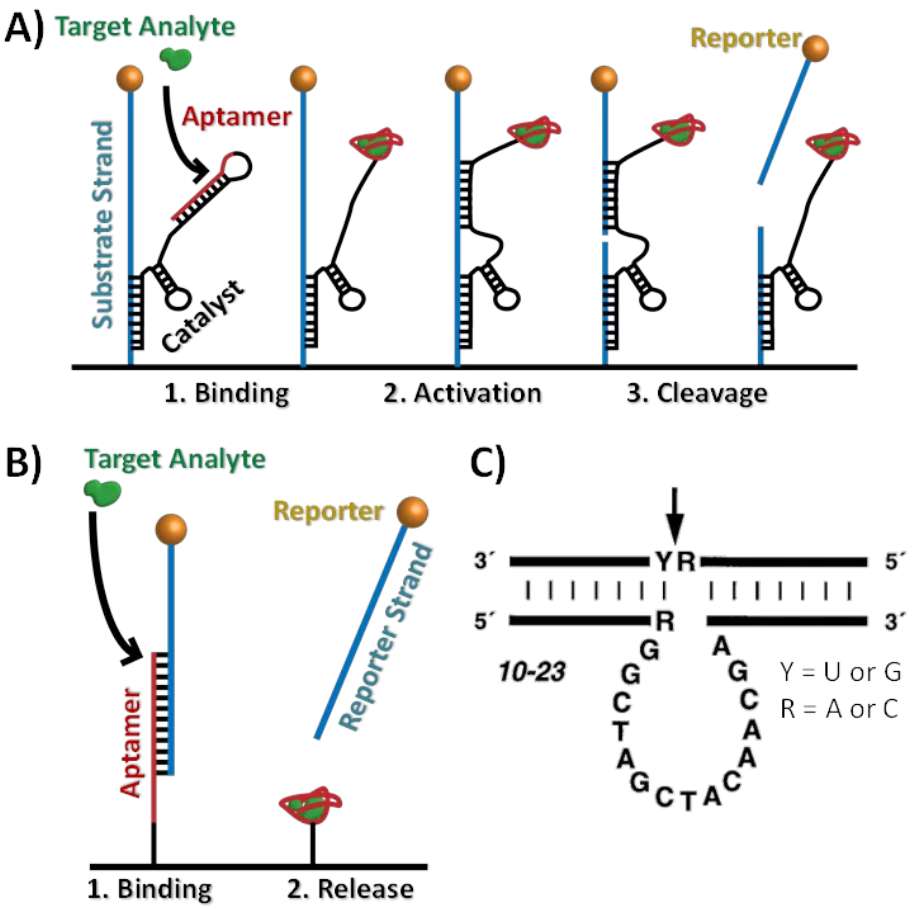

Figure 3.3 Aptamer-mediated amplification probe (AMProbe). (A) Aptazyme probes consist of a target-specific aptamer domain (red) coupled with a nucleolytic cleavage motif (black). Upon activation, the substrate strand (blue) is cleaved, yielding the irreversible release of the conjugated reporter element. (B) In the aptamer-release assay, a target analyte binds to an aptamer region (red), destabilizing the hybridized reporter strand (blue), leading to a release for downstream detection. (C) The 10-23 deoxyribozyme (DNAzyme) has been selected to rapidly cleave a target ribonucleobase as shown. This structure has been incorporated into our aptazyme constructs, labeled "Catalyst" in (A).

In addition to the low cost, simplicity, and stability of nucleic acid biorecognition elements, the reporter probe release strategy provides a number of advantages over standard affinity assays. This technique obviates the need for wash steps as reaction and release occur in a location separate from the amplification and readout region (Figure 3.9). Furthermore, a broad range of reporter tags can be conjugated to the release strand, facilitating a broad range of downstream detection mechanisms that are independent of the biorecognition mechanism. This versatility is particularly beneficial as it offers design flexibility when dealing with a variety of sample matrix compatibility and environmental requirements for specific RLR settings.

3.2.2 Design of AMProbe Release Structures

The AMProbe release structure was designed in a modular way to enable modification and extension to an array of substrates, targets, reporters, and sample matrices. The overall structure for an AMProbe consists of the following sequence motifs: base linker, aptamer complement, aptamer, and reporter (**Figure 3.16**).

A number of different aptamer sequences can be found in the literature, at times with multiple unique sequences for any given target antigen, however their affinity is often lower than required, or results are difficult to replicate in practice. These Critically-low Reliability Aptamer or "CRAptamer" sequences lack sensitive or specific affinity for their target sequence. In surveying the literature, we identified aptamers for a broad range of target molecules, though ultimately aimed to demonstrate a proof of concept with a high-affinity and well-studied motif. We thus studied several thrombin aptamer sequence motifs in order to identify the optimal binding sequence. We selected the 15bp thrombin sequence [5'-GGTTGGTGTGGTTGG-3'], reported by Bock et al. to have a K_D of approximately 200nM[63].

After selecting the appropriate aptamer motif for thrombin binding, a subset of potential reporter sequences were designed through a melting temperature analysis. The melting temperature (T_m), defined as the temperature at which half of a target sequences strands are hybridized (Equation 3.1), can be calculated with an array of tools. This melting temperature, in turn, can be used to define the length, composition, and configuration of nucleic acid sequences in order to optimize single- and multi-species binding kinetics.

$$T_m = \frac{\Delta H^\circ}{\Delta S^\circ + R\, ln([A]_{total} - [B]_{total}/2)}$$

Equation 3.1 Melting temperature equation. The melting temperature, T_m, is defined as the temperature at which half of a double-stranded DNA molecule will be dissociated into single strands. The equation above applies for short DNA sequences (< 70bp)[64,65]. ΔH^o and ΔS^o are the standard enthalpy and standard entropy for the sequence, respectively. R is the ideal gas constant. $[A]_{total}$ and $[B]_{total}$ are the total concentrations of each strand of DNA (where $[B]_{total} > [A]_{total}$).

Sequences were generally designed in order to minimize interactions that would interfere with the desired assay operation. A candidate oligomer sequence was selected through an iterative process including the following steps:

1. Core functional motifs are inserted (such as aptamer sequences).
2. Hybridization sequences are inserted as needed for oligomers to be used in multi-strand complexes. For the aptamer complex, sequences are designed to have minimal melting temperatures in the antigen-bound state (leading to rapid release of the reporter strand), while maintaining a high melting temperature in the antigen-unbound state (to reduce non-specific release of the reporter strand).
3. Flanking sequences are inserted as necessary (such as linker sequences). These may be randomly-selected sequences or poly-nucleotide repeat sequences.
4. Hairpin structures that would interfere with oligomer performance are removed through iterative modification. In general, unwanted hybridizations can be removed by editing GC-bonds in medial and/or distal regions of a hybrid motif.

5. Cross-hybridization that would interfere with multi-strand complex performance is removed through an iterative modification to.
6. In general, the GC content of any non-functional sequence is kept between ~40 - 60% in order to prevent unwanted interactions and to improve synthesis efficiency.

Starting with these *in silico* sequence designs, optimized structures were selected through empirical analysis of binding and release thermodynamics via both SPR and radiolabeling techniques, described in the following sections.

3.2.3 Surface-based Optimization of AMProbe Capture by SPR

The AMProbe assay relies on competitive binding of the target (thrombin) to the exposed aptamer. We thus performed an analysis with varying base pair hybridization overlap between the aptamer and reporter sequences. The amount of aptamer "covered" by the reporter oligo was varied between 5 – 7 bp (Table 3.3).

Table 3.3 Aptamer and reporter sequence design.

Aptamer Overlap with Reporter (bp)	Type	Name	Sequence
N/A	Base Linker	Biotin-DNA Base	TCACAGATGAGTAAAAAAAAAAAA
5	Aptamer	Thr-Apt_5bp_01	TTTTTTACTCATCTGTGAATTCTCTGGGTTGGTGTGGTTGG
	Aptamer-Control	Thr-Apt-Ctrl_5bp_01	TTTTTTACTCATCTGTGAATTCTCTGGTTGGTGTGGTTGG
	Reporter	Thr-Rep_5bp_01	TTTTTTACTCATCTGTGAATTCTCGGTTGGTGTGGTTGG
6	Aptamer	Thr-Apt_6bp_01	TTTTTTACTCATCTGTGAATTCTCTGGGTTG
	Aptamer-Control	Thr-Apt-Ctrl_6bp_01	TTTTTTACTCATCTGTGAATTCTCTGGTTGG
	Reporter	Thr-Rep_6bp_01	TTTTTTACTCATCTGTGAATTCTCGGTTGGT
7	Aptamer	Thr-Apt_7bp_01	CAACCCAGAGAAT
	Aptamer-Control	Thr-Apt-Ctrl_7bp_01	CCAACCAGAGAAT
	Reporter	Thr-Rep_7bp_01	ACCAACCGAGAAT

A surface-based approach was employed to analyze binding kinetics and thermodynamics for each of the designed AMProbe constructs. We performed SPR analysis of sequential binding on the Biacore T100 instrument. Briefly, the Biacore instrument enabled us to perform sequential loading of AMProbe constructs and target antigens to measure surface binding kinetics. The process for preparing the Biacore CM5 chips, along with testing binding of thrombin to AMProbe constructs, is presented in Figure 3.4.

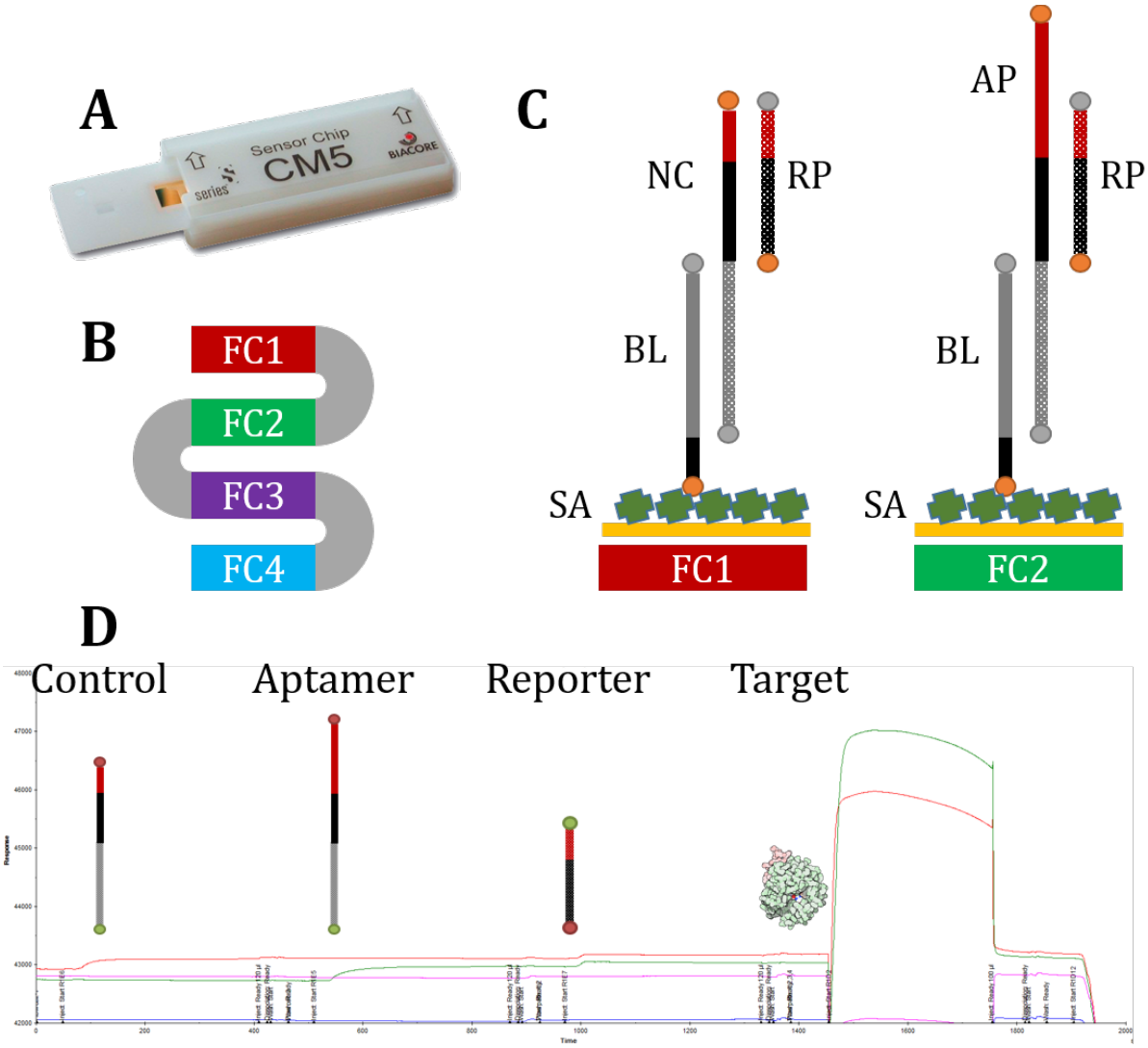

Figure 3.4 SPR assay procedure. (A) A Biacore CM5 chip was used as the assay substrate in a Biacore T100 instrument (**GE,**). (B) The CM5 chip has 4 flow channels (FC) that may be addressed individually or in sequence. In each step, the flow rate and time are controlled to ensure saturation (confirmed by sensorgram). (C) The chip was first prepared through the conjugation of streptavidin (SA) via NHS-EDC chemistry. A base linker (BL) oligo was subsequently bound to FC1 and FC2. A control oligo (NC) lacking the complete aptamer motif was bound to FC1 and an aptamer oligo (AP) was bound to FC2. A reporter oligo (RP) was bound to both FC1 and FC2 via hybridization to the control or aptamer strand, respectively. The thrombin target was flowed through both FC1 and FC2, with binding measured by sensorgram. The 5' end of oligos are indicated with an orange circle. (D) Sensorgram of the mass accumulation for each component. The red and green channels show mass accumulation in FC1 and FC2, respectively. Upon introduction of the thrombin target to both FC1 and FC2, a larger initial accumulation on FC2 is seen due to selective binding with the aptamer oligo.

The capture efficiency for each construct was determined through comparative analysis of normalized capture for each AMProbe construct. A Matlab script was developed

to enable rapid analysis of Biacore data files. The results for differing strands are presented in Figure 3.5.

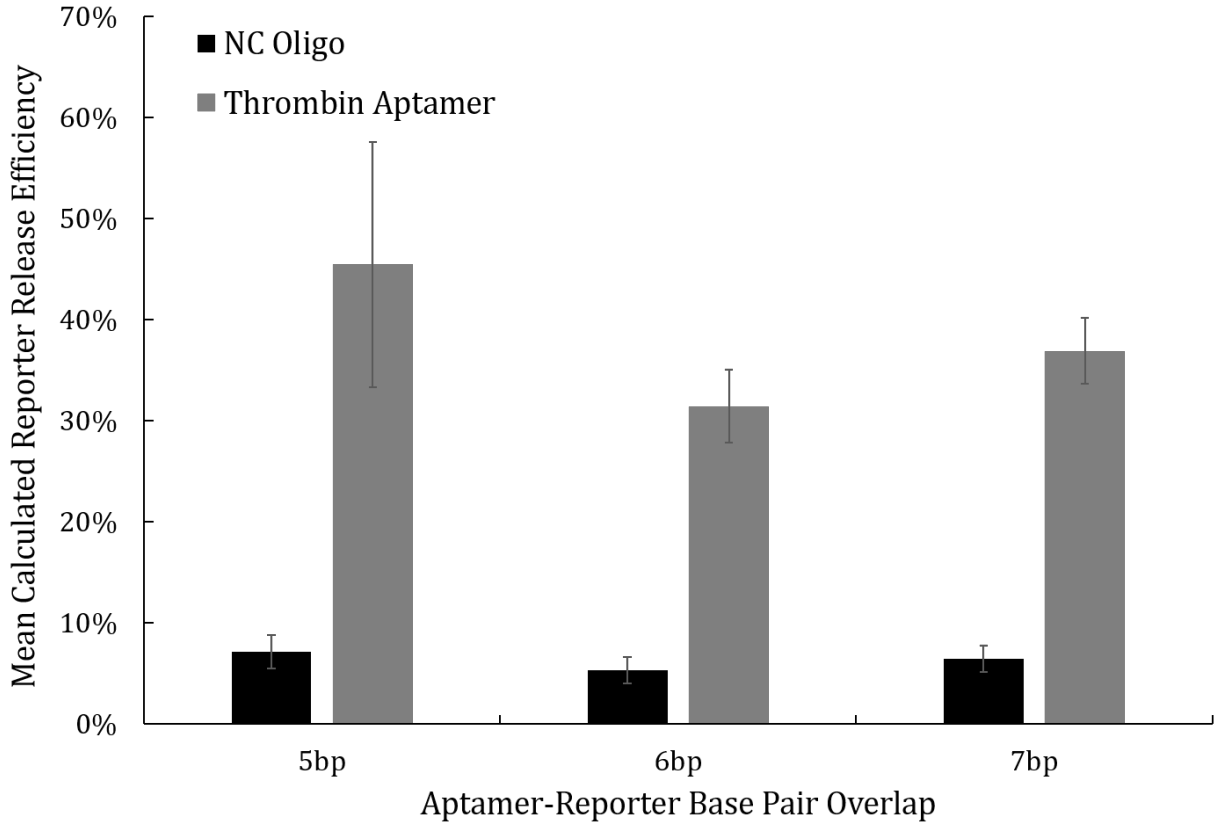

Figure 3.5 SPR analysis of AMProbe constructs. Release efficiency was estimated through an analysis of SPR shifts in the presence of injected thrombin target on a Biacore T100 instrument. A study was conducted for three different sequences with aptamer-reporter overlap varying between 5 – 7 bp (Table 3.3). Analysis was conducted in parallel for a negative control (NC) oligo lacking the full aptamer motif, as well as a thrombin aptamer oligo with the full aptamer motif. All tests were conducted in triplicate.

3.2.4 Solution-based optimization of AMProbe Release by Radiolabel Assay

The release efficiency of AMProbe constructs was further tested in a bead-based system to identify the optimal reporter hybridization configuration. While the surface-based SPR system is limited through indirect measure of target binding and reporter release by a coupled change in local index of refraction, this bead-based release assay directly measures the radiolabeled reporter molecules released from the particles. This method provides a more direct assessment of release efficiency as a function of thrombin target binding and reporter dehybridization.

We extended our SPR analysis to quantify release efficiency as a function of the reporter sequence, with the estimated T_m being reduced upon binding of a target to the aptamer motif. We designed 6 reporter sequences with a variation of expected bound and unbound T_m upon binding of thrombin to the thrombin aptamer motif (Figure 3.6).

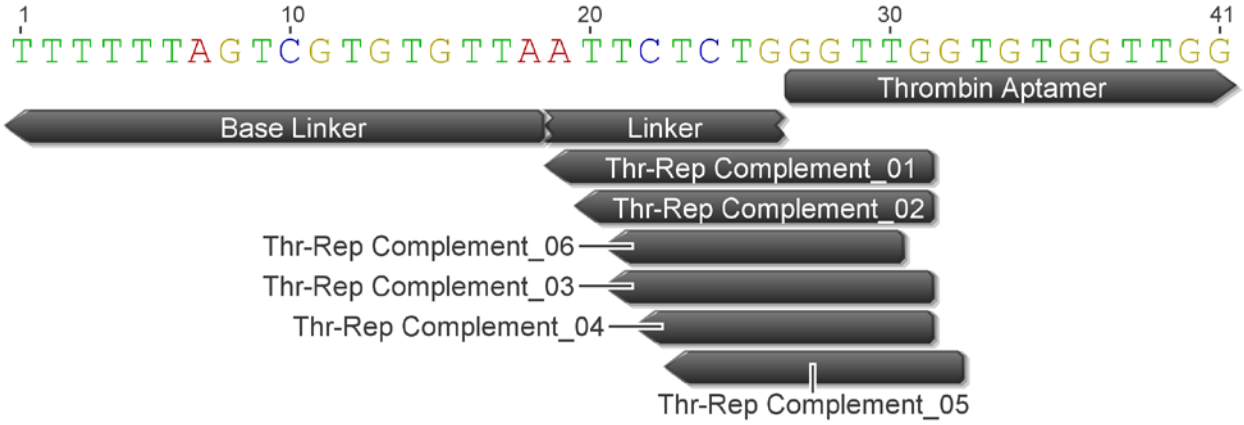

Figure 3.6 Reporter sequence designs. Reporter complement motifs for designs 1- 6 mapped onto the thrombin aptamer sequence (adapted from Thr-Apt_5bp_01 from the SPR analysis). The reporter sequences were designed to have a range of T_m when thrombin aptamer is bound or unbound (Table 3.4).

In an optimal configuration, the reporter would have a high T_m (stable hybridization) prior to target binding, and a low T_m (strand displacement and release) upon target binding. We have tested a range of reporter sequences (Table 3.4). The reporter has a natural hybridization T_m that is decreased upon destabilization through competitive binding of the target antigen to the aptamer region of the capture strand.

Table 3.4 Thrombin AMProbe reporter sequence designs.

Aptamer Overlap with Reporter (bp)	Type	Name	Sequence
N/A	Base Linker	Biotin-DNA Base	TCACAGATGAGTAAAAAAAAAAAA
5	Aptamer	Thr-Apt_5bp_01	TTTTTTACTCATCTGTGAATTCTCTGGGTTGGTGTGGTTGG
	Aptamer-Control	Thr-Apt-Ctrl_5bp_01	TTTTTTACTCATCTGTGAATTCTCTGGTTGGTGTGGTTGG
	Reporter	Thr-Rep_5bp_01	TTTTTTACTCATCTGTGAATTCTCGGTTGGTGTGGTTGG
6	Aptamer	Thr-Apt_6bp_01	TTTTTTACTCATCTGTGAATTCTCTGGGTTG
	Aptamer-Control	Thr-Apt-Ctrl_6bp_01	TTTTTTACTCATCTGTGAATTCTCTGGTTGG
	Reporter	Thr-Rep_6bp_01	TTTTTTACTCATCTGTGAATTCTCGGTTGGT
7	Aptamer	Thr-Apt_7bp_01	CAACCCAGAGAAT
	Aptamer-Control	Thr-Apt-Ctrl_7bp_01	CCAACCAGAGAAT
	Reporter	Thr-Rep_7bp_01	ACCAACCGAGAAT

A magnetic separation system was coupled with a radioactive ^{32}P reporter label to measure the relative release efficiency of each AMProbe construct (Figure 3.7). Briefly, AMProbe constructs were assembled to streptavidin-coated paramagnetic particles (PMPs), in the same configuration as the above SPR assay. The reporter oligos were each radiolabeled with ^{32}P in order to facilitate sensitive detection down to the pM range (in collaboration with the Doudna lab at UC Berkeley). A comparison of the ^{32}P signal from the

PMP-bound reporter and the reporters released into the supernatant upon magnetic separation yielded the relative release efficiency for each construct (Figure 3.7). See Appendix A.4.2 for a detailed protocol).

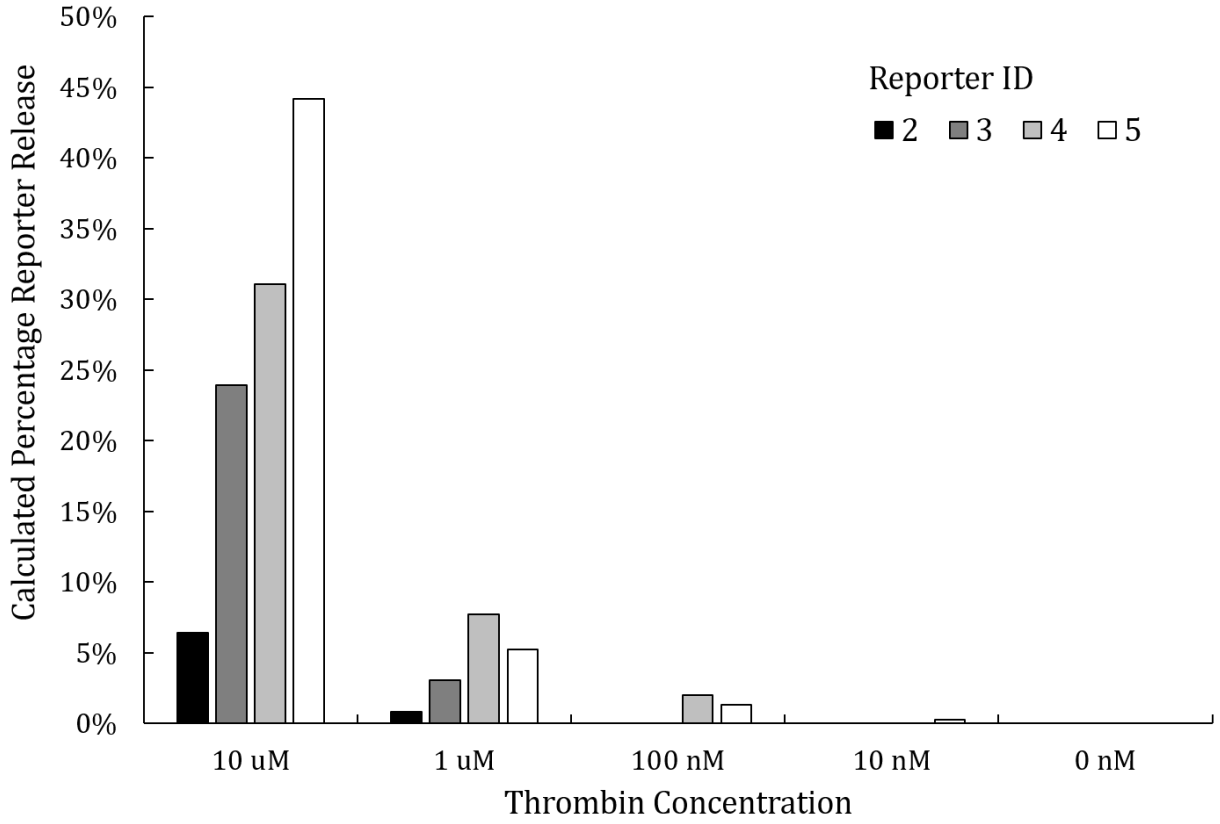

Figure 3.7 Radiolabel assay of AMProbe release. Radiolabeled reporter oligos were assembled with aptamer oligos into AMProbe constructs on streptavidin (SA) coated paramagnetic particles (PMPs). Functionalized PMPs were incubated with thrombin at a range of concentrations for 10 minutes. A magnet was used to separate out the supernatant, which was subsequently measured by radiometer for release quantification (see Appendix A.4.2 for a detailed protocol). A fraction of release was calculated by comparing radiometric readings from the initial PMP-bound constructs and the released supernatant.

The release efficiencies after a 10 minute exposure to 10μM thrombin were observed to be 6.4%, 23.9%, 31.0%, and 44.2% for AMProbe reporters 2, 3, 4, and 5, respectively (see Table 3.4 for reporter sequence information). Thr-5 and Thr-4 wer thus shown to be appealing candidates for AMProbe constructs, as expected due to the large differential between reporter melting temperature in the bound and unbound states. These results further corroborated the findings from SPR analysis (section 3.2.3).

3.3 Colorimetric Nanoplasmonic Probe Release Assay

3.3.1 Nanoplasmonic Catalytic Readout Overview

We have developed a robust mechanism to generate an optical readout from released AMProbe reporters. This configuration leverages an enzymatic reporter to generate a rapid

amplification of signal on a downstream nanoplasmonic substrate (NPS) (Figure 3.8). The NPS is designed in such a way that a nanoscale shift in geometry will result in a significant shift in plasmon resonance for the entire structure, yielding a macroscopic optical effect visible to the naked eye or a simple CCD camera (see Chapter 4 for a more thorough discussion of nanoplasmonic phenomena). Such structural color effects are commonly found in nature, yielding brilliant hues[66]. Sensors leveraging structural color offer a number of advantages over traditional fluorescent, chemiluminescent, and colorimetric assays. NPS sensors are highly tunable within a single substrate material, macroscopically visible without additional lighting or optics, and stable against photobleaching.

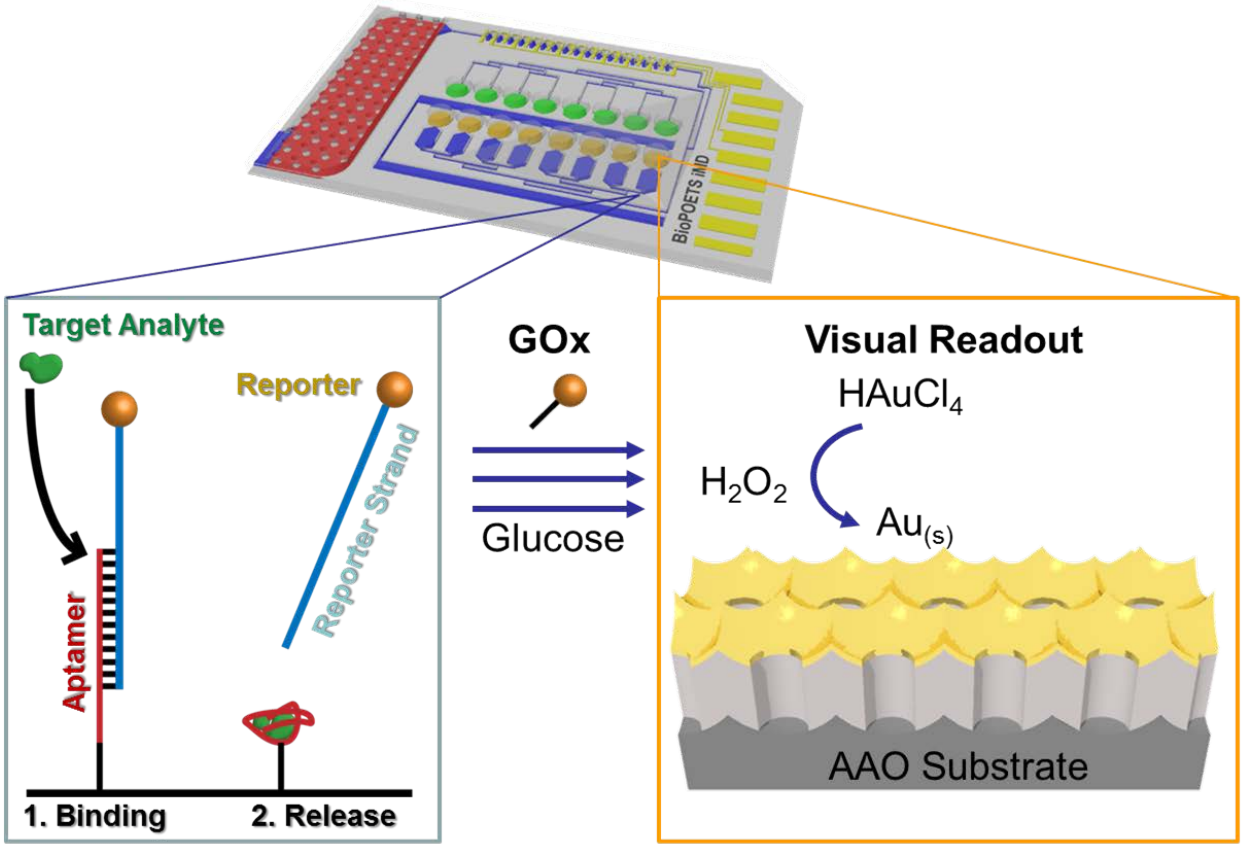

Figure 3.8 NPS readout of reporter AMProbe. The GOx-conjugated AMProbe is immobilized upstream and, upon target binding, dehybridization leads to the release of GOx. In an excess of lyophilized glucose and dried gold salt reconstituted by the sample in the downstream reaction chamber, GOx rapidly generates H_2O_2, causing gold reduction onto the NPS and an associated shift in reflectance. This shift leads to a visible color change.

Glucose oxidase (GOx) is a particularly attractive catalyst for point-of-care diagnostics due to its optimization for robust integration into microfluidic systems[67]. Enzyme stability has been improved through a number of methods, including the reduction of free thiol groups and the optimization of salt concentration and immobilization strategies[68]. Enzymes are classified by their Enzyme Commission (EC) number based on their activity, target, specificity, and other concerns. GOx, EC 1.1.3.4, is part of a class of

alcohol-specific oxidoreductase enzymes, and in the category 1.1.3 there are 29 enzymes whose reaction mechanisms involve the oxidation of a given substrate alongside the reduction of molecular oxygen to hydrogen peroxide[69]. GOx rapidly converts glucose into hydrogen peroxide (H_2O_2) and D-glucono-δ-lactone at rates between 10 to 1000 mM/min in microfluidic volumes, and activity can be preserved for up to 18 months at temperatures ranging from 20-30°C[67]. The (H_2O_2) byproduct becomes an active reactant for downstream redox reactions. GOx has been incorporated into diagnostic assays as early as 1977[70], and is commonly used in glucose sensors widely commercialized today.

The H_2O_2 generated by the reaction of reporter-conjugated GOx and glucose subsequently reduces the gold salt ($HAuCl_4$) in the NPS reaction chamber. We have selected anodized aluminum oxide (AAO) as the NPS for this assay due to its low cost to manufacture and its well-characterized plasmonic properties. Without the need for lithography, self-ordered nanophotonic crystals of AAO substrates are fabricated via a scalable anodization process involving exposure to specific acids and voltages that yield a tunable pore diameter and surface thickness[71]. Our group has previously tuned the dielectric properties of an AAO substrates by sputtering thin layers of silver[72]. This results in shifted plasmonic properties, and can even yield a visible color shift, which we have leveraged in this work.

3.3.2 Fabrication and Characterization of Nanoplasmonic Substrates

AAO substrates were fabricated through a standard process described previously[72]. Briefly, anodization is accomplished through the sequential processes of electropolishing, primary anodization, etching, secondary anodization, and pore widening (Figure 3.9). See Appendix A.7 for a detailed AAO fabrication protocol.

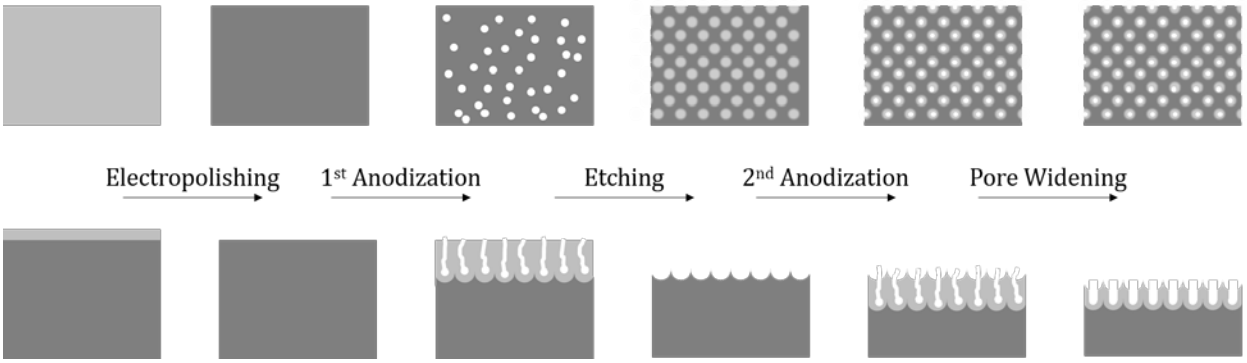

Figure 3.9 Aluminum anodization schematic. AAO substrates were fabricated in a process consisting of electropolishing, 1st anodization, etching, 2nd anodization, and pore widening.

Most importantly, the pore depth can be controlled as a function of secondary anodization time, leading to highly-tunable initial optical properties of AAO substrates. This property facilitates optimization of the assay for a range of catalytic rates, metals for reduction, and optical readouts (spectrophotometric or visual).

Although metal anodization is a common industrial process, most nanoplasmonic structures from AAO require high-purity aluminum starting substrate. We further reduced the cost of the NPS by implementing our system with off-the-shelf food-grade aluminum foil. Details of this procedure can be found in Appendix A.7. An overview of some of the optical properties for AAO substrates is shown in Figure 3.10.

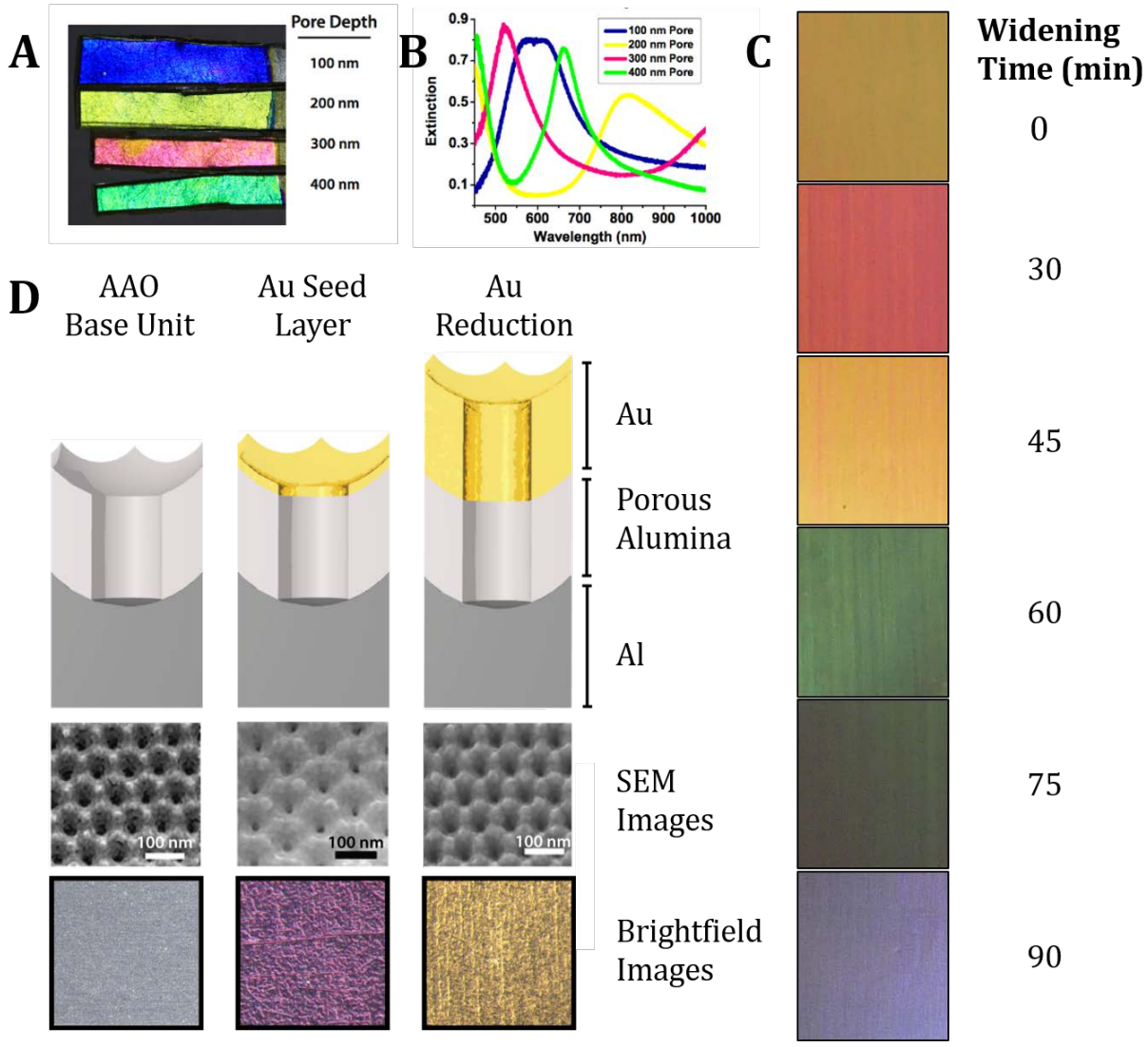

Figure 3.10 Colorimetric properties of nanoscale substrates. (A) The effect of pore depth on the optical reflection properties of the initial nanoplasmonic substrate. (B) Extinction curves indicating the entire visible spectrum can be achieved as a function of pore depth. (C) Varying optical properties of AAO substrates as a function of pore widening time. Images were taken after deposition of Au seed layer onto anodized Reynolds Heavy Duty aluminum (98.5% pure, 24 μm thick). Samples were anodized for 5 minutes at 40 V in 0.3M oxalic acid, with pore widening in 0.1M phosphoric acid at 30°C for varying times. Al is 98.5% Al, 24-micron thick foil. (D) The colorimetric GOx-mediated reduction of Au onto the AAO substrate was characterized visually.

3.3.3 GOx-mediated Catalytic Growth Proof of Concept

We developed a proof of concept GOx-mediated colorimetric reaction leveraging AAO substrates. In this assay, an AAO substrate seeded with a thin layer of gold was used for analysis. A mixture containing gold salt (HAuCl4) and glucose was initially incubated on the

substrate. GOx was added to the mixture and time lapse images were taken and characterized (Figure 3.11).

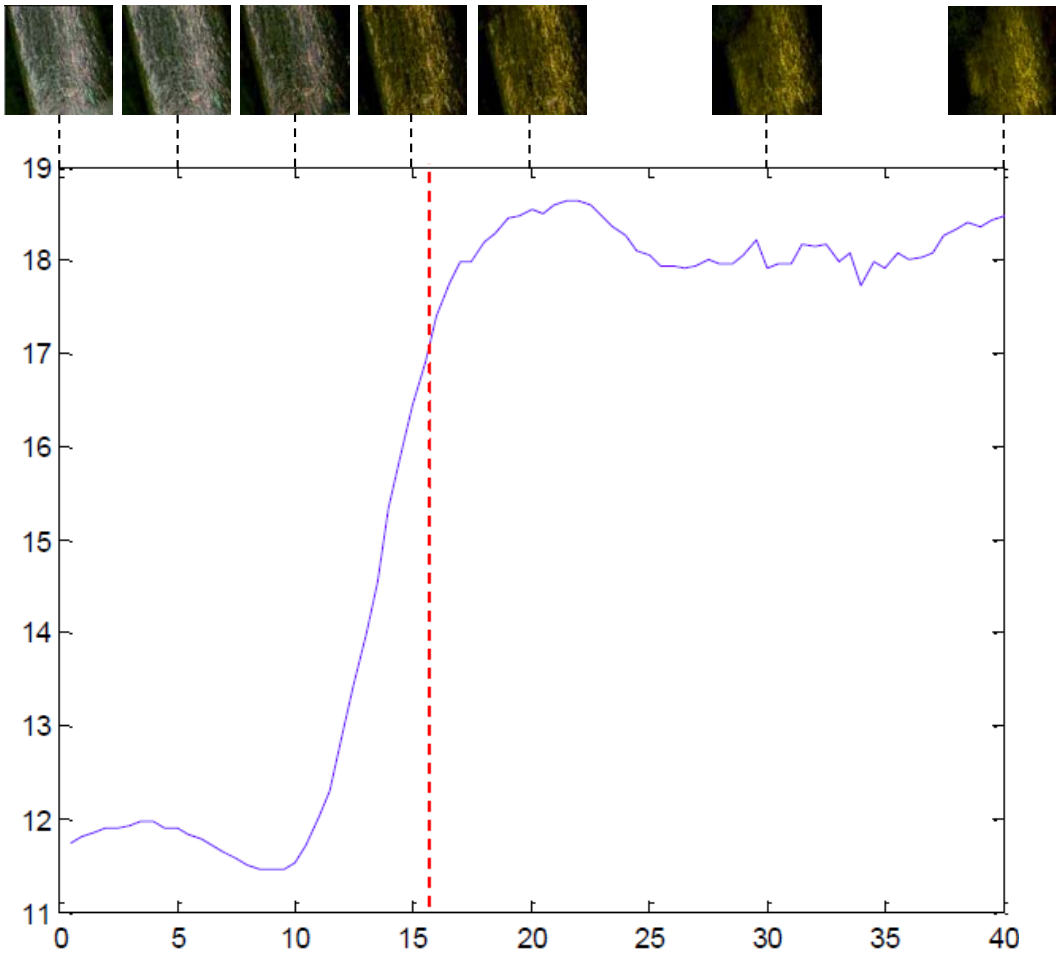

Figure 3.11 GOx-mediated catalysis proof of concept. An initial GOx reduction on an AAO NPS was performed. The AAO substrate was processed from 99.999% Al alloy according to our standard AAO preparation protocol (see Appendix A.7 for a detailed protocol). A reaction gasket chamber of PDMS was placed on the AAO substrate. A solution of Techni-Gold (Technic, Inc.) and glucose was mixed with 100μM 50kU GOx (MP Biomedicals) and placed in the reaction chamber on the AAO substrate. Images were taken over time and a chroma shift was observed within ~15 minutes.

We further performed a set of tests with varying GOx concentration and incubation time. These substrates were evaluated for both colorimetric and spectroscopic effects (Figure 3.12).

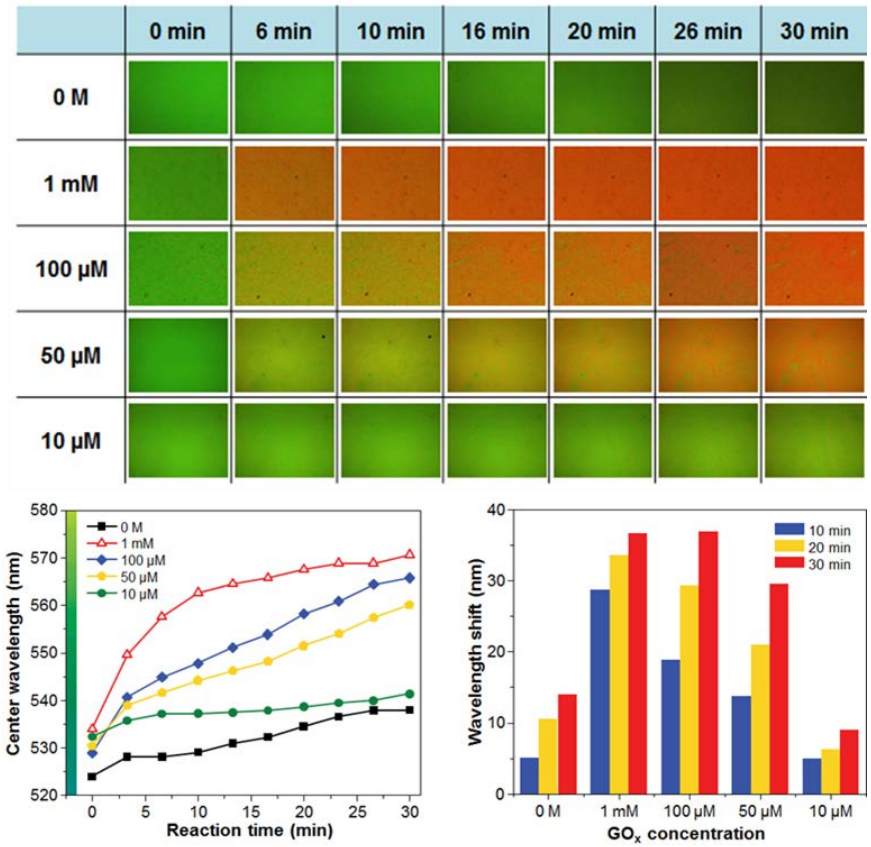

Figure 3.12 Characterization of chemical amplification by glucose oxidase-mediated reduction of gold onto a nanoplasmonic substrate. An AAO NPS was exposed to a Techni-Gold and glucose mixture, along with a varying concentration of 50kU GOx (MP Biomedicals). Images and spectra were taken over a 30 minute period in order to quantify the shift in reflectance.

3.3.4 On-chip Catalytic Growth

In order to assess the impact of reaction in confined microfluidic volumes, GOx-mediated reduction assays were performed on AAO-PDMS hybrid chips (Figure 3.13). Similar to the previous studies, a reaction mix was prepared containing Techni-Gold, glucose, and a varying concentration of 50kU GOx (MP Biomedicals), between 0 and 100 µM. Images were taken over the course of the reaction, with a color shift observed within ~30 minutes for a 100µM sample, and ~60 minutes for a 10nM sample.

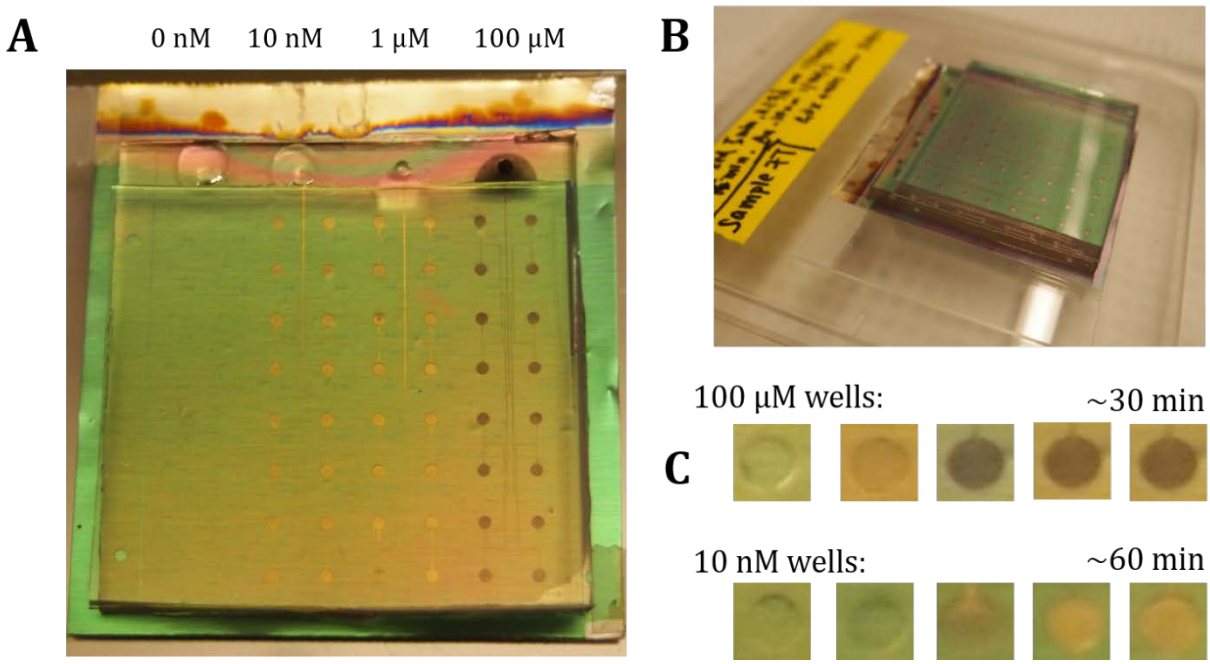

Figure 3.13 On-chip GOx-mediated reduction of gold on AAO substrate. (A) An AAO substrate was bonded to a PDMS microfluidic device to simulate performance of a released GOx reporter. Four separate inlets addressed 16 replicate reaction wells in a degas-loaded chip. Each inlet was loaded with a different GOx solution, including a negative control, 10nM, 1µM, and 100µM. (B) Image of chip reacting on benchtop at room temperature. (C) Significant color change was observed within ~30 minutes (100µM wells) or ~60 minutes (10nM wells).

We have further extended this catalytic assay format for use with silver nanoparticle (AgNP) catalysts. AgNP reporters offer improved stability and an increased rate of reaction over that observed with GOx reporters. We performed an antibody-based immunoassay to study the performance of AgNP reporters, yielding picomolar sensitivity within a 10 minute incubation window (see Appendix D.2 for further analysis). This assay demonstrates another promising reporter for use in an AMProbe diagnostic system coupled with NPS readout.

3.4 Isothermal Amplification Probe Release Assay

3.4.1 iAMProbe Release Assay Overview

These has been increasing interest in the development of platforms for simultaneous quantification of both nucleic acid and protein analytes. We have demonstrated the use of isothermal amplification to enable rapid, robust, and inexpensive quantification of nucleic acid biomarkers in RLR settings (see Chapter 2 for a more detailed overview of nucleic acid quantification). These same isothermal techniques can be coupled into an AMProbe system, yielding the potential for a unified diagnostic platform with a single, sensitive quantification mechanism (Figure 3.14)

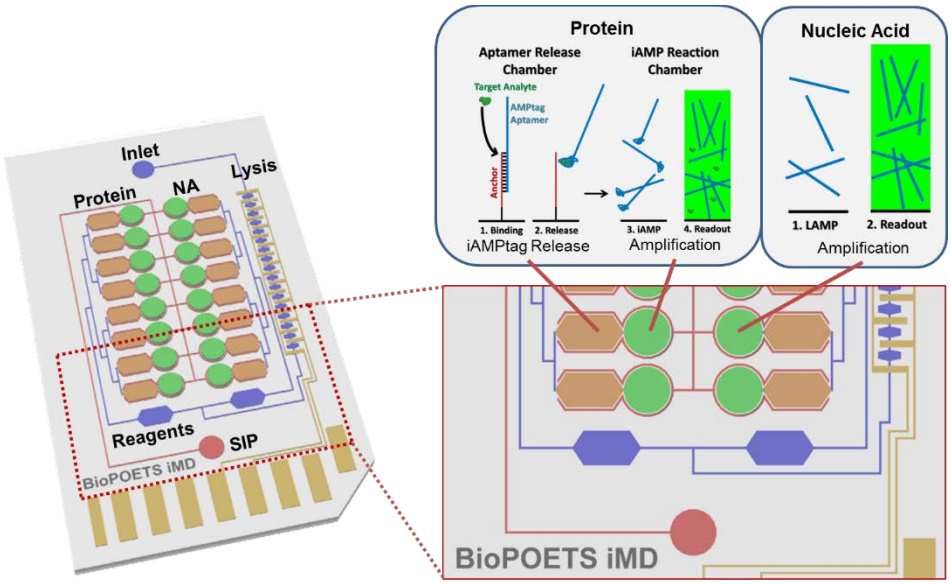

Figure 3.14 Isothermal AMProbe detection schematic. A multiplex nucleic acid (NA) and protein detection chip was designed for isothermal amplification of either a NA target or of a released AMProbe. The AMProbe construct is initially immobilized to the substrate by a biotinylated anchor strand. The reporter strand is released following target binding to the aptamer motif. The released reporter strand is quantified through real-time RPA analysis down-stream.

In order to obviate the need for slow and energy-intensive thermocycling, we have leveraged isothermal recombinase polymerase amplification (RPA)[73] (see **Chapter 2** for a detailed overview of RPA). This method of amplification utilizes a recombinase protein to insert primer sequences into double-stranded DNA (dsDNA) targets, with a strand-displacement polymerase facilitating subsequent DNA replication. In this way, we are able to achieve low-temperature (25-37°C) signal readout using a versatile DNA platform that can be readily conjugated into a number of detection formats.

3.4.2 RPA Assay Overview

As an alternative isothermal amplification mechanism, we have investigated recombinase-polymerase amplification (RPA). RPA was developed in 2006 as an isothermal amplification mechanism leveraging recombinase proteins to facilitate rapid dynamic annealing and dissociation of primer-template hybrids at low temperatures[73]. A summary of this amplification method is presented in Figure 3.15.

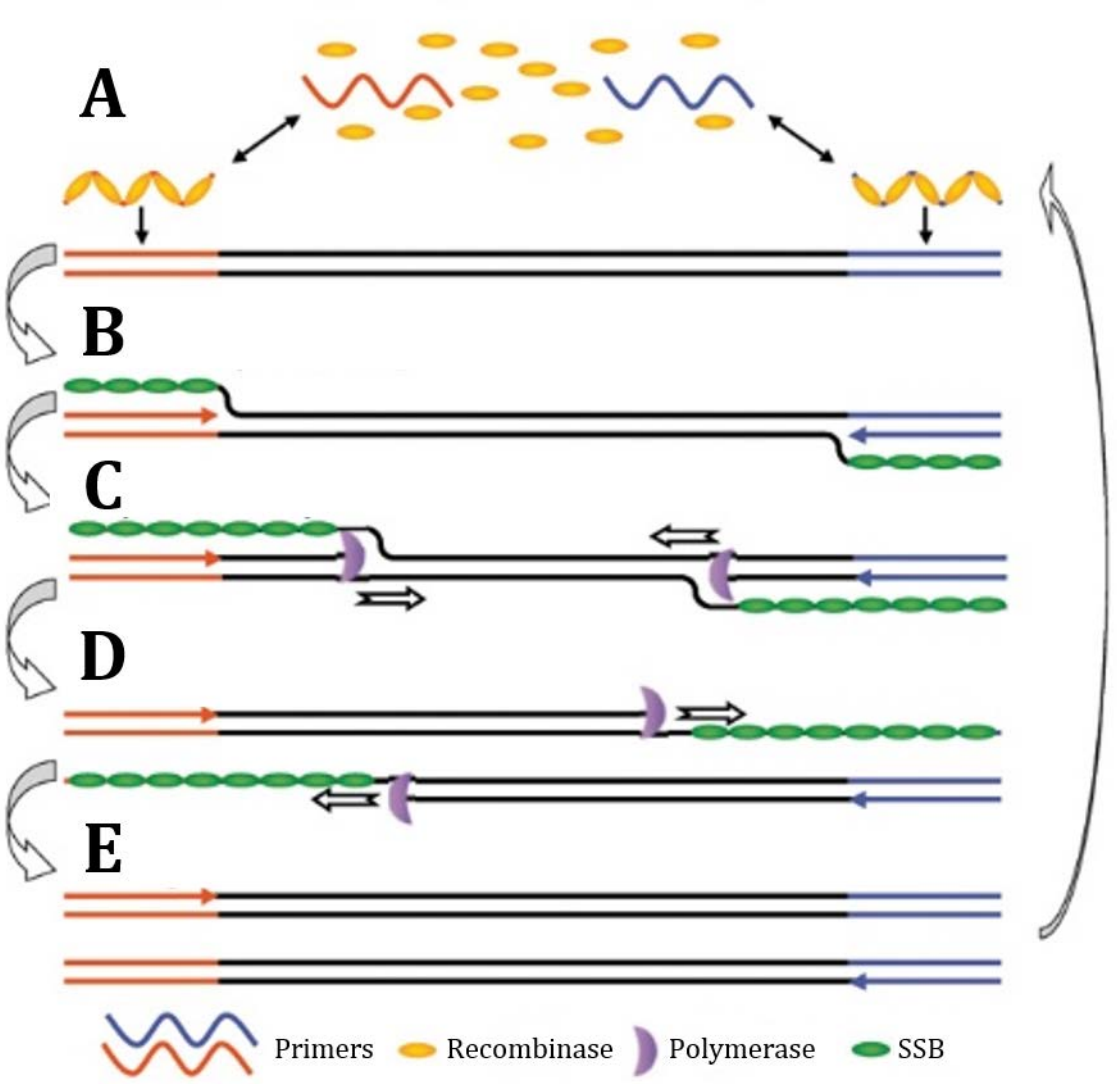

Figure 3.15 RPA assay mechanism. Figure adapted from TwistDx[74]. (A) Primer/recombinase complexes form and bind to target dsDNA. (B) Strand exchange forms a loop through which polymerization may occur. (C) Polymerase initiates synthesis. (D) dsDNA separates and polymerization continues. (E) Two amplicons duplexes are formed and the process continues to cycle on the new amplicons.

The RPA assay requires a recombinase, a single-stranded DNA-binding protein, and a strand-displacing polymerase in order to generate DNA amplicons, with the addition of a reverse transcriptase in order to generate amplicons from RNA targets. In the first step, the recombinase protein binds to the primers and facilitates a strand exchange to hybridize the primers with complementary sequences on the target strand. The single-stranded DNA-binding protein binds to the displaced strand of the target, preventing it from displacing the primer. The strand-displacing polymerase initiates synthesis of a new strand, displacing the initial target complement in the 3' direction of amplification. As with PCR, each round of amplification yields a duplication in target amplicons. Unlike PCR, thermocycling is required and the reaction proceeds continuously at the assay operating temperature.

The RPA mechanism offers several advantages over LAMP for diagnostics in RLR settings. The RPA assay is effective at room temperature, though the optimal amplification efficiency occurs at ~37°C. This lower temperature requirement enables analysis without the need for any heating elements, reducing power consumption and issues associated with microfluidic system heating (including evaporation, bubbles, and material failure). Furthermore, RPA can yield rapid results in less than 5 minutes, compared with a minimum assay time on the order of 20-40 minutes for LAMP. We expect this reaction rate could increase as the technology matures and becomes more widely available in commercial settings.

However, RPA also suffers from several limitations that prevent it from being a panacea in the isothermal amplification community. The assay proceeds so rapidly, it can be difficult to obtain any dynamic quantitative information such as what can normally be obtained through cycle and time thresholding in PCR or LAMP, respectively. This may be overcome by using a digital format to achieve quantitative results in a time-independent manner[75], though that solution may require significantly larger sample volumes and take up large chip areas (reducing multiplexing capabilities and requiring more reagents). Furthermore, the RPA assay currently requires multiple expensive proteins that are not readily available through commercial suppliers. Thus, anyone wishing to experiment with RPA and develop their own optimized kits will have to perform a significant amount of base work in cloning, expressing, and purifying these components. However, like LAMP, these reagents have been demonstrated to perform well from a resuspension of completely lyophilized reaction mix – giving hope that the assay could be adapted to a RLR settings in a robust and inexpensive manner. To date, RPA has been tested for a range of applications for infectious disease diagnosis.

3.4.3 iAMProbe Analysis on Surface

As an initial demonstration, we performed an AMProbe release assay on a flat substrate to simulate optimized conditions in a microfluidic chip (Figure 3.16). We immobilized an anchor strand to a streptavidin-coated glass slide via standard biotin-streptavidin coupling. We subsequently hybridized the AMProbe strand for thrombin recognition and detection by RPA. The RPA MRSA sequences and probes were adapted from . The composite sequences for this isothermal AMProbe (iAMProbe) are listed in Table 3.5.

Table 3.5 iAMProbe sequences.

Type	Name	Sequence
Anchor	Thrombin Anchor_02 Biotin	Biotin-TTTTTTAGTCGTGTGTGTATTCTCTCCCAACC
AMProbe	Thrombin RPAtag_02	CCCATGCGCATAGCGACTATGTAATCGTCATTGGCGGATCAAA CGTATTGTTAATTGAACAAGTGTACAGAGCATTTAAGATTAT GCGTGGAGTATGAATACTTATAGTGAAGGGAAGTTCTAGCTT TGCCGGTTGGTGTGGTTGGGAGA
Forward Primer	MRSA RPA Fwd_02	CCCATGCGCATAGCGACTATGTAATCGTCATTGGCGGATCAAA CG
Reverse Primer	MRSA RPA Rev_02	GGCAAAGCTAGAACTTCCCTTCACTATAAGTATTC
Probe	MRSA RPA Probe	TGTTAATTGAACAAGTGTACAGAGCATTTAAGATTATGCGTG GAG

The assay was performed on streptavidin-coated glass slide with silicone wells bonded on top to make isolated reaction chambers. The iAMProbe construct was generated through equimolar mixing of the anchor and aptamer probe sequences at 60°C for 10 minutes, followed by 10 minutes of annealing at room temperature. A set of 100x serial dilutions was prepared, with concentrations of the iAMProbe ranging from 1E-6 M to 1E-20 M. These dilutions were incubated in separate wells on the slide in order to find an optimal immobilization density. After a 15 minute incubation at room temperature, a series of wash steps were performed to remove unbound iAMProbe. Each chamber was incubated with either 0 mM or 1 mM thrombin for 10 minutes at room temperature. The solution was pipetted from each chamber and used as the template in an RPA quantification reaction on a Biorad CFX96 thermocycler (see Appendix A.1.3 for a detailed protocol).

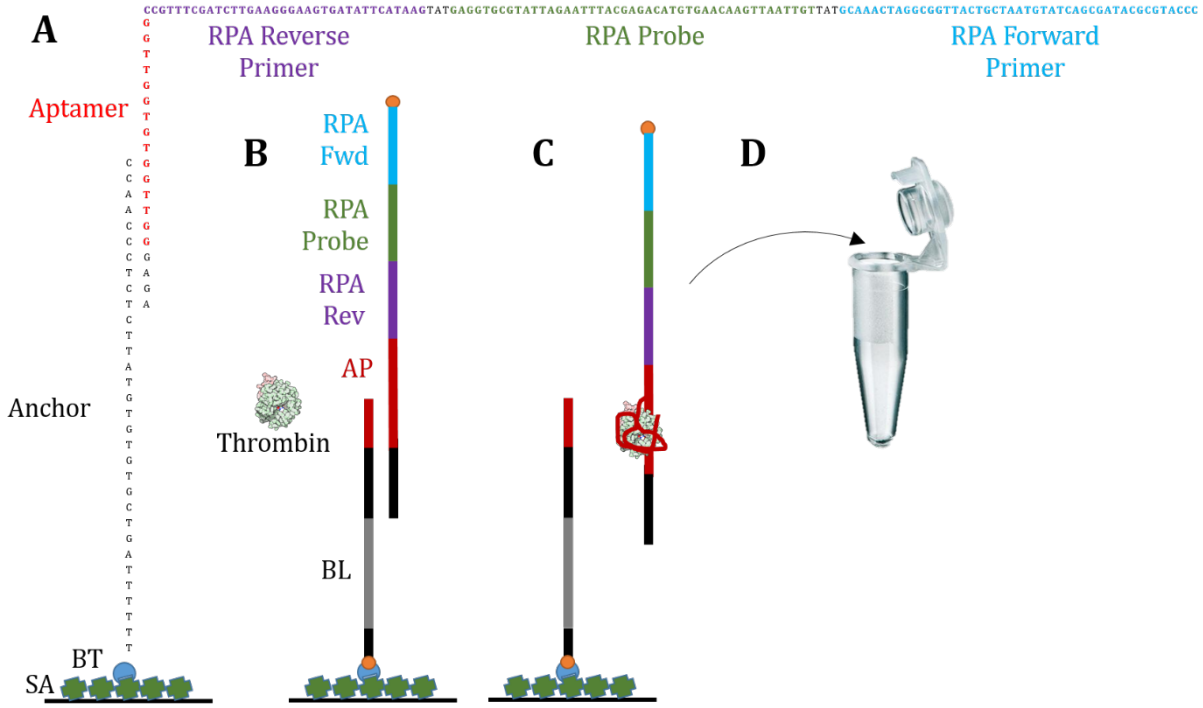

Figure 3.16 RPA iAMProbe assay schematic. (A) The iAMProbe construct consists of an anchor strand and an aptamer-amplification strand. The anchor strand has a 5' biotin (BT) for immobilization to streptavidin (SA) surfaces. The base linker (BL) acts as a bridge to the aptamer sequence. The aptamer-amplification strand has an aptamer motif (red) that selectively dehybridizes when bound to its thrombin target. A set of RPA amplification motifs are designed for downstream detection of released reporter molecules. An RPA forward primer (blue), reverse primer (purple), and probe (green) sequence are necessary for amplification. (B) In the assay, an iAMProbe construct is immobilized to an SA-coated glass slide. (C) Incubation with thrombin leads to aptamer binding and release or the reporter probe. (D) Released reporter probes are subsequently analyzed by real-time amplification in a Biorad CFX96 thermocycler.

The optimal surface coating was at 1E-14 M iAMProbe incubation on the glass slide. In this condition, the thrombin-incubated sampled showed a larger signal than the sample

receiving no thrombin (Figure 3.17). These results show promise for an aptamer-mediated release and downstream isothermal amplification.

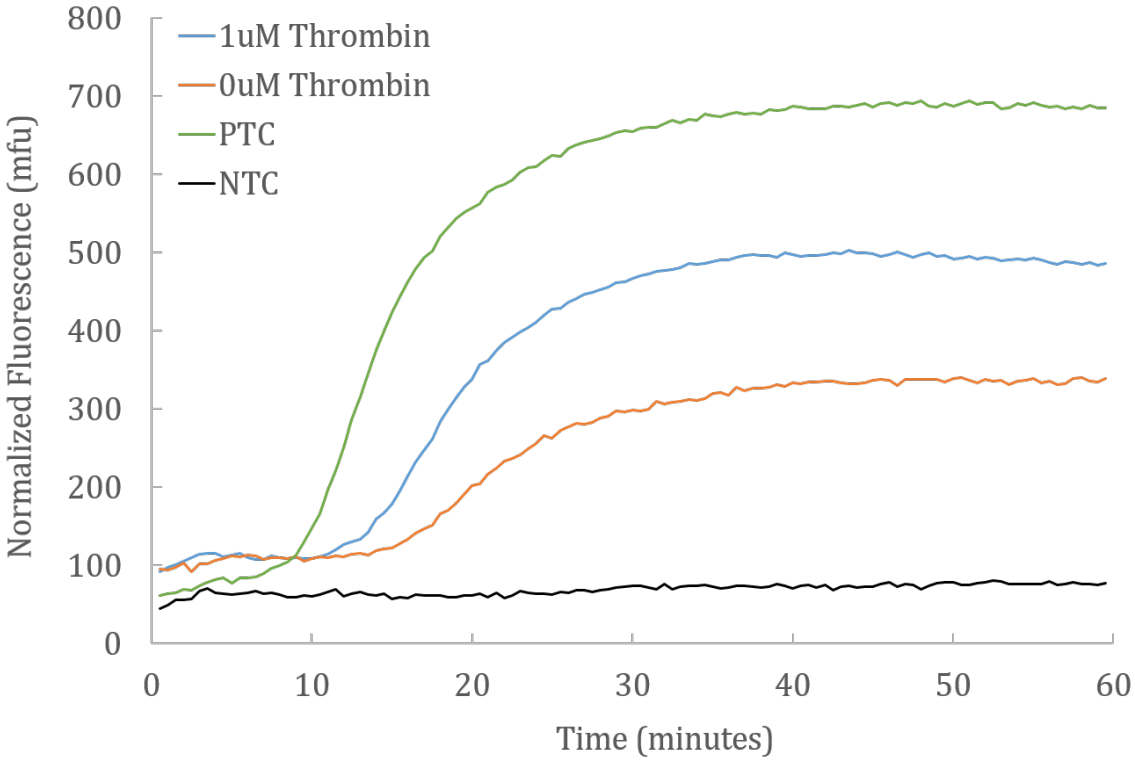

Figure 3.17 iAMProbe analysis on a flat substrate. RPA analysis was performed on the supernatant from a 10 minute incubation with either 1 μM or 0 μM thrombin. As expected, the 1 μM thrombin incubation led to a larger signal (lower time threshold for amplification). The signal observed in the 0 μM sample had a time threshold ~50% longer than that of the 1 μM sample, and with ~60% the saturation intensity. A positive template control (PTC) with 10^5 cop/mL of RPAtag_02 showed a positive signal greater than the 1 μM release supernatant. A negative template control (NTC) with water showed no signal.

3.5 Discussion

In this work we have demonstrated the components of an AMProbe assay mechanism, from the basic aptamer-mediated release of a reporter sequence to several downstream detection mechanisms. SPR and radiolabel assays showed release efficiencies of up to 45% with optimized AMProbe structures. We believe this release efficiency could be further enhanced by improving aptamer binding sensitivity and specificity through an optimized selection process[76] or through the introduction of non-native base pairs[20].

We demonstrated a nanoplasmonic mechanism for detecting released reporter molecules. We initially demonstrated the use of GOx as a reporter molecule bound to the reporter strand. We were able to observe colorimetric and spectrometric detection of GOx at levels as low as 50 μM. Confining the reaction volume to a microfluidic system further reduced the detection limit to as low as 10 nM. We subsequently implemented a capture

mechanism with an alternate silver nanoparticle catalyst to achieve detection as low as 10 pM within 10 minutes.

As an alternative downstream detection strategy, we demonstrated the iAMProbe assay with an integrated RPA amplification mechanism on the reporter strand. We were able to demonstrate the detection of 1 μM reporter strand in a slide-based assay. This mechanism enables simple implementation of a multiplexed nucleic acid and protein detection device with a single downstream detection mechanism. We believe this assay could further be enhanced through the implementation of downstream capture oligos to remove reporter strands that have been released non-specifically (through binding the aptamer sequence) and through concentrating the released reporter strand with capture oligos further downstream in the reaction chamber.

The assays and tools developed in this chapter hold promise for integration into a full protein diagnostic system that meets the operating criteria for use in RLR settings.

3.6 References

1. Berson, B. S. A. & Yalow, R. S. Quantitative aspects of the reaction between insulin and insulin-binding antibody. 1996–2016 (1959).
2. Lequin, R. M. Enzyme immunoassay (EIA)/enzyme-linked immunosorbent assay (ELISA). *Clin. Chem.* **51,** 2415–2418 (2005).
3. Engvall, E. & Perlmann, P. Enzyme-linked immunosorbent assay (ELISA) quantitative assay of immunoglobulin G. *Immunochemistry* **8,** 871–874 (1971).
4. Van Weemen, B. K. & Schuurs, A. H. W. M. Immunoassay using antigen—enzyme conjugates. *FEBS Lett.* **15,** 232–236 (1971).
5. Constantine, N. T. & Zink, H. HIV testing technologies after two decades of evolution. *Indian J. Med. Res.* **121,** 519–538 (2005).
6. Rao, A. R., Motiwala, H. G. & Karim, O. M. A. The discovery of prostate-specific antigen. *BJU Int.* **101,** 5–10 (2008).
7. Mitri, Z., Constantine, T. & O'Regan, R. The HER2 Receptor in Breast Cancer: Pathophysiology, Clinical Use, and New Advances in Therapy. *Chemother. Res. Pract.* **2012,** 743193 (2012).
8. Antibodies, C. on M. of P. M., Council, N. R., (U.S.), N. R. C. & (U.S, I. for L. A. R. *Monoclonal Antibody Production*. (1999). at <http://www.nap.edu/catalog.php?record_id=9450#toc>
9. Turner, A. P. F. BIOCHEMISTRY: Biosensors-Sense and Sensitivity. *Science (80-.).* **290,** 1315–1317 (2000).
10. Skottrup, P. D., Nicolaisen, M. & Justesen, A. F. Towards on-site pathogen detection using antibody-based sensors. *Biosens. Bioelectron.* **24,** 339–348 (2008).
11. Borrebaeck, C. A. K. Antibodies in diagnostics - from immunoassays to protein chips. *Immunol. Today* **21,** 379–382 (2000).
12. Berg, J. M., Tymoczko, J. L. & Stryer, L. *Biochemistry*. (W.H. Freeman, 2002). at <http://books.google.com/books?id=pMxpAAAAMAAJ>
13. Cantor, H., Simpson, E., Sato, V. L., Fathman, C. G. & Herzenberg, L. A. Characterization of subpopulations of T lymphocytes : I. Separation and functional studies of peripheral T-cells binding different amounts of fluorescent anti-Thy 1.2 (theta)

antibody using a fluorescence-activated cell sorter (FACS). *Cell. Immunol.* **15,** 180–196 (1975).
14. Blake, M. S., Johnston, K. H., Russell-Jones, G. J. & Gotschlich, E. C. A rapid, sensitive method for detection of alkaline phosphatase-conjugated anti-antibody on Western blots. *Anal. Biochem.* **136,** 175–179 (1984).
15. Alberts, B. *et al. Molecular Biology of the Cell*. (Garland Science, 2002). at <http://www.google.com/books?id=oYF4KAAACAAJ>
16. Chadd, H. E. & Chamow, S. M. Therapeutic antibody expression technology. *Curr. Opin. Biotechnol.* **12,** 188–194 (2001).
17. Wu, J. *et al.* Rapid development of new protein biosensors utilizing peptides obtained via phage display. *PLoS One* **6,** e24948 (2011).
18. Pavan, S. & Berti, F. Short peptides as biosensor transducers. *Anal. Bioanal. Chem.* **402,** 3055–70 (2012).
19. Jayasena, S. D. Aptamers: An Emerging Class of Molecules That Rival Antibodies in Diagnostics. *Clin Chem* **45,** 1628–1650 (1999).
20. Rohloff, J. C. *et al.* Nucleic Acid Ligands With Protein-like Side Chains: Modified Aptamers and Their Use as Diagnostic and Therapeutic Agents. *Mol. Ther. Nucleic Acids* **3,** e201 (2014).
21. Assaf Avihoo, Idan Gabdank, Michal Shapira & Danny Barash*. In Silico Design of Small RNA Switches. *NanoBioscience, IEEE Trans.* **6,** 4–11 (2007).
22. Tuerk, C. & Gold, L. Systematic Evolution of Ligands by Exponential Enrichment: RNA Ligands to Bacteriophage T4 DNA Polymerase. *Science (80-.).* **249,** 505–510 (1990).
23. Stoltenburg, R., Reinemann, C. & Strehlitz, B. SELEX--A (r)evolutionary method to generate high-affinity nucleic acid ligands. *Biomol. Eng.* **24,** 381–403 (2007).
24. Baum, D. & Silverman, S. Deoxyribozymes: useful DNA catalysts in vitro and in vivo. *Cell. Mol. Life Sci.* **65,** 2156–2174 (2008).
25. Li, Y. & Breaker, R. R. Deoxyribozymes: New players in the ancient game of biocatalysis. *Curr. Opin. Struct. Biol.* **9,** 315–323 (1999).
26. Breaker, R. R. DNA aptamers and DNA enzymes. *Curr. Opin. Chem. Biol.* **1,** 26–31 (1997).
27. Silverman, S. K. In vitro selection, characterization, and application of deoxyribozymes that cleave RNA. *Nucl. Acids Res.* **33,** 6151–6163 (2005).
28. Narayanaswamy, R. & Ellington, A. D. in 423–445 (2006). at <http://dx.doi.org/10.1007/3-540-27262-3_22>
29. Parisien, M. & Major, F. The MC-Fold and MC-Sym pipeline infers RNA structure from sequence data. *Nature* **452,** 51–55 (2008).
30. Zuker, M. & Stiegler, P. Optimal computer folding of large RNA sequences using thermodynamics and auxiliary information. *Nucleic Acids Res.* **9,** 133–148 (1981).
31. Hall, B., Hesselberth, J. R. & Ellington, A. D. Computational selection of nucleic acid biosensors via a slip structure model. *Biosens. Bioelectron.* **22,** 1939–1947 (2007).
32. Win, M. N. & Smolke, C. D. Higher-Order Cellular Information Processing with Synthetic RNA Devices. *Science (80-.).* **322,** 456–460 (2008).
33. Win, M. N. & Smolke, C. D. A modular and extensible RNA-based gene-regulatory platform for engineering cellular function. *Proc. Natl. Acad. Sci. U. S. A.* **104,** 14283–8 (2007).

34. Liu, J. & Lu, Y. Adenosine-Dependent Assembly of Aptazyme-Functionalized Gold Nanoparticles and Its Application as a Colorimetric Biosensor. *Anal. Chem.* **76,** 1627–1632 (2004).
35. Warsinke, A. Point-of-care testing of proteins. *Anal. Bioanal. Chem.* **393,** 1393–1405 (2009).
36. Cooper, M. a. Label-free screening of bio-molecular interactions. *Anal. Bioanal. Chem.* **377,** 834–42 (2003).
37. Ligler, F. S. Perspective on Optical Biosensors and Integrated Sensor Systems. *Anal. Chem.* **81,** 519–526 (2009).
38. Myers, F. B. & Lee, L. P. Innovations in optical microfluidic technologies for point-of-care diagnostics. *Lab Chip* **8,** 2015 (2008).
39. Fernandez-Suarez, M. & Ting, A. Y. Fluorescent probes for super-resolution imaging in living cells. *Nat Rev Mol Cell Biol* **9,** 929–943 (2008).
40. Jain, K. K. Applications of Nanobiotechnology in Clinical Diagnostics. *Clin Chem* **53,** 2002–2009 (2007).
41. Baptista, P. *et al.* Gold nanoparticles for the development of clinical diagnosis methods. *Anal. Bioanal. Chem.* **391,** 943–950 (2008).
42. Zhao, W., Ali, M. M., Aguirre, S. D., Brook, M. A. & Li, Y. Paper-Based Bioassays Using Gold Nanoparticle Colorimetric Probes. *Anal. Chem.* **80,** 8431–8437 (2008).
43. Burtis, C. A., Ashwood, E. R. & Bruns, D. E. *Tietz Textbook of Clinical Chemistry and Molecular Diagnostics*. (Elsevier Health Sciences, 2012). at <https://books.google.com/books?id=BBLRUI4aHhkC&pgis=1>
44. BERSON, S. A. & YALOW, R. S. Isotopic tracers in the study of diabetes. *Adv. Biol. Med. Phys.* **6,** 349–430 (1958).
45. YALOW, R. S. & BERSON, S. A. Assay of Plasma Insulin in Human Subjects by Immunological Methods. *Nature* **184,** 1648–1649 (1959).
46. Andreotti, P. E. *et al.* Immunoassay of infectious agents. *Biotechniques* **35,** 850–9 (2003).
47. Bolton, A. E. & Hunter, W. M. The labelling of proteins to high specific radioactivities by conjugation to a 125I-containing acylating agent. *Biochem. J.* **133,** 529–39 (1973).
48. Tamanaha, C. R., Mulvaney, S. P., Rife, J. C. & Whitman, L. J. Magnetic labeling, detection, and system integration. *Biosens. Bioelectron.* **24,** 1–13 (2008).
49. Waterfield, N. R. *et al.* Rapid Virulence Annotation (RVA): identification of virulence factors using a bacterial genome library and multiple invertebrate hosts. *Proc. Natl. Acad. Sci. U. S. A.* **105,** 15967–72 (2008).
50. Thomson, W. On the Electro-Dynamic Qualities of Metals: Effects of Magnetization on the Electric Conductivity of Nickel and of Iron. *Proc. R. Soc. London* **8,** 546–550 (1856).
51. Kotitz, R. *et al.* SQUID based remanence measurements for immunoassays. *IEEE Trans. Appl. Supercond.* **7,** 3678–3681 (1997).
52. Marinace, J. C. High sensitivity hall effect probe. 3–5 (1965).
53. Aytur, T. *et al.* A novel magnetic bead bioassay platform using a microchip-based sensor for infectious disease diagnosis. *J. Immunol. Methods* **314,** 21–29 (2006).
54. Kim, D.-K. *et al.* Label-Free DNA Biosensor Based on Localized Surface Plasmon Resonance Coupled with Interferometry. *Anal. Chem.* **79,** 1855–1864 (2007).
55. Raiteri, R., Grattarola, M., Butt, H.-J. & Skládal, P. Micromechanical cantilever-based biosensors. *Sensors Actuators B Chem.* **79,** 115–126 (2001).

56. Wang, R., Ruan, C., Kanayeva, D., Lassiter, K. & Li, Y. TiO2 Nanowire Bundle Microelectrode Based Impedance Immunosensor for Rapid and Sensitive Detection of Listeria monocytogenes. *Nano Lett.* (2008). at <http://pubs3.acs.org/acs/journals/doilookup?in_doi=10.1021/nl080366q>
57. Posthuma-Trumpie, G., Korf, J. & van Amerongen, A. Lateral flow (immuno)assay: its strengths, weaknesses, opportunities and threats. A literature survey. *Anal. Bioanal. Chem.* **393,** 569–582 (2009).
58. Verpoorte, E. Microfluidic chips for clinical and forensic analysis. *Electrophoresis* **23,** 677–712 (2002).
59. Shi, J., Yang, T. & Cremer, P. S. Multiplexing Ligand−Receptor Binding Measurements by Chemically Patterning Microfluidic Channels. *Anal. Chem.* (2008). at <http://pubs3.acs.org/acs/journals/doilookup?in_doi=10.1021/ac800912f>
60. Wang, D. Y. & Sen, D. A novel mode of regulation of an RNA-cleaving DNAzyme by effectors that bind to both enzyme and substrate. *J. Mol. Biol.* **310,** 723–734 (2001).
61. Wang, D. Y., Lai, B. H. Y. & Sen, D. A General Strategy for Effector-mediated Control of RNA-cleaving Ribozymes and DNA Enzymes. *J. Mol. Biol.* **318,** 33–43 (2002).
62. Lang, B. E. & Schwarz, F. P. Thermodynamic dependence of DNA/DNA and DNA/RNA hybridization reactions on temperature and ionic strength. *Biophys. Chem.* **131,** 96–104 (2007).
63. Bock, L. C., Griffin, L. C., Latham, J. A., Vermaas, E. H. & Toole, J. J. Selection of single-stranded DNA molecules that bind and inhibit human thrombin. *Nature* **355,** 564–6 (1992).
64. Owczarzy, R. *et al.* Predicting sequence-dependent melting stability of short duplex DNA oligomers. *Biopolymers* **44,** 217–239 (1997).
65. Owczarzy, R., Dunietz, I., Behlke, M. a, Klotz, I. M. & Walder, J. a. Thermodynamic treatment of oligonucleotide duplex-simplex equilibria. *Proc. Natl. Acad. Sci. U. S. A.* **100,** 14840–14845 (2003).
66. Kinoshita, S. & Yoshioka, S. Structural colors in nature: the role of regularity and irregularity in the structure. *Chemphyschem* **6,** 1442–59 (2005).
67. Wilson, R. & Turner, A. P. F. Glucose oxidase: an ideal enzyme. *Biosens. Bioelectron.* **7,** 165–185 (1992).
68. Gulla, K. C., Gouda, M. D., Thakur, M. S. & Karanth, N. G. Enhancement of stability of immobilized glucose oxidase by modification of free thiols generated by reducing disulfide bonds and using additives. *Biosens. Bioelectron.* **19,** 621–625 (2004).
69. Webb, E. C. *Enzyme Nomenclature 1992*. (Academic Press, 1992). at <http://www.amazon.com/Enzyme-Nomenclature-1992-NC-IUBMB/dp/0122271645>
70. Mattiasson, B. & Nilsson, H. An enzyme immunoelectrode Assay of human serum albumin insulin. *FEBS Lett.* **78,** 251–254 (1977).
71. Lee, M. H. *et al.* Roll-to-roll anodization and etching of aluminum foils for high-throughput surface nanotexturing. *Nano Lett.* **11,** 3425–30 (2011).
72. Choi, D., Choi, Y., Hong, S., Kang, T. & Lee, L. P. Self-Organized Hexagonal-Nanopore SERS Array. *Small* **9999,** NA (2010).
73. Piepenburg, O., Williams, C. H., Stemple, D. L. & Armes, N. A. DNA Detection Using Recombination Proteins. *PLoS Biol* **4,** e204 (2006).
74. TwistDx. *Appendix to the TwistAmp TM reaction kit manuals*.

75. Shen, F. *et al.* Digital isothermal quantification of nucleic acids via simultaneous chemical initiation of recombinase polymerase amplification reactions on SlipChip. *Anal. Chem.* **83,** 3533–40 (2011).
76. Blind, M. & Blank, M. Aptamer Selection Technology and Recent Advances. *Mol. Ther. Acids* **4,** e223 (2015).

Chapter 4: Nanoplasmonic Polymerase Chain Reaction

4.1 Introduction

4.1.1 Nucleic Acid Ampilfication Readout

Nucleic acid amplification has become a core tool in the qualitative and quantitative analysis of biomolecular samples[1]. A variety of thermocycling and isothermal amplification mechanisms have been developed[2], as well as a broad range of readout mechanisms, with gel electrophoresis[3] and fluorescence quantification[4] acting as workhorse analytical tools (see Chapter 2 for a more background on nucleic acid amplification in molecular diagnostics).

Nucleic acid amplification has also been adapted to *in situ* analysis of gene expression[5,6]. In these methods, nucleic acid sequences are imaged locally in order to study intra- and intercellular phenomena. However, these methods often lack amplification, have limited scaling of multiplexing, or require extensive sample processing.

An ideal readout mechanism would classify multiple amplification sequences, address a large multiplex, leverage robust materials, and minimize processing steps. Such an ideal method would also be amenable for implementation *in situ*. The implementation of such a mechanism would vastly extend the reach of nucleic acid testing in RLR settings. We have developed the nanoplasmonic polymerase chain reaction (NanoPCR) mechanism to meet these requirements.

4.1.2 Surface Plasmon Resonance

The optical properties of metallic nanoparticles have been studied for centuries, with some of the first written analysis coming from Michael Faraday in 1857[7]. Briefly, when light interacts with a metal nanoparticle, the oscillating electromagnetic waves excite the free electrons (or "plasmons") confined to the particle's surface. The quantum confinement of these electrons leads to an absorbance and scattering spectrum that is a function of particle geometry, size, and material, as well as interparticle distance in aggregates[8], leading to tunable "plasmon resonance" peaks. This phenomenon is also responsible for the deep reds found in stained glass windows, which contain colloidal gold nanoparticles. These plasmonic properties have been described analytically by the Mie solution for a spherical particle[9,10].

Localized surface plasmon resonance (LSPR) analysis has been applied in a range of molecular detection platforms with integrated nanoparticle sensors[11–16]. The critical value for LSPR is the peak "resonant" wavelength at which surface plasmons exhibit maximal absorption of incident radiation. The wavelength of this peak is a function of the dielectric properties at the interface between the metallic nanoparticle surface and the surrounding medium[10,17,18]. As LSPR is extremely responsive to these surface conditions, it has been leveraged for high-sensitivity quantification of biomolecules adsorbed to nanoparticle surfaces, including proteins[12,14,19], nucleic acids[20,21], and small molecules[15].

4.1.3 Gold Nanoparticle Molecular Ruler

There has been some indication that surface-immobilized double-stranded DNA (dsDNA) causes resonance shifts an order of magnitude larger than those generally observed in protein binding, suggesting the power of this technique for nucleic acid detection[20]. Our group previously found that the resonance shift was a function of nucleic acid length, enabling dsDNA sizing, in addition to quantification. Each additional DNA basepair caused an extended red-shifting of the peak resonant wavelength by approximately 1.24 nm. While this technique was initially applied to the observation of nucleic acid cleavage in the presence of restriction enzymes, similar principles may facilitate the quantification of growing dsDNA strands during nucleic acid synthesis and amplification.

4.1.4 NanoPCR Assay Overview

We have designed a localized nanoplasmonic PCR (NanoPCR) platform to measure nucleic acid length and content *in situ*. Thiolated forward primers are conjugated to gold nanoparticles and subsequently mixed with the assay buffer containing DNA targets and reverse primers (Figure 4.1). Thermocycling is conducted in a standard PCR machine. The resulting amplicons are bound to gold nanoparticles in a sequence-specific manner, with sizes determined by the relative placement of associated reverse primers. The LSPR spectrum for each particle is taken, revealing a resonance wavelength shift that is a function of the amplicon length, allowing for rapid sizing of nucleic acids during amplification.

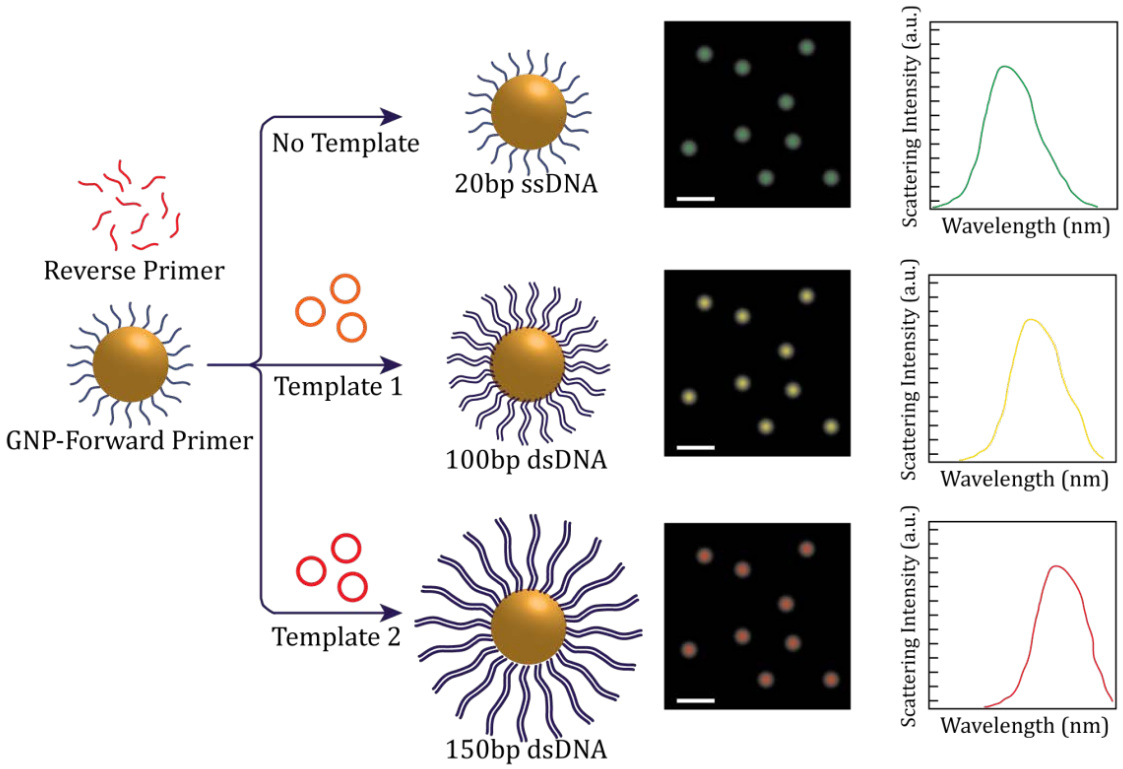

Figure 4.1 NanoPCR Platform. Gold nanoparticles are conjugated with forward primer (Au-Primer) and incubated with reverse primer. PCR reaction mix and a target DNA template (in this case a plasmid) are added to facilitate amplification. Thermocycling may be conducted

in a standard thermocycler or by illumination to generate a local heat gradient for the melting and annealing steps. True color dark field images show a red-shift as a function of amplicon length, confirmed by spectroscopy of individual particles. A single pair of primers may be designed to amplify a different region of each template used, with the only difference being the length of the contained amplicon. This helps mitigate any issues resulting from variation in primer melting temperature and subsequent reaction rates.

4.2 NanoPCR for Multiplexed Analysis

4.2.1 Design and Optimization of NanoPCR Primers

NanoPCR primers were designed to provide a range of amplicon lengths between 50 – 200 basepair (bp). Primers were designed to amplify a sequence in the rRNA large subunit methyltransferase CDS of *Staphylococcus aureus* (RefSeq ID NC_002952). This region was selected as a conserved region for the detection of methicillin-resistant *Staphylococcus aureus*. Forward and reverse primers were designed to flank a previously-generated taqman probe, in order to enable secondary quantification of amplification (Figure 4.2).

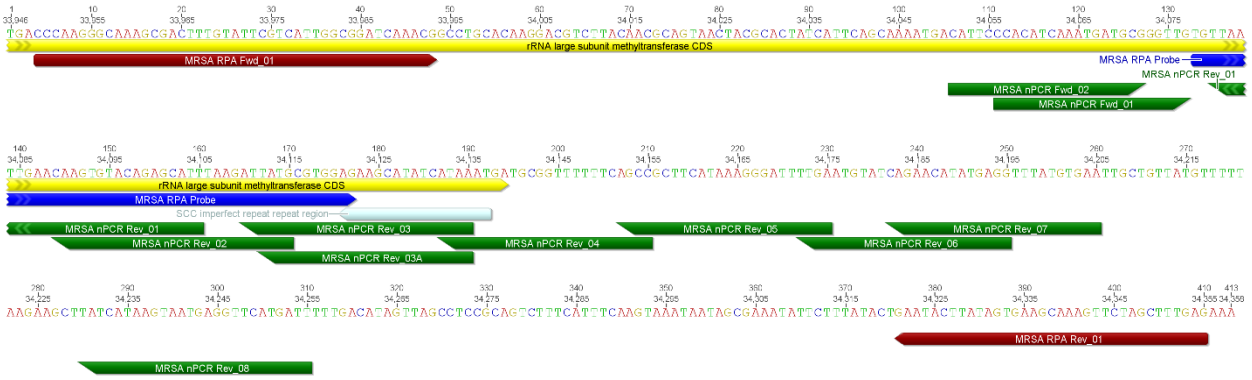

Figure 4.2 MRSA NanoPCR template and primers. A 413 bp subsequence from the *Staphylococcus aureus* genome (RefSeq ID NC_002952) is shown with primer and probe annotations. Forward and reverse primers for nanoPCR (green) are shown. Reverse primers were selected to give a range of amplicons between 50 – 200 bp. A taqman probe (blue) is also annotated, along with RPA primers that were designed previously (see Chapter 3.4 for more information on the RPA primers in an iAMProbe construct).

A forward primer was initially designed to meet primer criteria for length, T_m, and %GC (see Chapter 2 for more information on PCR primer design). A subset of 9 reverse primers were designed to meet similar primer criteria, with the additional requirement of producing an amplicon between 50 and 200bp in length when paired with the forward primer (Table 4.1).

Table 4.1 NanoPCR primer and target sequences.

Amplicon Size (bp)	Type	Name	Sequence
N/A	Forward	MRSA Fwd_01	CCACATCAAATGATGCGGGTTG
50	**Reverse**	**MRSA Rev_01**	**AATGCTCTGTACACTTGTTCAATTAA**
60	Reverse	MRSA Rev_02	CATAATCTTAAATGCTCTGTACACTTG
80	Reverse	MRSA Rev_03	TTATGATATGCTTCTCCACGCATAAT
80	**Reverse**	**MRSA Rev_03A**	**TTATGATATGCTTCTCCACGCATA**
100	Reverse	MRSA Rev_04	GGCTGAAAAAACCGCATCATTTAT
120	**Reverse**	**MRSA Rev_05**	**TCAAAATCCCTTTATGAAGCGGCT**
140	Reverse	MRSA Rev_06	CCTCATATGTTCTGATACATTCAA
150	**Reverse**	**MRSA Rev_07**	**TTCACATAAACCTCATATGTTCTG**
200	**Reverse**	**MRSA Rev_08**	**AATCATGAACCTCATTACTTATGATA**
N/A	**gBlock**	**MRSA 413bp**	TGACCCAAGGGCAAAGCGACTTTGTATTCGTCATTGGCGGATCA AACGGCCTGCACAAGGACGTCTTACAACGCAGTAACTACGCACT ATCATTCAGCAAAATGACATTCCCACATCAAATGATGCGGGTTG TGTTAATTGAACAAGTGTACAGAGCATTTAAGATTATGCGTGGA GAAGCATATCATAAATGATGCGGTTTTTTCAGCCGCTTCATAAA GGGATTTTGAATGTATCAGAACATATGAGGTTTATGTGAATTGC TGTTATGTTTTTAAGAAGCTTATCATAAGTAATGAGGTTCATGA TTTTTGACATAGTTAGCCTCCGCAGTCTTTCATTTCAAGTAAAT AATAGCGAAATATTCTTTATACTGAATACTTATAGTGAAGCAAA GTTCTAGCTTTGAGAAA

Standard quantitative PCR (qPCR) was performed in a Bio-Rad CFX96 instrument in order to assess the performance of designed primer sets (see Appendix A.1 for a detailed description of the qPCR protocol). From the initial set of primers, a subset of 5 reverse primers showed amplification for a positive template control (PTC) within 32 thermal cycles (highlighted in bold, Table 4.1), with no amplification of a negative template control (NTC) within 40 cycles (Figure 4.3). In PTC solutions, the template used was a 413bp gene block (IDT) at 100 copies/μL.

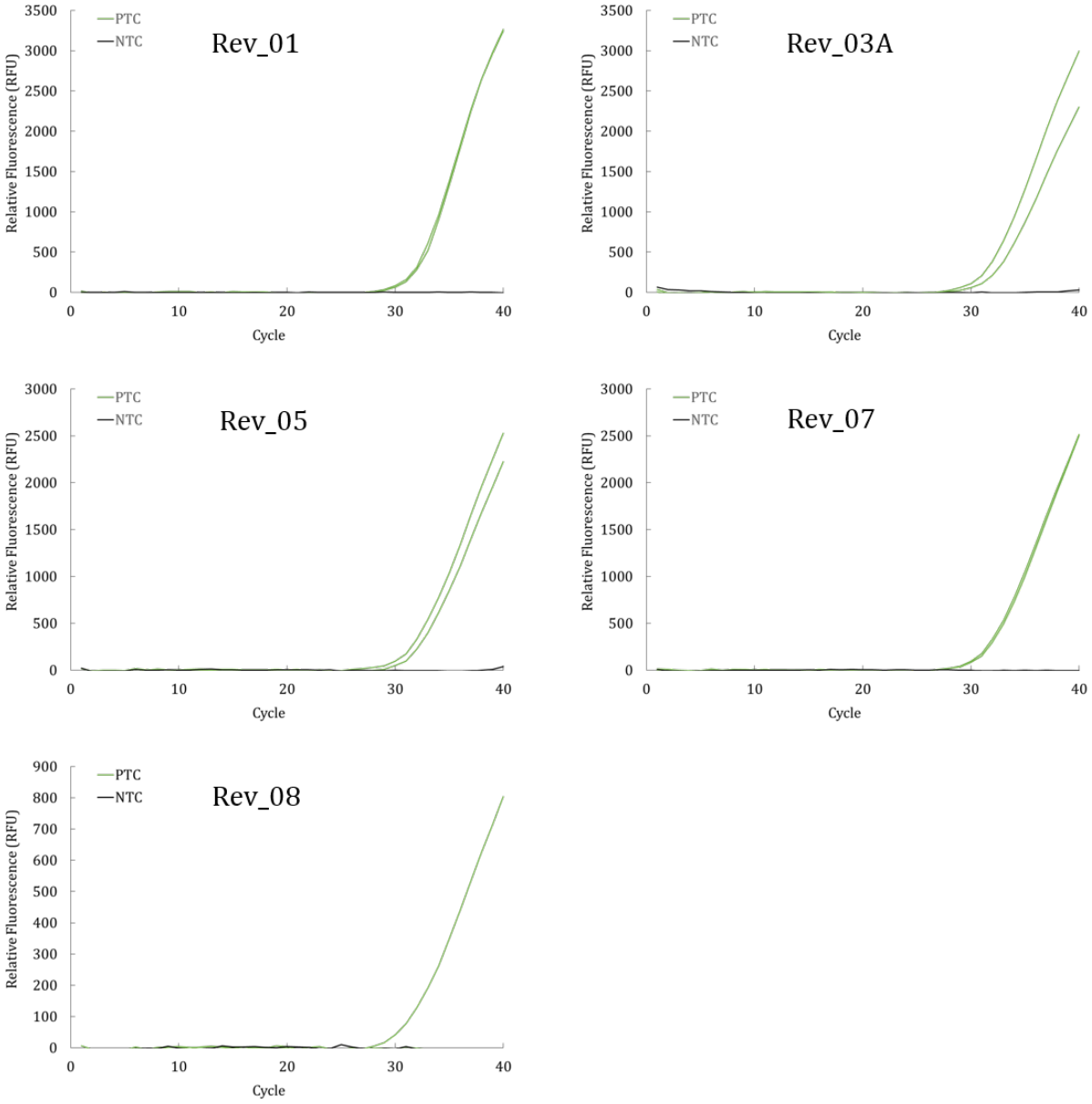

Figure 4.3 NanoPCR primer amplification confirmation. A qPCR assay was performed with the forward primer Fwd_01 and each of the reverse primer options. Results for a subset of the primers that did not show amplification for NTC within 40 cycles is shown.

A subsequent serial dilution analysis showed that MRSA Fwd_01 and MRSA Rev_01 have a sensitivity as low as 10 copies/μL of a MRSA gene block target (Figure 4.4). We thus confirmed that the selected primers would be viable for use in a nanoPCR confirguration.

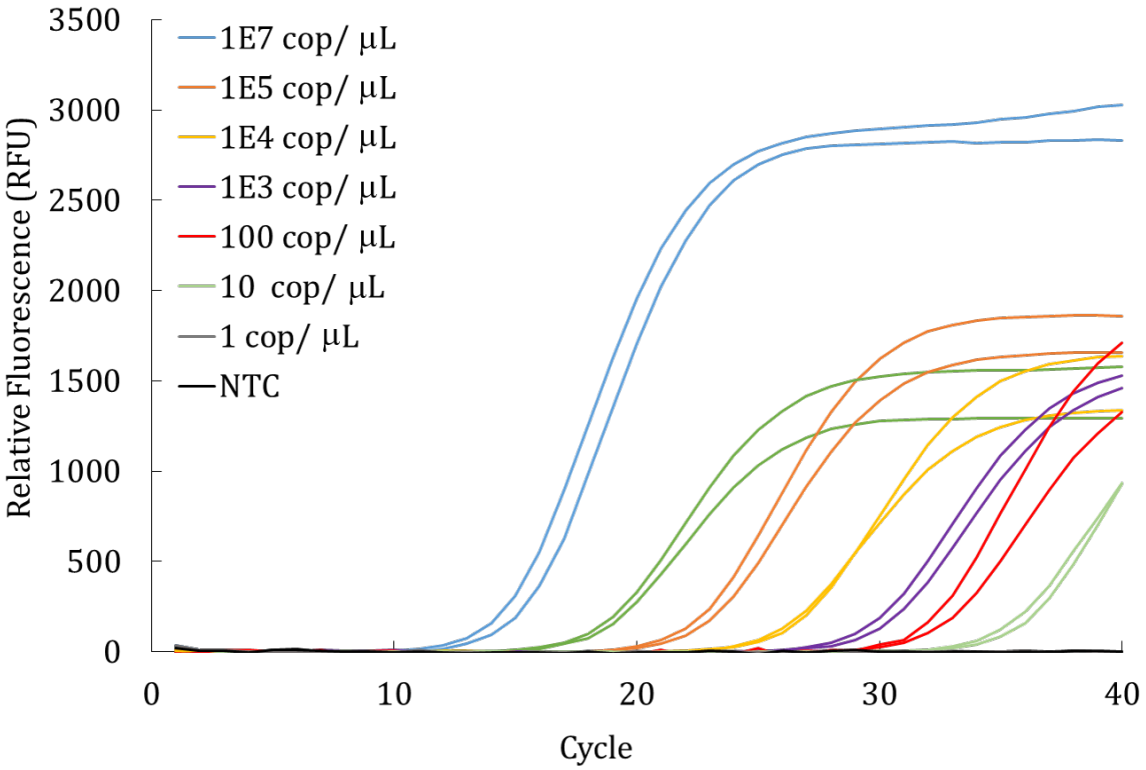

Figure 4.4 NanoPCR primer serial dilution. A qPCR assay was performed with the forward primer Fwd_01 and the reverse primer Rev_01 with a serial dilution of the 413bp MRSA gene block target, from 10^7 – 1 copies/µL, along with a negative control that received water with no template. This assay confirms that the primer sets have high sensitivity for amplification of the target gene block.

4.2.2 Preparation of NanoPCR Particles

NanoPCR particles were generated through a thiol-mediated binding of MRSA Fwd_01 primers to 15nm GNPs (BBI). NanoPCR particles were prepared in accordance with previously-described methods[22]. Briefly, a solution of Tris(2-carboxyethyl)phosphine (TCEP) was used to facilitate the reduction of disfulide groups on thiolated forward primer. This activated primer was incubated with the GNPs and unbound primer was subsequently removed through centrifugation steps (see Appendix A.5 for a detailed GNP-primer conjugation protocol.

4.2.3 Fluorescent Analysis of NanoPCR Amplification

Primers conjugated to GNPs were used in standard qPCR format reactions to confirm amplification of the MRSA target sequence in optimal conditions (see Appendix A.1 for a detailed description of the qPCR protocol). However, in repeated attempts, we were unable to produce a fluorescent signal from SYBR Green assay (data not shown). We confirmed that the thiolated primer was able to generate a fluorescent signal prior to conjugation to GNPs. We therefore believe either the GNP was inhibiting amplification, or the GNP was quenching the fluorescent signal from SYBR Green due to local absorption. The latter is most likely the case, given the absorption spectrum for GNPs of this size.

4.2.4 Darkfield Analysis of NanoPCR

In order to assess whether an amplification was occurring, but was just not visible via fluorescent analysis, we performed an analysis in a dark field hyperspectral imaging platform (Cytoviva). Briefly, ~5 μL of the amplicon solutions from qPCR analysis of GNP-conjugated forward primers were pipetted onto glass slides for imaging. The hyperspectral imaging system provides a spectral analysis of each pixel in a darkfield image, enabling multiplexed nanoplasmonic shift analysis (see Appendix A.5.4 for a detailed protocol).

Our initial results showed promise, with a moderate plasmonic shift observed between PTC and NTC reactions (Figure 4.5). Further investigation is needed to confirm the dependence of nanoplasmonic shift on the length of anticipated amplicon.

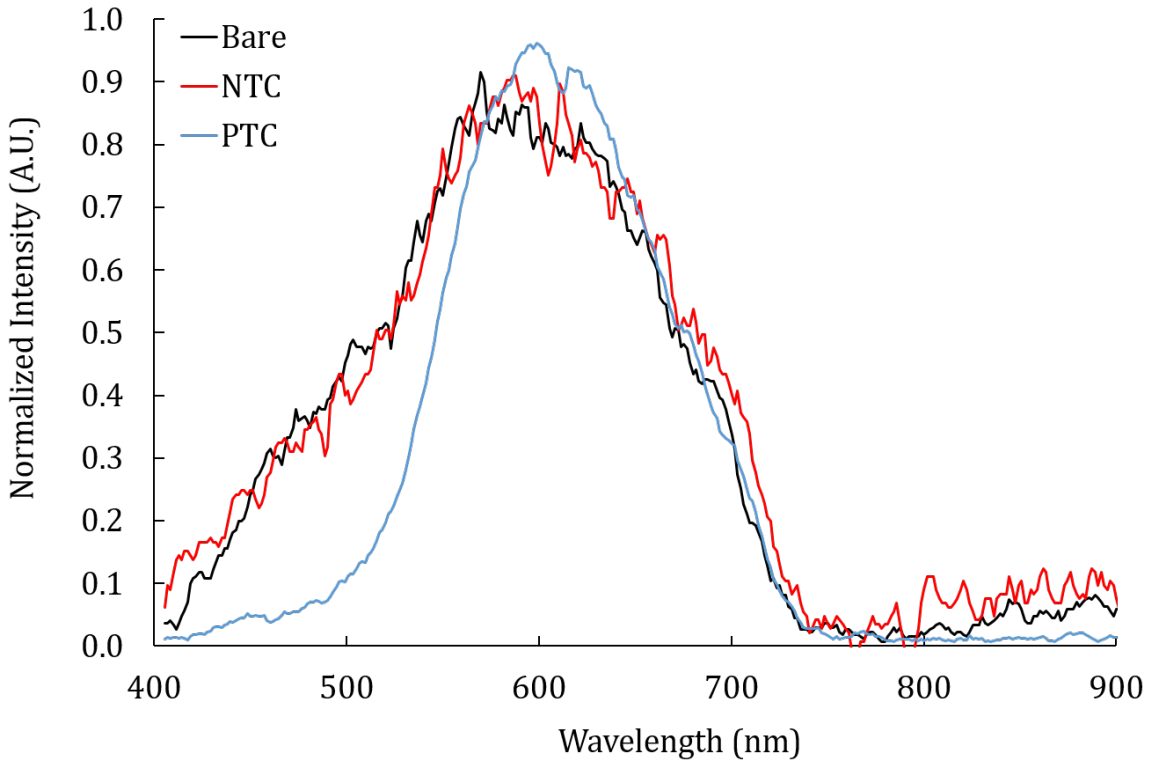

Figure 4.5 Initial hyperspectral analysis of nanoPCR amplification. Hyperspectral images were taken of qPCR reaction mixes after 40 cycles of amplification on a Biorad CFX96 thermocycler. The reactions were run using Fwd_01 thiolated primer conjugated to 20nm GNPs (BBI). The reverse primer used was Rev_08, leading to a 200 bp expected amplicon size. The PTC reaction was exposed to 10^5 copies/μL of MRSA 413 bp gene block and the NTC reaction had only water with no template. Solutions of bare 20nm GNPs with no conjugated primer (black), NTC product (red), and PTC product (blue) were imaged on a Cytoviva hyperspectral imaging platform. Representative spectra from imaged nanoparticles are shown.

4.3 Discussion

In this chapter we have shown the initial work required to develop a nanoPCR system. We have developed a model assay system to generate amplicons in a range of lengths. We created a system of primers conjugated to GNPs for spectral analysis and performed initial experiments on a hyperspectral imaging platform, with early results indicating a resonance shift for GNPs with after amplification.

In future work, we plan to further enhance amplification through the introduction of an additional polyethylene glycol (PEG) spacer to improve primer availability for amplification. Treatment with a thiolated PEG after primer-GNP conjugation may also improve primer availability by reducing interactions with the GNP surface. The plasmon shift as a function of amplicon length must also be characterized by both gel electrophoresis and hyperspectral imaging.

Furthermore, the true power of the nanoPCR assay lies in the use of the nanoplasmonic substrate as a heat generation platform as well. Further work to optimize the geometry of the nanoplasmonic substrate in order to produce thermal gradients required to drive PCR will facilitate new applications in nucleic acid analysis. This photothermal nanoPCR will enable high-sensitivity nucleic acid analysis while preserving spatiotemporal resolution. This could lead to significant applications for *in vivo* systems. Further, an optimization of the photothermal effect can lead to an inexpensive and robust PCR machine that is driven with simple LED's. Such a system would have significant implications for use in RLR settings.

4.4 References

1. Debnath, M., Prasad, G. B. K. S. & Bisen, P. S. *Molecular Diagnostics: Promises and Possibilities*. (Springer Netherlands, 2010). at <http://www.springerlink.com/content/978-90-481-3260-7#section=656588&page=1>
2. Craw, P. & Balachandran, W. Isothermal Nucleic Acid Amplification Technologies for Point-of-Care Diagnostics: A Critical Review. *Lab Chip* (2012). doi:10.1039/c2lc40100b
3. RAYMOND, S. & WEINTRAUB, L. Acrylamide Gel as a Supporting Medium for Zone Electrophoresis. *Science (80-.).* **130,** 711–711 (1959).
4. Epstein, J. R., Biran, I. & Walt, D. R. Fluorescence-based nucleic acid detection and microarrays. *Anal. Chim. Acta* **469,** 3–36 (2002).
5. Tyagi, S. Imaging intracellular RNA distribution and dynamics in living cells. *Public Health* **6,** 331–338 (2009).
6. Fernandez-Suarez, M. & Ting, A. Y. Fluorescent probes for super-resolution imaging in living cells. *Nat Rev Mol Cell Biol* **9,** 929–943 (2008).
7. Faraday, M. The Bakerian Lecture: Experimental Relations of Gold (and Other Metals) to Light. *Philos. Trans. R. Soc. London* **147,** 145–181 (1857).
8. Ghosh, S. K. & Pal, T. Interparticle Coupling Effect on the Surface Plasmon Resonance of Gold Nanoparticles: From Theory to Applications. *Chem. Rev.* **107,** 4797–4862 (2007).
9. Mie, G. Beiträge zur Optik trüber Medien, speziell kolloidaler Metallösungen. *Ann. Phys.* **330,** 377–445 (1908).

10. Ross, B. M. & Lee, L. P. Comparison of near- and far-field measures for plasmon resonance of metallic nanoparticles. *Opt. Lett.* **34,** 896–898 (2009).
11. Yang, M., Kostov, Y., Bruck, H. A. & Rasooly, A. Gold nanoparticle-based enhanced chemiluminescence immunosensor for detection of Staphylococcal Enterotoxin B (SEB) in food. *Int. J. Food Microbiol.* **133,** 265–271 (2009).
12. Baptista, P. V., Koziol-Montewka, M., Paluch-Oles, J., Doria, G. & Franco, R. Gold-Nanoparticle-Probe-Based Assay for Rapid and Direct Detection of Mycobacterium tuberculosis DNA in Clinical Samples. *Clin Chem* **52,** 1433–1434 (2006).
13. Liu, G., Doll, J. & Lee, L. High-speed multispectral imaging of nanoplasmonic array. *Opt. Express* **13,** 8520–8525 (2005).
14. Rosi, N. L. & Mirkin, C. A. Nanostructures in Biodiagnostics. *Chem. Rev.* **105,** 1547–1562 (2005).
15. Choi, Y., Park, Y., Kang, T. & Lee, L. P. Selective and sensitive detection of metal ions by plasmonic resonance energy transfer-based nanospectroscopy. *Nat Nano* **4,** 742–746 (2009).
16. Lindquist, N. C., Lesuffleur, A., Im, H. & Oh, S.-H. Sub-micron resolution surface plasmon resonance imaging enabled by nanohole arrays with surrounding Bragg mirrors for enhanced sensitivity and isolation. *Lab Chip* **9,** 382–387 (2009).
17. Link, S., Wang, Z. L. & El-Sayed, M. A. Alloy Formation of Gold−Silver Nanoparticles and the Dependence of the Plasmon Absorption on Their Composition. *J. Phys. Chem. B* **103,** 3529–3533 (1999).
18. Khlebtsov, N. G. Determination of Size and Concentration of Gold Nanoparticles from Extinction Spectra. *Anal. Chem.* (2008). at <http://pubs3.acs.org/acs/journals/doilookup?in_doi=10.1021/ac800834n>
19. Niemeyer, C. M. Nanoparticles, Proteins, and Nucleic Acids: Biotechnology Meets Materials Science. *Angew. Chemie Int. Ed.* **40,** 4128–4158 (2001).
20. Liu, G. L. *et al.* A nanoplasmonic molecular ruler for measuring nuclease activity and DNA footprinting. *Nat Nano* **1,** 47–52 (2006).
21. Shen, H. B., Hu, M., Wang, Y. B. & Zhou, H. Q. Polymerase chain reaction of nanoparticle-bound primers. *Biophys. Chem.* **115,** 63–66 (2005).
22. Lu, Y. & Liu, J. Preparation of aptamer-linked gold nanoparticle purple aggregates for colorimetric sensing of analytes. *Nat. Protoc.* **1,** 246–252 (2006).

Chapter 5: Conclusions and Future Work

5.1 Overview

In this work, several assays and tools have been presented to enable molecular diagnostics in remote and low-resource (RLR) settings. These tools included innovations in fluidic actuation, signal transduction, signal amplification, and result readout. In order to meet the diverse clinical needs in RLR settings, both nucleic acid and protein detection systems were developed. Initial tests have been performed on a range of simulated and clinical specimens, yielding promising results that can now be further developed into fully integrated diagnostic solutions.

5.2 Nucleic Acid Detection

The fundamental biochemical assay for nucleic amplification was optimized for use in RLR settings. The isothermal LAMP assay was adapted for selective amplification of SNPs encoding drug resistance in *M. tuberculosis*. Unique primers were demonstrated to yield differential amplification that was significantly enhanced through the addition of 3' destabilizing bases. This assay mechanism was further confirmed in the detection of *M. tuberculosis* in samples from infected patients.

Steps were taken to enhance the efficiency of this nucleic acid analysis platform through improved sample loading mechanisms. A novel microfluidic solution isolated pump (μSIP) was developed to increase fluidic loading rates, and to enable bubble-free loading of dead-end chambers. Both active and passive μSIP systems offer an attractive means to load fluid samples in RLR settings.

The entire nucleic acid test was coupled with a microfluidic biomolecular amplification reader (μBAR) to demonstrate a hand-held genetic analyzer for use in RLR settings. The performance of the μBAR system was characterized and amplification was confirmed with a model analytical system.

The microfluidic technologies implemented in the μBAR system can now be integrated with upstream sample preparation mechanisms in a matrix- and target-specific manner. This will yield a truly integrated system requiring minimal operator effort. Furthermore, multiplexed assays can be designed to leverage the differential SNP amplification mechanism with additional loci associated with drug resistance. As an additional step, the μBAR may be simplified through the introduction of an imaging readout based on the camera built into an off-the-shelf mobile device. This would provide an inexpensive, versatile, and robust means collect, analyze, and transmit amplification data.

5.3 Protein Detection

A robust aptamer-mediated amplification probe (AMProbe) system was demonstrated for the detection of the model protein, thrombin. This system was designed to transduce a protein biorecognition event into the release of an oligo strand containing a reporter component. The designed reporters included catalysts for downstream colorimetric or electrochemical analysis, isothermal amplification target sequences, and gene translation sequences for fluorescent analysis.

Release efficiencies of up to 45% were demonstrated for AMProbe constructs. Furthermore, a downstream nanoplasmonic readout mechanism was developed that enabled detection of released reporter down to 10pM. Alternatively, an isothermal AMProbe (iAMProbe) configuration was demonstrated to achieve a 1μM sensitivity in a surface-based assay.

The AMProbe constructs can now be further enhanced through optimization of the affinity for the target protein by leveraging several recently-developed advances in aptamer design. Furthermore, sensitivity can be decreased through the implementation of concentrating "capture" oligos immobilized downstream of the release reaction. Specificity may be further enhanced through the introduction of non-specific "capture" oligos immobilized downstream to selectively hybridize with unbound aptamer sequences. The nanoplasmonic readout may be further optimized with varying reaction chamber geometry, as well as catalyst reporter composition. Additionally, a fully-integrated system with both protein and nucleic acid detection can now be developed using iAMProbe constructs for downstream isothermal amplification of released reporters in parallel with the amplification of nucleic acid targets.

5.4 Nanoplasmonic PCR

A novel system for photothermal nanoplasmonic PCR (nanoPCR) was designed in order to enhance the speed, simplicity, cost, and multiplex of nucleic acid amplification. The system consisted of a nanoplasmonic substrate (in this case gold nanoparticles), that would yield plamon resonance peak shifts proportional to the length of amplicons on the surface. An initial demonstration of this assay was performed in a hyperspectral imaging system.

In future work, the amplification efficiency can be improved through additional surface modifications to the nanoplasmonic substrate. Further, planar surface substrates may also be adapted to this assay configuration, simplifying the process of peak shift analysis to operate in a mode similar to standard surface plasmon resonance instruments. Perhaps more importantly, the properties of these planar or colloidal nanoplasmonic substrates may be leveraged to drive the PCR assay. Illumination can be used to generate localized resistive heating that facilitates rapid thermocycling just in the local environment where PCR is taking place, and not in the entire bulk solution as is done in traditional PCR. This configuration may be further extended to intracellular analysis of nucleic acid expression through the use of colloidal plasmonic substrates.

5.5 Integrated Molecular Diagnostics

The systems described in this work demonstrate many individual components of diagnostic device that meets the needs of RLR settings. In some cases, these components were further integrated to provide a portion of the overall assay pipeline, as in the μBAR system. However, future work must be done to create a complete system, from sample extraction to result transmission and interpretation. Sample preparation remains the primary hurdle in this effort for many complex sample matrices. However, the modular nature of the systems described here lends them to strategic implementation in an integrated molecular diagnostic for nucleic acid and protein targets. Such a system promises to bring powerful healthcare tools into the hands of the global population.

Appendix

A Protocols

A.1 Quantitative PCR

A.1.1 Materials

Quantitative PCR (qPCR) assays were performed using SsoFast Evagreen 2x reaction mix containing a Evagreen SYBR dye (Invitrogen). Forward and reverse primers were added to a final concentration of 200 nM in a final 1x reaction mix containing the template solution and water. Oligos were generally ordered lyophilized, resuspended to 1 – 1,000 μM in water, and stored at -20°C until needed.

A.1.2 PCR primer design

PCR primers were generally designed using online tools such as PrimerQuest® (IDT). In some cases, our custom Matlab script was used to generate primers (see Appendix C.1).

A.1.3 PCR analysis in Bio-Rad CFX96

Final reaction mixes were placed in a PCR reaction tube or plate at volumes of 20 or 25 μL per reaction. The reaction vessel was stored on ice until use, if not used immediately. The tube(s) or plate were placed in the CFX96 heating block and instructions were followed to conduct PCR in accordance with recommended procedures for the reaction mix used.

A.2 Loop-mediated isothermal amplification

A.2.1 Materials

LAMP reactions were either performed using a LoopAMP reaction mix and FD dye (Eiken), or using a custom reaction mix preparead using the reagents listed in Appendix A.2.2. Chemicals were generally purchased from Sigma Aldrich or New England Biosciences and primers were purchased from IDT.

A.2.2 Cost comparison of LoopAMP kit vs. custom LAMP mix

The overall cost of custom LAMP mix was ~$0.025 per μL, or ~$61 to fill a 96-well plate of 25 μL reactions. This is ~13% of the cost to comparably fill a 96-well plate with LoopAMP kit (~$464). A cost break-down for solid and solution components of the custom LAMP mix are provided in Table A.1 and Table A.2, respectively. Reagents are from Sigma or New England Biosciences. Primers are from Integrated DNA Technologies (IDT).

Table A.1 Costs of solid components of custom LAMP mix

Reagent	Molecular Weight (g/mol)	Mass (g)	Moles	Cost	Cost/ mole	Concentration/ Reaction	Moles/ reaction	Cost/ reaction	Percent of Cost
Tris Buffer	127.2	100	0.786164	$74	$94.13	0.02	0.0000005	$0.00	0.00743%
KCl	74.55	500	6.706908	$31	$4.59	0.01	0.00000025	$0.00	0.00018%
$MgSO_4 \cdot 7H_2O$	246.47	500	2.028644	$30	$14.79	0.008	0.0000002	$0.00	0.00047%
$(NH_4)_2SO_4$	132.14	100	0.756773	$14	$18.76	0.01	0.00000025	$0.00	0.00074%
MnCl2	197.91	100	0.50528	$22	$43.94	0.001	0.000000025	$0.00	0.00017%
Calcein	622.53	5	0.008032	$103	$12,761.87	0.00005	1.25E-09	$0.00	0.00252%

Table A.2 Costs of solution components of custom LAMP mix

Reagent	Concentration (M)	Volume (L)	Moles	Cost	Cost/mole	Rxn Concentration (M)	Moles/ reaction	Cost/ reaction	Percent of Cost
Betaine	5	0.0015	0.0075	$20	$2,666.67	0.8	0.00002	$0.05	8.42%
dATP	0.1	0.00025	0.000025	$60	$2,400,000	0.0014	0.000000035	$0.08	13.26%
dCTP	0.1	0.00025	0.000025	$60	$2,400,000	0.0014	0.000000035	$0.08	13.26%
dGTP	0.1	0.00025	0.000025	$60	$2,400,000	0.0014	0.000000035	$0.08	13.26%
dTTP	0.1	0.00025	0.000025	$60	$2,400,000	0.0014	0.000000035	$0.08	13.26%
Bst Polymerase (units/L)	8000000	0.001	8000	$244	$0.03	320000	8	$0.24	38.52%
Tween 20 (%)	1	100	100	$27	$0.27	0.2	0.000005	$0.00	0.00022%

A.2.3 LAMP primer design

LAMP primers were generally designed using the web-based tool PrimerExplorer V4 (Eiken). For the detection of *M. tuberculosis* drug susceptibility, LAMP primers were selected through the following steps:

1. Identify tuberculosis drug resistance mutations in the TB Drug Resistance Mutation Database (tbdreamdb.com).
2. Identify high-confidence SNPs for resistance to several first/second line *Mtb* drugs.
3. Align these SNPs within genes on the entire *Mtb* genome H37Rv (RefSeq NC_000962).
4. Generate target sequences containing the SNP and +/- 200 bp flanking sequences.
5. Use Primer Explorer V4 (Eiken) to design primer sets agains these sequences.
6. Place F1 and B2 primers fixed around the SNP (use a 22bp size).
7. Display primers with "Sort = None" to see all results.
8. Select highly ranked primer set and save the primer file list.
9. Use the primer info file as an upload to generate the loop primers.
10. Add each of the 6 regions to Geneious (F3, F2, F1, B1c, B2c, B3c).
11. FIP = 5'-F1c-F2-3' and BIP = 5'-B1c-B2-3'. F3, B3, LPF, and LPB primers are directly provided.

A.2.4 LAMP solution preparation

LAMP reaction solutions were either prepared from stock solutions (Table A.3). Either a LoopAMP 2x Reaction Mix or a custom LAMP 2x Reaction Mix was used (adapted from Tomita et al.[1]). Either the LoopAMP Fluorescent Detection (FD) dye was used, or a mixture of Calcein and $MnCl_2$ was added. In general, 10% excess was prepared in order to account for liquid loss during transfer steps (Table A.3 is thus preparing 6 reactions).

Table A.3 LAMP solution preparation from stock.

# Reactions			**1 reaction**	**6.6 reactions**
Reagents	[Stock]	[Final]	Volume (μL)	Volume (μL)
2x Reaction Mix (X)	2	1	12.5	82.5
FIP Primer (μM)	20	1.6	2	13.2
BIP Primer (μM)	20	1.6	2	13.2

Loop-F (μM)	20	0.8	1	6.6
Loop-B (μM)	20	0.8	1	6.6
F3 (μM)	20	0.2	0.25	1.65
B3 (μM)	20	0.2	0.25	1.65
Fluorescent Detection (X)	25	1	1	6.6
***Bst* Polymerase (X)**	25	1	1	6.6
Template (cop/uL)	25	1	1	6.6
H2O			3	19.8
Total Volume (uL)			**25**	**165**

A.2.5 Plasmid preparation

Plasmids were prepared in accordance with the IDT Custom Gene Synthesis Protocols (http://www.idtdna.com/catalog/CustomGeneSyn/). The following steps were performed to prepare plasmid stocks:

1. Resuspend Plasmids
    1. Centrifuge tube ~1 minute prior to opening to ensure DNA is on the bottom.
    2. Resuspend DNA in 20 μL of 1x TE Buffer.
    3. Incubate tube at room temperature for 30 minutes, then vortex for 20 seconds.
    4. Centrifuge for 1 minute.
    5. Create working stock: Add 1 μL of 0.1 μg/mL stock to 999 μL of H_2O.
    6. Store the working stock at -20°C.
2. Transform Competent *E. coli* (based on IDT Gene Synthesis Protocol and E. cloni 10G protocol MA05N1.6)
    1. Pre-chill all microcentrifuge tubes on ice. Pre-warm hot bath to 42°C.
    2. Thaw E. Cloni Chemically Competent Cells (Cat. #60108-1, Lucigen) on ice for ~10 – 20 minutes.
    3. Add 40 μL E. Cloni cells to each tube (on ice).
    4. Add appropriate amount of plasmid (1 – 2 μL) or (+)/(-) control to each tube. Stir with pipette tip gently and incubate on ice for 30 minutes.
    5. Heat shock tubes for 45 seconds in 42°C hot bath.
    6. Return tubes to ice for 2 minutes.
    7. Add 960 μL Recovery Medium (Lucigen) at room temperature to each tube.
    8. Place tubes in warm room at 37°C on a shaker (250rpm).
    9. Pre-warm agar plates to 37°C (M9 Minimal Salts –Amp, Teknova Cat. #M1245)
    10. Plate transformed cells (either 10 μL or 100 μL) onto agar plates. Spread evenly on the plate and let it sit for 10 minutes at room temperature.
    11. Place the plates upside-down at 37°C. Allow to incubate on plates until colonies form (more than 1 day).
    12. Inoculate an individual colony from the plate into LB Broth + Amp and incubate at 37°C.

For the destabilized primers, the H37RV and D435V plasmids were at a molecular weight of ~1479938.5 g/mole. The solutions at 10^4 cop/μL were thus equivalent to ~27 fM.

A.2.6 LAMP Analysis in Bio-Rad CFX96

Final reaction mixes were placed in a PCR reaction tube or plate at volumes of 20 or 25 μL per reaction. The reaction vessel was stored on ice until use, if not used immediately. The tube(s) or plate were placed in the CFX96 heating block and a LAMP procedure was followed with a temperature generally around 60 – 63°C for up to 120 minutes, with fluorescence image capture in the green channel every 30 seconds.

A.2.7 LAMP Analysis in microfluidic chip

LAMP reaction chips were used for microfluidic analysis. Chips were prepared according to Appendix A.6. Assembled chips were stored in a vacuum for 35 – 60 minutes to degas the PDMS. Chips were vacuum sealed if they were not used immediately. Otherwise, sample was immediately loaded into inlets and the device was placed into the μBAR. Standard assays on the μBAR generally involved a 120 minute reaction at ~60°C.

In cases where reagents were lyophilized on chips, the appropriate solutions were pipetted into the reaction chambers on an inverted PDMS slab. This slab was placed in a petri dish and incubated at -80°C for 15 mins. The petri dish was then immediately transferred to a Labconco FreeZone 4.5 Plus lyophilization chamber. The pressure generally reached 0.021 mBar or below. The petri dish was incubated overnight to ensure it is completely dried. The chip is then bonded to a glass slide or PCR tape as desired.

A.2.8 LAMP Analysis of human-derived M. tuberculosis samples

Human-derived *M. tuberculosis* samples were provided by our collaborators in the National Centre for Tuberculosis Excellence at Tygerberg. These samples had been treated according to the following procedure:

1. Prepare 2% NaOH/NALC (MycoPrep, Becton Dickinson)
2. Add equal amounts of sputum and MycoPrep reagent (total volume should not exceed 20 mL) to a 50 mL centrifuge tube.
3. Vortex 20 seconds.
4. Invert tube to ensure solution contacts all of the sputum.
5. Let stand at room temperature for 20 seconds.
6. Mix every 5 minutes by gentle inversion (do not treat for longer than 20 minutes).
7. Add sterile PBS to the 45 mL mark of the tube to stop decontamination.
8. Invert tube 3 times to mix.
9. Place centrifuge tube in the biosafety cabinet and remove protective lid.
10. Centrifuge tube at 3000 rcf for 15 minutes at 4°C.
11. Carefully pour supernatant into a screw top bottle, leaving the pellet in the tube.
12. If sputum smears are done, make a smear of the concentrated pellet.
13. Use a pipette to add 1.5 mL of sterile PBS buffer to the tube.
14. Recap the tube and vortex for 5 seconds to resuspend the pellet.

Samples were analyzed as described in Appendices A.2.6 and A.2.7.

A.3 Recombinase polymerase amplification

A.3.1 Materials

TwistAMP™ Basic kits were purchased (TwistDx) for DNA analysis. Primers were purchased from IDT.

A.3.2 RPA Solution Preparation

RPA reaction mixes were prepared in accordance with the TwistDx product manual TA01cmanual (Revision E). An example RPA reaction preparation for 2 replicates of a PTC and 2 replicates of a NTC is shown in Table A.4.

Table A.4 RPA reaction solution preparation from stock.

# Reactions		**1**	**PTC**	**2.2**	**NTC**	**2.2**
Reagents	[Stock]	Volume (μL)	[Final]	Volume (μL)	[Final]	Volume (μL)
Rehydration Buffer	1.69491	29.5	1	64.9	1	64.9
Forward Primer (uM)	10	2.1	0.42	4.62	0.42	4.62
Reverse Primer (uM)	10	2.1	0.42	4.62	0.42	4.62
Exo Probe (uM)	10	0.6	0.12	1.32	0.12	1.32
Magnesium Acetate (mM)	280	2.5	14	5.5	14	5.5
Template (cop/uL)	100	10	20	22	0	0
H2O		3.2		7.04		29.04
Total Volume (uL)		**50**		**110**		**110**

A.3.3 RPA Analysis on CFX96 Thermocycler

Final reaction mixes were placed in a PCR reaction tube or plate at volumes of 50 μL per reaction. The reaction vessel was transferred to the CFX96 heating block immediately upon addition of the magnesium acetate. The mix was incubated between 20 – 37°C for up to 60 minutes, with fluorescence image capture in the green channel every 10 – 30 seconds.

A.4 Aptamer binding and reporter release analysis

A.4.1 Surface plasmon resonance analysis

Surface plasmon resonance studies of binding and release kinetics were performed on a Biacore™ T100 instrument. Stock solutions were prepared and loaded into the reagent tubes appropriately. Programs were designed to test sequential injection of each part of the AMProbe construct in order to ensure adequate mass accumulation on the surface. Assays were performed as described in Figure 3.4.

A.4.2 Radiolabel analysis

Radiolabel assays were performed in collaboration with the Doudna Lab according to the below procedure:

1. Preparation of nuclease-free 20x SSC buffer (3.0-M NaCl, 0.3-M sodium citrate)

1. Add 87.7-g NaCl and 44.1-g trisodium citrate to 400-mL DEPC-treated water. Add 10-N HCl to a final pH of 7.2 then bring the final volume up to 500-mL. Dispense into aliquots and sterilize by autoclaving.
2. Prepare a stock of 0.5x SSC buffer for use with the remainder of the procedure.

2. Preparation of SA-PMPs for use
    1. Obtain a new tube of SA-PMPs (600-µL in a 1.5-mL centrifuge tube) and gently flick or vortex to resuspend the particles. The particle should remain suspended for at least 3-minutes without forming a visible pellet.
    2. Annealing the biotinylated DNA: Prepare a solution of 2.4-µM biotinylated DNA and any other oligos which should be hybridized to the DNA in 500-µL solution (1.2-nmol total DNA). Add 13-µL of 20x SSC buffer to bring the final SSC concentration to 0.5x. Incubate in a heat block at 65°C for 10-min, then cool to room temperature for 10-min.
    3. Washing the SA-PMPs: Place the tube in a magnetic stand and wait 30-s for the particles to fully aggregate on the side of the tube. Carefully remove the supernatant without disturbing the particles, then add 300-µL of fresh 0.5x SSC buffer to wash the particles. Gently flick or vortex to resuspend the particles and repeat for 3 washes. After the last wash, resuspend the particles in 100-µL of 0.5x SSC buffer. The particles should be used within 30-minutes of washing for optimal retention of activity.
    4. Add the contents of the annealing reaction to the washed particles and incubate for 10-min, gently inverting and mixing every 1 to 2-min. Isolate the particles, pull off the supernatant, and resuspend the particles in 100-µL 0.5x SSC buffer in preparation for hybridizing the reporter DNA to the aptamer structure.
3. Adding the reporter DNA
    1. Prepare a solution of 2.4-µM P32-labeled DNA in 500-µL water (1.2-nmol total DNA) and add to it 13-µL of 20x SSC buffer to bring the final SSC concentration to 0.5x. Prepare a separate aliquot of the 2.4-µM P32-labeled DNA to measure the activity of P32 present ("P32 mix").
    2. Add the contents of the tube containing reporter DNA to the tube containing the particles. Mix by gently flicking or vortexing before bringing the contents of the tube to 50°C on a heat block for 10-min and cooling to room temperature for another 10-min.
    3. Place the tube in a magnetic stand and wait 30-s for the particles to aggregate. Carefully pull off the supernatant and store in a tube to measure the activity of P32 present ("SN or Supernatant").
    4. Wash the particles 3 times with 300-µL 0.5x SSC buffer. Save each of these washes in a tube to measure the activity of P32 present ("Wash 1", "Wash 2", "Wash 3"). Resuspend the particles in 300-µL 0.5x SSC buffer after the washes are finished.
    5. Resuspend the particles by gently flicking or vortexting the tube and dispense 50-µL aliquots into separate tubes. 5 of these aliquots can be

used for the thrombin/adenosine capture and release experiments. The remaining aliquot should be saved to measure the activity of P32 present ("AW or After Wash"). This helps us confirm how much P32 is left on the beads prior to target addition.

4. Target capture and P32 release
    1. From the previous step, each tube containing fully assembled aptamer structures with P32 reporter should have been divided into 6 aliquots, 5 of which can be used for the target capture and P32 release experiments.
    2. For characterization of the sensitivity of release, add 10-µL of thrombin/adenosine at different concentrations to each tube containing 50-µL of particles prepared with the fully assembled aptamer structure and P32-labeled reporter DNA. Mix by gently flicking or vortexing and incubate each tube at room temperature for 30-min. Pull off the supernatant with the help of the magnetic stand and store in a tube to measure the activity of P32 present ("T"). The particles should be saved and resuspended in 60-µL 0.5x SSC buffer to measure the activity of any residual P32 left on the beads ("R").
    3. For determination of the optimal incubation time, add 10-µL of 10-µM thrombin/adenosine to each tube containing 50-µL of particles prepared with the fully assembled aptamer structure and P32-labeled reporter DNA. Mix by gently flicking or vortexing and incubate each tube at room temperature for varying amounts of time (5-min, 10-min, 20-min, 30-min, 60-min). Pull off the supernatant with the help of the magnetic stand and store in a tube to measure the activity of P32 present ("T"). The particles should be saved and resuspended in 60-µL 0.5x SSC buffer to measure the activity of any residual P32 left on the beads ("R").

A.4.3 iAMProbe analysis

iAMProbe tests were performed on a glass slide with silicone wells according to the following procedure:

1. iAMProbe Construct Preparation
    1. Prepare a mix of 7.5 µL 20x SSC buffer, 30 µL Thrombin Anchor_02 Biotin, 30 µL Thrombine RPAtag_02, and 232.5 µL H_2O.
    2. Incubate mixture at 60°C for 10 minutes.
    3. Anneal mixture at room temperature for 10 minutes.
    4. Prepare 7 100x dilutions into 0.5x SSC buffer (5 µL solution + 495 µL 0.5x SSC). This will lead to 8 total dilutions ranging between 1E-6 and 1E-20 M.
2. Glass Slide Preparation
    1. Use KNK cutter to cut two rows of 8 silicone wells (3 mm diameter, 4.5 mm pitch).
    2. Place the silicone chambers onto a streptavidin-coated glass slide.

3. Pipet each dilution of iAMProbe construct into two separate wells on the glass slide.
4. Incubate iAMProbe on glass slide for 15 minutes at room temperature.
5. Carefully remove the remainder of the solution in each well.
6. Wash the wells to remove unbound iAMProbe.
    1. Incubate 0.1x SSC buffer in each well for 10 minutes at room temperature (pipet up and down 10x when removing).
    2. Repeat the above step a total of 4 times.
    3. Incubate 0.5 mg/mL BSA in each well for 10 minutes at room temperature (to block non-specific reactions).
    4. Wash each well twice with 0.1x SSC buffer (10 minute incubation, pipet up and down 10x).
    5. Wash each well once with HBSP buffer (10 minute incubation, pipet up and down 10x). Slide is now ready for use.

3. Thrombin Release Assay
    1. Add 10 μL of 1 μM thrombin (in HBSP buffer) to each of 8 top row chambers.
    2. Add 10 μL of 0 μM thrombin (just HBSP buffer) to each of 8 bottom row chambers.
    3. Incubate both for 10 minutes at room temperature.
    4. Remove all 10 μL from each well and transfer to a PCR plate for use as the templates in a set of RPA reactions.

A.5 DNA conjugation to gold nanoparticles

A.5.1 DNA design for conjugation

PCR primers were designed as described in Appendix A.1. Primers were designed to generate amplicons between 50 and 200 bp in length. They were additionally constrained to have a probe hybridization region within the amplicons.

A.5.2 DNA conjugation to gold nanoparticles

The procedure to conjugate thiolated DNA to gold nanoparticles was adapted from Liu and Lu[2].

1. De-protect thiolated primers
    1. Prepare 10mM TCEP. TCEP should be prepared fresh each time.
    2. Pipette 9uL of 1mM thiolated primer into a microcentrifuge tube.
    3. Add 1μL of 500mM acetate buffer (pH 5.2) and 1.5μL of 10mM TCEP to each tube to activate the thiol-modified DNA. Incubate the sample at room temperature for 1 hour.
2. Prepare DNA-GNP conjugation vials
    1. Fill disposable scintillation vials (20 ml volume) with 12M NaOH.
    2. Incubate vials for 1 hour at room temperature.
    3. Rinse the vials with large amounts of deionized water and then Millipore water.
    4. Dry vials with N_2 for later use.

3. Prepare gold nanoparticles
    1. Use 50ml of 15 nm GNPs (BBI, 1.4E12 particles/mL)
    2. Centrifuge at 16,110 RCF and remove 44 mL supernatant. Note: centrifuging > 3 times leads to aggregation due to destabilization of the citrate cap (this is in equilibrium with the solution). For 10 nm particles, it is recommended to centrifuge at 14,000 rpm for 30 mins. For 20 nm particles it is recommended to centrifuge at 14,000 rpm for 5 mins.
    3. Split 6 mL into 2 scintillation vials.
4. Conjugate DNA to GNPs
    1. Transfer 3mL of the already prepared 15nm gold nanoparticles (BBI, 1.4E12 particles/mL) to each of the two NaOH-treated glass vials.
    2. Slowly add the TCEP-treated thiol DNA with gentle shaking by hand.
    3. Cap the vials and store them in the dark at room temperature for at least 16 hours. Magnetic stirring may also be applied to facilitate the reaction.
    4. Add 30uL of 500mM Tris acetate (pH 8.2) buffer dropwise to each vial with gentle hand shaking. The final Tris acetate concentration is 5mM.
    5. Add 300uL of 1M NaCl dropwise to each vial with gentle hand shaking. Store the two vials in the dark for at least another day before use.
5. Removal of Unattached Primers
    1. Centrifuge conjugated DNA-GNP solution at 14,000 rpm for 30 mins and remove the supernatant.

A.5.3 Analysis of DNA-GNP conjugates in Bio-Rad CFX96

The prepared DNA-GNP conjugates were used as primers in a standard PCR reaction mix as described in A.1. Final reaction mixes were placed in a PCR reaction tube or plate at volumes of 20 or 25 μL per reaction. The reaction vessel was transferred to the CFX96 heating block and instructions were followed to conduct PCR in accordance with recommended procedures for the reaction mix used. Fluorescent quantification was performed in the green channel at the end of each cycle, for up to 40 cycles.

A.5.4 Analysis of DNA-GNP conjugates in Cytoviva System

The products of the DNA-GNP PCR reaction in Appendix A.5.3 were analyzed in a dark field hyperspectral imaging system (Cytoviva). Slides were prepared with 5 – 10 mL of each sample under a glass cover slip. Cytoviva immersion oil was used to create contact between the slide and the imaging optics. Images were captured and spectra isolated from individual particles.

A.6 PDMS chip fabrication

A.6.1 Overview of PDMS chip fabrication

Soft lithography is the process by which a microfluidic device is rapidly prototyped from a mold composed of patterned photoresist on a silicon substrate (Figure A.1). First a mold is made through spinning a thin coat of photoresist onto a silicon wafer and UV exposing the photo resist to generate a hardened pattern that remains after the development

phase. SU-8 is a commonly used photoresist in this process, and mylar masks are frequently designed and used for UV patterning. Once the SU-8 mold has been created, PDMS devices can be generated by pouring the liquid base components and allowing them to solidify. The PDMS device is then removed from the mold and bonded to a substrate to form the bottom of the channels via oxygen plasma bonding.

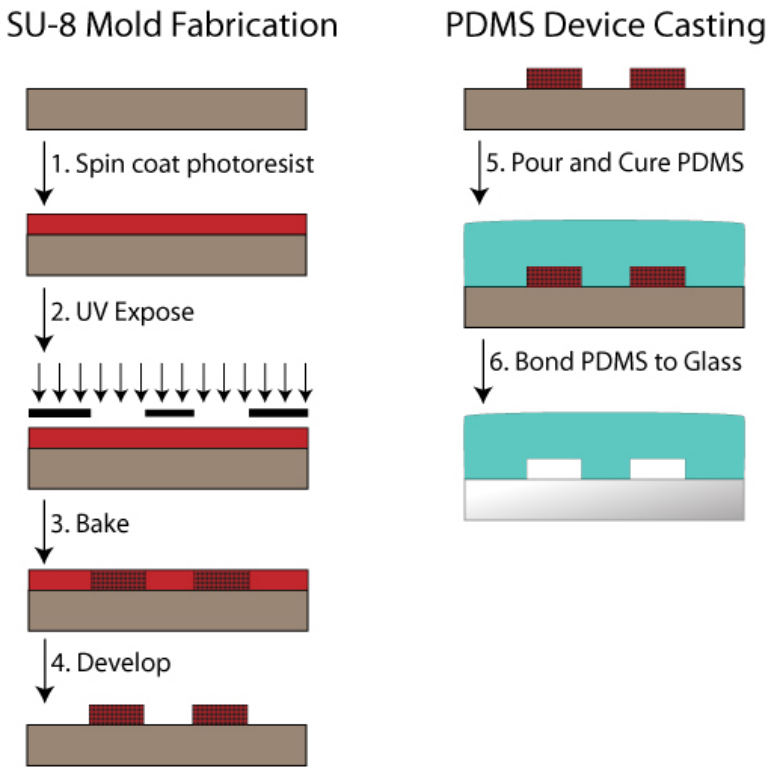

Figure A.1 Soft lithography to prototype microfluidic devices.

A.6.2 Materials

SU-8 photoresist (Microchem) is selected based on viscosity in order to achieve desired channel heights. Propylene glycol monomethyl ether acetate (PGMEA, Sigma Aldrich) is used as a developing solution to remove unhardened photoresist. Silicon wafers (University Wafer) are used as the main substrate of the mold. Polydimethylsiloxane is composed of a primary reagent mixed with a cross-linking initiator reagent at a 10:1 w/w ratio (Sylgard 184 Silicone Encapsulant Clear, Dow Corning). Glass slides or PCR tape are used to form the bottom of the microfluidic channels. Furthermore, PCR tape proved a powerful means to decrease gas permeability across the upper surface of the PDMS device. Like glass substrates, the PCR tape can also be bonded to PDMS through an oxygen plasma reaction.

A.6.3 Mask design tips

Masks were generally designed in AutoCAD. A few notes on microfluidic design:

1. In order to stabilize SU8 mold, try to get a 1:1 aspect ratio of height to width for any given channel.

2. No structure (control or flow) can be fabricated having an aspect ration lower than 1/10. The aspect ratio is defined as the quotient of the structure height to the minimum lateral dimension (height/width). Structures with lower aspect ratios are prone to collapse. If a feature is wider than this design rule permits, support posts must be added to ensure the aspect ratio is no lower then 1/10 in-between posts (i.e. posts every 100μm for a 10μm high structure).
3. Make inlets ~1mm in diameter, and draw a 4mm diameter circle around the inlets (in junk layer) to keep you from putting anything within 3mm of your inlets. At a minimum, the outer circle should be 2mm.
4. If more than one chip is designed on a wafer there must be at least 2 mm spacing between the borders of adjacent devices.
5. Minimum center to center punch spacing for 20 guage I/O's is 1500 μm. Minimum center to center spacing for 15 guage I/O's is 2000 μm.
6. Leave a ring of approximately 0.5cm (5000micron) free around the mold perimeter. This area should be void of any design or critical chip area since photoresist uniformity is least reliable around the perimeter of a wafer.

A.7 Anodized aluminum oxide fabrication

A.7.1 Overview of AAO fabrication

A hexagonally ordered array of pores is formed in an oxide film when aluminum metal is anodized in acidic solutions. This ordering arises from mechanical forces between neighboring pores as the Al is anodized to form Al_2O_3 and undergoes volume expansion. The average pore spacing, width, and depth of the resulting oxide film depend on the anodization conditions, including electrolyte composition, Al purity, current density, time, temperature, and other reaction kinetic factors such as stir rate. Well-ordered AAO templates are known to be formed from 19 – 25 V in sulfuric acid, 40 V in oxalic acid, and 160 – 195 V in phosphoric acid, with sulfuric acid forming the smallest pores (~7 nm) and phosphoric acid producint the largest pores (~300 nm). Oxalic acid forms an intermediate pore size (~50 nm).

A.7.2 Materials

1. 1 L jacketed beaker connected to Neslab RTE7 water circulator and Digital One temperature controller, placed over magnetic stirrer
2. 5.25" diameter acrylic cover placed over beaker with slots cut out for Cu wire (gauge 12) with alligator clips (ACE 22-14 AWG) for electrical contact with sample
3. BK precision 1623A power supply (0 to 60 V, 1.5 A maximum current) with leads to drive anodization reaction
4. Pt electrode (99.99%, 1 x 1 in) and Al sample attached to alligator clips and immersed in anodizing solution up to maskant line
5. Aluminum foil (99.999%, 0.5 mm, area = 2.0 x 2.0 in^2)
6. Isopropyl alcohol, 70-% v/v (67-63-0, MSDS)
7. AC 828T maskant (MSDS)

8. Ethanol, 100-% (64-17-5, MSDS)
9. Perchloric acid, 60-% (7601-90-3, order, MSDS)
10. Oxalic acid (114-62-7, order, MSDS)
11. Chromic acid (7738-94-5, order, MSDS)
12. Phosphoric acid, 85-% wt (7664-38-2, order, MSDS)

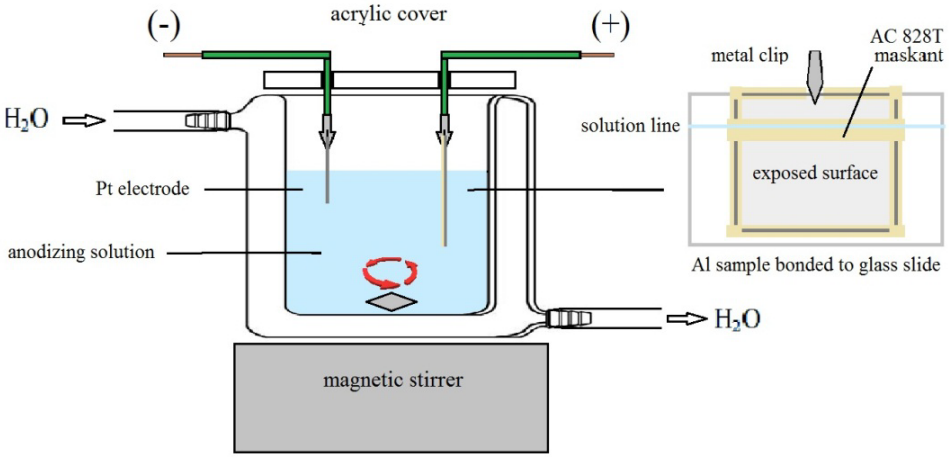

Figure A.2 Anodization setup. A fluidic cooling sheath and magnetic stirrer provide environmental control while a power supply and Pt electrode facilitate electrolytic reactions during the anodization process.

A.7.3 Anodization of aluminum

Anodization of Pure Al Alloy (99.5% pure annealed 1050 Al alloy, CometMetals Inc.)

1. Pretreatment – Loading Al
    1. Use tin snips to cut a 2 x 2 in piece of Al alloy.
    2. Place Al alloy on a large glass slide.
    3. Working in a fume hood, block the underside of the Al with AC 828T Maskant adhesive (resistant to acids).
    4. Dry the muskant at room temperature for ~30 minutes (or shorter in 60°C oven).
2. Electropolishing – Remove Aluminum Oxide
    1. Set temperature on the sheath coolant to 7°C.
    2. Prepare a solution of 400 mL 100% EtOH (Rossville Gold Shield, 200-proof) and 100 mL 60% perchloric acid (Sigma Aldrich #311413). A new solution should be prepared if the solution appears contaminated with black specs, or if it has been used more than 5 times for electropolishing.
    3. Start the magnetic stirrer rod at 350 rpm.
    4. Preprogram the power supply for 20 V and turn the current to the max setting to prevent the system from being current-controlled.

5. Rinse the Al alloy and Pt electrode sample with IPA and dH_2O. Attach the (+) end of the power supply to the Al alloy and the (-) end to the Pt electrode. And submerge them to the appropriate lines in the solution.
6. After 30 seconds of submersion, switch on the power supply and increase the stir speed to 1050 rpm. The current should be less than 1 A with ~0.07 A per cm^2 of exposed Al surface. Allow the reaction to run for exactly 4 minutes. A gray film will form and peel away after ~1 minute of electropolishing.
7. After 4 minutes, switch the power supply off and remove the Al alloy and Pt electrode from the solution and rinse with IPA for 10 seconds, followed by dH_2O for 10 seconds. Then dry both off with N_2. Immediately begin the next step as the Al alloy will begin to oxidize in air. The surface of the alloy should be smooth and shiny after electropolishing.

3. 1^{st} Anodization – Oxalic Acid
    1. Set temperature on sheath coolant to 14^oC. Pour the electropolishing solution back into its container and clean the beacker with IPA followed by dH_2O.
    2. Prepare the 1^{st} anodization solution by adding 18.9 g of oxalic acid (99.999% purity, Sigma Aldrich, #658537) to 500 mL of dH_2O. Agitate white flakes until they are completely dissolved.
    3. Add the 1^{st} anodization solution to the beaker with a clean stir bar and set the stir speed to 350 rpm.
    4. Preprogram the power supply to 40 V.
    5. Once the solution temperature is stable at 14oC, place the Al alloy and Pt electrode in the solution as before, connecting the (+) and (-) leads in the same manner. After 30 seconds, switch the power supply on and allow the anodization to proceed for 10 – 12 hours. The current should fall to 0.01 A immediately and slowly rise about 0.04 A to 0.06 A for the duration of the anodization. If the current continues to increase or bubbles are observed at the edges of the maskant, there is a leak and the experiment should be halted as both the Pt electrode and the oxalic acid solution may be damaged.
    6. After 10 to 12 hours, the Al sample should appear a dark and dull yellow. Turn off the power and carefully remove the Al alloy and the Pt electrode from the solution and clean as before. After the first anodization, the alloy samples may be stored indefinitely, so additional Al samples can be prepared for the next step, which has a capacity for etching up to 4 samples at once. The maskant can also be carefully removed at this point.
4. Etching
    1. Prepare the etching solution by adding 9.0 g of chromium trioxide (99.99% purity, Sigma Aldrich, #675644) and 20.2 mL of 85.0%wt H_3PO_4 to dH_2O up to a 500 mL volume. The solution should appear bright reddish-orange color due to the dichromatic ion in solution.

2. Set temperature on sheath coolant to 65°C. This will take up to 50 minutes, so do not introduce the next etching solution until the beaker is at least at 55°C to minimize evaporative loss. Introduce a clean stir bar and set the stir speed to 125 rpm.
3. Attach up to 4 samples to the two clips after cleaning them with IPA and dH_2O. Orient the samples such that they are back-to-back. Place the samples in the etching solution and incubate for 6 – 8 hours.
4. Once etching has completed, remove the Al alloy samples and place them in a bath of hot dH_2O. Remove each sample from the dH_2O bath and dry with N_2 before placing in a sealed vacuum chamber for storage (in order to prevent oxidation). Alternatively, the Al alloy samples can be placed in a baker, filled with N_2, and then have the top quickly sealed off with multiple layers of parafilm. Start ramping the sheath temperature down to 14°C.

5. 2nd Anodization – Anodize to Desired Depth (100 nm/min)
    1. The procedure is the same for the 1st anodization except for the following differences:
        1. Use a fresh 0.3 M oxalic acid solution to guarantee consistency with the second anodization.
        2. Prepare a hot dH_2O bath in which the samples are immersed immediately following anodizaing so that any residual acid will be cleaned from the pores.
    2. Andoize the sample for the desired time (100 nm/min). Connect a multimeter in series with the electrochemical circuit to more precisely characterize the anodization current in this step.
    3. After washing and drying with N2, the sample should appear faintly colored with tints ranging from bluish-purple to pale yellow to aqua-teal to pinkish-red (increasing anodization time). Anodizing for 5 minutes should produce a pinkish-red tone.
6. Pore Widening – Widen Desired Amount (~50 nm/min)
    1. Prepare a 0.1 M phosphoric acid solution and increase the sheath temperature to 30°C . Set the stir speed to 350 rpm.
    2. Immerse the Al alloy in the solution for the desired time.

<u>Anodization of Reynolds Al Foil (20 μm thickness, heavy-duty foil)</u>

1. Pretreatment – Loading Al
    1. Place Al foil on a large glass slide. Smooth the foil as flat as possible.
    2. Working in a fume hood, block the underside of the Al with AC 828T Maskant adhesive (resistant to acids).
    3. Dry the muskant at room temperature for ~30 minutes (or shorter in 60°C oven).
2. 1st Anodization
    1. Anodize the Al foil sample as above in 500 mL of 0.3 M oxalic acid solution at 14°C, 40 V, and 350 rpm for the desired time. Switch the power supply on exactly 10 seconds after introducing the Al foil into the solution.

2. Carefully cut the Al foil from the maksant and dry in N_2.

3. Pore Widening – Widen Desired Amount (~50 nm/min)
    1. Prepare a 0.1 M phosphoric acid solution and increase the sheath temperature to 30°C with a stir speed of 350 rpm.
    2. Immerse the Al foil in the solution and incubate to the desired time, following the same procedure as with the above pure foil.

A.7.4 Gold film deposition

Anodized Al samples from above were seeded with a thin film of gold through a sputtering process. First, a 2 nm Cr layer was sputtered, followed by a 10 nm Au layer. These samples were then ready for testing.

B CAD Design & Prototypes

B.1 PDMS Chip Design

B.1.1 LAMP Chips

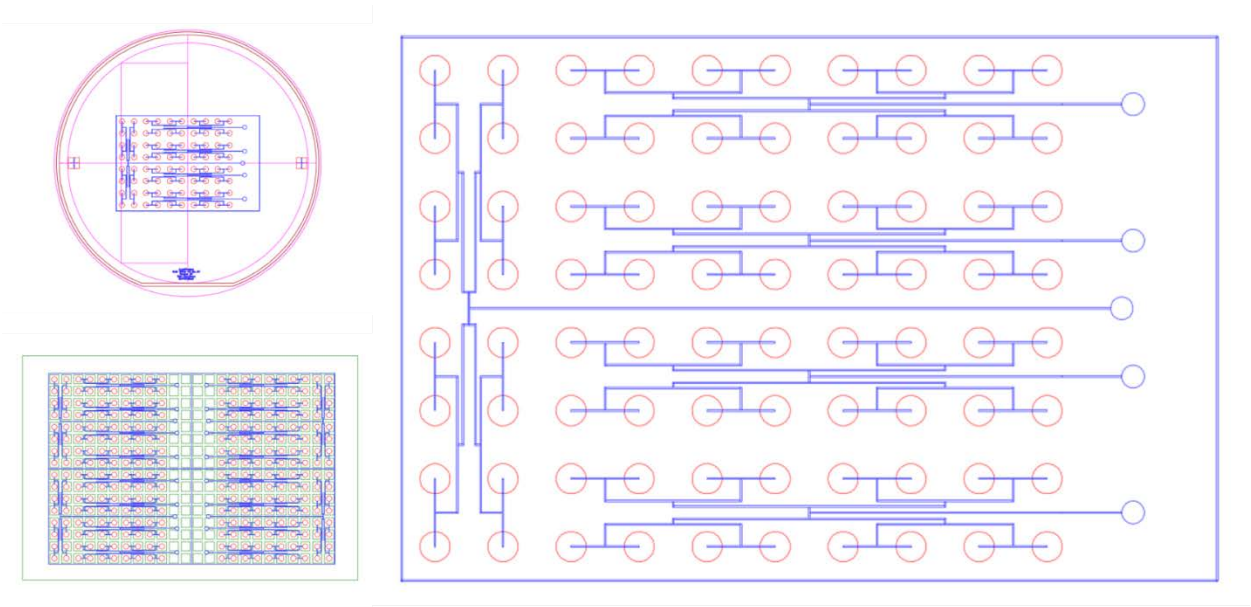

Figure B.1 Initial LAMP chip design. [2010-10-04] The initial chip was designed to align with a 384 well plate (bottom-left). The chip was designed to have 5 inlets with channels (blue) leading to downstream reaction chambers (red).

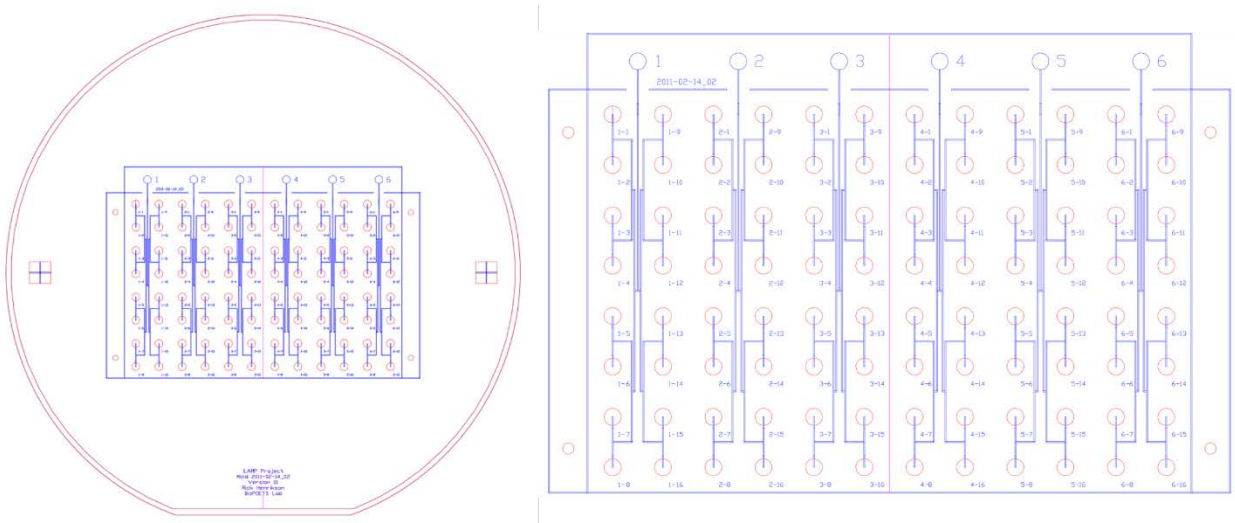

Figure B.2 Standard LAMP analysis chip for μBAR. [2011-02-14] The standard LAMP chip design used in μBAR assays.

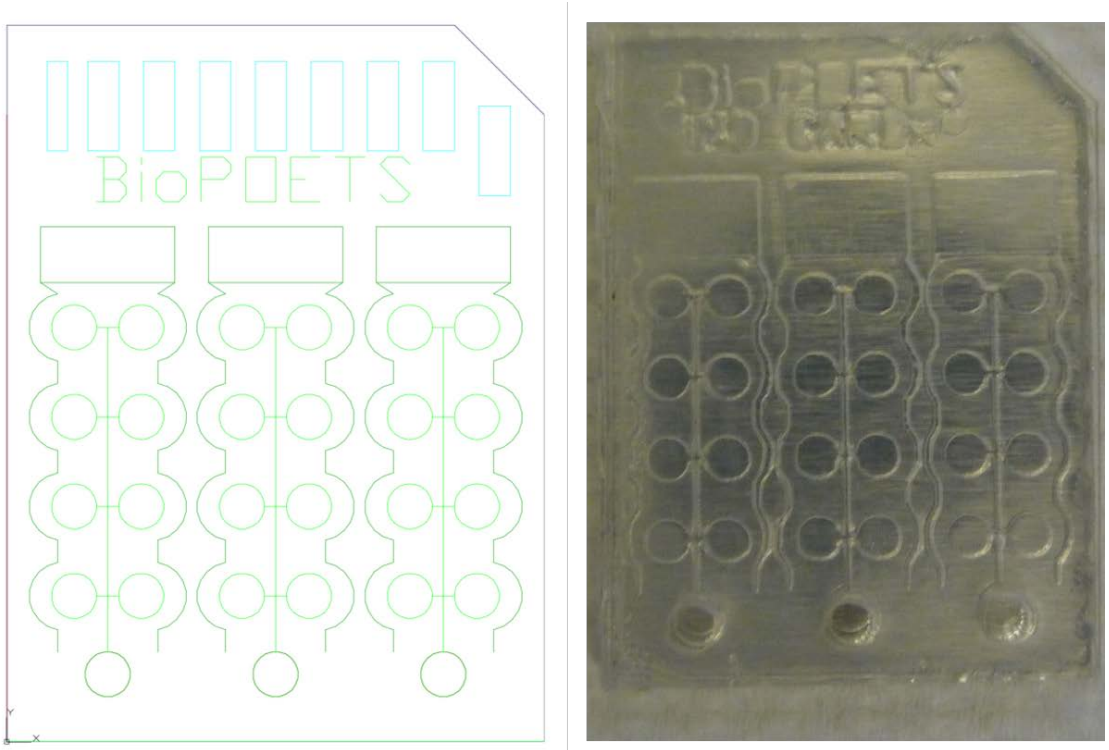

Figure B.3 Enhaned μSIP loading chip. [2012-01-06] A modification to an SD card format chip in order to enhance loading of an AAO-backed chip. The flanking μSIP channels significantly improved loading speed.

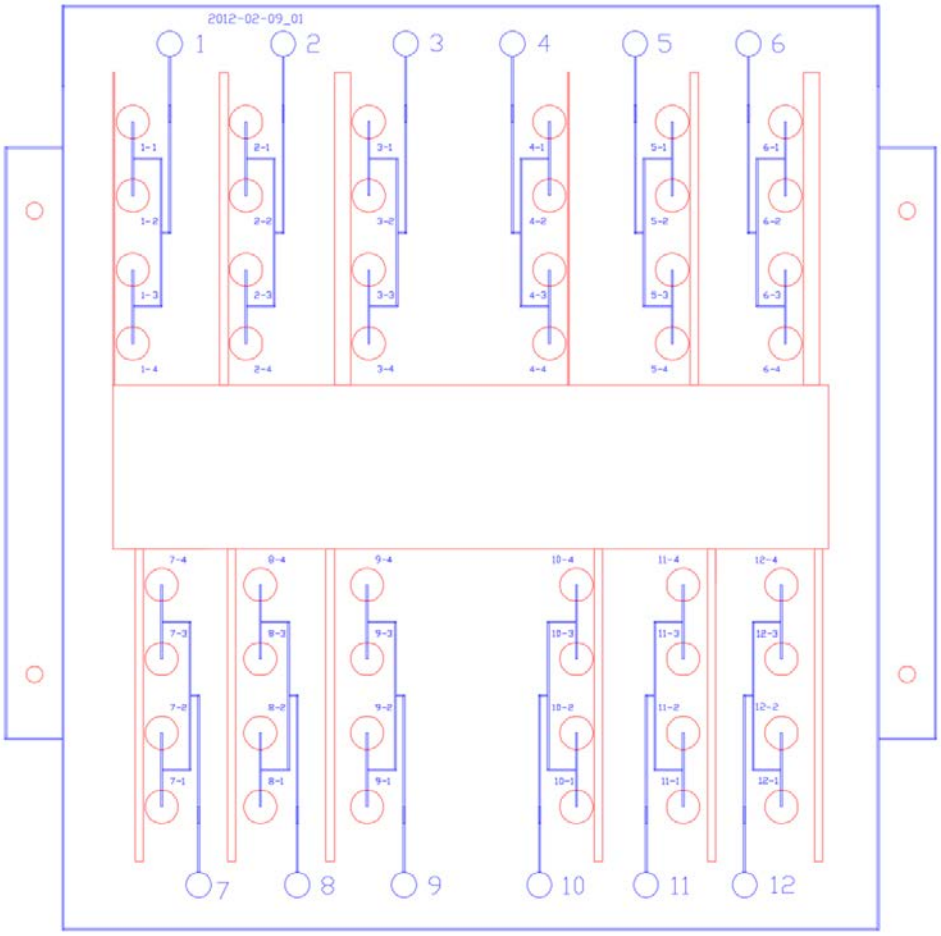

Figure B.4 μSIP optimization chip. [2012-02-09] A chip was designed with flanking μSIP channels of varying widths and distances from the dead end reaction chambers in order to characterize loading phenomena.

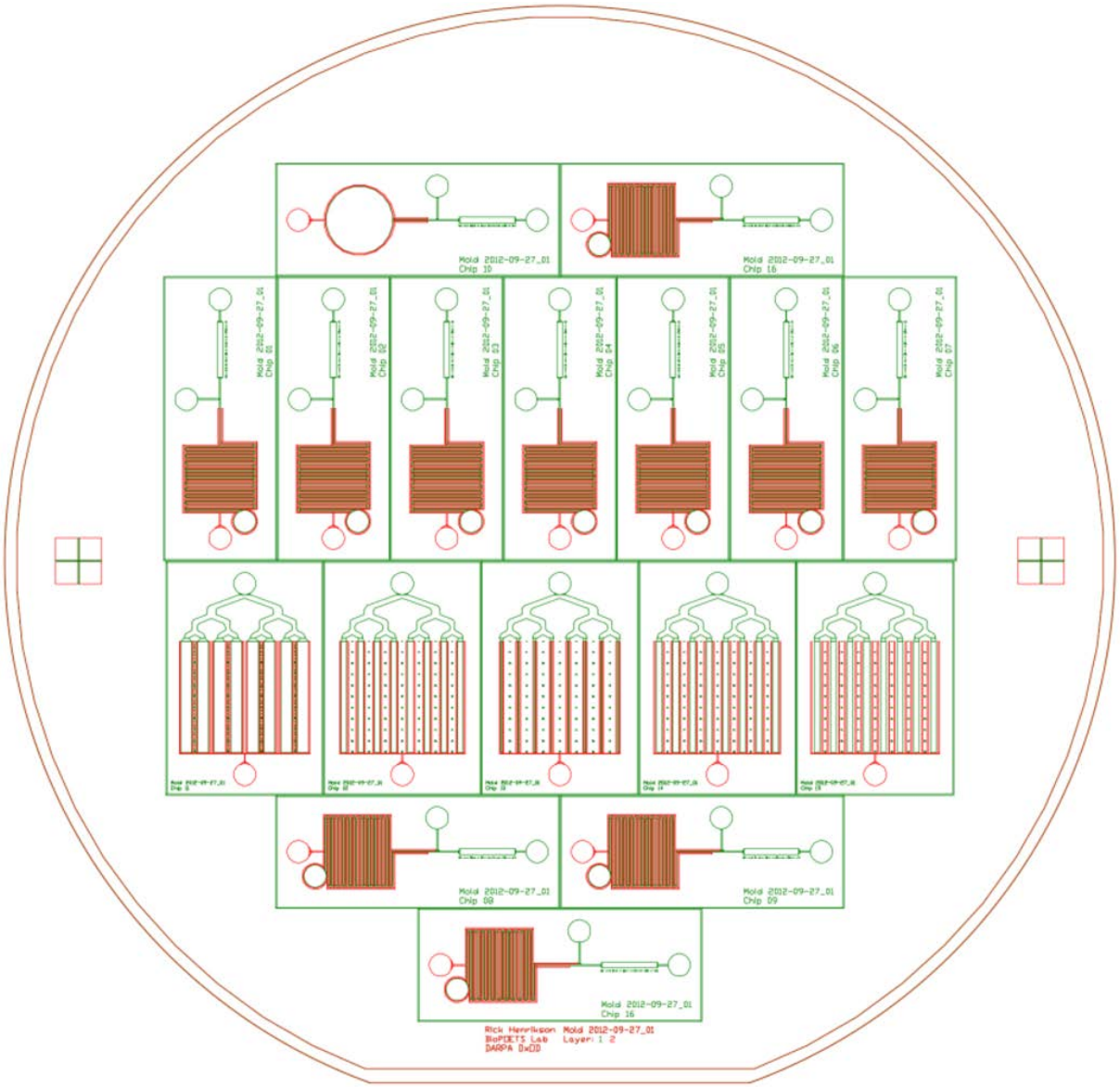

Figure B.5 Extensive μSIP loading test chip. [2012-09-27] A chip designed with multiple configurations of active μSIP flanking channels to assess the impact of channel widths and distances on loading rates.

B.1.2 AMProbe Chips

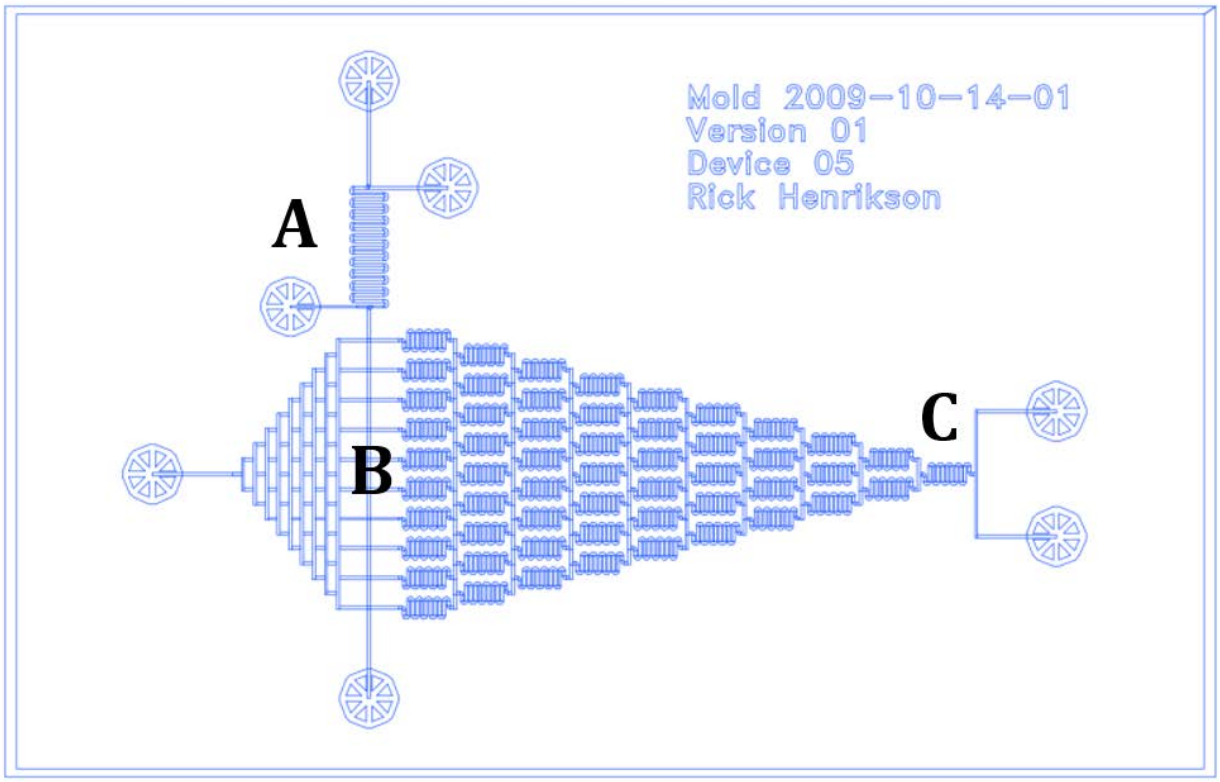

Figure B.6 Initial AMProbe chip design. [2009-10-14] (A) The sinuous AMProbe incubation channel. Flanking inlets on the left and right were designed to enable patterning of AMProbes prior to an assay. (B) A gradient of reaction intersections for the release reporter to interact with – enabling a broader dynamic range. (C) Inlets to generate a concentration gradient for the reporter reactant (such as hybridization capture probes, catalytic reagents, etc.)

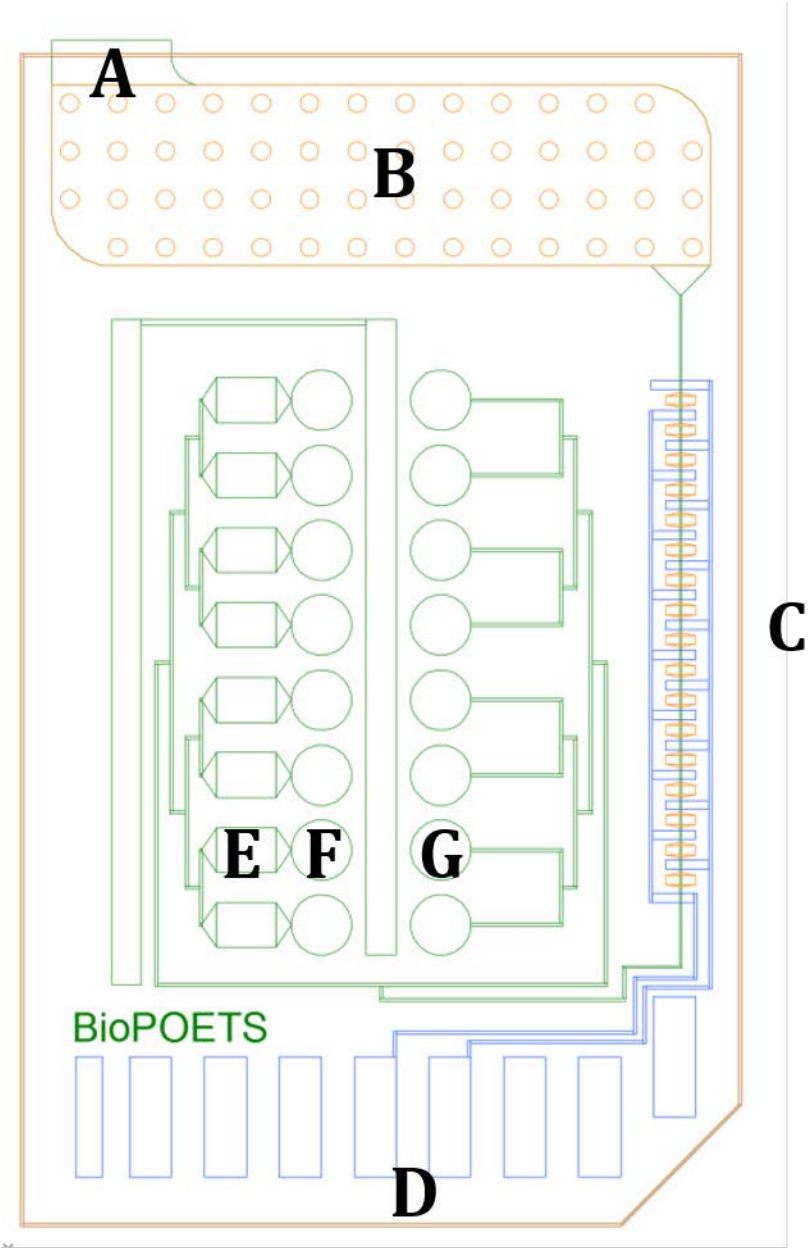

Figure B.7 Integrated Protein and Nucleic Acid Detection Chip. [2012-04-26] (A) Lateral inlet for combined degas and capillary action sample loading. (B) Sample loading and cell sedimentation chamber. (C) Alternating interdigitated electrodes with trenches to slow cell transit for electrochemical lysis. (D) Source and drain for interdigitated electrodes. (E) AMProbe protein-mediated release chamber. (F) AMProbe reaction and readout chamber. (G) Isothermal nucleic acid amplification chamber.

C Sequences

Please note: All sequences are provided in 5' → 3' direction, unless otherwise noted.

C.1 Plasmids

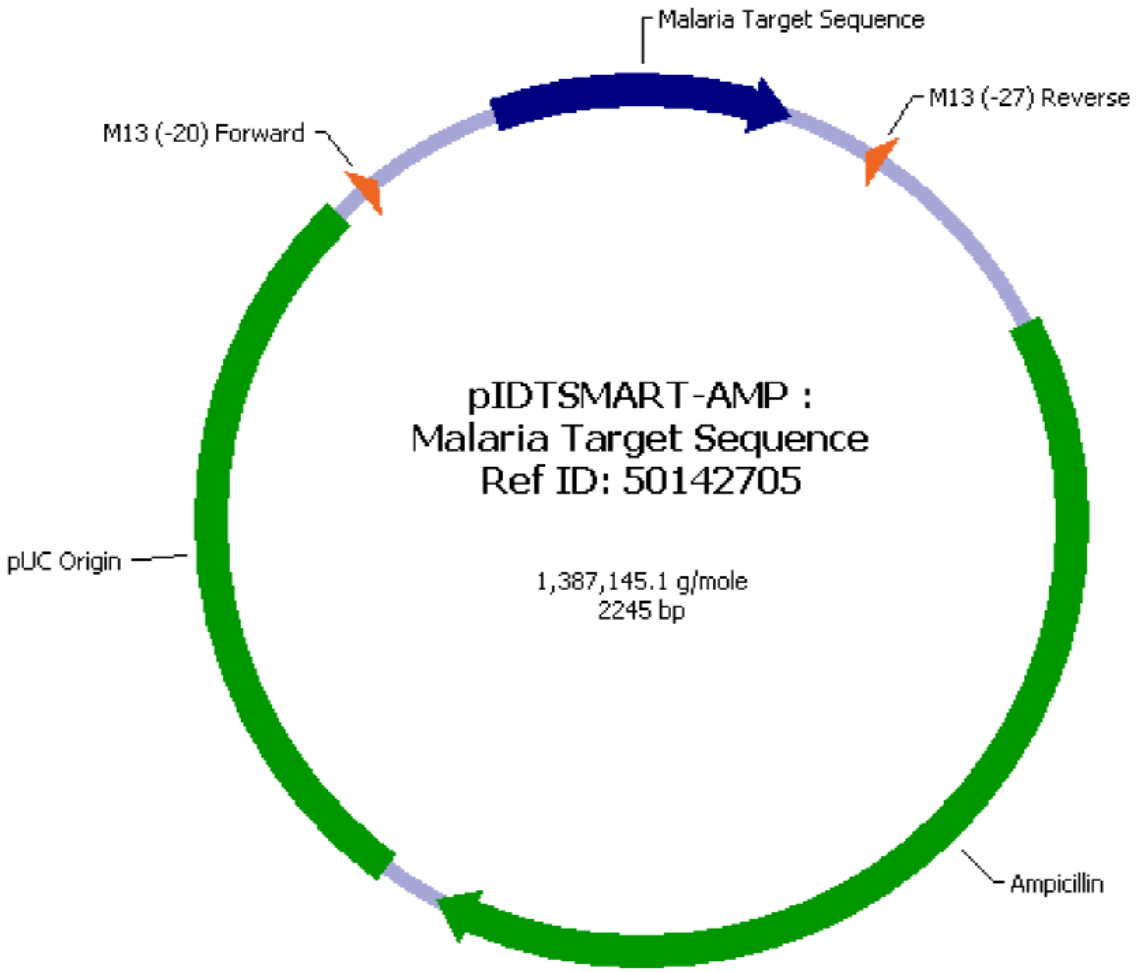

Figure C.1 Malaria plasmid.

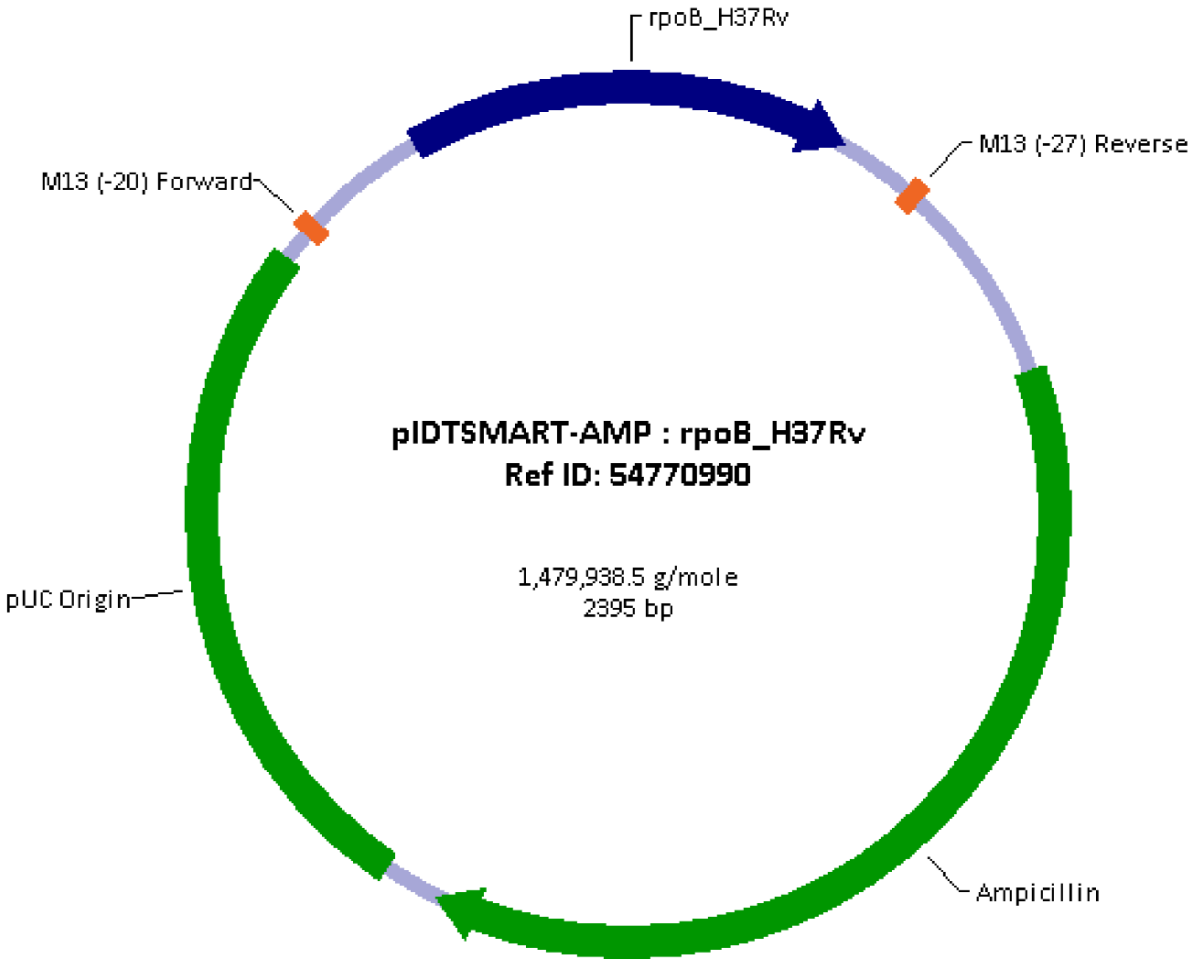

Figure C.2 H37Rv plasmid.

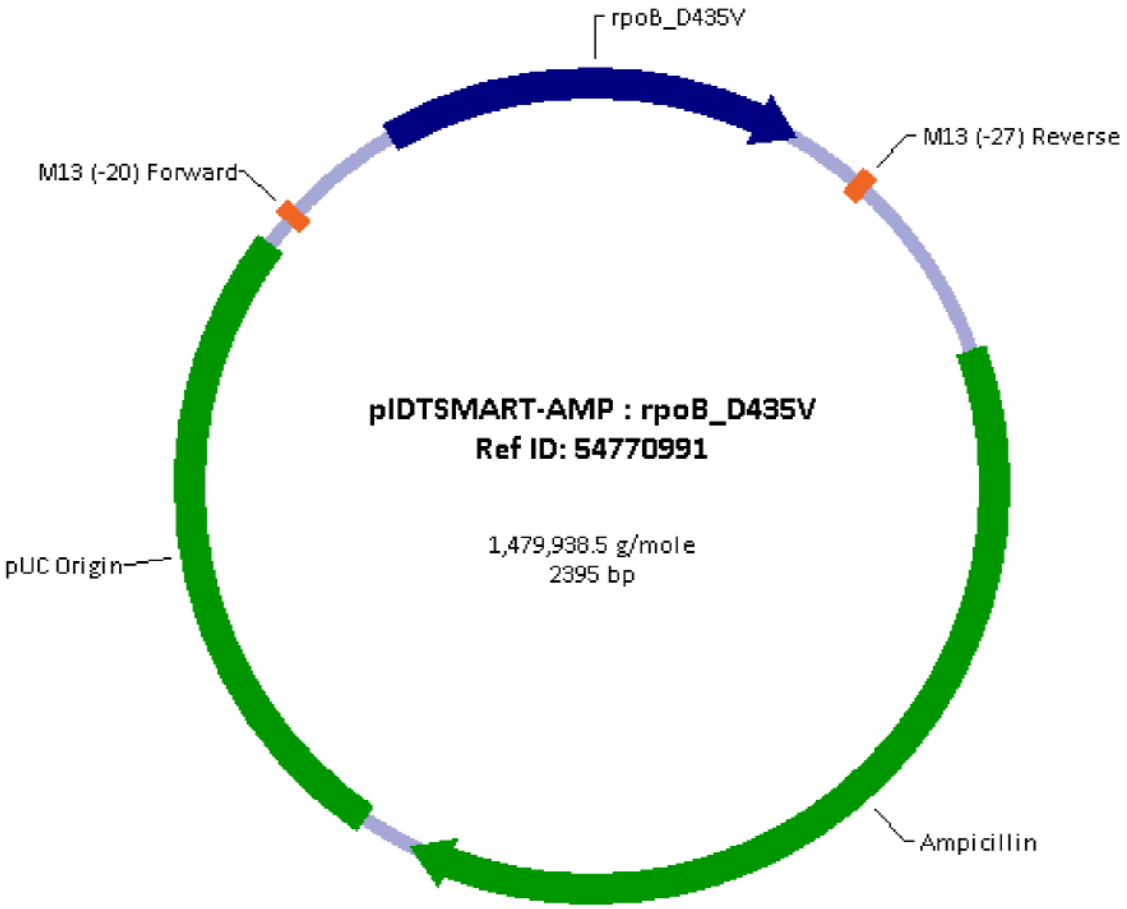

Figure C.3 D435V plasmid.

D Supplemental Data

D.1 LAMP Reaction Data

D.1.1 Optimization of [Calcein] and [$MnCl_2$]

In order to optimize the concentration of calcein and $MnCl_2$ in LAMP reactions, visual inspection was performed on plates with a range of dilutions for each reagent. Unless otherwise specified, all reactions were performed using a custom 2x reaction mix (see A.2.4). In all positive reactions, an HIV DNA plasmid template at 10^6 copies/μL was used as the target, with appropriate HIV LAMP primers. Reactions were performed with an amplification incubation at 63°C for 120 minutes in a Biorad CFX96 thermocycler. Plate and chip images were taken using an Invitrogen SYBR© Safe imager™ blue light transilluminator in a dark room.

An initial optimization was performed by a matrix of 5x serial dilutions, with calcein ranging between 250 - 0.0032 μM and $MnCl_2$ ranging between 1000 - 0.032 μM final concentration in a LAMP reaction of 20μL (Figure D.1).

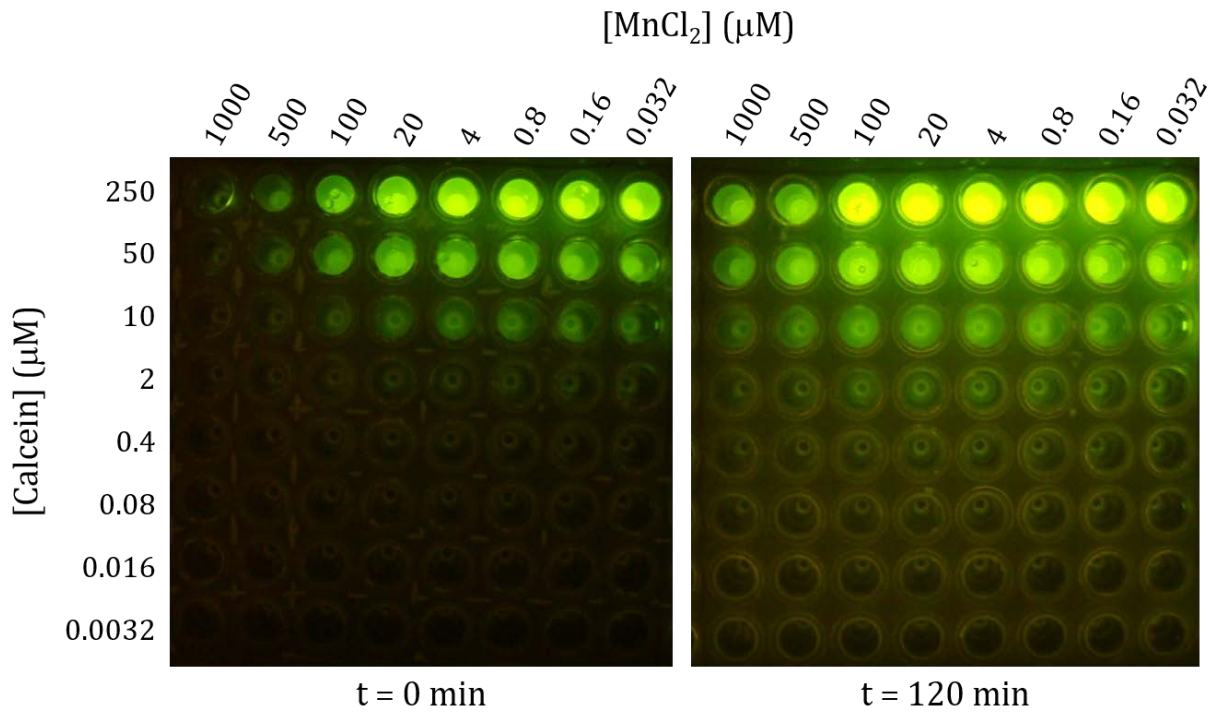

Figure D.1 Initial optimization of calcein and $MnCl_2$ for visual readout.

Solutions from selected wells above (endpoint reactions) were subsequently loaded into microfluidic chips to confirm visibility of fluorescence in the microfluidic system (Figure D.2).

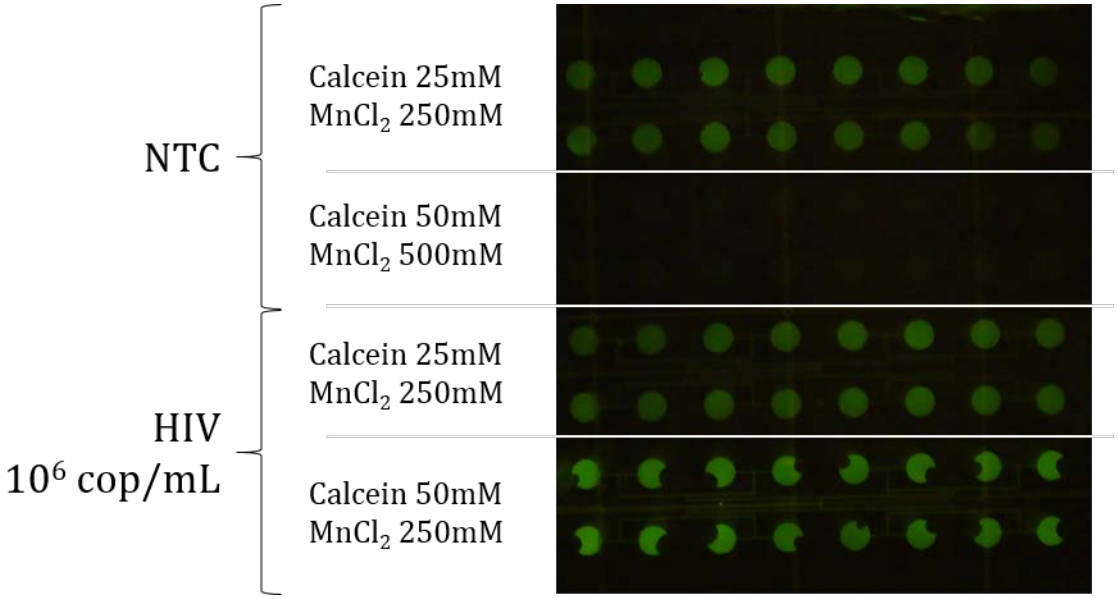

Figure D.2 Visualization of LAMP products in a microfluidic LAMP chip.

We subsequently performed a narrowed-in optimization, using an $MnCl_2$ concentration of 1488 μM and a serial dilution range for calcein. In this way, we identified an optimal concentration of calcein for visual readout at 27.28 μM (Figure D.3).

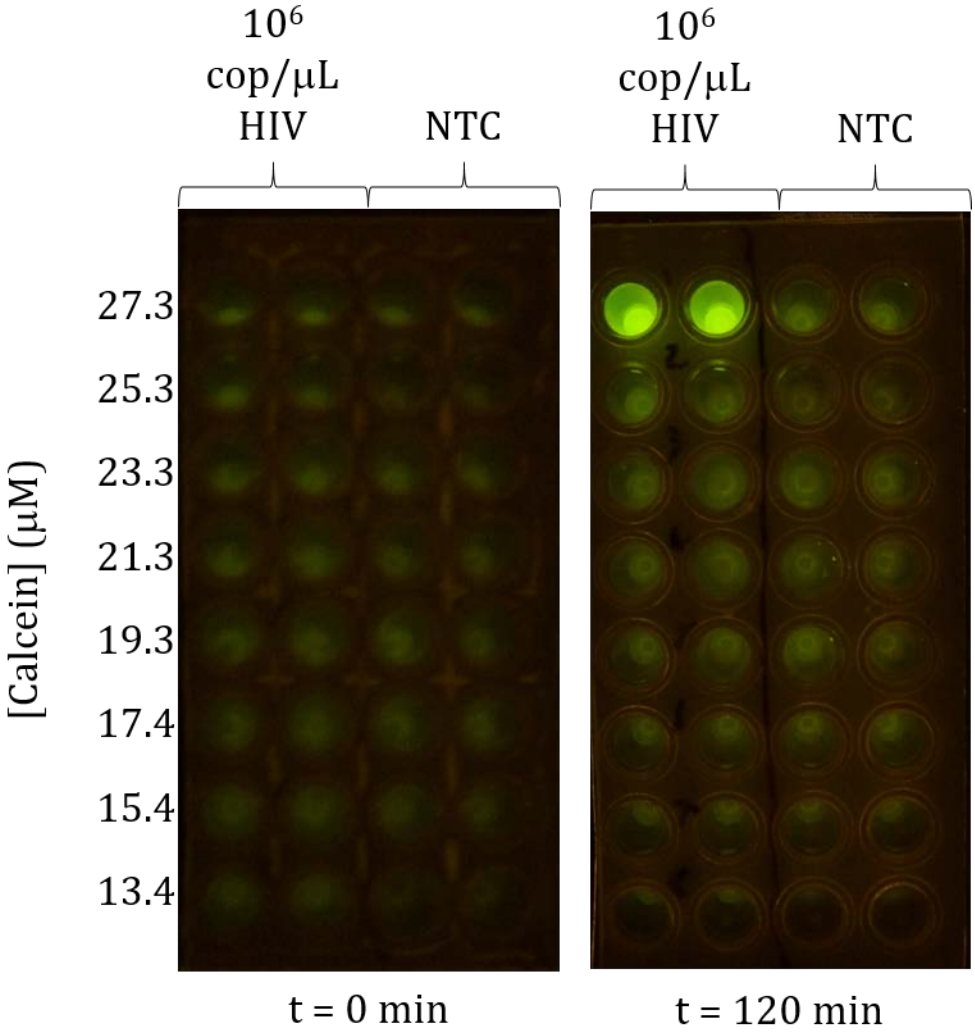

Figure D.3 Subsequent optimization of calcein and MnCl2 for visual readout. Optimal differential fluorescence after 120 minutes incubation was found at 27.28 μM calcein.

D.1.2 μBAR System Characterization

We performed a range of tests in order to characterize the performance of the μBAR instrument[74]. We first characterized the fluorescence sensitivity of the mBAR instrument by introducing different known concentrations of calcein (the fluorophore used in our LAMP assays) into the microfluidic device and observing the relative changes in photoamplifier output across all reaction chambers (Figure D.4A). For this experiment, we developed a slightly modified chip which included a serpentine channel connecting all of the reaction wells in series. This allowed us to sequentially introduce higher calcein concentrations (Figure D.4B) while ensuring that the chip placement/geometry was fixed. We repeated this

experiment with 3 independent chips (marked with red, blue, and green circles) and found that detector output as a function of concentration followed a linear trend over four orders of magnitude. To determine the sensitivity of the instrument to fluorescence changes, we calculated the Instrument Detection Limit (IDL) as the concentration that produces a signal three times greater than the noise standard deviation of the instrument for a given time resolution. In the case of real-time nucleic acid amplification signals, a time resolution (BW^{-1}) of 2 min is sufficient. In that case, the noise standard deviation of the μBAR is 5 mV_{rms}, leading to an IDL of approximately 600 pM with the μBAR. As most nucleic acid amplification reactions involve fluorophore concentrations that are orders of magnitude higher than this (typically 1–10 μM), this is more than sufficient to carry out these kinds of assays. We further examined the nonuniformity of photoamplifier sensitivity across the detection array. Because the LED lighting does not lead to uniform illumination, and due to some internal scattering within the chips, the amount of light reaching each reaction chamber is slightly different. By calculating the linear slope of amplitude change as a function of concentration change (i.e. sensitivity) at each well (Figure D.4C), we can normalize subsequent assay runs so that intensities can be directly compared across the chip. Although the chip was designed with 96 reaction chambers in a 12 x 8 configuration, we determined that it was not possible to use assay results from the outermost chambers due to excitation light scattering at the edges of the device. This limitation could easily be overcome in subsequent designs. We therefore restrict our analysis to the 60 innermost reaction chambers (6 x 10 array).

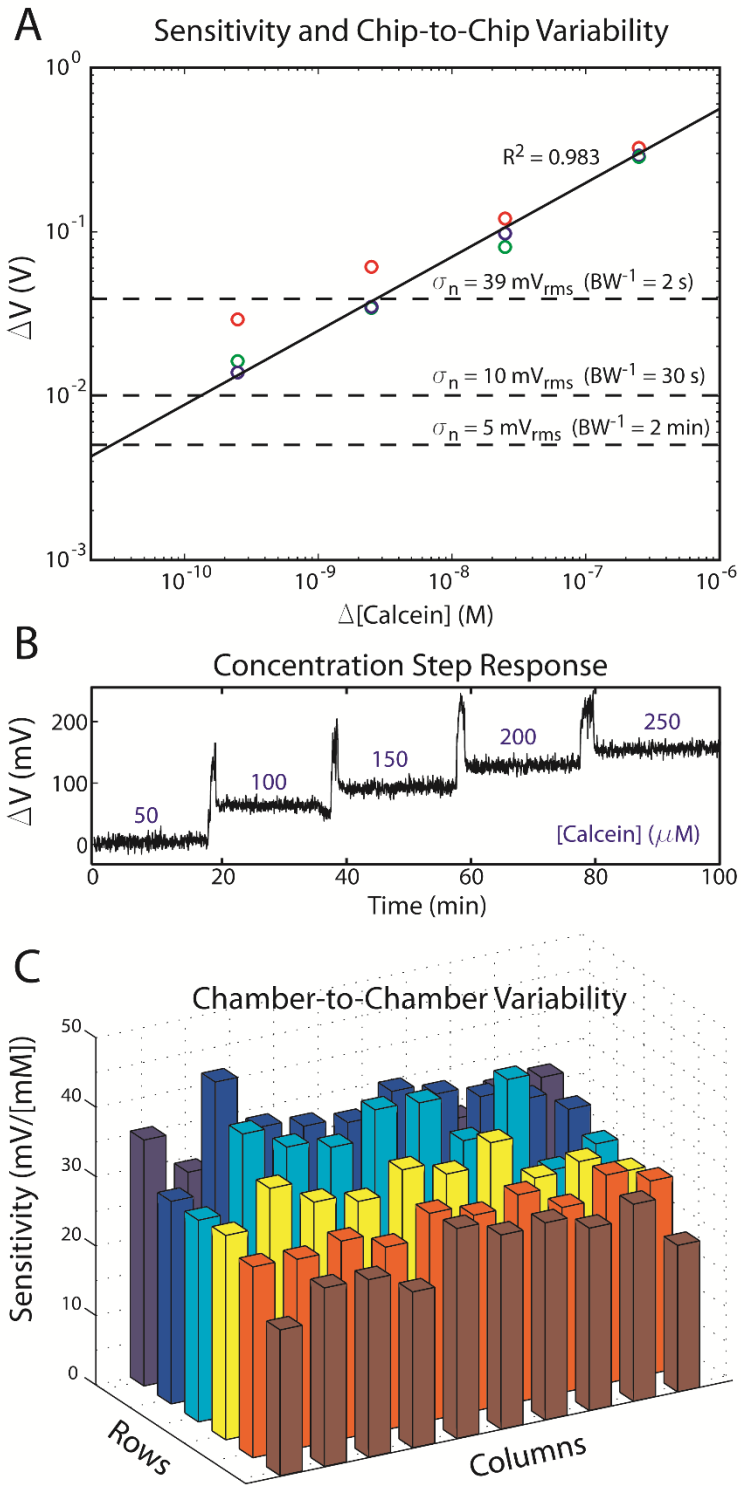

Figure D.4 Fluorescence sensitivity and linearity. (A) Different concentrations of calcein were introduced into a microfluidic cartridge and the corresponding change in photoamplifier voltage was recorded. The circles indicate the mean signal amplitude across all reaction wells for three different chips (red, green, and blue). As expected, the relationship between calcein concentration and photoamplifier output is linear (R^2=0.983). Limit of detection can be evaluated by determining when this trend line crosses the noise

floor of the instrument at a given bandwidth. At a time resolution (BW^{-1}) of 2 min, the μBAR can distinguish changes in calcein concentration of 30 pM, which is orders of magnitude below the fluorophore concentrations typically used in nucleic acid amplification reactions. (B) 50 μM steps of calcein are clearly visible in the photoamplifier output and this output remains stable for a constant concentration. (C) Due to the nature of the illumination scheme and the lack of optics, there is some nonuniformity of sensitivity across the 6 x 10 reaction chamber array. However, we take this into account and normalize each well by its mean sensitivity, shown here. In this graphic, the illumination LEDs and sample inlets are located above the topmost row.

We next examined the spatial uniformity and temperature regulation performance of the μBAR's internal ITO substrate heater. We used an infrared thermal camera to examine the surface of a PDMS device on top of the ITO heater with the case removed (Figure D.5A). For the 6 x 10 array of reaction chambers in the center of the chip, we found a temperature distribution of 60 ± 1.25°C (Figure D.5B). By comparison, modern mid-range thermocyclers have a well-to-well temperature nonuniformity of 1–2°C during a plateau phase. We then embedded a commercial thermocouple temperature probe (Fluke 87V) within the PDMS microfluidic device and calibrated the on-board temperature feedback (from a thermistor positioned on the underside of the ITO heater) with the actual chip temperature. Following calibration, we found excellent agreement between the μBAR's temperature setpoint and the independently measured chip temperature (Figure D.5C).

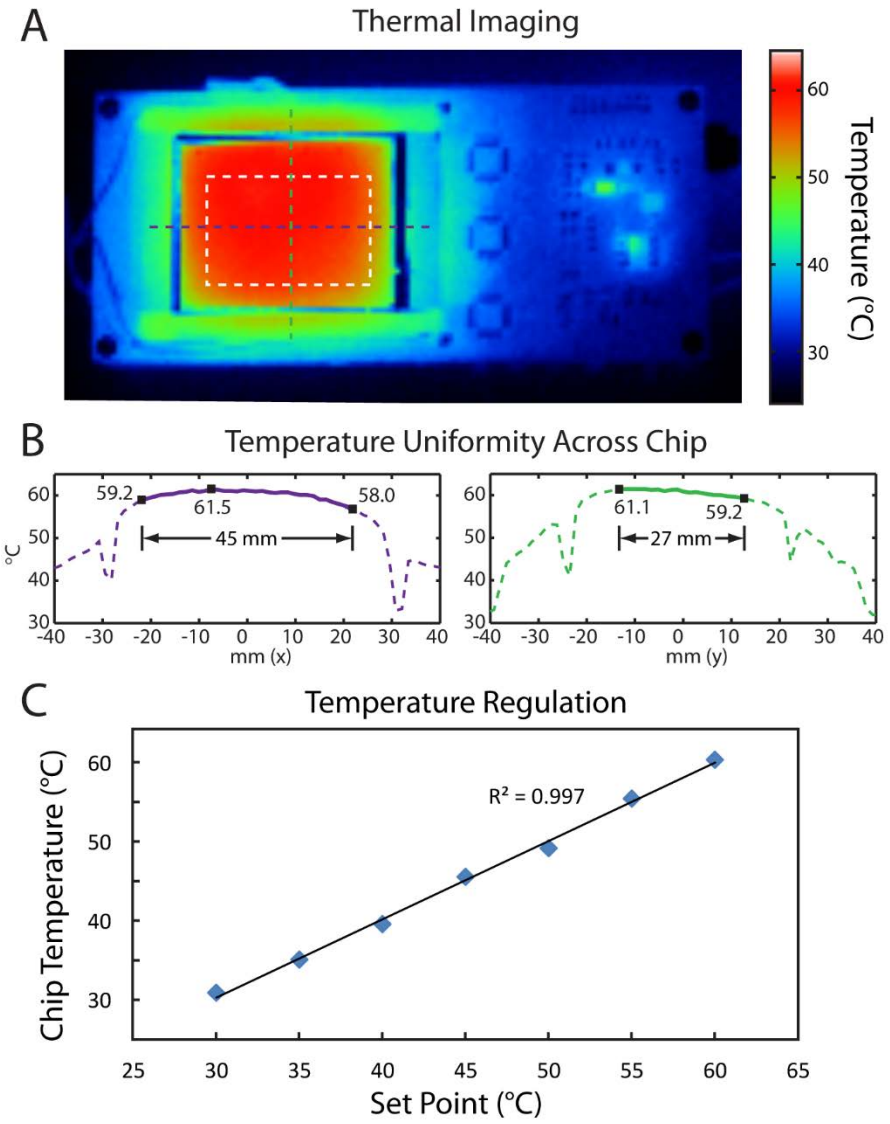

Figure D.5 Heater uniformity and stability. (A) Infrared thermal image of the μBAR (case removed) at 60°C. The white box indicates the extent of the 6 x 10 reaction chamber array. (B) Linescans through this region indicate a temperature uniformity of ± 1.25°C. (C) Chip temperature, as measured with a thermocouple directly embedded in the PDMS, versus μBAR temperature set point.

The μBAR can either be operated from a 5V DC wall power source or from a lithium polymer battery (3.7V nominal voltage). During battery operation, the battery discharge leads to a decreasing battery voltage, and it's important that this not significantly affect LED intensity, photoamplifier sensitivity, or temperature over the course of a typical 2 hour assay run, because any time-varying signal might obscure the assay results. Using a chip with a constant dye concentration, we directly compared photoamplifier output and temperature for wall power and battery power (Figure D.6). We found that both wall power and battery power lead to a small linear drift in photoamplifier output (0.21 and 0.08 mV/min, respectively) which was well below the amplitude of a typical LAMP assay (.10 mV/min, see

Figure D.6). Both wall power and battery power resulted in a steady temperature of 60°C ± 0.1 (standard deviation).

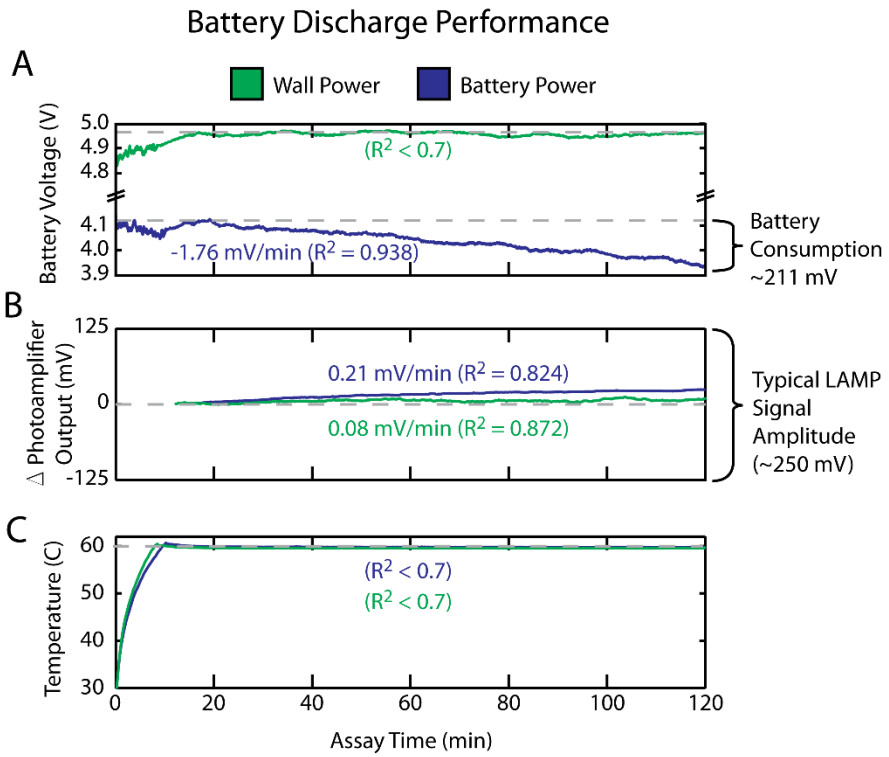

Figure D.6 Battery discharge performance of the μBAR. The μBAR maintains constant LED intensity and chip temperature over a 2 hr period when operated from a battery. Since a battery's voltage decreases as it is discharged, we wanted to ensure that this would not obscure results of the assay by either causing drift in the photoamplifier output or chip temperature. In this experiment, the battery voltage decreases linearly by 211 mV over the course of the assay run (A). This, however, does not significantly impact the intensity of the LEDs/photoamplifier sensitivity (B), or temperature stability (C), as compared with a constant (wall) power source. Dashed lines show the values of battery voltage, photoamplifier output, and temperature at t=20 min, linear regressions are calculated and slopes are reported for R^2 values >0.7. There is no significant change in temperature for either wall or battery power. Photoamplifier output shows a slight time dependant drift in both cases (7.5 mV/min for wall power and 2.5 mV/min for battery power), but this drift is significantly lower than the signal amplitudes which we see in a typical LAMP assay (~250 mV, see Figure D.4), so we consider it acceptable.

D.2 Colorimetric Nanoplasmonic Readout

The colorimetric nanoplasmonic readout was further extended with additional catalytic reporter molecules. Silver nanoparticle reporters showed a significantly enhanced reduction of gold and accompanying reflectance spectra peak shift in the AAO substrate (Figure D.7).

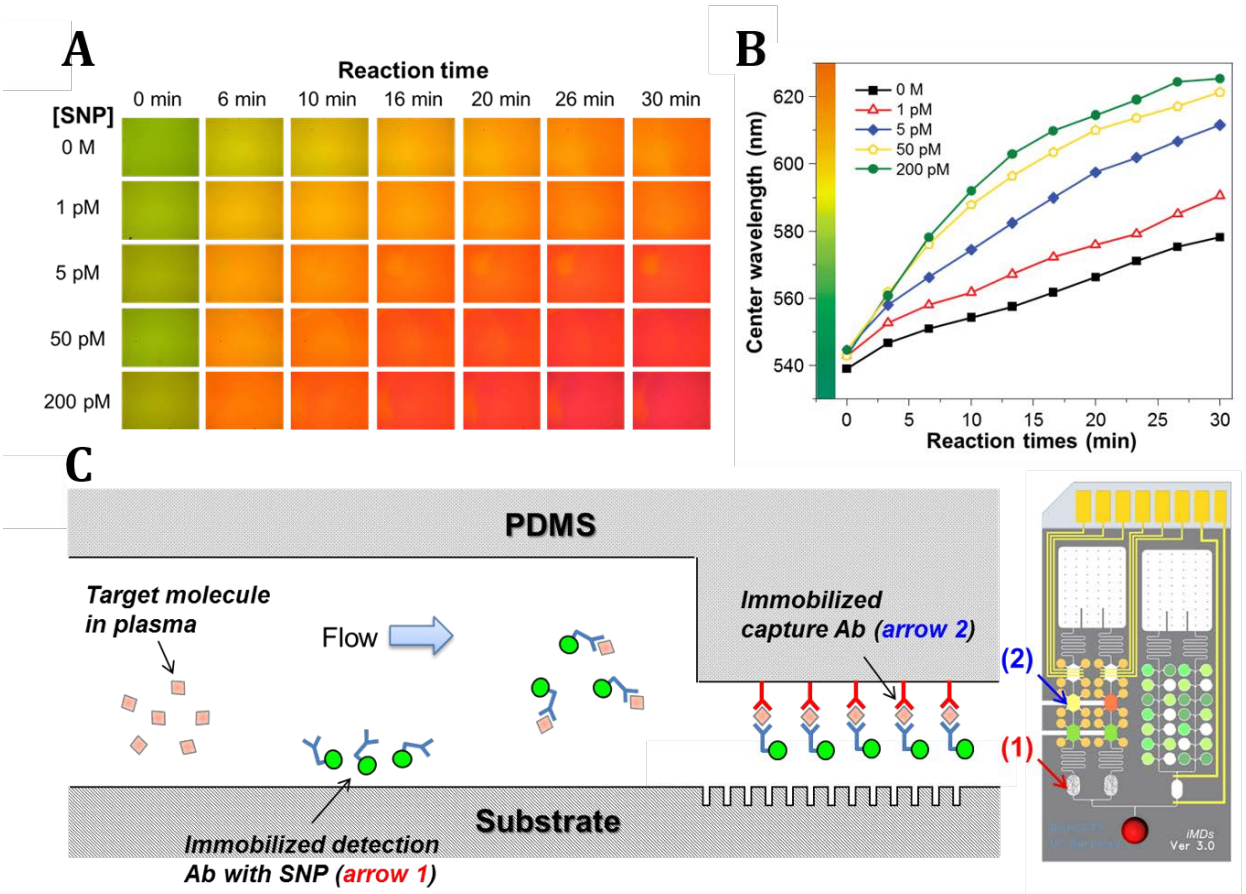

Figure D.7 Colorimetric response of AAO optical biosensor by silver nanoparticle-mediated Au reduction. (A) Optical microscopy images. (B) Shifts in peak wavelength in reflectance spectra for the AAO optical biosensor as a function of reaction time with different silver nanoparticle concentrations. The reactants were 1 µL 50 mM HAuCl4 solution and 1 µL silver nanoparticle dispersion with different concentration. (C) Schematic cross-sectional illustration of iMDs with single-step enzyme-linked immunosorbent assay (ELISA) for protein detection.

E References

1. Tomita, N., Mori, Y., Kanda, H. & Notomi, T. Loop-mediated isothermal amplification (LAMP) of gene sequences and simple visual detection of products. *Nat. Protoc.* **3,** 877–882 (2008).
2. Lu, Y. & Liu, J. Preparation of aptamer-linked gold nanoparticle purple aggregates for colorimetric sensing of analytes. *Nat. Protoc.* **1,** 246–252 (2006).
3. Carson, K. L. Flexibility - the guiding principle for antibody manufacturing. *Nat Biotech* **23,** 1054–1058 (2005).
4. Ross, B. M. & Lee, L. P. Comparison of near- and far-field measures for plasmon resonance of metallic nanoparticles. *Opt. Lett.* **34,** 896–898 (2009).

5. Ghosh, S. K. & Pal, T. Interparticle Coupling Effect on the Surface Plasmon Resonance of Gold Nanoparticles: From Theory to Applications. *Chem. Rev.* **107,** 4797–4862 (2007).